Functions of the transcription factor Lyl-1 in the hematopoietic development of the embryo : Focus on yolk sac macrophages and hematopoietic stem cells

Deshan Ren

NNT:2019SACLS189

Thèse de doctorat

Functions of the transcription factor Lyl-1 in the hematopoietic development of the embryo:

Focus on yolk sac macrophages and hematopoietic stem cells

Thèse de doctorat de l'Université Paris-Saclay
préparée à l'Université Paris-Sud

École doctorale n°577:
Structure et Dynamique des Systèmes Vivants (SDSV)
Spécialité: Sciences de la vie et de la santé

Thèse présentée et soutenue à Villejuif, le 8 juillet 2019 par

Deshan REN

Composition du Jury :

Dr. Pierre BOBE Université Paris-Sud	Président
Dr. Julien Y. BERTRAND Université de Genève	Rapporteur
Dr. Charles DURAND Sorbonne Université	Rapporteur
Dr. Thomas MERCHER Institut Gustave Roussy	Examinateur
Dr. Rachel GOLUB Institut Pasteur	Examinatrice
Dr. Isabelle GODIN Université Paris-Sud	Directrice de thèse

UNIVERSITE PARIS-SUD

École doctorale n°577 "Structure et Dynamique des Systèmes Vivants"

Institut Gustave Roussy

DISCIPLINE: BIOLOGIE

THÈSE DE DOCTORAT

Soutenue le 8 Juillet 2019

Par Deshan REN

Functions of the transcription factor Lyl-1 in the hematopoietic development of the embryo: Focus on yolk sac macrophages and hematopoietic stem cells

Composition du jury:

Rapporteurs:	Dr. Charles DURAND	Sorbonne Université
	Dr. Julien Y. BERTRAND	Université de Genève
Examinateurs:	Dr. Rachel GOLUB	Institut Pasteur
	Dr. Thomas MERCHER	Institut Gustave Roussy
Président:	Dr. Pierre BOBE	Université Paris Sud
Directrice de thèse:	Dr. Isabelle GODIN	Université Paris Sud

ACKNOWLEDGEMENTS

This work is the result of the untiring and fulfilling efforts at Institut Gustave Roussy, a place I call my second home under the supervision of Dr. Isabelle GODIN. It is my pleasure to be able to thank the people who have provided their kind help and support to me during these 4 years.

First of all, I would express my perpetual and sincere gratitude to my supervisor, Dr. Isabelle GODIN, for introducing, leading and guiding me into this wonderful world of embryonic research. Thank you for your patience, which I tested many a times. Your mentorship during these 4 years of professional training opened my eyes to this amazing world of research. Your wisdom and implausible suggestions have made me into the researcher that I am today. You have taught me a lot and I will always be grateful to you for so many things. Thank you for introducing me to your family and treating me like family. Your mentoring was not only that of a supervisor but also a friend. Where I not only learnt science, but also how to be a person who is righteous and honesty.

Sincere thanks to Dr. Julien Y. BERTRAND and Dr. Charles DURAND who spent a lot of their precious time to improve my manuscript and come up with very insightful comments. You definitely increased my perception and helped me a lot in finalizing my work. I would like to thank the other members of my thesis committee: Dr. Pierre BOBE, Dr. Thomas Mercher for taking out time from their busy schedules to review my work. A very sincere gratitude to Dr. Rachel GOLUB for not only being my thesis jury but also the advisor of my study.

Next, I must also acknowledge my team: I would like to thank Dr. Shoutang Wang, who was a companion for more than 2 years in the lab, and for his scientific assistance and kind help with my studies and life in France. Your humor and jokes

during lunch gave us a lot of pleasure. I would like to thank Claudia Santos and Sonia Benhamouche for your encouragement and assistance.

I would like to thank Dr. William VAINCHENKER, Dr. Dr. Isabelle PLO, Dr. Hana RASLOVA and Dr. Monika WITTNER for your kindness support during my study.

I would like extend a special thanks to Mr. Rameez ISHAQ for his encouragement and friendship and for his critical support whenever I requested it. I truly have been lucky to meet you in the lab and I will definitely miss you. I would like to thank Dr. Tao Song & Dr. Longsheng Zheng for the fun weekends during their 3 year stay in Villejuif. A warm gratitude to the Chinese people in IGR: Dr. Yanyan Zhang; Dr. Liang He; Dr.Heng Zhou; Dr. Yinxing Ma; Dr. Peng Liu and Dr. Liwei Zhao; Dr. Guo Chen; Dr. Jiang Hu and Mr. Wei Xie for your support and encouragement. Cheers for the young researchers in U1170: Dr. Lise Secardin; Tracy Dagher; Graciela Rabadann; Francesca BASSOVALENTINA; Dr. Mira KHOURY; Dr. Alessandro Donada; Dr. Brahim ARKOUN and Dr. Anita Roy.

I would like to acknowledge the friends I have made in Paris: Mr. Bingrun Liu, Miss Jiajia Guo, and Mr. Dawei Liu and those happy, optimistic and talkative people from Northeast of China who give me a lot of cheering up. Dr. He Huang and Dr. Zuowei Zhu and your group of students from ENS Cachan for sharing your get together during the lonely weekend.

Last but not least I would like to thank my family, particularly my parents, for all the support you provided me throughout my entire life. My girlfriend Yu Pingping for your sacrifice and understanding during the past years. And I hope I will not let you down in any way in the future.

Finally, I would like to thank the China Scholarship Council. This thesis would not have been possible without the fellowship from China Scholarship Council.

Index

Abbreviations

AGM: Aorta-gonad-mesonephros

ALL: Acute lymphoblastic leukemia

AML: Acute myeloblastic leukemia

β-Gal:β-Galactosidase

bHLH: Basic helix-loop-helix

CLP: Common myeloid progenitor

CSF1: Colony stimulating factor-1

DCs: Dendritic cells

DEGs: Differentially expressed genes

DN: Double-Negative

E: Embryonic day

EHT: Endothelial to hematopoietic transition

EMP: Erythro-myeloid progenitor

EoBP: Eosinophil–basophil progenitor

ER: Estrogen receptor

FDG: Fluorescein di-β-galactopyranoside

FDR: False discovery rate

FL: Fetal liver

GMP: Granulocyte–monocyte progenitors

GSEA: Gene Set Enrichment Analysis

HIAC: Hematopoietic Intra-Aortic Cluster

HSCs: Hematopoietic stem cells

HSPC: Hematopoietic stem and progenitor cells

IFN-α: Interferon α

ILCs: Innate lymphoid cells

IRF8: Interferon regulatory factor 8

LDA: Limiting dilution assay

Lmo2: LIM domain only 2

LRP: Low density lipoprotein receptor-related protein

LSK: Lineage- Sca-1^{+}cKit^{+}

LTR: Long-term reconstitution

Lyl-1: Lymphoblastic leukemia derived sequence 1

M-CSF: Macrophage colony-stimulating factor

MEP: Megakaryocyte–erythrocyte progenitors

MΦ: Macrophages

$M\Phi^{Prim}$: Primitive MΦ

$M\Phi^{T\text{-}Def}$: Transient definitive MΦ

MIF: Macrophage migration inhibitory factor

MPS: Mononuclear phagocyte system

NES: Normalized enrichment score

NF-κB: Nuclear factor k-light-chain enhancer of activated B core

NK: Natural killer

P-Sp: Paraaortic splanchnopleura

Runx1: Runt-related transcription factor 1

S: Somite pair

T-ALL: T-cell Acute Lymphoblastic Leukemia

TAM: Tamoxifen

TLR4: Toll-like receptor 4

TGF-β: Transforming growth factor-β

VE-cadherin: Vascular endothelial cadherin

WT: Wild type

YS: Yolk sac

Organization of the thesis

During ontogeny, hematopoietic progenitors are generated in three independent waves, the first two (primitive and transient definitive) develop from the yolk sac (YS) before the appearance of hematopoietic Stem Cells (HSCs) that occurs later in the Aorta-Gonad-Mesonephros (AGM), in the third and definitive wave.

Both Tal1/SCL and its paralog Lyl-1 belong to the transcriptional complex that regulates hematopoietic progenitor development. While Tal-1/SCL is mandatory for the specification of hematopoietic progenitors from the three embryonic waves, to date the functions of Lyl-1 during developmental hematopoiesis remains largely unknown. Previous work from our team has detected that Lyl-1 and Tal1/Scl were expressed in an overlapping pattern in the early YS and newly generated AGM HSC, suggesting Lyl-1 plays some important roles during hematopoiesis ontogeny. Few years ago, our team started to investigate the role of Lyl-1 during developmental hematopoiesis and my research project focused on the function of Lyl-1 during the development of YS macrophage (MΦ) and of HSC.

Here, I give you a brief organisation of the thesis:
Firstly, I will give the general background (Introduction chapter) regarding the different steps of developmental hematopoiesis, including the three waves of hematopoiesis. I will develop in more details the current knowledge on YS MΦ and HSC development. I will also give the information about the regulation of hematopoiesis by transcription factors and focus on the data currently available for Lyl-1.
In the results part, I will first report previous data regarding the function of Lyl-1 during YS MΦ development that were obtained Shoutang Wang, as I participated to this project. I further continued this project by the RNA-seq analysis of YS MΦ progenitors and this part of results will be present secondly. The last part will report the data I have obtained on the function of Lyl-1 during HSCs development.
Lastly, I will present the conclusion and perspective of the research project.

Figure List

Introduction figures:

Results part 1 figures:

Results part 2 figures:

Results part 3 figures：

1. Introduction

1.1 The adult hematopoietic system

In adult mammals, the blood cells are composed of a variety of cell types that travel in the blood vessels to reach the different tissues, where they provide oxygen (erythrocytes), produce platelets that are essential for clotting processes (megakaryocytes) and provide the first barrier of defense against environmental pathogens, through the clearing of exogenous particles and cellular debris (macrophages and neutrophils). Mammalian life is impossible in the absence of any of these erythro-myeloid cells. Specific defenses against pathogens and the elimination of abnormal cells (tumors) are carried out by cells of the lymphoid lineage — T cells, B cells and natural killer (NK) cells (Laurenti and Gottgens, 2018). And these blood cells are constantly replenished by progenitors produced by a rare population cells from the bone marrow, which are the hematopoietic stem cells (HSCs).

The *in vivo* proof for the multipotent capacity of HSCs was first discovered based on bone marrow transplantation experiments aimed to protect mice from lethal irradiation (Jacobson et al., 1951). Since then, progress in the phenotypic and functional characterization of these progenitors led to the isolation of HSCs and has made the hematopoietic system a paradigm in stem cell biology. Thus, HSC are characterized by two classical stem cell properties, multipotency and self-renewal. Multipotency is defined by the capacity of a single cell to give rise to a differentiated progeny comprising different cell types, including erythrocytes, myeloid cells, megakaryocytes, dendritic cells, lymphoid cells and natural killer cells. The self-renewal capability means that they can give rise to HSCs themselves without differentiation, which is very important to keep its proper pool. The property of HSC is proved by *in vivo* long-term reconstitution (LTR) experiments. By contrast, fate-committed progenitors are defined by a restricted lineage differentiation capacity (most often bi- or uni-lineage) and the absence or a limited self-renewal capability, so that they are usually exhausted within the first 2–3 weeks after transplantation (Laurenti and Gottgens, 2018).

The integrity of blood system depends on the differentiation of HSCs into the different lineages of blood cells. The characterization of progenitor populations downstream of HSCs provided the blueprint of the first classical hierarchical model of hematopoiesis. In this model, the first branching point distinguishes lymphoid potential from all other lineages (erythroid, myeloid and

megakaryocytic), followed by several further branches on either side of the hierarchy tree progressing from multi- to bi- then uni-potent progenitor and mature blood cells. The subsequently discovery of other immune-phenotypic markers during the years 2005 to 2015 led to revise several details of the branching tree, including subdivision of the multipotent progenitor compartment into several distinct subpopulations, lymphoid and myeloid fates remaining associated until further down the tree making it the current most prevailing model (Figure 1) of hematopoiesis (Laurenti and Gottgens, 2018).

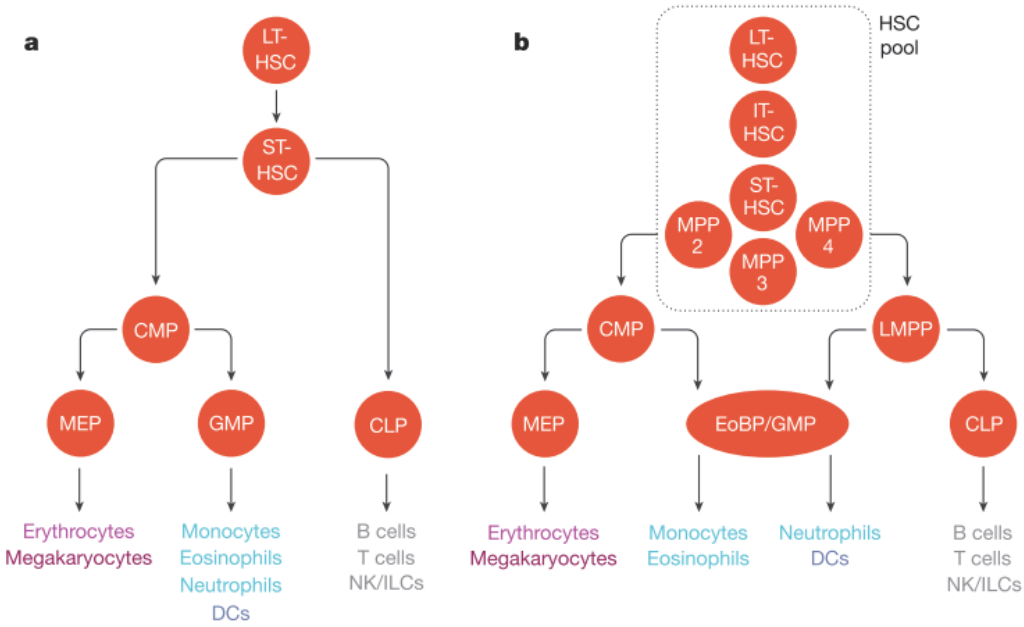

Figure 1: Hierarchical models of hematopoiesis.
a, Visualization of the classical hierarchical model of hematopoiesis: HSCs are represented as a homogeneous population. Downstream HSC, the first lineage bifurcation separates the myeloid and lymphoid branches via the common myeloid progenitor (CMP) and common lymphoid progenitor (CLP) populations. **b**, During the years 2005–2015, this visualization incorporates new findings: the heterogeneity of the HSC pool both in terms of self-renewal (vertical axis) and differentiation properties (horizontal axis), the myeloid and lymphoid branches remain associated via the lymphoid-primed multipotent progenitor (LMPP) population, the GMP compartment is shown to be fairly heterogeneous.
DCs, dendritic cells; EoBP, eosinophil–basophil progenitor; GMP, granulocyte–monocyte progenitors; LT, long-term; ILCs, innate lymphoid cells; MEP, megakaryocyte–erythrocyte progenitors; NK, natural killer cells; ST, short-term. From (Laurenti and Gottgens, 2018)

1.2 Development of hematopoietic system

1.2.1 Three waves of embryonic hematopoietic progenitors: general information

Though adult HSCs reside in the bone marrow of mammalian, they are not generated there, but originate from a population generated *de novo* during ontogeny. During mouse ontogeny, the hematopoietic system is absolutely different from the hierarchical models of hematopoiesis described in the adult. The hematopoietic system initiates with HSCs independent hematopoiesis (Palis, 2016) and is established in three distinct successive waves which are temporally and spatially restricted, each producing specific blood progenitors. This process involves three main anatomical sites: the extra-embryonic yolk sac (YS), the intra-embryonic aorta-gonad-mesonephros region (AGM) and the fetal liver (FL) (Cumano and Godin, 2007). The YS blood island is the first site of hematopoiesis in mammalian embryos, and the AGM is the site for HSC generation, while FL provides a microenvironment for HSC proliferation, maturation and differentiation (Khan et al., 2016).

During hematopoiesis ontogeny, the first two waves of hematopoietic progenitors are generated in the YS and are called respectively primitive wave and “transient definitive” wave **(Figure 2)**. These two waves share as a common feature the ability to produce cells from the erythro-myeloid lineage, but they differ by several features (for more details, see below). The third wave is the definitive wave, which produce multipotent hematopoietic progenitors with long term reconstitution (LTR) activity in the aorta region, called the paraaortic splanchnopleura (P-Sp) at embryonic day (E) 9, then AGM at E10. During development, progenitors from three waves of hematopoietic cells sequentially migrate to and colonize the FL, then some of them colonize the thymus, the spleen and finally the BM **(Figure 3)**. The first two waves generated in the YS are also called HSC independent hematopoietic waves (Palis, 2016), since they initiate hematopoiesis prior to the generation of HSCs.

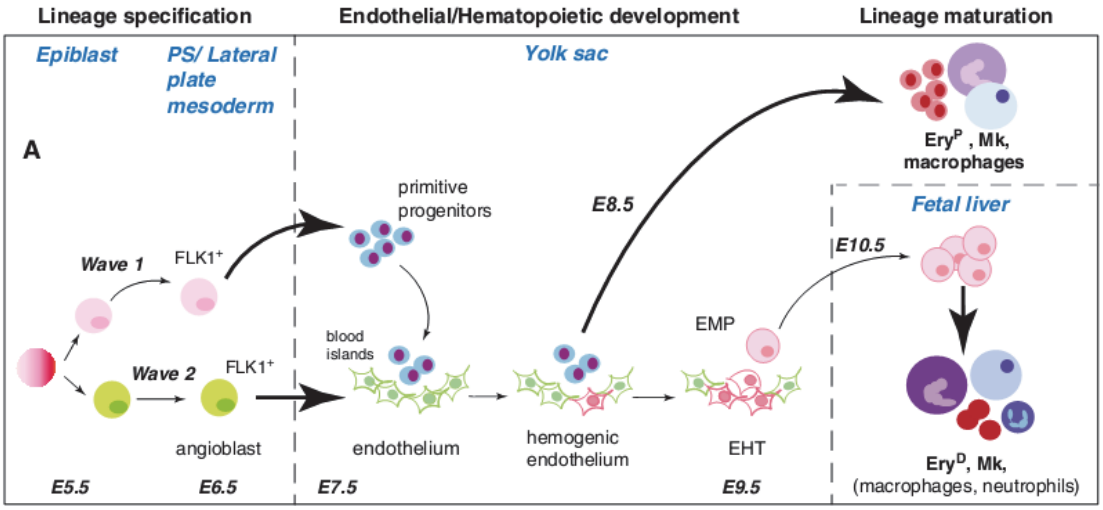

Figure 2: Two waves of specification, development, and maturation stages of hematopoietic waves in YS. From (Porcher et al., 2017).

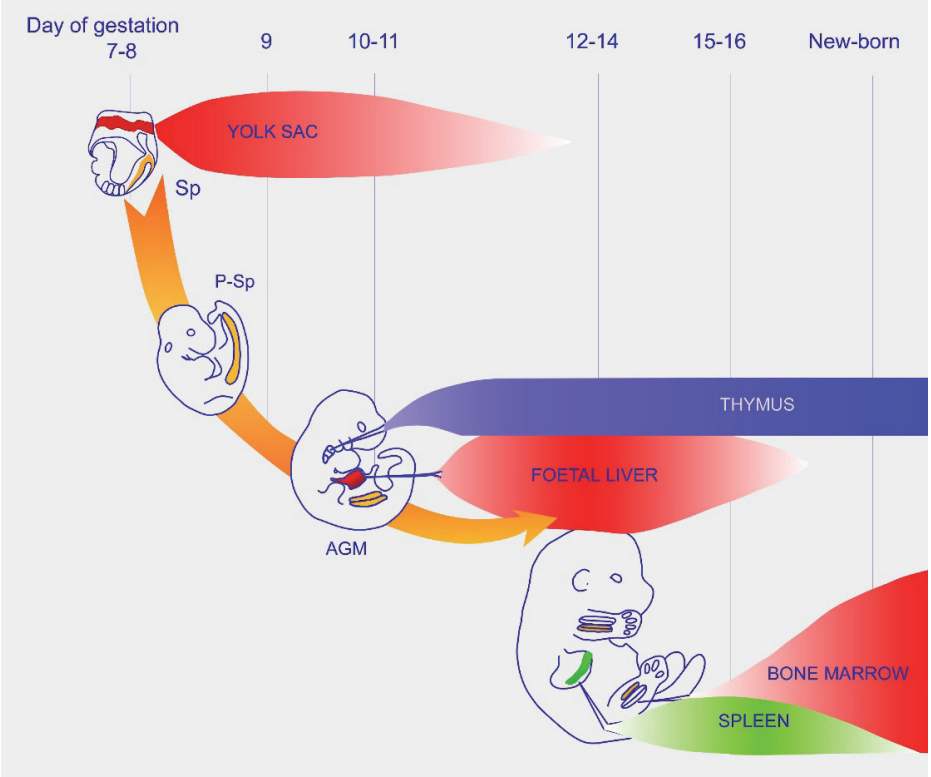

Figure 3: Schematic illustration of the successive hematopoietic sites during mouse ontogeny.
An illustration of a mouse shows the hematopoietic sites and organs during embryonic development (two independent hematopoietic sites: yolk sac and P-Sp/AGM; intermediate site: fetal liver; hematopoietic organs: first the thymus, then the spleen and, finally, the bone marrow; here, the placenta has not been considered to be a hematopoietic organ,). P-Sp/AGM: Paraaortic Splanchnopleura/Aorta-Gonad-Mesonephros region.

1.2.2 The primitive wave

The primitive wave initiates in the YS blood islands from E7 before the establishment of blood circulation (McGrath et al., 2003) and produces precursors with either erythroid, macrophage (MΦ) or megakaryocytic potential (Palis et al., 2001; Palis et al., 1999). After circulation between the YS and embryo proper is connected at the E8.25 stage (Ji et al., 2003; McGrath et al., 2003), these precursors and their progenies enter the blood stream and soon mix with the progenitors derived from the transient definitive, then the definitive waves and their mature progenies (Kingsley et al., 2004). Contrary to progenitors from the transient definitive and definitive waves, which give rise to mature erythrocyte, MΦ or megakaryocytes trough bi-potential intermediate progenitors (EMk and GM), in the primitive wave erythrocyte, MΦ or megakaryocytes are produced by monopotent progenitors (Tober et al., 2007). The primitive erythrocyte progenitors (EryP-CFCs) will produce large, nucleated, embryonic βH1-globin-expressing erythroid cells, which differ from definitive erythrocytes from the 2nd wave and 3rd waves, which are small, enucleate and express only adult globins. Further studies indicate that primitive erythropoiesis, megakaryopoiesis and MΦ develop independently of cMyb (Gomez Perdiguero and Geissmann, 2013; Schulz et al., 2012; Tober et al., 2008). Though primitive and definitive erythropoiesis have been well characterized, little is known about the differences between primitive and definitive megakaryopoiesis, as well as primitive and definitive MΦ regarding on their development and specific functions. Actually, primitive MΦ progenitors and 2nd wave EMP share some common feature as their immune-phenotype evolution during differentiation to mature MΦ (Bertrand et al., 2005b), so that they are sometimes referred to as early and late EMP (Hoeffel and Ginhoux, 2015, 2018). Information regarding MΦ development in the embryo will be further developed in chapter 1.3.

1.2.3 The transient-definitive wave: EMP and HSC-independent B- and T-lymphoid potential

The 2nd wave of hematopoiesis in the YS gives rise to erythro-myeloid progenitors (EMPs) starting from E8.0 (Palis, 2016), concomitantly with the establishment of blood circulation (McGrath et al., 2003). This wave is more complex than the primitive one, as EMP has a multilineage potential and produces mature blood cells in a differentiation pathway that is similar to the adult. Still, progenitors from this wave lack a long-term reconstitution potential and have been thus termed the ‘‘transient definitive’’ wave. This wave is thus distinct from the

primitive wave, which is also transient but lacks multipotent progenitors and from the third wave, which shows long-term maintenance capacity (McGrath et al., 2015a). Progenitors from the 2nd wave give rise to definitive erythrocytes, MΦ, megakaryocytes, which will mature and differentiate mainly in the FL, after its colonization. Recent research has suggested that the 2nd wave of hematopoiesis could also give rise to rare progenitors which will later give rise to B1a cells (Yoshimoto et al., 2011) and T cells (Boiers et al., 2013), but these progenitors are distinct from EMPs and develop before the beginning of HSC generation, making this wave of hematopoiesis more complex. McGrath *et al.* have suggested that EMPs could be distinguished by their phenotype from primitive progenitors: they express higher levels of CD41 and cKit at E8.5, whereas primitive erythrocytes progenitors display a $CD41^{low}$ $cKit^{low}$ phenotype. At E9.5, the EMPs population displays a $c\text{-}Kit^{+}CD41^{+}CD16/32^{+}$ phenotype, differing from maturing primitive cells such as $c\text{-}Kit^{-}CD16/32^{+}CD45^{hi}$ primitive MΦ and $c\text{-}Kit^{-}CD41^{hi}Gp1b\beta^{+}$ primitive megakaryocytes (McGrath et al., 2015a). However, the differences between primitive MΦ progenitors and EMPs still remain unclear.

1.2.4 The definitive wave: Development of hematopoietic stem cell

The third wave of hematopoiesis initiates in the intra-embryonic compartment, in a site that contains the developing aorta, gonads, and mesonephros. This site is called first Paraaortic Splanchnopleura (P-Sp) from E9 and it further develops into the AGM after E10. Bona fide HSC, characterized by their ability to perform long term mutilineage reconstitution (LTR) of irradiated adult recipient are generated in this P-Sp/ AGM region. Once generated, these cells migrate to FL where their number dramatically expand. Finally, they migrate to the bone marrow, where they will be responsible for the adult hematopoiesis (Ciau-Uitz et al., 2014). *In vivo* LTR experiments confirmed that only progenitors from the 3rd wave of intra-embryonic can provide HSC that confers long term reconstitution potential (Cumano et al., 1996; Cumano et al., 2001; Ganuza et al., 2018). The intra-embryonic HSCs generated in the AGM region (E10: 30-35 somite pairs (S)), are characterized by a high expression level of c-Kit, a low level of CD41, and a low to negative expression of CD45. They also express several markers, which expressions are common with endothelial cells, such as CD31, CD34 and AA4.1 (Bertrand et al., 2005a).

At this early stage (E10), HSC do not yet express MHC-I molecules and thus cannot engraft normal adult recipient mice. However, they can successfully perform multilineage LTR when transferred into immune-deficient $Rag2^{-/-}\gamma c^{-/-}$ mice that lack natural killer cell, as well as B and T

lymphoid cells (Bertrand et al., 2005a) or into neonatal recipient mice (Arora et al., 2014). Soon after E10.5 (35S) in the AGM and after they migrate to FL, HSC acquire a $CD45^+$ and $MHC\text{-}1^+$ phenotype (Kieusseian et al., 2012) and the ability to perform LTR in normal adult recipient (Arora et al., 2014).

As blood circulation between the YS and the embryo is established just after the formation of the first primitive wave (McGrath et al., 2003), from then on, progenitors from all three waves are mixed in the blood stream and can be found within the YS, the AGM, the FL and other tissue such as the placenta (McKinney-Freeman et al., 2009), making it difficult to delineate the contribution of each wave to hematopoiesis.

1.2.5 Cross talk between waves of hematopoiesis

Overall, the ontogeny of the hematopoietic system is a precise and complex process, in which each wave gives rise to progenitors with different differentiation and maintenance potentials **(Figure 4)**. While HSCs are indispensable for lifelong support of blood cells production up to postnatal life, already functional blood cells are also required for the development of early mammalian embryos prior to the emergence of HSCs (Palis, 2016).

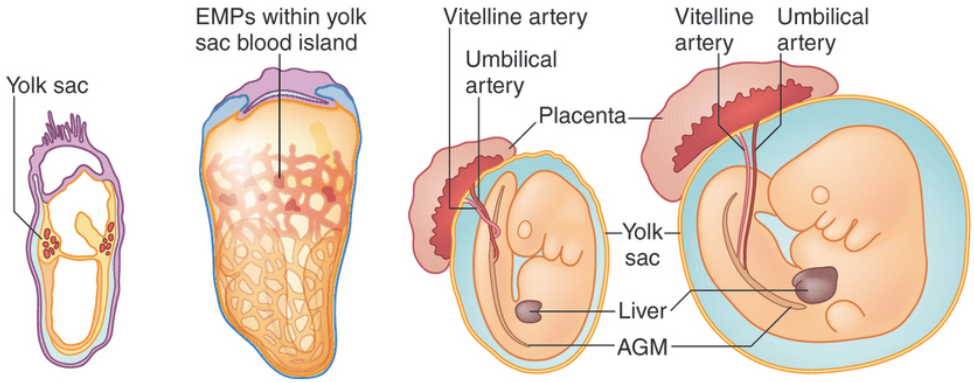

	Embryonic stage			
	E7	**E8.25**	**E9**	**E10.5**
Wave 1	Primitive erythroid progenitors macrophages megakaryocytes	Primitive erythroid progenitors macrophages megakaryocytes	Primitive macrophages	Primitive macrophages
Wave 2		EMPs	EMPs B lymphoid cells T lymphoid cells	EMPs (yolk sac) B lymphoid cells (AGM, yolk sac) T lymphoid cells (AGM, yolk sac)
Wave 3				Hematopoietic stem cells (AGM)

Figure 4: Hematopoietic sites and different output of each hematopoietic wave during ontogeny.
The first wave originates in the YS and produces primitive erythrocyte, MΦ and megakaryocytes. The second wave produces erythroid-myeloid (EMP) and lymphoid-biased progenitors that can reconstitute lethally irradiated recipients after experimental transplantation, but spontaneously disappear before adulthood in their native environment. The third wave produces conventional fetal HSCs that will develop into quiescent adult HSCs that sustain post-natal hematopoiesis. From(Yoder, 2014).

Embryos deprived of functional Tal1 die in utero as early as E9.5 (Robb et al., 1995) due to the complete absence of primitive erythropoiesis (Fujiwara et al., 1996), suggesting a pivotal role of the primitive wave of hematopoiesis. Embryos which lack functional EMPs from the 2nd wave (Frame et al., 2013), such as cMyb knockout embryos (Mucenski et al., 1991), will die around E15.5, also pointing out the importance of 2nd wave for hematopoiesis. Actually, besides providing the erythroid and myeloid cells that support embryogenesis, progenitors from these two waves will further provide the pro-inflammatory environment (that will be further discussed in chapter 1.4.2) required for HSC generation in the third wave (Palis, 2016). Collectively, all these research show that progenitors from these three waves, which show a spatial-temporal overlap in early embryo, work together closely to establish the proper hematopoiesis system.

1.3 Development of macrophage progenitors in the YS

1.3.1 Tissue resident MΦ

MΦ, one of the multifaceted cells of the hematopoietic system, can be found in all tissues **(Figure 5)** where they form the tissue resident MΦ population. They perform roles ranging from the regulation of development, the maintenance of homeostasis to the immune surveillance of pathogens (Wynn et al., 2013). For a long time, adult MΦ were considered as continuously replenished by bone marrow HSCs through monocyte intermediates. However, this view was overturned by several works which evidenced that most adult tissue resident MΦ are generated during embryonic development and that they can self-renew locally without an input from HSC derived monocytes from the bone marrow (Sieweke and Allen, 2013).

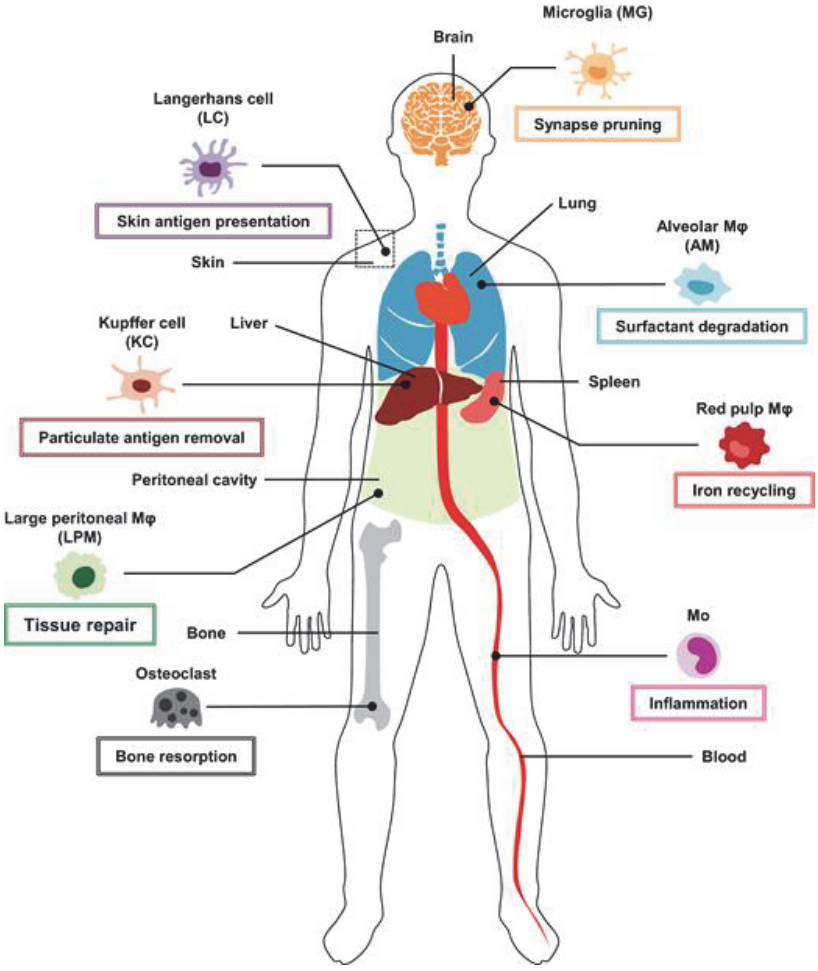

Figure 5: Localization and functions of resident MΦ subpopulations.

Resident MΦ are distributed in various tissues such as the CNS, skin, lung, spleen, liver, bone, blood and serosal cavities. From (Kurotaki et al., 2017)

About 4 decades ago, Van Furth and colleagues proposed the ‘‘mononuclear phagocyte system’’ (MPS) concept which group together peripheral blood monocytes, tissue resident MΦ and their precursors in the BM (van Furth et al., 1972) and it was firmly believed that tissue resident MΦ were supplied by progenitors from the BM. This view was challenged in the early 2000s with the experiments on Langerhans cells (epidermal MΦ) showing that these cells are resistant to high doses irradiation and that the repopulation originates from host remaining Langerhans cells, whereas monocytes were all repopulated from donor progenitors after congenic BM transplantation (Merad et al., 2002). A similar phenomenon was also observed for brain microglia (Ajami et al., 2007). With the advance of fate mapping technology, several lineage tracing experiments proved that most of tissue resident MΦ, ranging from brain microglia and liver Kupffer cells to epidermal Langerhans cells, arise from embryonic progenitors and maintain themselves through self-renewal (Ginhoux and Guilliams, 2016). The current knowledge on

different origin of tissue resident MΦ is summarized in **Figure 6**.

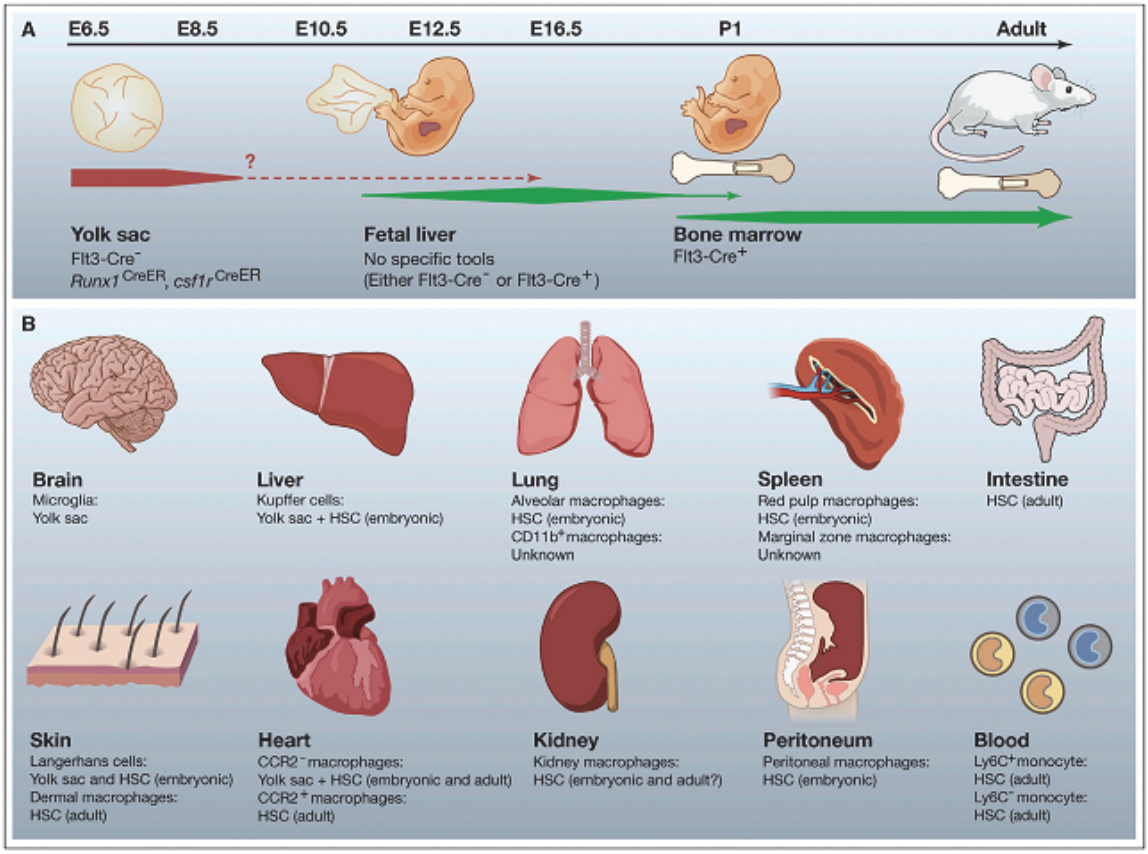

Figure 6: Origin of tissue resident MΦ.

(A) Different fate mapping strategies used to identify the origin of tissue resident MΦ: Csf1rCreER and Runx1 for YS derived MΦ and Flt3-cre for either FL-HSC or bone marrow HSC derived MΦ. (B) The origin of several different tissue resident MΦ: microglia are soley derived from YS; liver Kupffer cells arise from YS derived progenitors and embryonic HSC, etc. From (Epelman et al., 2014b).

1.3.2 Fate-mapping analysis of MΦ ontogeny

1.3.2.1 Fate mapping strategies

Defining the precise origin and developmental pathway of tissue-resident MΦ should help refine our understanding of the role of these cells in various diseases and enable to design novel MΦ-targeted therapies. Lineage-tracing methods provide the possibility to trace embryonic MΦ differentiation into adulthood. The most frequently used tool for lineage-tracing is the cre-loxP–mediated recombination system which was first discovered and named by Sternberg and Hamilton in 1981 using P1 bacteriophage system (Sternberg and Hamilton, 1981). The cre recombinase, once expressed, irreversibly removes the loxP-flanked DNA region, leaving a permanent modification of the DNA sequence. Since then, it was widely used especially in mammalian studied, because it allows researchers to interrogate the function of genes in

specific cell types, and it can also be used as a labeling system (McLellan et al., 2017). The conditional gene expression is designed by flanking a stop sequences by loxP between the promoter and a gene coding sequence for reporter markers (fluorescent markers for example), and the Rosa26 locus is most frequently used as a reporter gene driver due to its ubiquitous and strong expression pattern (Zambrowicz et al., 1997). Furthermore, the temporal control of Cre activity is designed to precisely target genes at specific development times. One of the most frequent strategy for timed gene targeting uses the fusion of ligand-binding domains of steroid hormone receptors, such as estrogen receptor (ER) or modified ER (Mer): without the ligand for these receptors, the cre activity is blocked by the heat shock protein Hsp90, which forms heterodimers with cre protein in the cytoplasm and prevents it for accessing the DNA. In the presence of the ligand such as tamoxifen (TAM), the modified cre protein is released from Hsp90 heterodimer, translocates into the nucleus and exerts its recombining function. Recently, several fate-mapping mouse lines have been used to investigate the ontogeny of MΦ.

1.3.2.2 Various inducible models used to analyze MΦ ontogeny

Ginhoux *et al.* made use of the inducible runx1-MER-Cre-MER labeling system at around E7.0 to label early YS MΦ progenitors prior to the development of HSC. He demonstrated that microglia derives from MΦ progenitors originating in the YS, that was considered as primitive (Ginhoux et al., 2010).

CSF-1R is the receptor for colony stimulating factor-1 (CSF-1) or macrophage colony-stimulating factor (M-CSF), which is expressed by E8.5 YS MΦ. Schulz *et al.* making used the inducible Csf1r-Mer-iCre-Mer mouse line to lineage trace MΦ development at E8.5. They found that YS MΦ seed the different embryonic tissues and contribute later to adult resident MΦ in several tissues, such as liver Kupffer cells, epidermal Langerhans cells and brain microglia (Schulz et al., 2012). One thing that need to be pointed out is that these tissue resident MΦ developed normally in the absence of cMyb, confirming that these MΦ are derived from primitive YS hematopoiesis since cMyb is required for transient definitive hematopoiesis and HSC generation but not primitive YS hematopoiesis (Mucenski et al., 1991).

The tyrosine kinase receptor cKit (CD117) is expressed by all hematopoietic progenitors of early

YS and FL stages to adult progenitors in the BM. Sheng *et al.* used a new cKit-MercreMer mouse strain to trace the origin of adult MΦ. By targeting cKit-expressing progenitors at different developmental time points, they conclude that all microglia derives from YS progenitors, since lineage tracing after E11.5 never labeled microglia (Sheng et al., 2015).

Tie2 is expressed in endothelial cells, YS progenitors and HSCs (Cumano and Godin, 2007). Thus, by injecting TAM into Tie2MeriCreMer at different development time points could help to understanding the origin of different hematopoietic progenitors during development. Gomez *et al.* demonstrated that an early injection of TAM (E6.5) could target hematopoietic progenitors from all waves during embryo development, whereas induction performed at later stages (from E10.5) only highly targets HSCs (Gomez Perdiguero et al., 2015). By comparing the targeting efficiency at different induction time points, they evidenced that the vast majority of adult tissue-resident MΦ in the liver (Kupffer cells), lung (alveolar MΦ), epidermis (Langerhans cells) and brain (microglia) originates from YS-derived progenitors.

During lineage commitment, adult HSCs transiently express Flt3 (Boyer et al., 2011), which provides a good model to genetically label adult HSC derived cells (Flt3-Cre). For the MΦ lineage, blood monocytes derived from Flt3+ HSC do not replace Flt3 negative tissue MΦ populations under normal situation, even over long periods of time (Epelman et al., 2014b). But we have to be cautious when we try to interpret the ontogeny of Flt3-derived MΦ cells. Though, Flt3-Cre could help trace the differentiation of adult HSCs, it cannot clarify the contribution of the first 2 waves of hematopoiesis to tissue resident MΦ, because MΦ progenitors from both primitive and transient definitive waves do not express Flt3. In addition, during fetal liver hematopoiesis, Flt3 has a very limited lineage tracing efficiency (Epelman et al., 2014a; Hoeffel et al., 2015). So, due to these limitations, Flt3-cre tracing is reliable only in adult stage.

1.3.2.3 Ontogeny of tissue resident MΦ: contribution and limitation of fate mapping studies

All these fate-mapping studies provided a lot information on the ontogeny of different tissue resident MΦ. For example, the consensus now is that mouse brain microglia are exclusively derived from YS progenitors (Ginhoux et al., 2010; Gomez Perdiguero et al., 2015). Still, they have few inevitable defects regarding the lineage tracing efficiency and accuracy, because

factors such as Runx1, Tie2 and cKit are not specific markers for any waves of progenitors and they are expressed by all progenitors during development. Moreover, contrary to previous claims, recent research by Senserrich *et al.* on inducible cre-loxP system showed that a significant Cre activity persists in mouse blood cells for 72 h after 4-OH-TAM injection (Senserrich et al., 2018). Such extended recombination activity *in vivo* is a potential source of misinterpretation, particularly in analysis of dynamic developmental processes during early stages of embryogenesis.

1.3.3 Contribution of YS hematopoiesis to microglia population

As mentioned before, both waves of hematopoietic progenitors in the YS have the capability to give rise to MΦ within a short time window and, up to now, no immune-phenotypic markers can distinguish the two MΦ progenitors generated from the respective progenitors (Bertrand et al., 2005b). Both waves of progenitors show a $CD45^{-}cKit^{+}$ phenotype and mature into MΦ in an A1 to A3 phenotype progression **(Figure 7)** as indicated by their increased expression of MΦ markers, such as CX3CR1 and F4⁄80.

Even though fate-mapping studies using different markers confirmed the YS origin of microglia (Kierdorf et al., 2013; Sheng et al., 2015), the contribution of primitive and transient definitive YS wave of MΦ progenitors to microglia remains unclear. To date, 3 models of YS hematopoiesis contribution to microglia have been proposed **(Figure 8)**. The first model corresponds to the results from (Gomez Perdiguero et al., 2015). Combining inducible Tie2cre and inducible Csf1r fate-mapping mouse models, they proposed that YS EMP are the common source of the vast majority of adult tissue-resident MΦ, including brain microglia. The second model proposed by (Hoeffel et al., 2015), claims that most tissue resident MΦ including those from spleen, gut, kidney, lung and skin are derived from late cMyb+ YS EMPs which seed the fetal liver and go through a fetal monocytes state, while brain microglia are derived from so-called “early YS EMPs” without monocytic intermediates. These “early YS EMPs” from (Hoeffel et al., 2015) most probably correspond to the YS primitive progenitors, as they share a common phenotype with YS EMP progenitors, but do not differentiate into MΦ through monocytic intermediates (Bertrand et al., 2005b).

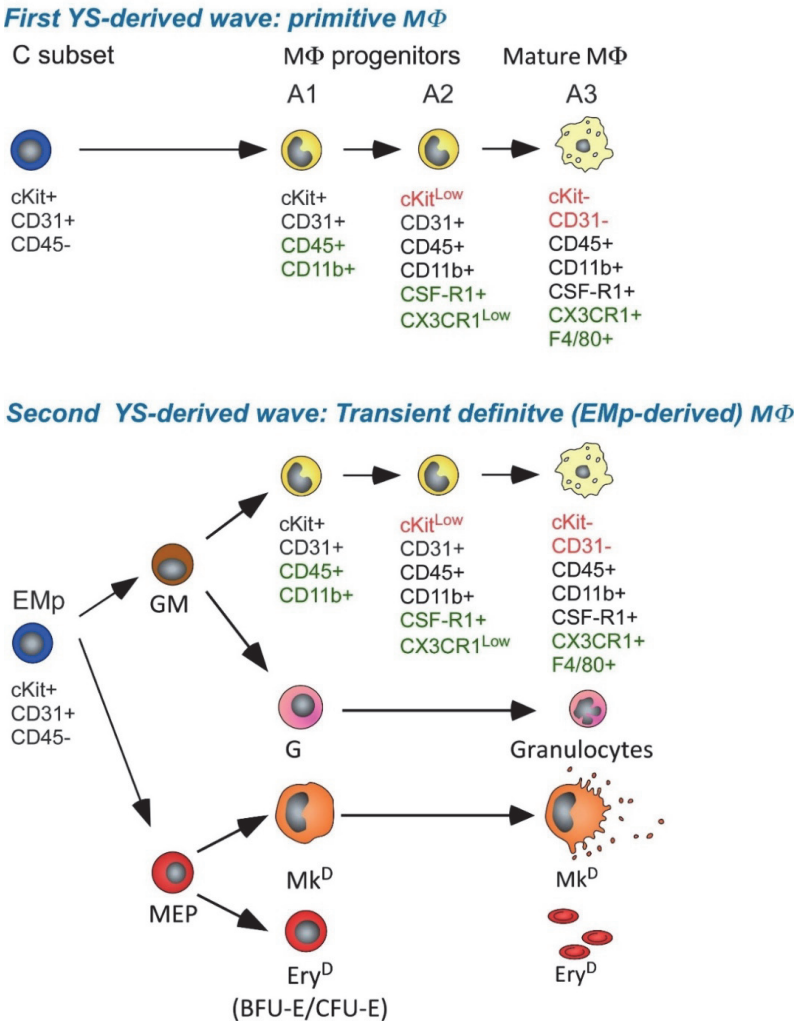

Figure 7: Two distinct MΦ waves generated from YS progenitors.
Ery indicates erythrocytes; Gr, granulocytes. Two waves of MΦ progenitors are generated in a narrow spatial and time overlap pattern and by now, no phenotypic markers can distinguish them. From (Bertrand et al., 2005b).

The last model corresponds to the observation obtained by (Sheng et al., 2015) using the inducible cKit-cre mouse model to trace the progeny of cKit progenitors at different time points. Induction at E7.5 to E9.5 led to the labeling of all brain microglia and partially of epidermal Langerhans cells. On the contrary, targeting at E8.5 efficiently labeled other tissue resident MΦ. Even if there is some disagreement on the origin of several tissue resident MΦ, all three models agree on one fact: brain microglia are only derived from YS progenitors. However, the precise contribution of primitive vs. EMP-derived MΦ progenitors is still under debate. Nevertheless, in all the fate-mapping experiments mentioned above, only a subset of microglia was labeled in adult mice, leaving open the possibility that they are other sources of microglia progenitors. Indeed, two researches on zebrafish confirmed that two distinct microglia progenitors exist in

zebrafish (Ferrero et al., 2018; Xu et al., 2015). In zebrafish, the spatial-temporal and lineage difference of the three waves of hematopoiesis is easier to discriminate than that in mammals (Bertrand et al., 2007), the researchers could reach the conclusion that primitive MΦ progenitors give rise to embryonic microglia and also that the definitive wave generated the adult microglia (Ferrero et al., 2018; Xu et al., 2015). More recently, the discovery of two microglia subpopulations (canonical, non-Hoxb8 lineage-labeled microglia and Hoxb8 lineage-labeled microglia) added new fuel to the dispute on microglia ontogeny (De et al., 2018). Indeed, it is difficult so far to separate progenitors from the three hematopoietic waves using cell surface markers, due to their overlapping generation stages and similar immune-phenotype (Bertrand et al., 2005a; Bertrand et al., 2005b; Inlay et al., 2014.; Lee et al., 2016; McGrath et al., 2015a; McGrath et al., 2015b).

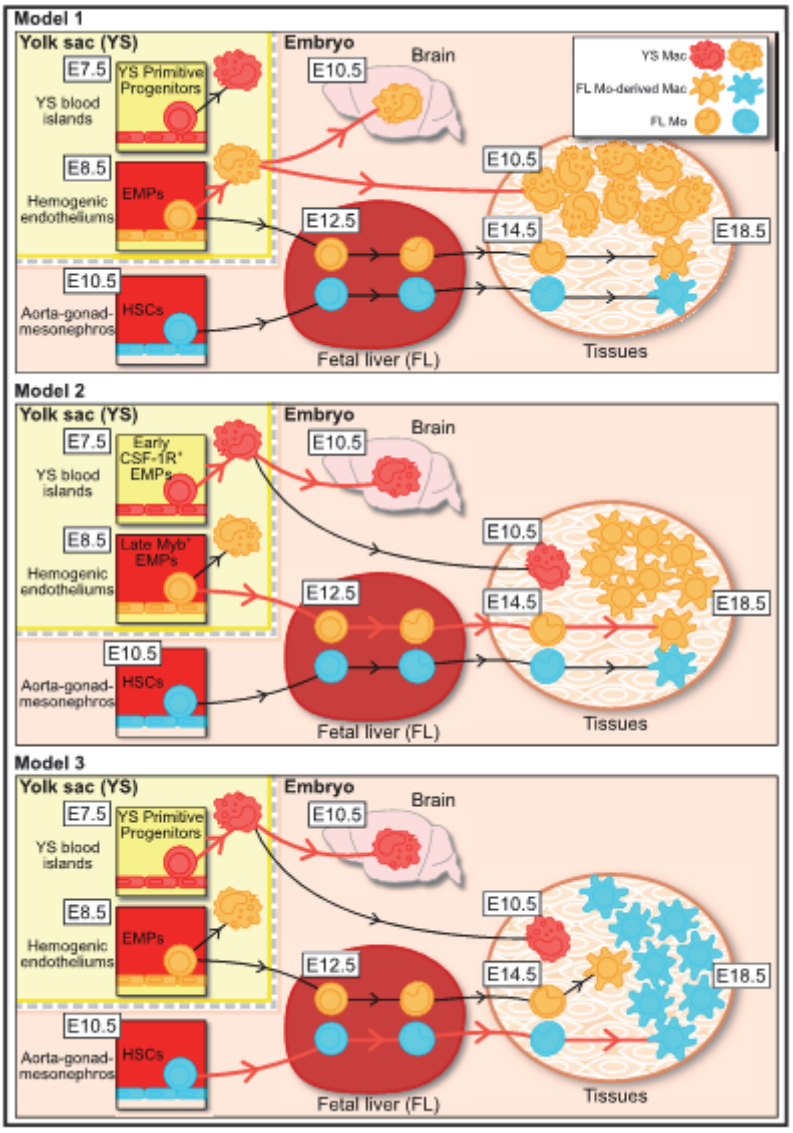

Figure 8. Three different models of fetal MΦ ontogeny.
The first model corresponds to the work of Gomez Perdiguero et al. (2015), the second to the work of Hoeffel et al. (2015), and the last to Sheng et al. (2015). Red arrow indicates the proposed major path of ontogeny and differentiation in each model. Cell colors are matched to their proposed origins. For example, whereas model 1 considers the contribution of FL monocytes unlikely, models 2 and 3 propose that these cells represent the main precursors of fetal MΦ populations, with the exception of microglia, which arise predominantly from cMyb-independent YS MΦ **From (Ginhoux and Guilliams, 2016).**

These discordant results on microglia ontogeny from the currently available inducible fate-mapping mouse models reveals the difficulty of performing in utero labeling of specific hematopoietic populations that all arise within a very narrow temporal window during development (Bertrand et al., 2005b; Ferrero et al., 2018). Also, we have to always keep in mind that during embryonic development, the time of mouse mating (plug time) does not always mean the exact fertilization time of the eggs. Even within the same litter, up to 20 hours difference can be observed in the development stage of individual embryos. Thus, a better understanding of molecular signature restricted to each wave of hematopoietic progenitors and the identification of new markers specific for each waves is required to fully address the microglia ontogeny process.

1.3.4 Factors that regulate the development of MΦ in the embryo

It is important to clearly understand the factors which are involved in embryonic MΦ development, because they contribute to tissue resident MΦ in the adult and more importantly, because modification/defects of early embryonic progenitors, such as microglia progenitors, have been linked to the development of neurodevelopmental and/or neuropsychiatric disorders at later stages (Chen et al., 2010; Mass et al., 2017).

CSF-1 and its receptor CSF-1R is very important for the differentiation of adult MΦ. Ginhoux *et al.* confirmed that CSF-1R is expressed in early embryonic microglia and YS MΦ. He showed that deletion of CSF-1R, but not that of CSF-1, greatly reduces the production of YS MΦ leading to the absence of microglia (Ginhoux et al., 2010). Similarly, Langerhans cells are absent from Csf1r KO mice, but present in Csf1 op/op mice. Further in-depth analysis of microglia and Langerhans cells formation confirmed that another ligand for CSF-1R, IL-34, is required for the homeostasis of microglia and Langerhans cells (Greter et al., 2012; Wang et al., 2012).
Another growth factor shown to be required for MΦ development is the transforming growth

factor-β (TGF-β). Butovsky *et al.* have demonstrated that TGF-β signaling pathway is required for adult microglia to keep their characteristic molecular signature and that microglia are absent in TGF-β1–deficient mice (Butovsky et al., 2014). Yu *et al.* showed that TGF-βR signaling is also required for the development of embryonic alveolar MΦ and for their maintenance during adult life (Yu et al., 2017).

Experiments from Schulz *et al.* have shown that cMyb is required for the development of HSC derived MΦ whereas it is dispensable for YS myelopoiesis (Schulz et al., 2012). cMyb was previously suggested dispensable for unilineage primitive wave MΦ generation but required for definitive hematopoiesis (Clarke et al., 2000), suggesting primitive wave MΦ are cMyb independent while EMP derived MΦ are cMyb dependent (Ginhoux and Guilliams, 2016).

Kierdorf *et al.* demonstrated that Pu.1 KO embryos lack microglia at E14, while IRF8 KO mice have a reduced number of microglia. Further analysis on YS A1 and A2 MΦ progenitors proved that Pu.1 is required for A1 MΦ progenitors generation and IRF8 is needed for the survival, differentiation from A1 to A2 (Kierdorf et al., 2013) and late stage MΦ maturation (Hagemeyer et al., 2016).

Benefiting from the Immunological Genome (ImmGen) Project (https://www.immgen.org/), immunologists discovered a core MΦ signature and more importantly some genes specifically expressed by tissue specific resident MΦ (Gautier et al., 2012). For example, Sall1 is very important for adult brain microglia identity (Buttgereit et al., 2016) and Id3 is important for liver Kupffer cell development (Mass et al., 2016), for more information please see **Figure 9**.

Engraftment experiments suggested that even if part of the microglia signature can be acquired by engrafted MΦ/progenitors from other tissues (van de Laar et al., 2016), the core signature of tissue resident MΦ cannot be recapitulated even after a long period of time, suggesting that both environmental and cell ontogeny intrinsic programs strictly control the function of each subsets of MΦ (Bennett et al., 2018). Moreover, transcriptomic and epigenetic landscapes of engrafted MΦ differ from host microglia and they show discrete responses to peripheral inflammation challenge, as compared to host microglia (Shemer et al., 2018). So, it is important to clarify the bone fide origin of each tissue resident MΦ (Ginhoux and Guilliams, 2016).

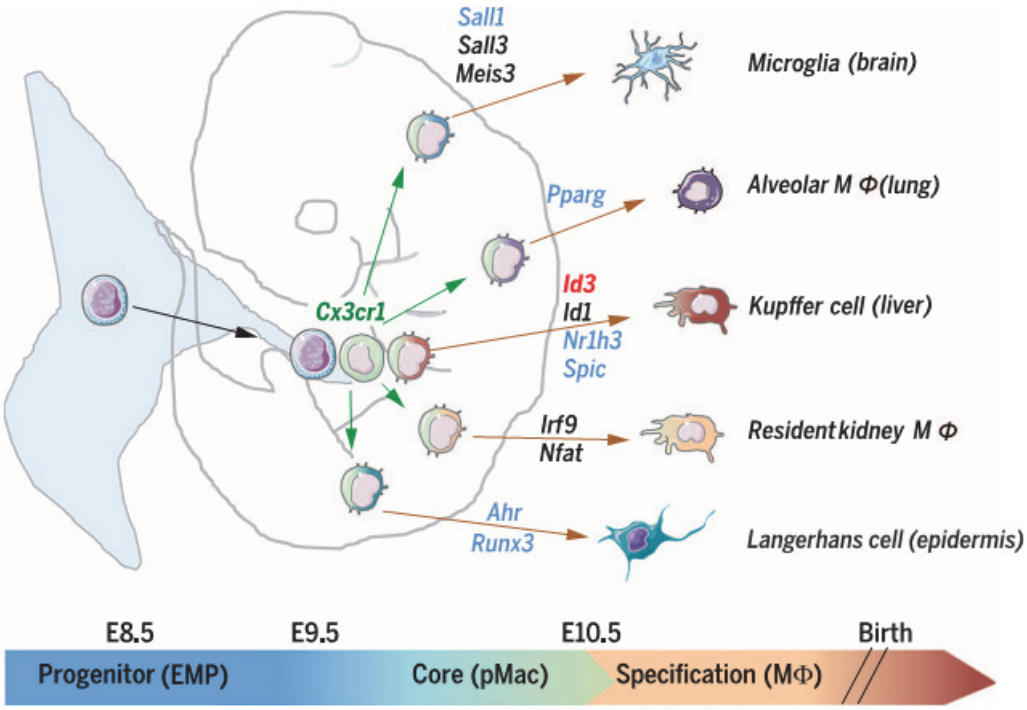

Figure 9: Tissue resident MΦ specification.
YS MΦ progenitors colonize the FL and give rise to MΦ precursors (pMacs) that acquire a core MΦ transcriptional program and will colonize the embryo and initiated the expression of tissue-specific transcriptional regulators, such as sall1 and sall3 for microglia, Id3 for Kupffer cell development. From (Mass et al., 2016).

1.4 HSC development and factors involvement

1.4.1 HSCs markers during development

HSCs are *de novo* generated within in the ventral part of the embryonic dorsal aorta (Bertrand et al., 2005a; Taoudi and Medvinsky, 2007). This generation process involves the transformation of a specific type of endothelial cells, called hemogenic endothelium, that gives rise to HSC through a process called endothelial to hematopoietic transition (EHT) (Ciau-Uitz and Patient, 2016; Clements and Traver, 2013). The AGM contains a low number of HSC, calculated repopulating units after limiting dilution reconstitution experiments, which corresponds to a low HSC number at the early stage of their development. *In vivo* experiments have proved that AGM HSC are able to sustain long term reconstitution of hematopoiesis when transplanted into adult mice with B, T cell and NK cell deficiency (Arora et al., 2014; Cumano et al., 2001; Vo et al., 2018) or more engraftment permissive wild-type neonatal recipients (Arora et al., 2014).

Indeed, HSCs are a rare population of cells during both development (Kumaravelu et al., 2002; Morrison et al., 1995) and adult stage (Benz et al., 2012), it counts less than 1 in 10, 000 cells from the tissue/organ where they reside. Purifying authentic HSC from heterogeneous cellular populations is necessary to understand the features of those extremely rare and precious cells and promote their therapeutic application. Since the first purification methods available for transplantable HSCs with the help of fluorescence-activated cell sorting system, extensive research has been applied to perfect the purification efficiency of HSC (Spangrude et al., 1988). Many studies during the past few decades have attempted to identify their specific markers, and now flow cytometry based strategies coupled with stringent LTR assay (secondary transplantation competitive, limiting dilution) have made it possible to sort HSC with high purity in mice (Benz et al., 2012; Kim et al., 2006).

HSCs from different stages of development exhibit quite different phenotypic and cell cycle features. Embryonic HSC shows very high proliferation rate, with 95 and 100% of HSCs actively cycling during embryonic development, while more than 90% of HSC remain quiescent in the adult (Pietras et al., 2011).

Researchers have shown that multipotent HSCs in E10.5 AGM express c-Kit, AA4.1, CD31, low level of CD41, and are mainly negative for CD45 (Bertrand et al., 2005a) and positive for vascular endothelial cadherin (VE-cadherin) (Rybtsov et al., 2014). Later, at E11, they will express CD45 (Zhou et al., 2016a). From E12.5, the site enriched for HSC is the FL where HSCs expand dramatically. At this time, they are enriched in the $Lin^{-}Sca\text{-}1^{+}c\text{-}Kit^{+}$ $CD201^{+}$ $VE\text{-}cadherin^{+}$ $Mac\text{-}1/CD11b^{low}$ population (McKinney-Freeman et al., 2012; Zhou et al., 2016a), where Lin^{-} indicates the negative expression of markers specific for mature cells in various lineages, such as Ter119 for erythrocytes, CD19 for B cells and CD3 for T cells. Mac-1/CD11b, which is used as a Lin- marker for myeloid cells in the adult, cannot be used at early stages of FL hematopoiesis because researchers have shown that embryonic HSCs express low level of Mac-1/CD11b (Hills et al., 2011; Kim et al., 2005; Morrison et al., 1995). From E13.5, HSCs share a common phenotype with adult bone marrow HSCs, being enriched in the $Lin^{-}CD45^{+}Sca\text{-}1^{+}$ $c\text{-}Kit^{+}CD201^{+}CD150^{+}$ $CD48^{-}$ population, called ESLAM (Benz et al., 2012; McKinney-Freeman et al., 2012). (See Table1 for a summary of canonical HSC markers at different stages of mouse development).

Despite the increasing knowledge about HSCs development, the exact fate decision of HSC generation and the precise underlying molecular mechanism that control HSC are not fully understood. Here, I will introduce some aspects regarding the development of HSC during ontogeny relating to inflammatory signals and transcription factors.

Table 1: Canonical markers for murine hematopoietic stem cells at different developmental stages.

Stage	Phenotypes	reference
E10 AGM HSC	$CD45^{-low}AA4.1^{+}CD31^{+}CD41^{low}$ c-Kit^{+} VE-$cadherin^{+}CD43^{+}$	(Batsivari et al., 2017; Bertrand et al., 2005a)
E11 AGM HSC	$CD31^{+}CD45^{+}CD41^{low}$c-$Kit^{+}CD201^{high}$ VE-$cadherin^{+}CD43^{+}$	(Batsivari et al., 2017; Bertrand et al., 2005a; Zhou et al., 2016a)
E12 FL HSC	Lin^{-}sca-1^{+}c$Kit^{+}CD11b^{low}CD201^{+}$	(Hills et al., 2011; Morrison et al., 1995; Zhou et al., 2016a)
E13-E14 FL HSC	Lin^{-}sca-1^{+}c$Kit^{+}CD45^{+}CD150^{+}CD48^{-}$ $CD201^{+}$ (ESLAM)	(Benz et al., 2012; Kim et al., 2006; McKinney-Freeman et al., 2012)
Adult BM HSC	Lin^{-}sca-1^{+}c$Kit^{+}CD45^{+}CD150^{+}CD48^{-}$ $CD201^{+}$ (ESLAM)	(Benz et al., 2012; McKinney-Freeman et al., 2012)

1.4.2 Hematopoietic transcription factors involved in HSC development

The great interest in stem cell–based therapies have emphasized the importance of understanding the molecular mechanisms by which cells choose their fate and mature/differentiate towards a particular lineage. In hematopoiesis, the specification of mesoderm cells to HSCs is precisely controlled by cell intrinsic and extrinsic factors. Among them, cell intrinsic transcription factors play a pivotal role in controlling the progression of the hematopoiesis landscape (Porcher et al., 2017). During past few decades, plenty of work has been focused on identifying transcription factors that govern HSCs specification, maintenance and differentiation and researchers have established several key regulators of the HSCs program (Wilson et al., 2009).

The basic helix-loop-helix (bHLH) transcription factor, T-cell acute lymphocytic leukemia 1 (Tal1/Scl) has been classified as a master regulator of hematopoiesis because it is absolutely required for the specification of YS progenitors and HSCs (Robb et al., 1995; Shivdasani et al.,

1995), as well as for their subsequent differentiation into erythroid and megakaryocytic lineages (Curtis et al., 2004). As the name Tal1 itself indicates, it was first discovered in chromosomal translocations into the T cell receptor δ (TCRδ) locus of T-cell Acute Lymphoblastic Leukemia (T-ALL) patients (Begley et al., 1989; Chen et al., 1990; Finger et al., 1989). Around the same time, several other transcription factors essential for hematopoiesis have also been identified in genetic translocation leading to leukemia. These include LIM domain only 2 (Lmo2) (Boehm et al., 1991), lymphoblastic leukemia derived sequence 1 (Lyl-1)(Mellentin et al., 1989) and runt-related transcription factor 1 (Runx1), also named AML1 for Acute Myeloid Leukemia 1 (Miyoshi et al., 1991).

Tal1/Scl null embryos do not survive beyond E9.5 due to the complete absence of YS primitive erythropoiesis and myelopoiesis. Homozygous *Lmo2* knockout mice have a similar phenotype and die around E10.5 due to the failure of YS primitive erythropoiesis (Warren et al., 1994). This is a more striking phenotype than the one of other important regulators of early hematopoiesis such as Runx1 or Gata2, because null embryos of *Gata2* can survive until E11.5 (Tsai et al., 1994) and *Runx1* knockout embryos die around E12.5 (Okuda et al., 1996) from the lack of HSCs development. Further *in vitro* and *in vivo* chimera experiments using *Tal1/Scl*$^{-/-}$ embryonic stem cells to bypass the early embryonic death confirmed that this transcription factor is also required for HSCs generation (Porcher et al., 1996). Similarly, *Lmo2*$^{-/-}$ mouse embryonic stem cells did not contribute to any hematopoietic lineage in adult chimeric mice, which confirmed that Lmo2 is also required for HSCs generation (Yamada et al., 1988). Indeed, in situ hybridization expression analysis demonstrated the expression of Lmo2 is associated with the intraembryonic hemogenic sites (Manaia et al., 2000). Unlike Tal1/Scl, Lmo2 does not bind to DNA promoter directly but rather works as a bridge, bringing together other transcription factors such as Tal1/Scl and Gata1/2 to form the transcriptional complexes (Wadman et al., 1997).

The Gata family of transcription factors belongs to a zinc finger family, which comprise six molecules, namely Gata1 to Gata6. Among them, Gata1 and Gata2 were mostly investigated regarding hematopoiesis. Gata1 is required for both primitive and definitive erythrocyte development. Knock out of *Gata1* leads to a differentiation block at the pro-erythroblast stage (Fujiwara et al., 1996). Beside erythrocytes, Gata1 is also important to other hematopoietic cell differentiation such as megakaryocytes (Vyas et al., 1999) and basophils (Nei et al., 2013). Gata2

is expressed by both embryo AGM HSC (Minegishi et al., 1999) and adult bone marrow HSC (Orlic et al., 1995). Knockout of *Gata2* leads to failure of definitive hematopoiesis and early embryo death, suggesting an important role in definitive hematopoiesis (Tsai et al., 1994). Further study has discovered either Gata1 or Gata2 were capable to initiate primitive hematopoietic development because they can compensate each other, as evidenced by combined knockout of Gata1 and Gata2 where erythroid cell formation is completely blocked (Fujiwara et al., 2004).

Runx1, another transcription factor frequently found in translocation leading to leukemia, is also essential for the development of definitive hematopoiesis. Embryos with homozygous mutation of *Runx1* die around E12.5 and showed comparatively normal YS primitive erythropoiesis, but a defect in HSCs formation (Okuda et al., 1996). Conditional depletion of *Runx1* at late adult stage also proved that it contributes to different hematopoietic lineages differentiation, such as lymphoid cells and megakaryocytes, but it is not required for HSCs maintenance (Ichikawa et al., 2004). Heterozygous $Runx1^{+/-}$ and $Gata2^{+/-}$ mice are both viable with only slight HSCs defects, 25% percent of $Runx1^{+/-}$:$Gata2^{+/-}$ offspring would be expected in double cross $Runx1^{+/-}$ with $Gata2^{+/-}$ mice. However, no viable $Runx1^{+/-}$:$Gata2^{+/-}$ offspring were obtained after the cross of this two lines (Wilson et al., 2010), confirming these two genes are synthetic lethal alleles and compensate each other during hematopoietic development. Also, comparative molecular genomics and chromatin study have suggested that the expression of Runx1 is regulated by Tal1/Scl and Gata2, which are recruited to the promoter region of Runx1 (Nottingham et al., 2007).

The ETS family transcription factor Pu.1 is not necessary for HSCs generation, but is important for HSCs maintenance and the commitment to other lineage, such as myeloid lineage determination (Graf and Enver, 2009). *Pu.1* knockout mice die due to hematopoietic failure around E18.5 (Kim et al., 2004). They display a reduced HSCs number in the FL and a defective differentiation into common myeloid progenitors (CMPs) and common lymphoid progenitors (CLPs). Comprehensive genome-wide binding profiles of hematopoietic transcriptional regulators in hematopoietic progenitor cells revealed a close collaboration of a heptad of transcription factors (Tal1/Scl, Lyl-1, Lmo2, Gata2, Runx1, Erg, and Fli-1) in keeping HSCs homeostasis (Wilson et al., 2010) **(Figure 10)**. Unlike other factors, which knockout leads to

embryonic death, *Lyl-1* deficient mice are viable (Capron et al., 2006), but exhibit several defects (see next chapter). However, the function of Lyl-1 during embryonic hematopoiesis remains largely unknown.

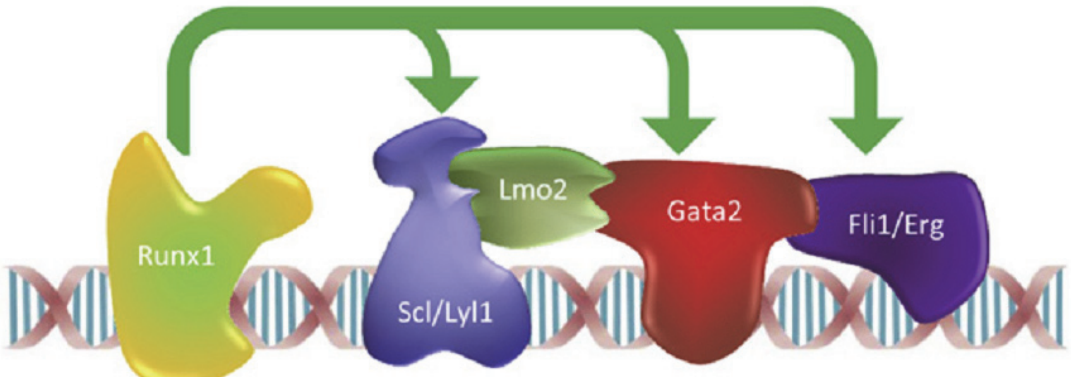

Figure 10: Schematic representation of hematopoietic transcription factors in HSCs.
From (Wilson et al., 2010)

1.4.3 Extrinsic regulation of HSC emergence

Apart from the cell intrinsic transcription factors, extrinsic signaling, plays important roles in the process of HSC generation. The studies focusing on how cell extrinsic environment influence the generation of HSC during development have provided lots of insights to decipher the extrinsic signaling in promoting HSC formation in AGM. Due to the limited scope of the thesis, I will briefly discuss several well-known microenvironment signals have been proved vital to HSC formation, such as notch, WNT (Bigas et al., 2013) and bone morphogenetic protein (BMP) (Robin and Durand, 2010) and recently identified pro-inflammation signaling required for HSC emergence during ontogeny (Clapes et al., 2016; Hayashi et al., 2019).

Notch is a highly conserved signaling pathway that plays multiple roles in cell fate decision and differentiation during development (Bigas and Espinosa, 2012). In mammals, four Notch receptors (Notch 1 to 4) and five ligands (two Jagged ligands (Jag1–2) and three Delta-like ligands (Dll1, 3, 4) have been identified. Notch2, Notch3 and Notch4 have been shown to be involved in vasculogenesis while Notch1 is implicated in hematopoiesis (Bigas et al., 2013). Mouse mutants in Notch1 related signaling such as *Notch1*, *Jag1* or *Rbpj* are embryonic lethal and exhibit severely impaired HSC generation together with the expansion of the aortic

endothelial cell population, indicating a strong regulation of the EHT process by Notch1-Jag1 signaling (Gama-Norton et al., 2015; Robert-Moreno et al., 2008). *Notch1*$^{-/-}$ embryos keep a normal primitive hematopoiesis, but die due to the severe defect in HSC generation (Kumano et al., 2003). Consistent with this observation, research on zebrafish have shown that Notch1 is only required for HSC generation and not for yolk sac EMP production, and thus distinguishes the two waves of definitive hematopoiesis (Bertrand et al., 2010). Molecular pathway analyses have shown that Notch1 activates several important hematopoietic transcription factors such as Runx1, Gata2 and Hes1/5 during the early stage of AGM HSC specification. However, Notch1 is not required for late maturation of HSCs (Souilhol et al., 2016).

Wnt signaling is another highly conserved pathway important for cell fate decision and cell polarity decision (Richter et al., 2017). The Wnt signaling pathways comprise 19 glycoproteins ligands, 10 Frizzled receptors, and 2 low density lipoprotein receptor-related protein 5 (LRP5) or LRP6 co-receptors (Angers and Moon, 2009). The ligands and receptors for Wnt signaling are expressed in the endothelium of the AGM region (Corrigan et al., 2009). Wnt signaling is very important for blood vessel development, as the loss of Wnt ligands such as β-catenin leads to a defective vascular patterning and hemorrhage, finally leading to embryonic lethality around E11.5 (Cattelino et al., 2003). The first evidence of a role for Wnt signaling in the generation of HSC was obtained from a reporter zebrafish line using a β-catenin activation response (Goessling et al., 2009), in which AGM HSC formation could be induced by prostaglandin E2 through a β-catenin-dependent manner. The specific deletion of β-catenin in mouse embryonic endothelium using Ve-Cadherin-cre led to the failure of HSC generation. The production of AGM HSC is also reduced when E10.5 embryos are treated with pharmacological compounds that inhibit the activation of β-catenin/Wnt signaling (Ruiz-Herguido et al., 2012). Another non-canonical Wnt pathway, Wnt16, is important for HSC specification, since HSCs are absent or reduced in *Wnt16* zebrafish morphants. Further analysis revealed that Wnt16 is required for the expression of Notch ligands Dlc and Dld (Clements et al., 2011).

BMP signaling is essential for mesoderm induction and its commitment to a hematopoietic fate. Among them, BMP4 became the most important factor during hematopoietic development, as it induces the formation of the ventral mesoderm, where the HSC will be generated (Maeno et al., 1996). BMP4 is expressed in a polarized way in the mesenchyme underlying the dorsal aorta

(Marshall et al., 2000; Pimanda et al., 2007a), which is thought to play a role during the development of HSC (Marshall et al., 2000; Pimanda et al., 2007a; Taoudi and Medvinsky, 2007) . BMP4 is important for the expression of several hematopoietic transcription factors such as Tal1/Scl and Runx1 (Gupta et al., 2006; Wilkinson et al., 2009). Moreover, adding BMP4 to human cord blood cells *in vitro* (Bhatia et al., 1999) or to isolated mouse AGM increased the HSC output (Durand et al., 2007), suggesting their important role in HSC generation.

Recent studies have suggested that pro-inflammatory signaling is also required for proper HSC emergence during ontogeny (Clapes et al., 2016; Hayashi et al., 2019). It was long believed that HSCs did not respond directly to inflammatory signals, but many groups have now proved that several different cytokines and tonic inflammatory signaling are required for HSCs emergence during both zebrafish and mouse development **(Figure 11)** (Luis et al., 2016). Li *et al.* have demonstrated that interferon signaling is very important for HSC production, since mice embryos lacking Interferon α (IFN-α) or IFN-γ and zebrafish morphants devoid of IFN-γ or IFN-α activity had significantly less AGM HSPCs compared to WT (Li et al., 2014). He *et al.,* using embryos deficient in Toll-like receptor 4 (TLR4) signaling, showed that TLR4–NF-κB (nuclear factor k-light-chain enhancer of activated B core) signaling is important for HSCs formation (He et al., 2015). Mechanically, TLR4 promotes HSPC specification through the activation of Notch signaling which is required for both zebrafish and mouse hematopoietic development. Espin-Palazon *et al.* found that TNF-α promotes HSC emergence through Notch and NF-κB signaling pathways (Espin-Palazon et al., 2014). One thing needs to keep in mind is that all these inflammatory ligands/cytokines are produced by local endothelial cell or HSC independent hematopoiesis from the YS, since at this stage no mature immune cell derived from HSC has formed yet. For example, Espin-Palazon *et al.* found that primitive myeloid cells (MΦ and neutrophils) express TNF-α in zebrafish embryos. They further demonstrated that primitive neutrophils are the main source of TNF-α using *Irf8* zebrafish morphants (Espin-Palazon et al., 2014). Almost the same time, Li *et al.* identified endothelial cells, MΦ and HSCs as the main source of inflammatory cytokines in murine and zebrafish embryos (Li et al., 2014). However, the function of the MΦ lineage during HSC ontogeny is not yet well defined. MΦ have been suggested to control HSC migration in zebrafish embryos (Travnickova et al., 2015), since MΦ depletion result in an increase of number of HSC remaining in the AGM. The exact source of inflammatory signal in mouse embryos is still largely unknown (Clapes et al., 2016), but as a

potential main producer of cytokines in the mouse embryos, the HSC independent MΦ lineage probably promotes HSC emergence.

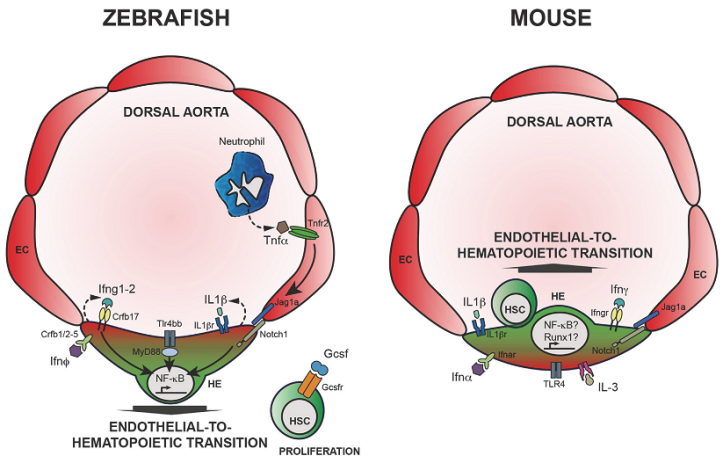

Figure 11: Inflammatory signaling is required for HSC emergence.
Left panel: In zebrafish embryos, the specification of HSC depends on TLR4 signaling, Neutrophils-derived TNFα, or the downstream products IL1β or IFN-φ that activates Notch signaling or NF-κb signaling. Right panel: In mouse embryos, IFN-α, IFN-γ, as well as Il-1β, IL-3, and TLR4 are required for proper HSC specification, possibly by engaging Notch1, Runx1 and/or NF-κB signaling, but the exact source of inflammatory signals is still unclear. **From(Clapes et al., 2016).**

1.5 The function of Lyl-1 in hematopoiesis

1.5.1 Current knowledge on Lyl-1

The transcription factor Lyl-1was first identified in 1989 in the chromosomal translocation t(7; 19) leading to T-ALL (Mellentin et al., 1989). Lyl-1 belongs to the class II bHLH transcription factor family. bHLH proteins possess two highly conserved and functionally different domains, the helix-loop-helix domain facilitates the formation of homo- or hetero-dimers and an extra basic region of about 15 amino acid residues that is adjacent to the HLH domain which will specifically binds to DNA (Kodama and Sano, 2006). Importantly, protein dimerization formation leads by the HLH domain is independent of, but necessary for DNA binding, as two basic regions are required for DNA binding activity. Class II bHLH transcription factors often activate or repress transcription by binding to target gene sequences as heterodimers with E-proteins (Fairman et al., 1993).

T-ALL accounts for about 15% and 25% of in pediatric and adult acute lymphoblastic leukemia (ALL) respectively (Chiaretti and Foa, 2009; Pui et al., 2004). Molecular studies have identified aberrant expression in T-ALL of several transcription factors essential for developmental

hematopoiesis, including Tal1/Scl, Lmo1/Lmo2 and Lyl-1 (Ferrando et al., 2002). About 10% of pediatric and 25% of adult T-ALL are associated with Lyl-1 genetic alterations (Pui et al., 2004). Lyl-1 is a close relative to Tal1/Scl, as Lyl-1 and Tal1/Scl displayed more than 80% amino acid similarity in the bHLH domain, and both of them are involved in leukemogenesis by closely interacting with the leukemia oncogene proteins Lmo1/Lmo2 (Curtis et al., 2012; Ferrando et al., 2002).

Mouse experiments confirmed that 30% of transgenic mice overexpressing Lyl-1 would develop a T- or B-cell malignant lymphomas (Zhong et al., 2007). Lukov *et al.*, by overexpression Lyl-1 through retroviral transduction in bone marrow progenitor cells, evidenced that Lyl-1 could expand hematopoietic progenitors and increase the peripheral output of T-cell through an increased proliferation and suppressed apoptosis of progenitor cells. These observations suggested that a pro-leukemic effect of Lyl-1 in early hematopoietic progenitors could cause an aberrant expansion of malignant cells (Lukov et al., 2011). Further research showed that the interaction of Lyl-1 and Lmo2 was essential for Lmo2 to initiate an early T- ALL transformation (McCormack et al., 2013). Meng, *et al.* proposed that Lyl-1 may also be a potential oncogenic factor in AML, since Lyl-1 is also highly expressed in the majority of patients with acute myeloblastic leukemia (AML) or high-risk myelodysplastic syndrome. By forcing Lyl-1 expression in myeloid cells, they found that Lyl-1 might contribute to the aberrant growth, disrupted differentiation pattern and drug resistance of AML cells (Meng et al., 2005). Recent research confirmed the role of Lyl-1 in the progression to AML and its ability to induce the stem cell-like gene expression profiles and self-renewal in thymocytes by crossing a NUP98-HOXD13 transgenic oncogenic mouse line with Lyl-1 knockout mice (Shields et al., 2019).

Beyond the field of leukemia research, Lyl-1 has been found expressed in other cell types, such as endothelial cells, B-cells, and HSCs (Curtis et al., 2012). Data acquired from Lyl-1 knockout mice has indicated few other functions of Lyl-1. By now, two *Lyl-1* Knockout mouse models have been generated **(Figure 12)**. The first *Lyl-1* knockout model was generated by inserting a β-galactosidase/Neomycin cassette into the fourth exon of *Lyl-1* (*Lyl-1*^{lacZ}), replacing the locus comprising the functional HLH domain and the entire 3' end of the Lyl-1 gene, while the 5' N-terminus of Lyl-1 is kept (Capron et al., 2006). The insertion of the *β-galactosidase* reporter gene allows the tracking of Lyl-1 expression (Giroux et al., 2007). The second knockout mouse model was designed to delete the whole coding sequence of *Lyl-1* (*Lyl1*^{Mg} strain) (Souroullas and

Goodell, 2011). These two models show little phenotype differences and display a similar HSCs defect, demonstrating that that the presence of the N-terminus of *Lyl-1* in the *Lyl-1*^{lacZ} model has a relatively minor residual function.

Pirot *et al.* demonstrated that Lyl-1 plays important roles in keeping endothelial barrier homeostasis. In syngeneic tumors implant experiments, the neovascularization process in *Lyl-1* knockout mice led to the development of vessels with enlarged lumens, reduced pericyte coverage and increased permeability (Pirot et al., 2010). Lyl-1 was also found required for the formation of a mature endothelial barrier in the lungs of adult mice, as Evans blue dye extravasation, edema and leukocyte infiltration were higher in the parenchyma of the lungs of *Lyl-1* knockout mice than in wild-type littermates (Pirot et al., 2014).

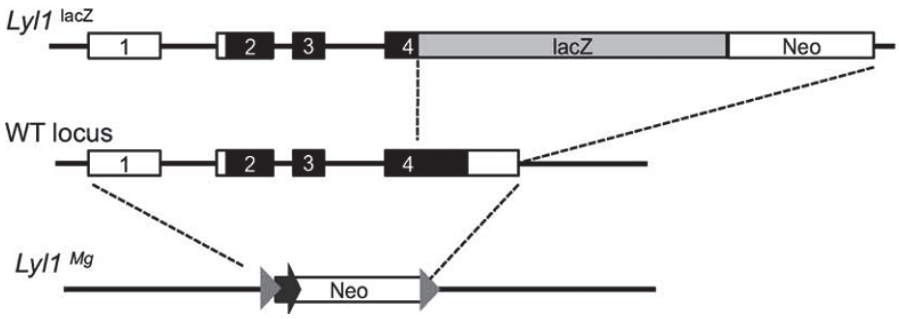

Figure 12: The two Lyl-1 knockout mouse models.
Lyl-1^{LacZ} represents the mouse model we used, in which the functional HLH domain in the C-terminus is replaced by a *lacZ/Neo* cassette. *Lyl1*^{Mg} represent another mouse model, in which all the coding regions have been deleted. From (Souroullas and Goodell, 2011).

Capron *et al.* found that Lyl-1 is expressed by E14 FL and bone marrow HSCs. HSPC from Lyl-1 knockout E14 FL and adult BM were severely impaired in their competitive reconstituting abilities. They also exhibited a defective B cell differentiation (Capron et al., 2006). Zohren *et al.* demonstrated that Lyl-1 is also required for early T lineage progenitor maintenance. Specifically, Lyl-1-deficient early T lineage and thymocyte progenitors exhibited an increased apoptosis, impaired expansion and a blocked differentiation at the $CD8^{-}CD4^{-}$ double-negative 2 (DN2) stage (Zohren et al., 2012).

1.5.2 Redundancy with Tal1/Scl

A close comparison analysis on Lyl-1 and Tal1/Scl expression patterns during mouse

development suggested they have redundant functions, as well as distinct roles during embryonic development and postnatal life (Giroux et al., 2007; Pirot et al., 2010; Visvader et al., 1991). Indeed, using in situ hybridization, the expression of both Tal1/Scl (Silver and Palis, 1997) and Lyl-1 transcripts was observed in the extra-embryonic YS-blood islands at E7.5 (Giroux et al., 2007). As stated above, mice Knockout of *Tal1/Scl* die in utero because the complete absence of primitive erythropoiesis (Robb et al., 1995) suggesting it has a critical role in YS hematopoiesis. A recent single-cell RNA-seq data of early embryos showed that primitive erythroid cells express both *Tal1/Scl* and *Lyl-1*. Moreover, the expression of Lyl-1 could substitute that of Tal1/Scl in primitive erythroid cells when its expression was significantly reduced (Chiu et al., 2018). The loss of *Tal1/Scl* leads to absence of all hematopoietic progenitors, showing that this factor is critical for the genesis of HSCs (Robb et al., 1995; Shivdasani et al., 1995). However, as I mentioned before, Tal1/Scl is not required for the maintenance of postnatal HSCs, as a conditional knockout of Tal1/Scl in adults has no impact on long-term HSC repopulation (Curtis et al., 2004; Mikkola et al., 2003).

The two *Lyl-1* knockout mouse lines exhibited reduced number of HSCs in both the fetal liver and adult bone marrow (Capron et al., 2006; Souroullas and Goodell, 2011), suggesting that *Lyl-1* is critical for normal maintenance of HSC function. *Lyl-1:Scl*-conditional double knockout mice revealed that a single allele of *Lyl-1* in *Tal1/Scl* null HSCs was sufficient to maintain hematopoiesis whereas rapid loss of HSCs was observed due to significantly increased apoptosis when both *Tal1/Scl* and *Lyl-1* were deleted (Souroullas et al., 2009), confirming *Lyl-1* is critical for the maintenance of adult HSC function. These results suggest *Lyl-1* and T*al1/Scl* share some overlap and distinct role in HSCs formation and maintenance. Despite the homologous and expression pattern similarities between *Lyl-1* and *Tal1/Scl* in hematopoiesis, it is clear that both genes have distinct role in embryonic hematopoiesis. Although *Lyl-1* is dispensable for the early mouse development, its precise role in early embryonic hematopoiesis has not been well studied. My work will present you some results I obtained on investigating the function of *Lyl-1* on early embryonic hematopoiesis, specifically on YS MΦ progenitors and HSCs.

Objectives of the thesis research

As already documented in the introduction part, each of the two hematopoietic waves that arise in the YS produce a population of MΦ progenitors, so that the YS harbours both primitive MΦ ($MΦ^{Prim}$), which derive from monopotent MΦ progenitors, and transient definitive MΦ ($MΦ^{T\text{-}Def}$), which arise from the differentiation of Erythro-myeloid progenitors (EMP). However, due to their similar phenotype and overlapping generation, their exact contribution to resident MΦ, including microglia in the brain, is still unclear. Recent results obtained by Shoutang Wang have shown that Lyl-1 marks the primitive MΦ ($MΦ^{Prim}$). I continued his research by investigating the function of Lyl-1 on MΦ progenitors during the YS stage. So, the first part of my thesis aims to address the following questions:

1. What is the molecular difference between $MΦ^{Prim}$ progenitors with EMP derived $MΦ^{T\text{-}Def}$ progenitors from the second wave? And does $MΦ^{Prim}$ progenitors has a microglia biased expression pattern?
2. What are the functions of Lyl-1 during $MΦ^{Prim}$ progenitor development?

Our team discovered that Lyl-1 is expressed by early AGM HSCs a few years ago, but the function of Lyl-1 during HSCs development remained largely unknown. The second theme of my project was to investigate the role of Lyl-1 in the development of HSCs trying to answer the following questions：

3. Is Lyl-1 involved in third wave HSCs development? If yes, what are the consequences of Lyl-1 invalidation on HSCs development?
4. What are the mechanisms underlying HSCs defect in Lyl-1 mutants?

2 Results

2.1 The role of Lyl-1 in the development of YS MΦ progenitor and microglia

Microglia are multifunctional tissue resident MΦ, which play different roles during brain development. They are required for the proper shaping of neuron synapses through a mechanism called pruning, and an abnormal microglia activity has been associated with many neurodegenerative diseases (Hammond et al., 2018). We first proposed that microglia derive from YS progenitors a long time ago (Alliot et al., 1999) and this was later confirmed by the results obtained from several fate mapping mouse models (Ginhoux et al., 2010; Gomez Perdiguero et al., 2015; Kierdorf et al., 2013). Two HSC independent waves of hematopoiesis progenitors are generated in the YS and both of them give rise to MΦ (Bertrand et al., 2005b; Palis et al., 1999). However, due to their similar phenotype and overlapping generation (Bertrand et al., 2005b), their exact contribution to microglia is still unclear. Here we name the primitive wave derived MΦ ($MΦ^{Prim}$) and transient definitive wave derived MΦ ($MΦ^{T\text{-}Def}$).

Previously, by making use of the lacZ reporter from the *Lyl-1*^{lacZ} mice, Shoutang Wang found that Lyl-1 specifically marks E9 YS $MΦ^{Prim}$ progenitors as well as embryonic microglia. Moreover, Lyl-1 inactivation leads to an increased production of $MΦ^{Prim}$ progenitors in the YS and to a transient decrease of the microglia pool at E12 and in the newborn. The arrested increase of microglia content in *Lyl-1*$^{LacZ/LacZ}$ brain at E12 resulted from a reduced proliferation. Moreover, our collaborators who analyzed the effects of Lyl-1 inactivation in the adult found that it leads to an abnormal activation of adult microglia, to a disrupted synaptic pruning and neuronal connectivity, ultimately leading to social anxiety like behavior.

My part in this project was to analyze the effect of Lyl-1 inactivation on the distribution and morphology of microglia. I found that Lyl-1 deficiency also provoked morphological changes in *Lyl-1*$^{LacZ/LacZ}$ microglia at E12, which displayed a reduced number and extent of ramifications compared to wild type microglia.

Altogether, we identify Lyl-1 as an expression marker for YS $MΦ^{Prim}$ progenitors and as an important regulator for microglia development.

Lyl-1 links primitive macrophages and microglia development to neuropsychiatric disorders

Shoutang Wang[1, †, *], Thomas Blank[2, *], Deshan Ren[1], Anna-Lila Kaushik[1, ††], Katrin Kierdorf[2], Marius Schwabenland[2], Audrey Dujardin[2, 3], Jonas-Frederic Sauer[4], Marlene Bartos[4], Gabriel Matherat[1], Yann Lécluse[5], Thomas Bienert[6], Dominik von Elverfeldt[6], William Vainchenker[1], Hana Raslova[1], Isabelle Plo[1], Marco Prinz[2, 7, #], Isabelle Godin[1, #]

[1] Gustave Roussy, INSERM U1170, Villejuif; Université Paris-Saclay, France.

[2] Institute of Neuropathology, Faculty of Medicine, University of Freiburg, Freiburg, Germany.

[3] INSERM Unité 1052, Centre de Recherche en Cancérologie de Lyon (CRCL), Lyon, France.

[4] Institute for Physiology I, Systemic and Cellular Neurophysiology, Faculty of Medicine, University of Freiburg, Freiburg, Germany.

[5] PFIC, lUMS AMMICa (US 23 INSERM / UMS 3655 CNRS; Gustave Roussy, Villejuif, France

[6] Dept. of Radiology, Medical Physics, University Medical Center Freiburg, Faculty of Medicine, University of Freiburg, Germany

[7] BIOSS Centre for Biological Signalling Studies, University of Freiburg, Freiburg, Germany.

Present addresses: [†] Department of Pathology and Immunology, Washington University School of Medicine, St. Louis, MO, 63110, USA; [††] Cabinet Plassereau, F-75009 Paris, France;

, # Equal contributions;

Correspondence and requests for materials should be addressed to Isabelle.Godin@gustaveroussy.fr (ORCID: 0000-0001-8577-8388)

Summary

The regulation of developmental hematopoiesis by most hematopoietic transcription factors has been extensively studied, except for the bHLH transcription factor Lyl-1. When analysing how Lyl-1 may impact mouse developmental hematopoiesis, we found that Lyl-1 marks YS-derived primitive macrophage ($M\Phi^{Prim}$) progenitors, as well as embryonic microglia, tissue macrophages of the central nervous system. During ontogeny, microglia, emerge from hematopoietic stem cell-independent progenitors originating from the yolk sac (YS). Neuropsychiatric diseases are often hallmarked by neuronal dysfunction and associated microglia activation. Factors impairing YS development may thus lead to neuropsychiatric disorders. We show that Lyl-1 disruption alters microglia development with far reaching consequences, since it leads to decreased cortical dendritic spine density and impaired neuronal activity, as well as impaired social interactions with increased anxiety-like behaviour.

We thus identify Lyl-1 as a critical regulator of $M\Phi^{Prim}$ and microglia development, whose disruption impacts microglia development and functionality, leading to a distinct neuropsychiatric phenotype.

Impact statement

The disruption of the transcription factor Lyl-1, which regulates macrophage and microglia development, leads to impaired brain function.

INTRODUCTION

Amongst the components of the transcription factor network that regulate the various features of hematopoietic cells, Tal-1/Scl, Lmo2, Runx1 and Gata2 stand out as the major regulators of hematopoietic progenitor development during ontogeny *(Pina and Enver, 2007; Wilson et al., 2010). Tal-1/Scl*, *Lmo2* and *Gata-2* belong to a transcriptional complex, which also includes the basic helix-loop-helix transcription factor lymphoblastic leukaemia-derived sequence 1 (*Lyl-1*). Like its paralog *Tal-1/Scl*, *Lyl-1 (Capron et al., 2006)* was initially identified in chromosomal translocations leading to paediatric T-cell acute lymphoblastic leukaemia. Contrary to Tal-1/Scl, which is mandatory for the specification of all hematopoietic progenitors in the embryo *(Curtis et al., 2012; Porcher et al., 2017)*, the function of Lyl-1 during developmental hematopoiesis remains largely unknown.

During embryonic development, hematopoietic progenitors are generated in three successive waves *(Palis, 2016)*. The two first waves occur prior to HSC generation in the yolk sac (YS). This ***HSC-independent hematopoiesis*** comprises first the ***primitive hematopoietic wave***, with the transient production of progenitors with embryonic specific features. The second YS wave, called ***transient definitive wave,*** provides for a limited duration progenitors (mostly erythro-myeloid) that display classical differentiation features. Finally, the hematopoietic stem cells (HSC) are generated in the aorta region in the third and ***definitive hematopoietic wave***. These HSC immediately migrate to the foetal liver where they mature and amplify to ultimately provide the HSC population that will maintain lifelong hematopoiesis in the adult bone marrow *(Cumano and Godin, 2007).*

While addressing the function of Lyl-1 during the earliest steps of developmental hematopoiesis, we found that Lyl-1 expression marks only a subset of macrophage (MΦ) progenitors in the early YS, suggesting that Lyl-1 expression might characterize one of the two YS haematopoietic waves. Indeed, these two waves share as a common feature, the ability to produce a erythro-myeloid progeny, so that they are sometimes referred to as early and late EMP *(Hoeffel and Ginhoux, 2018)*. However, in the earliest and primitive wave (from E7.25), mature primitive erythrocytes, megakaryocytes and MΦ ($M\Phi^{Prim}$) are produced by monopotent progenitors *(Bertrand et al., 2005b; Palis et al., 1999),* in a cMyb-independent pathway *(Mucenski et al., 1991; Schulz et al., 2012)*. In contrast, in the transient-definitive wave, the production of mature transient definitive MΦ ($M\Phi^{T\text{-}Def}$) depends on cMyb expression *(Frame et al., 2013; Hoeffel et al., 2015; Schulz et al., 2012).* $M\Phi^{T\text{-}Def}$ progenitors arise from the progressive differentiation of

erythro-myeloid progenitors (EMP) via the production of granulo-monocytic (GM) progenitors, and ultimately of granulocytes (G) and MΦ progenitors, in a differentiation pathways similar to that found in the adult *(McGrath et al., 2015a).* Progenitors from the two waves rapidly mix within the YS and systemic blood flow *(McGrath et al., 2003)* and specific features of the MΦ progenitors in each wave remain poorly defined *(McGrath et al., 2015b).* We here show that Lyl-1 expression discriminates $M\Phi^{Prim}$ from EMP-derived $M\Phi^{T-Def}$ progenitors and that inactivation of Lyl-1 HLH domain leads to an increased production of those $M\Phi^{Prim}$ progenitors.

To assess whether Lyl-1 marks and regulates other MΦ populations in the embryo, we focused on microglia, the resident MΦ population in the nervous system, as the simplest to analyse. Indeed, fate mapping studies indicate that most tissue of the developing embryo harbours resident MΦ of various origin (for a review, see *(Ginhoux and Guilliams, 2016; Hoeffel and Ginhoux, 2018)*). In this instance, microglia stands out as it appears to develops from MΦ progenitors originating from the YS *(Ginhoux et al., 2010; Gomez Perdiguero et al., 2015; Kierdorf et al., 2013; Schulz et al., 2012)*, prior to the production of HSC, thus confirming a developmental model that we had previously put forward *(Alliot et al., 1999).* While addressing this issue, we found that Lyl-1 expression marks the entire microglia population in the embryo. Furthermore, Lyl-1 appeared to regulate microglia development from its earliest stage, since Lyl-1 deficiency led to an increased production of MΦ progenitors in the early brain, as it did in the YS.

Microglial cells play pleiotropic functions in the normal and pathological brain. During development, they shape the neural network through synaptic pruning mechanism and thus impaired microglial function is thought to be involved in the development of disorders such as autism, schizophrenia or obsessive-compulsive disorders *(Paolicelli et al., 2011; Prinz and Priller, 2014; Zhan et al., 2014).* Consequently, factors impairing the development of hematopoietic cells in the YS may lead to deficient microglia development and eventually to neurodevelopmental and/or neuropsychiatric disorders.

Our investigation performed at later development of microglia stages pointed to two transient reduction of the microglia pool size in Lyl-1 mutant, first at mid-gestation and later in the new-born. Remarkably, Lyl-1 inactivation also impacted neurodevelopmental processes, as shown by a defect in synaptic pruning, reduced neuronal firing, altered functional brain connectivity, together with an aberrant behaviour, which resembles characteristics of social anxiety disorder in humans.

RESULTS

2.1.1 Lyl-1 expression marks YS MΦ progenitors in the early YS and brain

Lyl-1 expression pattern during ontogeny essentially overlaps with that of Tal-1/SCL, as both factors are similarly expressed in the developing cardiovascular and hematopoietic systems, suggesting that Lyl-1 regulates developmental hematopoiesis *(Giroux et al., 2007)*. A requirement for functional Lyl-1 during developmental processes was also suggested by a significantly decreased litter size and increased perinatal lethality in *Lyl-1$^{LacZ/LacZ}$ (Capron et al., 2006)* compared to wild type (WT) strains ***(Fig. 1a)***. We first explored Lyl-1 functions during YS hematopoiesis by characterizing the progenitors produced by WT, *Lyl-1$^{WT/LacZ}$* and *Lyl-1$^{LacZ/LacZ}$* YS in clonogenic assay. To do so, E8-YS were maintained in organ culture for 1 day (E8 OrgD1-YS): this culture system (Cumano et al., 1996; Cumano et al., 2001) allows the development of progenitors from both primitive and transient definitive waves, while avoiding the contamination by progenitors from the definitive wave that may occurs through the blood flow once YS and intra-embryonic vasculature have connected at E8.25 (4-5 somite-stage (S))*(McGrath et al., 2003).*

We observed an increased production of MΦ colonies from *Lyl-1$^{WT/LacZ}$* and *Lyl-1$^{LacZ/LacZ}$* OrgD1-YS, compared to WT. The yield of other progenitor types was unmodified, including those endowed with the potential to generate MΦ colonies, such as EMP and GM ***(Fig. 1b)***.

Using FACS-Gal assay, where the β-Galactosidase activity reporting Lyl-1 expression is detected using its fluorescent substrate FDG, we noticed that the entire YS MΦ progenitor population (cKit$^+$CD45$^+$CD11b$^+$) expressed Lyl-1 at E9, while at E9.5 as well as in E8-OrgD1-YS, two MΦ progenitor subsets discriminated by their FDG/Lyl-1 expression, were present in the YS ***(Fig. 1c, d; Fig S1)***.

Since fate mapping analyses established that resident MΦ in the developing brain arise from YS MΦ progenitors *(Gomez Perdiguero et al., 2015; Hoeffel et al., 2015; Sheng et al., 2015)*, we investigated in parallel the distribution of FDG$^+$/Lyl-1$^+$ and FDG$^-$/Lyl-1$^-$ subsets in the YS and brain of E10 WT and *Lyl-1$^{LacZ/LacZ}$* by FACS-Gal analysis. While E10-YS comprised both FDG$^+$/Lyl-1$^+$ and FDG$^-$/Lyl-1$^-$ MΦ progenitor subsets, the brain from the same embryos essentially harboured FDG$^+$/Lyl-1$^+$ MΦ progenitors (***Fig. 1d***). Similarly, mature MΦ (F4/80$^+$) in E10-YS were also sub-divided into FDG$^+$/Lyl-1$^+$ and FDG$^-$/Lyl-1$^-$ subsets, whereas in the corresponding brain, they were exclusively FDG$^+$/Lyl-1$^+$ ***(Fig. 1d)***.

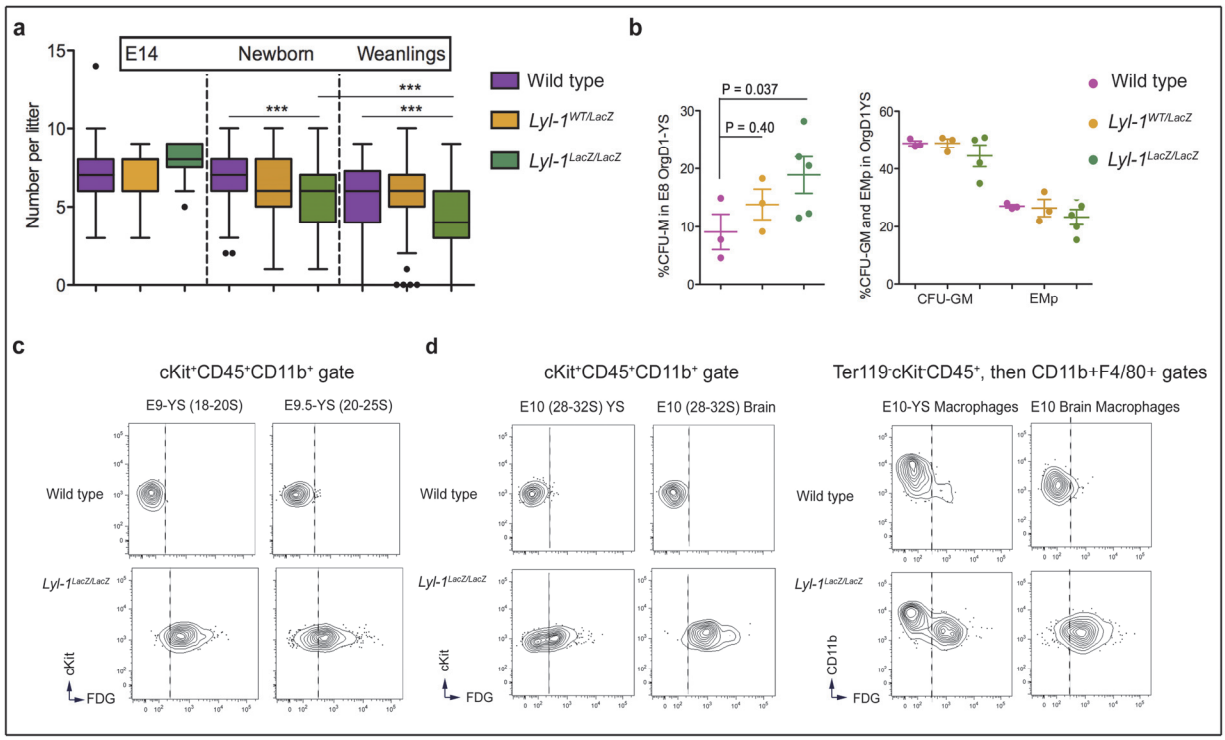

Figure 1: Lyl-1 marks MΦ progenitors from early YS and brain.

a. Lyl-1 deficiency leads to an increased perinatal lethality: The number of *Lyl-1*$^{LacZ/LacZ}$ embryo per litter was unmodified at E14 (left), but the number of living new-borns (middle) was reduced. The number of weanlings was further reduced in *Lyl-1*$^{LacZ/LacZ}$ mutants (right) with a significant increase of neonatal lethality until P15 (main occurrence between P1 and P5: data not shown). *Lyl-1*$^{LacZ/LacZ}$ mutants had a balanced sex ratio (data not shown). WT x *Lyl-1*$^{LacZ/LacZ}$ and WT x WT mice had similar numbers of E14 embryos, new-borns and weanlings. E14: n = WT: 35; *Lyl-1*$^{WT/LacZ}$: 35; *Lyl-1*$^{LacZ/LacZ}$: 29. New-borns and weanlings: n = WT: 150; *Lyl-1*$^{WT/LacZ}$: 95; *Lyl-1*$^{LacZ/LacZ}$: 284. Tuckey box plot; unpaired t-test.

b. Lyl-1 deficiency leads to an increased production of MΦ progenitors in the early YS: Left: Clonogenic potential of E8 OrgD1-YS cells: The production of MΦ progenitors (CFU-M) was increased in *Lyl-1*$^{LacZ/LacZ}$ OrgD1-YS (n=3-5, each sample contained 3 to 6 YS; plots show mean ± s.e.m.; Unpaired t-test). The size of the MΦ colonies and the cell morphology was similar for all 3 genotypes (data not shown). Right: The distribution of other progenitors, including those with myeloid potential (EMP and GM), was similar in WT, *Lyl-1*$^{WT/LacZ}$ and *Lyl-1*$^{LacZ/LacZ}$ E8 OrgD1-YS.

c. While all MΦ progenitors in E9-YS expressed FDG/Lyl-1, E9.5-YS harboured two populations discriminated by their FDG/Lyl-1 expression. Lyl-1 expression in MΦ progenitors was analysed by FACS-Gal assay where the β-Gal fluorescent substrate FDG was used as a reporter for Lyl-1 expression. The contour plots in WT samples indicate the level of non-specific background β-Gal activity/FDG labelling in WT samples.

d. E10 YS harboured both FDG$^+$/Lyl-1$^+$ and FDG$^-$/Lyl-1$^-$ MΦ progenitors. In the corresponding brain, only FDG$^+$/Lyl-1$^+$ MΦ progenitors were present (left). FDG$^+$/Lyl-1$^+$ and FDG$^-$/Lyl-1$^-$ mature MΦ coexisted in E10-YS, while in the corresponding brain all F4/80$^+$ cells (A3 subset) expressed FDG$^+$/Lyl-1$^+$ (right). Representative profiles of 3 independent samples, each consisting of 3-4 YS or brains of the same embryos *(See Fig. S1 for the gating strategy)*.

2.1.2 Lyl-1 expression discriminates MΦ^{Prim} progenitors from EMP-derived MΦ$^{T\text{-}Def}$ progenitors

As stated before, after E9.5 the YS contains MΦ^{Prim} progenitors from the first YS wave and MΦ^{T-Def} progenitors originating from the differentiation of EMPs and then GM progenitors from the transient definitive wave. Because the entire MΦ progenitor population expressed Lyl-1 at E9, while both FDG$^+$/Lyl-1$^+$ and FDG$^-$/Lyl-1$^-$ populations coexisted in the YS after E9.5, we hypothesized that Lyl-1 may mark MΦ^{Prim} progenitors which arise from the earliest wave. As MΦ^{Prim} and MΦ$^{T\text{-}Def}$ progenitors cannot be discriminated by phenotype *(Bertrand et al., 2005b)*, we investigated the three known features that discriminate the two waves: the earliest stage of appearance of primitive MΦ^{Prim} progenitors, the monopotent status of primitive progenitors *(Bertrand et al., 2005b; Palis et al., 1999)* and its independency of cMyb expression for its development *(Mucenski et al., 1991; Schulz et al., 2012).*

EMP and GM progenitors that give rise to MΦ$^{T\text{-}Def}$ progenitors in the transient definitive wave appear in the E8.25-YS, after the 3-5 Somite (S) stage *(Bertrand et al., 2005b; Palis et al., 1999)*. FACS-Gal assay performed at E8 (0-5S) ***(Fig. 2a)***, when only MΦ^{Prim} are present, demonstrated that most FDG$^+$/Lyl-1$^+$ cells (69.27% ± 0.33%) co-expressed CD11b and CD31, thus qualifying as MΦ^{Prim} progenitors. Conversely, all CD11b$^+$CD31$^+$ MΦ^{Prim} progenitors displayed FDG/Lyl-1 expression. The other MΦ population (CD45$^+$CD11b$^+$CD31-F4/80$^+$) present at this early stage corresponds to mature MΦ, which were previously shown to have a maternal origin *(Bertrand et al., 2005b)*. Moreover, when submitted to clonogenic assays, FDG$^+$/Lyl-1$^+$ cells sorted from *Lyl-1$^{WT/LacZ}$* E8-YS consistently produced MΦ colonies (72.78±9.65%; n=3), amounting 1-4 MΦ progenitors per YS, a value consistent with published data *(Bertrand et al., 2005b; Palis et al., 1999).* Additionally, both FACS-Gal ***(Fig. 2a)*** and clonogenic ***(Fig. 2b)*** assays pointed to an increased amount of MΦ progenitors in *Lyl-1$^{WT/LacZ}$* compared to WT-YS, concordant with our previous observation ***(Fig. 1b)***.

Contrary to MΦ^{Prim} that differentiate from monopotent progenitors, MΦ$^{T\text{-}Def}$ arise from EMP progenitors that also generate GM progenitors and granulocytes (McGrath et al., 2015b). We therefore characterized in clonogenic assay the differentiation potential of FDG$^+$/Lyl-1$^+$ and FDG$^-$/Lyl-1$^-$ cell fractions of cKit$^+$CD45$^+$CD11b$^+$ myeloid progenitors sorted from E10-YS that harbour both primitive and transient definitive/EMP-derived waves ***(Fig. 2C)***. All samples produced few non-myeloid contaminants, in similar non-significant amounts. Within myeloid colonies, WT E9-YS myeloid progenitors nearly exclusively produced MΦ colonies, while MΦ,

as well as GM and G colonies were generated from E10-YS myeloid progenitors. The colony output of $FDG^+/Lyl\text{-}1^+$ progenitors from E10-YS overlapped with that of E9-YS, as it was limited to the production of MΦ colonies, thus further pointing to a restriction of Lyl-1 expression to $M\Phi^{Prim}$ progenitors. In contrast, the $FDG^-/Lyl\text{-}1^-$ cell fraction gave rise to GM, G and MΦ colonies, confirming their transient definitive/EMP-derived status.

Primitive hematopoietic populations have been characterized as independent of cMyb for their development, contrary to their transient-definitive and definitive counterparts (Gomez Perdiguero and Geissmann, 2013; Hoeffel et al., 2015; McGrath et al., 2015b; Tober et al., 2008). The restriction of Lyl-1 expression to $M\Phi^{Prim}$ progenitors was also strengthened by the observation of a low level of *cMyb* expression in RT-qPCR analyses: *cMyb* expression, normalized to the mean expression value obtained for WT E10-YS, was compared to sorted $FDG^+/Lyl\text{-}1^+$ and $FDG^-/Lyl\text{-}1^-$ MΦ progenitors ($cKit^+CD45^+CD11b^+$) from *Lyl-1*$^{WT/LacZ}$ E10-YS. $FDG^-/Lyl\text{-}1^-$ MΦ progenitors displayed *cMyb* levels similar to $Sca1^+cKit^+$ progenitors from E12 foetal liver, used as positive control for definitive, *cMyb*-dependent progenitors. In contrast, $FDG^+/Lyl\text{-}1^+$ YS progenitors expressed *cMyb* levels similar to E9-YS $M\Phi^{Prim}$ progenitors, strengthening their primitive status and lineage relationship ***(Fig. 1h)***. MΦ progenitors from E10-brain also expressed *cMyb* levels similar to E9-YS $M\Phi^{Prim}$ progenitors, in frame with previous evidence pointing to a cMyb-independent development of microglia, namely the normal amount of microglia found in mice lacking the cMyb transcription factor *(Kierdorf et al., 2013; Schulz et al., 2012).*

Altogether, these results show that Lyl-1 expression discriminates $M\Phi^{Prim}$ from $M\Phi^{T\text{-}Def}$ progenitors in the early embryo.

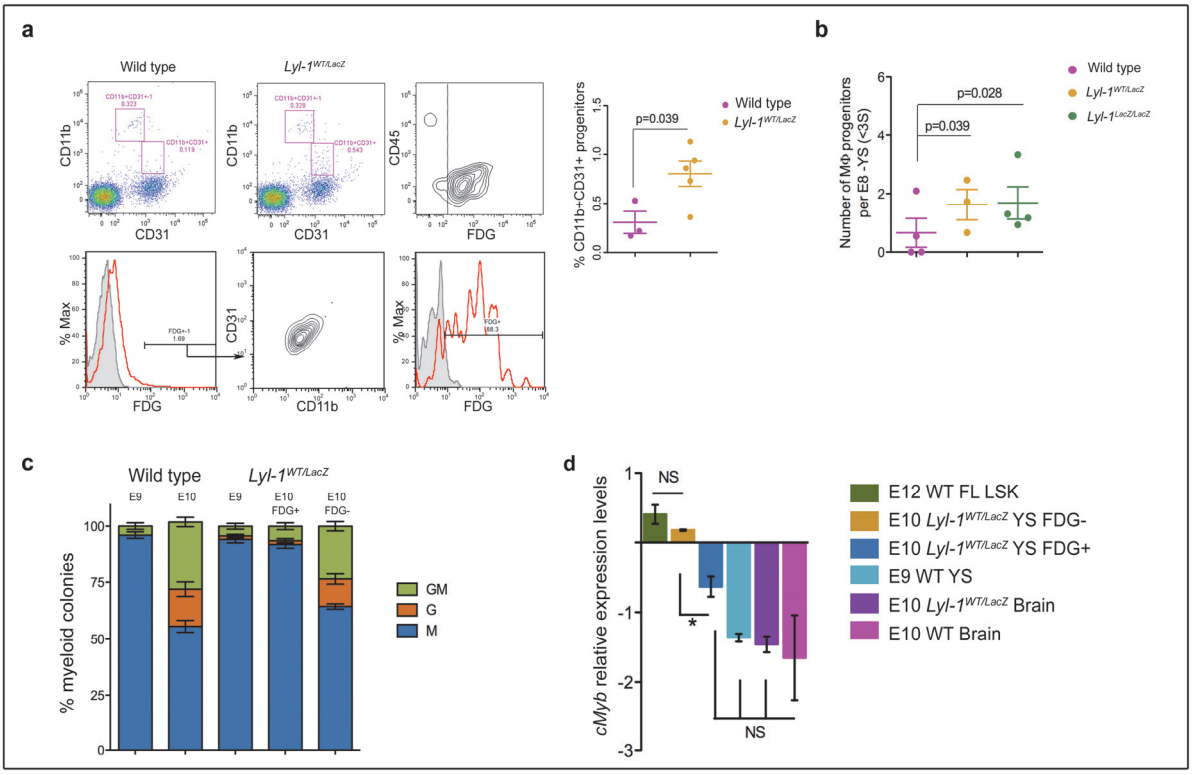

Figure 2: Lyl-1 expression discriminates MΦ^{Prim} progenitors from EMP-derived MΦ$^{T\text{-}Def}$ progenitors.

a. MΦ^{Prim} progenitors express Lyl-1. Upper panel: Flow cytometry profiles of WT (left) and *Lyl-1$^{WT/LacZ}$* (middle left) E8-YS (0-3S). CD11b$^+$CD31$^-$ MΦ (top gate) corresponded to maternal MΦ. The CD11b$^+$CD31$^+$ MΦ progenitor subset (lower gate), which displays FDG/Lyl-1 expression, was enlarged in *Lyl-1$^{WT/LacZ}$* YS (right; n=3). Lower panel: Within the FDG$^+$/Lyl-1$^+$ subset from *Lyl-1$^{WT/LacZ}$* E8-YS (left) most cells co-expressed CD31 and CD11b$^+$ (middle). Conversely, all MΦ progenitors within the CD11b$^+$CD31$^+$ gate displayed FDG/Lyl-1 expression (left). Grey histogram indicates non-specific background β-Gal activity/FDG levels in WT samples.

b. Lyl-1 regulates the production of MΦ^{Prim} progenitors. In clonogenic assays, less than one EMP and/or GM progenitor per E8-YS was detected in WT and mutant samples, confirming that the assay was performed at a time when EMP-derived- MΦ progenitors were absent. The majority of the 25-30 colonies per YS were Ery^P (60 to 80% in the 3 genotypes). The number of MΦ colonies obtained from E8-YS (0-3S) was increased in *Lyl-1$^{WT/LacZ}$* and *Lyl-1$^{LacZ/LacZ}$* compared to WT (left). Other progenitors were occasionally and randomly found in the *Lyl-1$^{WT/LacZ}$* FDG$^+$/Lyl-1$^+$ fraction including EMPs (0.81%±0.66; n=3). (n=3-5, each sample contained 5-10 YS; plots show mean ± s.e.m.; Unpaired t-test).

c. FDG/Lyl-1 positive and negative myeloid progenitors produce a distinct progeny: The type of progenitors produced by sorted cKit$^+$CD45$^+$CD11b$^+$ myeloid progenitors was determined by clonogenic assays using E9 WT and *Lyl-1$^{WT/LacZ}$* YS (<18S; n=7), and E10 WT YS (n=15) in 3 independent experiments. At E10, myeloid progenitors from *Lyl-1$^{WT/LacZ}$* YS were subdivided into FDG/Lyl-1 negative (n=15) and positive (n=12) fractions (5 independent experiments). Samples were biological replicates comprising 6-8 YS. 100 to 150 cKit$^+$CD45$^+$CD11b$^+$ cells per condition were platted in triplicate. FDG$^+$/Lyl-1$^+$ progenitors essentially produced MΦ colonies, while FDG$^-$/Lyl-1$^-$ progenitors produced also GM and G colonies, thus belonging to the transient definitive wave.

d. RT-qPCR quantification of *cMyb* expression levels in cKit$^+$CD45$^+$CD11b$^+$ MΦ progenitors sorted from WT E9-YS, WT and *Lyl-1$^{WT/LacZ}$* E10-YS and brain, as well as from the FDG/Lyl-1 positive and negative

MΦ progenitors fractions from *Lyl-1*$^{WT/LacZ}$ E10-YS. Lin^{-}Sca^{+}cKit^{+} (LSK) progenitors from WT E12 foetal liver (FL) were used as positive control. FDG^{+}/Lyl-1^{+} MΦ progenitors from E10-YS and E10 brain expressed *cMyb*$^{Low/Neg}$ levels similar to E9-YS, which characterize the primitive YS wave. In contrast, the FDG^{-}/Lyl-1^{-} fraction expressed significantly (paired t-test, p=0.033) higher *cMyb* levels, similar to LSK cells from E12-FL. *cMyb* expression levels are shown on a Log^{2} scale, normalized to the mean expression value obtained for WT E10-YS, considered as 1.

2.1.3 Lyl-1 deficiency leads to a defective differentiation of MΦ in the YS and of microglia in early brain

Previous studies have established that MΦ progenitors colonize the brain from E9 *(Alliot et al., 1999; Ginhoux et al., 2010)* and that this microglia settlement stage *(Matcovitch-Natan et al., 2016)* endures till E11. FACS-Gal assay demonstrated that Lyl-1+ MΦ progenitors are present in the brain from the onset of its colonisation ***(Fig. 3a)*** and that Lyl-1 is expressed in the whole F4/80^{+} microglia population throughout the settlement period ***(Fig. 3b)***. The presence of Lyl-1^{+} microglia at the earliest stage of brain colonization (E10) suggests that already differentiated MΦ may also participate in this colonization.

During YS development, both MΦ^{Prim} progenitors and MΦ$^{T\text{-}Def}$ progenitors originate from cKit^{+}CD31^{+}CD45^{-} progenitors (C subset), which subsequently acquire CD11b and CD45 expression (A1 subset). Further MΦ progenitors differentiation is first characterized by cKit down-regulation (A2 subset), then by the concomitant down-regulation of CD31 and up-regulation of F4/80 and CX$_3$CR1 (A3 subset) *(Bertrand et al., 2005b).* Lyl-1 expression in A1-A2-A3 subsets was analysed in *Cx3cr1*$^{WT/GFP}$ YS and brain at E10, when all three subsets are present. Lyl-1 expression was detectable throughout the differentiation of MΦ/microglia, with a decreasing level from A1 to A3 subsets ***(Fig. 3c)***. To evaluate the effect of *Lyl-1* deficiency, we monitored the distribution of A1-A2 and A3 MΦ subsets in E10-YS and brain using the *Cx3cr1*$^{WT/GFP}$*:Lyl-1*$^{LacZ/LacZ}$ double mutant strain which we established. The size of the whole MΦ population appeared similar in all three genotypes, with A1 progenitors predominating in the YS and A3 mature MΦ prevailing in the brain. In both locations, the A1 to A3 distribution was highly impacted by *Lyl-1* deficiency that led to an increased A1 pool and a reduced A3 pool ***(Fig. 3d)***. It thus appears that, besides its function in the regulation of the size of the MΦ progenitor pool, Lyl-1 also regulates the differentiation towards mature MΦ/Microglia.

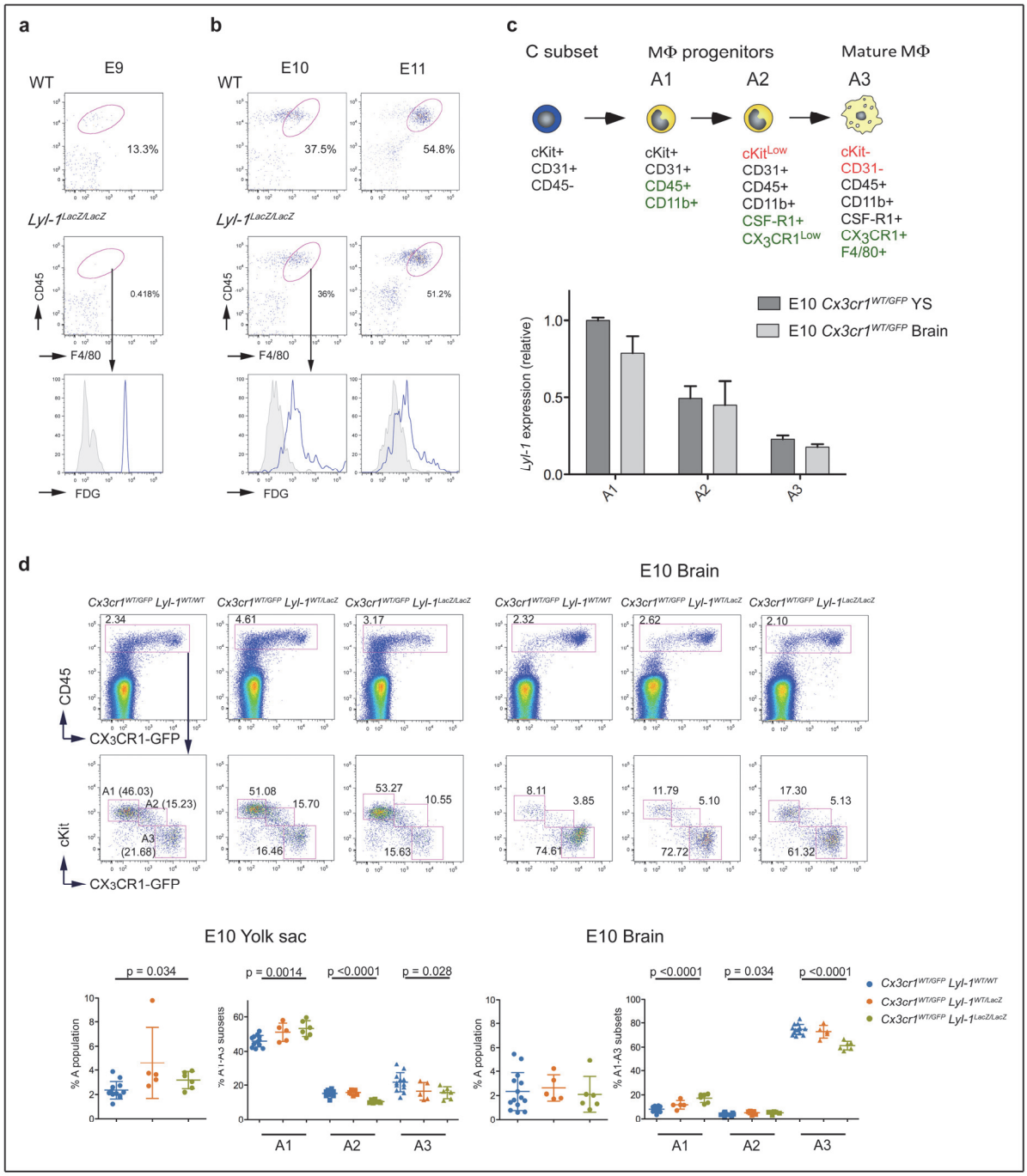

Figure 3: Lyl-1 regulates the differentiation towards mature MΦ/microglia.

a. FDG/Lyl-1 expression in brain at the onset of the brain colonisation stage. The rare CD11b+ F4/80$^{low\text{-}neg}$ cells present in the brain at E9 are FDG/Lyl-1 positive**.** Grey histograms indicate non-specific background β-Gal activity/FDG levels in WT samples.

b. Lyl-1 marks the entire F4/80+ microglia population from the beginning of brain colonisation. Grey histograms indicate non-specific background β-Gal activity/FDG levels in WT samples.

c. Phenotype of MΦ subsets. MΦ develop from cKit^{+}CD31^{+}CD45^{-} progenitors (C subset). MΦ progenitors first acquire the expression of CD11b and CD45 (A1 subset), then down-regulate cKit expression (A2 subset). The differentiation to mature MΦ is hallmarked by the concomitant down-regulation of CD31 and up-regulation of F4/80 and CX_3CR1 (A3 subset).

d. *Lyl-1* expression during MΦ progenitor differentiation. RT-qPCR analyses of *Lyl-1* expression in the MΦ subsets isolated from the YS and corresponding brains of *Cx3cr1$^{WT/GFP}$* embryos at E10. *Lyl-1* is expressed by the 3 subsets and its expression level decreases upon differentiation. Expression levels

were normalized to the mean value obtained for *Cx3cr1*$^{WT/GFP}$ A1 progenitors (n=3). The whole A1-A2-A3 subsets sorted from YS and corresponding brains were processed, independently of the cell numbers obtained for both tissues. Consequently, this assay does not quantify the difference in Lyl-1-expressing cells in both sites, but qualitatively supports the decrease of Lyl-1 expression upon MΦ differentiation similarly occurs in both sites.

d. Defective MΦ progenitor differentiation in the YS and brain of Lyl-1 mutant embryos. Distribution of A1-A2 and A3 MΦ subsets E10-YS (left) and brain (right) from *Cx3cr1*$^{WT/GFP}$*:Lyl-1*$^{WT/WT}$, *Cx3cr1*$^{WT/GFP}$*:Lyl-1*$^{WT/LacZ}$ and *Cx3cr1*$^{WT/GFP}$*:Lyl-1*$^{LacZ/LacZ}$ embryos. The size of the whole MΦ population was similar in the three genotypes in both YS and brain (Top panel), but *Lyl-1* deficiency modified the distribution of the MΦ subsets (middle and lower panel) with an increased size of the A1 subset and a reduced A3 pool (5-12 independent analyses, each sample cumulating 6-8 YS or brain. Plots show mean ± s.e.m.; Unpaired t-test).

2.1.4 Lyl-1 inactivation impairs microglia development at two development stages

Having defined Lyl-1 implication in the initial steps of microglia settlement in the brain, we turned to later stages of microglia development. Cytometry and confocal analyses ***(Fig. S2a, b)***, as well as database analyses (NCBI-GEO accession number GSE79812) *(Matcovitch-Natan et al., 2016)*, confirmed the continuous expression of Lyl-1 in microglia until adulthood. We therefore examined the impact of *Lyl-1* inactivation on the microglia pool size during development. By comparing the kinetics of microglia development in WT and *Lyl-1*$^{LacZ/LacZ}$ whole brain suspensions, we identified E12 as the first step when microglia expansion was impacted by the mutation ***(Fig. 4a).*** A more precise microglia quantification using Percoll purification confirmed the arrested increase of microglia content in *Lyl-1*$^{LacZ/LacZ}$ brain at E12 ***(Fig. 4b)***. This resulted from a reduced proliferation ***(Fig. 3c)*** rather than increased apoptosis ***(Fig. S3c)***. Moreover, *Lyl-1* deficiency also provoked morphological changes in E12 *Cx3cr1*$^{WT/GFP}$*:Lyl-1*$^{LacZ/LacZ}$ microglia which displayed a reduced number and extent of ramifications when compared to *Cx3cr1*$^{WT/GFP}$ microglia ***(Fig. 4d; Fig. S3a, b)***. Interestingly, from E14, the microglia pool size returned to levels similar to WT embryos, a recovery that may partly be attributed to a highly reduced apoptosis level in *Lyl-1*$^{LacZ/LacZ}$ microglia compared to WT at E14 ***(Fig. 4b; Fig. S3c)***.

Both cytometry analyses and quantification of Iba-1-positive microglia in brain sections resulted in the identification of P0-P3 as a second developmental stage altered in *Lyl-1*$^{LacZ/LacZ}$ mice. At that stage, the number of cells per *Lyl-1*$^{LacZ/LacZ}$ brain was significantly decreased compared to WT brain ***(Fig. 4e)***, a feature that was not observed at earlier stages ***(Fig. S3d)***. The same was true for the recovery of CD11b^{+} cells (*Lyl-1*$^{LacZ/LacZ}$: 87.18±0.37x10^{3}; n=9; WT:

140.96±0.91x10^3; n=9). Consequently, loss of Lyl-1 triggered a nearly 2-fold reduction of the microglia population, in accordance with the decreased microglia counts performed *in situ* ***(Fig. 4e)***. Moreover, at P0-P3 altered microglia development was also supported by a dimorphic morphology characterized by decreased ramification numbers ***(Fig. 4f)***. The reduction of the microglia pool size at perinatal stages appeared transient, since a normal cell number was detected in the adult brain by cytometry analyses and Iba-1^+ microglia cell counting ***(Fig. S3e)***. Such transient decrease of the microglia pool size occurs during normal development in postnatal weeks 2-3 *(Zhan et al., 2014)*, but also in *Cx3cr1* mutant mice during the 1st postnatal week *(Paolicelli et al., 2011)*. This indicates a highly dynamic control of the microglia pool size during key steps of neural development that seems preserved in the Lyl-1 mutant, with the exception of the E12 and P0-P3 time-points. At this later stage, the reduction of brain cellularity in *Lyl-$1^{LacZ/LacZ}$* mice points to Lyl-1 as a possible regulator of the trophic function of microglia on CNS cells *(Antony et al., 2011; Ueno et al., 2013)*.

The identification of E12 and P0-P3 as key stages for Lyl-1 function in microglia development was further confirmed by RT-qPCR analyses of the expression of a set of genes essential for MΦ (*Pu.1*, *Csf1-r*, *Mafb*) and/or microglia (*Runx1*, *Cx3cr1*, *Irf8*) development and function, as well as known regulators of developmental hematopoiesis (*Tal1, Lmo2, Runx1*) and related factors (*Tcf3*/E2A, *Tcf4*/E2.2) ***(Fig. 4g, h; Fig. S3g)***. Overall, the temporal evolution of these genes in wild type microglia correlated with previous reports *(Kierdorf et al., 2013; Matcovitch-Natan et al., 2016)* (NCBI-GEO accession number GSE79812). This time course analyses highlighted the down-regulation of *Csf1-r*, *Irf8* and *Lmo2* in *Lyl-$1^{LacZ/LacZ}$* microglia at both E12 and P0-P3, while the *Cx3cr1* signal decreased only at E12. Interestingly, *Lyl-1* expression was unmodified in *Cx3cr1$^{GFP/GFP}$* mutants, suggesting that Lyl-1 may regulate *CX_3CR1* expression in microglia. Indeed, *Cx_3cr1*, as well as *Irf8* and *Lmo2*, belong to potential Lyl-1 target genes (Wilson et al., 2010). *Mafb* expression levels in *Lyl-$1^{LacZ/LacZ}$* microglia transiently decreased at P0-P3 and later returned back to WT expression levels. As Mafb represses self-renewal of resident MΦ (Soucie et al., 2016), this transient decrease may be linked to the recovery of a normal microglia quantity of in the adult. The expression levels of *Pu.1*, *Tcf3*/E2A and *Tcf4*/E2.2 were unmodified in *Lyl-$1^{LacZ/LacZ}$* microglia irrespective of analysed stages, while *Runx1* expression was only affected after birth. The expression of *Tal-1/Scl* was decreased at E14 and increased after birth, suggesting that this *Lyl-1* paralog *(Curtis et al., 2012)* does not compensate for *Lyl-1* deficiency during embryonic stages of

microglia development, but may do so during postnatal stages ***(Fig. S3g)***.

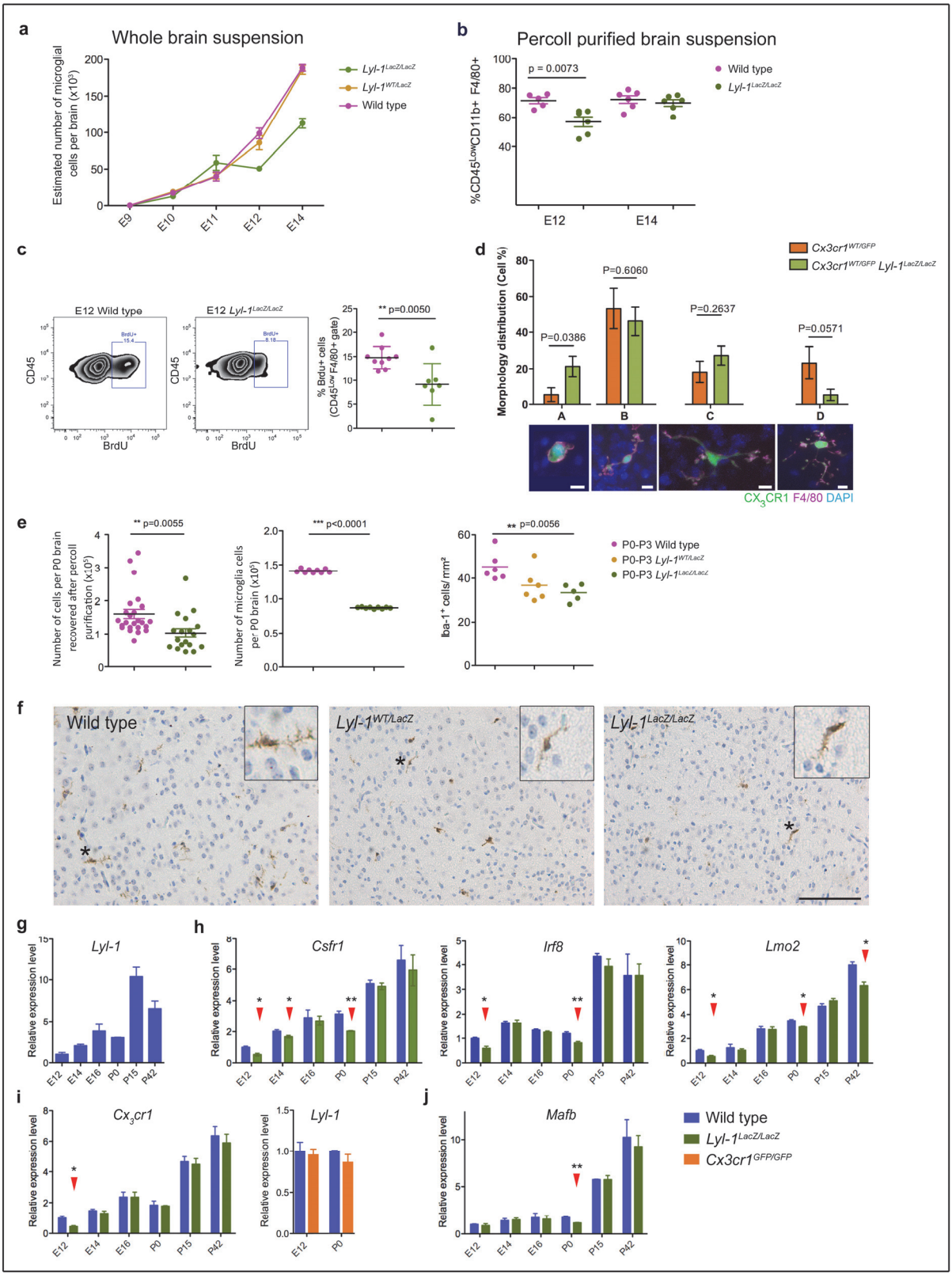

Figure 4: Lyl-1 deficiency leads to transient reductions of the microglia pool at E12 and P0-P3.

a. Kinetic evolution of $CD11b^{+}F4/80^{+}CD45^{-/low}$ microglia estimated number *(see methods)* in WT, *Lyl-1*$^{+/LacZ}$ and *Lyl-1*$^{LacZ/LacZ}$ brain. Microglia development in *Lyl-1*$^{WT/LacZ}$ embryos was similar to that of WT embryos. At E12, microglia content was reduced two fold in *Lyl-1*$^{LacZ/LacZ}$ brains compared to WT and *Lyl-1*$^{WT/LacZ}$ brains. Afterwards, the growth rate was similar to WT and *Lyl-1*$^{WT/LacZ}$ microglia.

Microglia were quantified in whole brain preparation (for WT, *Lyl-1*$^{WT/LacZ}$ and *Lyl-1*$^{LacZ/LacZ}$ respectively n=: E9: 6, 7, 4; E10: 9, 9, 5; E11: 6, 5, 7; E12: 6, 6, 6; E14: 8, 6, 6).
b. Percoll purification was performed after E12 to more precisely assess the microglia content of the brain. The microglia quantification obtained using this procedure confirmed the decreased size of the microglia pool at E12, as well as the recovery of a normal pool size at E14. Plots show mean ± s.e.m.; Unpaired t-test.
c. A reduced microglia proliferation may account for the reduced microglia number at E12, as shown by the two folds decrease (right) of BrdU-labelled cells in *Lyl-1*$^{LacZ/LacZ}$ (middle) compared to WT (left) brains. Plots show mean±s.e.m.; Unpaired t-test.
d. At E12, *Cx3cr1*$^{WT/GFP}$*:Lyl-1*$^{LacZ/LacZ}$ microglia displayed a reduced number and extent of ramifications compared to their *Cx3cr1*$^{WT/GFP}$ counterpart. Bottom: Microglia morphology was classified into subtypes depending on the number of main ramifications (A: none, B: 2, C: 3 and D:>3). Top: Microglia deprived of ramifications predominated in *Lyl-1*-deficient microglia. 65 and 61 cells were respectively acquired from the midbrain of E12 *Cx3cr1*$^{WT/GFP}$ and *Cx3cr1*$^{WT/GFP}$*:Lyl-1*$^{LacZ/LacZ}$ embryos (For each genotype, brains from 12 embryos were acquired in 3 independent experiments). Microglia were identified by *Cx3cr1*-driven GFP expression and F4/80-APC immuno-staining. Bar=10μm. Plots show mean±s.e.m.; Unpaired t-test.
e. In *Lyl-1*$^{LacZ/LacZ}$ new-born, the cellularity of the brain was consistently lower than in WT (left), and so was the estimated microglia number (middle). A reduced microglia pool size was also supported by the count of Iba-1^{+} microglia in *Lyl-1*$^{LacZ/LacZ}$ midbrain section (right). Plots show mean ± s.e.m.; Unpaired t-test.
f. Immuno-histochemical Iba-1 labelling of P1 microglia showed a reduced ramification of microglia in *Lyl-1*$^{WT/LacZ}$ brain sections. Bar=50 μm.
g. Kinetic evolution of *Lyl-1* expression levels in WT microglia from embryonic stages to adulthood. An increased expression of *Lyl-1* from embryonic stages to adulthood was also inferred from timeline RNA-seq data *(Matcovitch-Natan et al., 2016)* (GEO accession number GSE79812).
h. Quantitative RT-PCR analyses also point to E12 and P0 as key development stages regulated by Lyl-1. CD11b^{+}F4/80^{+}CD45^{low} microglia were isolated at sequential development stages. Bar graphs show the kinetic of expression of genes modified in *Lyl-1*$^{LacZ/LacZ}$ microglia (arrowheads), normalized to the mean expression value in WT E12 microglia (n=3). Error bars indicate s.e.m. Unpaired t-test.
I. *Cx3Cr1* and Lyl-1 expression in mutant microglia. The expression level of *Cx3CR1*, analysed as in h, was decreased in Lyl-1 mutant at E12, while *Lyl-1* expression level was unmodified in *CX3CR1*$^{GFP/GFP}$ microglia at E12 and in the new-born.
J. *Mafb* expression in mutant microglia. *Mafb* expression level, analysed as in h, was reduced in the microglia of *Lyl-1*$^{LacZ/LacZ}$ new-borns.

2.1.5 Effects of Lyl-1 inactivation in the adult: defective microglia and impaired social behavior

In adult brains, *Lyl-1* deficiency had no detectable impact on the gross architecture of the hippocampal or cerebellar brain region ***(Fig. S4a-h)***. Notably, the number of microglia was identical in hippocampus and cortex and no cellular infiltrates such as MAC-3^{+} MΦ or CD3^{+} T-cells were detected in *Lyl-1*$^{LacZ/LacZ}$ brains. No APP-positive axons, indicating neuronal damage, were observed, and brain endothelial cells were intact ***(Fig. S4i)***. RNA-seq data analyses of microglia isolated by FACS revealed that *Lyl-1* deficiency affects genes associated with neuropsychiatric disorders like autism spectrum disorder (ASD) and anxiety ***(Fig. 5a)***.

The increased expression of *Mios*, *Mapk8*, *Ccr6* and *Nod2* genes suggested an activated microglial phenotype. This was confirmed by immuno-fluorescent labelling of cortical sections, where an increased percentage of Iba1+ microglia also expressed CD68 *(Doorn et al., 2014)*, a marker for actively phagocytic microglia ***(Fig. 5b)***. Further support for an activated phenotype came from morphometric analysis of cortical microglia, which appeared slightly hyper-ramified in *Lyl-1*-deficient mice as indicated by increased filament dendrite volume ***(Fig. 5c)***. Since RNA-seq data indicated expression changes of genes related to psychiatric disorders in *Lyl-1*-deficient microglia, we searched STRING, a protein-protein interaction network, to identify potential interaction partners of Lyl-1, which were also related to this group of disorders. Predicted interactions involved NOTCH1, HDAC1, TRIM33 and TCF12, which represent proteins related to pathological anxiety and ASD ***(Fig. 5d)***.

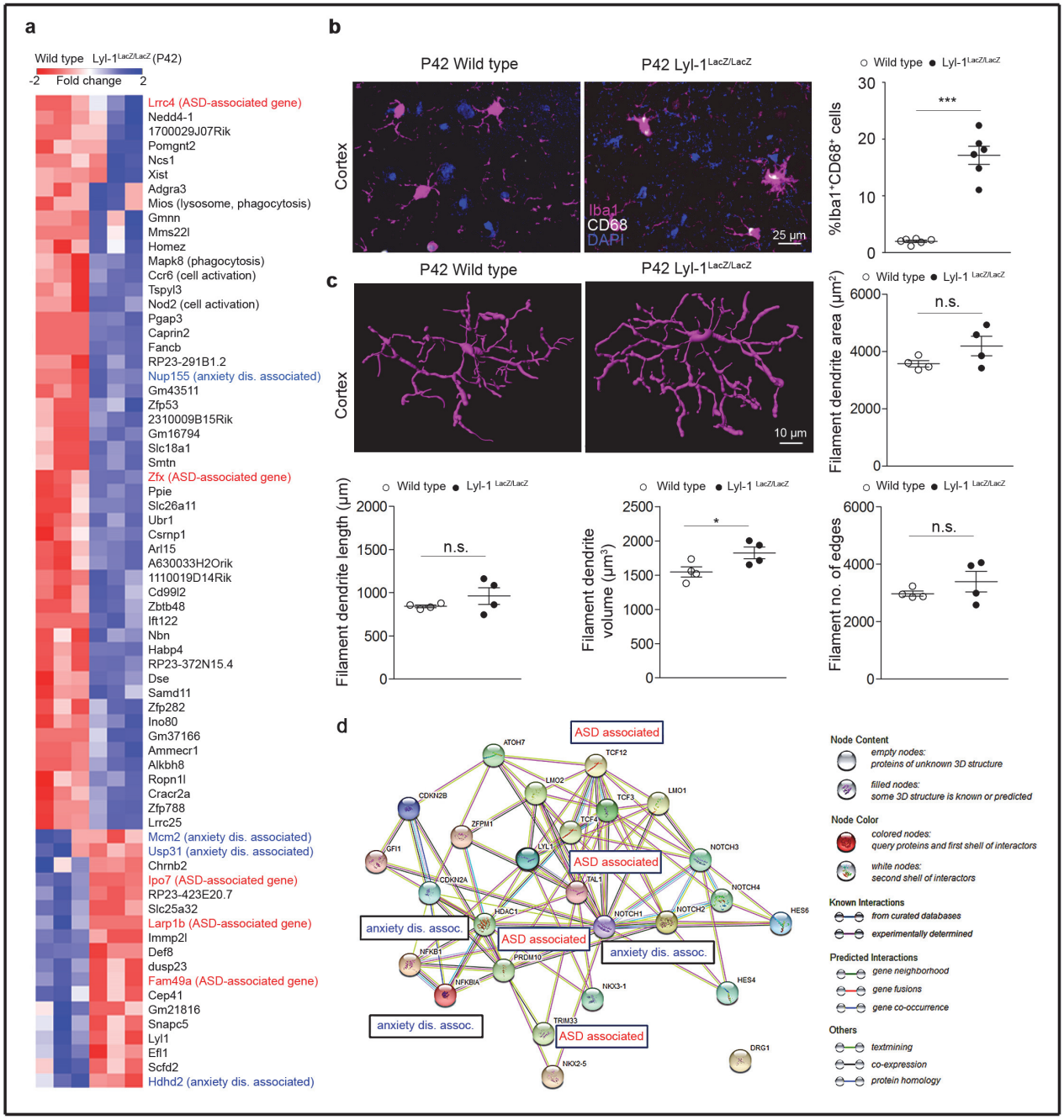

Figure 5: Lyl-1 deficiency alters transcriptomic profile and activation status of microglia in the adult brain.

a. RNA-seq heatmap showing differentially expressed (p<0.05) genes in microglia isolated from WT and *Lyl-1*$^{LacZ/LacZ}$ mice at P42.

b. Immunofluorescence labelling of the cortex of WT (left) and *Lyl-1*-deficient (right) mice at P42: Iba1^{+} (magenta) microglia co-localization with the lysosomal marker CD68^{+} (white) and DAPI-stained nuclei (blue) (Bar=25 µm). Right: Quantification of percentage Iba1^{+}+CD68^{+} microglia in the cortex of WT (open circles) and *Lyl-1*$^{LacZ/LacZ}$ (closed circles) mice. Each symbol represents data from one mouse. Three cortical sections were analysed per mouse (Unpaired *t* test, data are mean ± s.e.m., p<0.001 (***), n.s.; not significant.).

c. Three-dimensional (3D) reconstruction of cortical microglia in WT and *Lyl-1*$^{LacZ/LacZ}$ mice at P42 (Bar=10 µm). IMARIS based morphometric analysis of cortical microglia isolated from WT (open

circles) and *Lyl-1*$^{LacZ/LacZ}$ (closed circles) mice at P42. Each symbol represents data of one animal. Ten cells per mouse were reconstructed. Statistical analysis: unpaired *t* test, * = $p<0.05$, n.s.= non-significant.
d. STRING based functional protein association network of Lyl-1 (black circle) with indicated association to anxiety or ASD *(Bevins and Besheer, 2006; Kaneko-Goto et al., 2013; Kobayakawa et al., 2007)*.

Impaired social behaviour and reduced neuronal connectivity in Lyl-1-deficient animals

A spectrum of behavioural tests was performed to detect potential behavioural manifestations in *Lyl-1*-deficient mice. While *Lyl-1*-deficient mice showed no signs of depressive-like behaviour measured in the forced swim test (FST) ***(Fig. 6a)*** or abnormal self-grooming behaviour ***(Fig. 6c)***, they spent less time in the open arms of the elevated plus maze (EPM), indicating increased anxiety-like behaviour ***(Fig. 6b)***. In the three-chamber social interaction test, *Lyl-1*-deficient animals showed less preference to interact with an unfamiliar mouse compared to an object ***(Fig. 6d).*** In the social novelty test, *Lyl-1*-deficient mice spent less time with an unfamiliar mouse compared to the time spent interacting with a familiar mouse ***(Fig. 6e)***. Social interaction can be indirectly affected by disturbed olfaction *(Sullivan et al., 2015)* or hippocampal memory *(Rubin et al., 2014)*. This was not the case in the present experiments since *Lyl-1* deficiency did not interfere with olfactory avoidance ***(Fig. 6f)*** or novel object recognition, a hippocampal memory task ***(Fig. 6g, h)***. Combining the data of all behavioural tests results in a phenotype of increased anxiety, social fear and avoidance of social situations, which corresponds to cardinal behavioural symptoms of ASD *(Schuetze et al., 2017)* and social anxiety disorder in humans *(Morrison and Heimberg, 2013)*.

To understand the underlying functional connectivity (FC) across brain regions, we performed resting state functional magnetic resonance imaging (rsfMRI). Independent component (IC) analysis revealed brain regions for *Lyl-1*-deficient and WT groups, which can be attributed to the anterior cingulate cortex (ACC). Seed-based analysis with the IC of the ACC showed decreased FC in *Lyl-1*-deficient animals compared to WT ***(Fig. 6i, left)*** within ACC, hippocampus, motor/auditory/somatosensory cortex, thalamus, amygdala, caudate putamen and hypothalamus ***(Fig. 6i, right)*** (uncorrected, $p < 0.001$). While the vast majority of functional brain connections were impaired in *Lyl-1*-deficient mice, we also found cases of enhanced FC, as seen between the dentate gyrus and the left anterior hypothalamus. The FC matrices of each group, shown on a mouse glass brain ***(Fig. 6j,k)***, illustrate the generally decreased FC in the *Lyl-1*-deficient group between ACC and distant brain regions. The ACC

was chosen as seed because this brain region is particularly involved in the formation of social anxiety disorder *(Doruyter et al., 2016; Robinson et al., 2014)*.

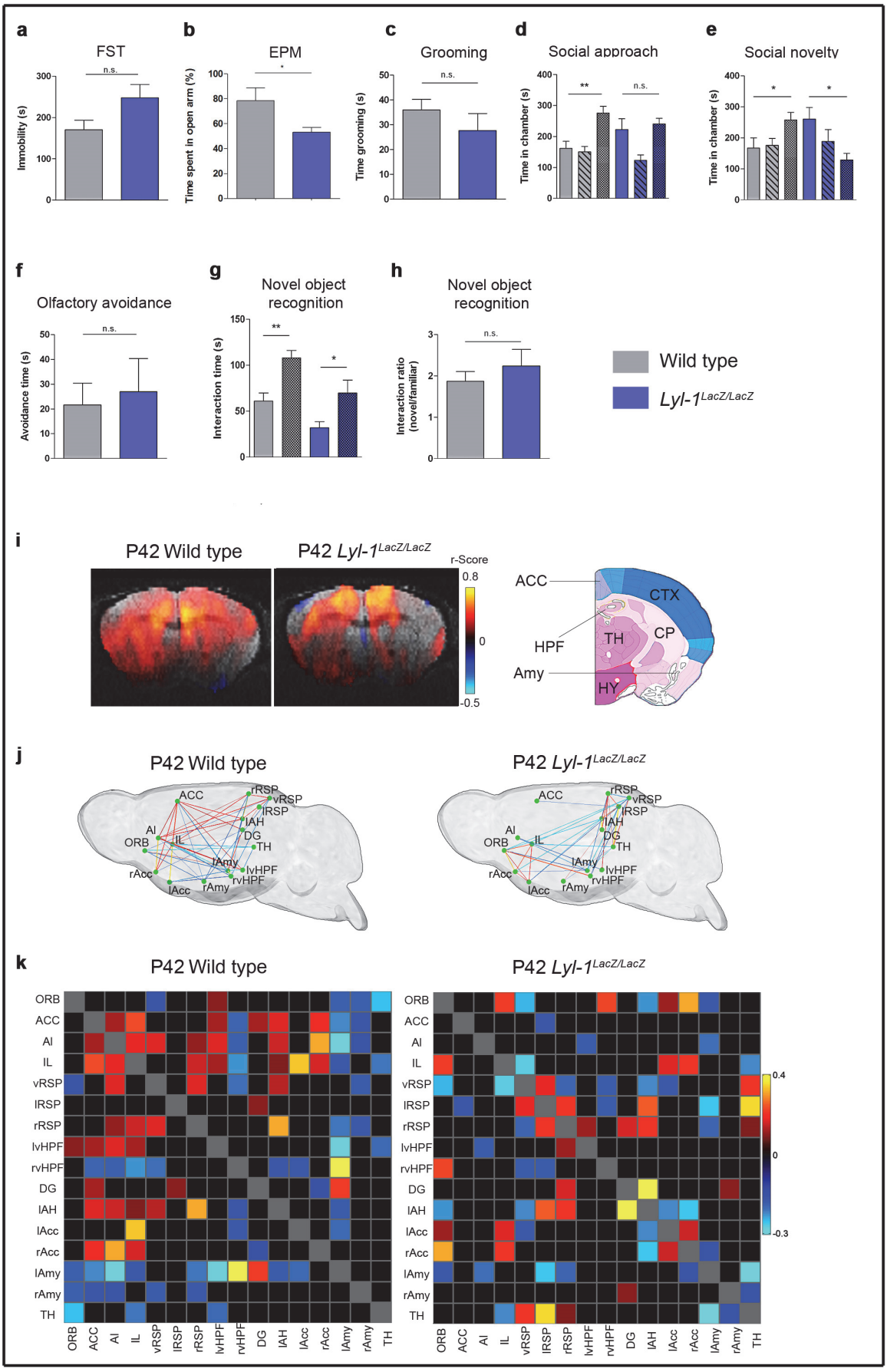
a
FST
Immobility (s)
n.s.
b
EPM
Time spent in open arm (%)
*
c
Grooming
Time grooming (s)
n.s.
d
Social approach
Time in chamber (s)
**
n.s.
e
Social novelty
Time in chamber (s)
*
*
f
Olfactory avoidance
Avoidance time (s)
n.s.
g
Novel object recognition
Interaction time (s)
**
*
h
Novel object recognition
Interaction ratio (novel/familiar)
n.s.
Wild type
Lyl-1LacZ/LacZ
i
P42 Wild type
P42 Lyl-1LacZ/LacZ
r-Score
0.8
0
-0.5
ACC
CTX
HPF
TH
CP
Amy
HY
j
P42 Wild type
P42 Lyl-1LacZ/LacZ
ACC
rRSP
vRSP
lRSP
AI
lAH
DG
ORB
IL
TH
lAmy
lvHPF
rAcc
rvHPF
lAcc
rAmy
k
P42 Wild type
P42 Lyl-1LacZ/LacZ
ORB
ACC
AI
IL
vRSP
lRSP
rRSP
lvHPF
rvHPF
DG
lAH
lAcc
rAcc
lAmy
rAmy
TH
0.4
0
-0.3

Figure 6: Lyl-1 deficiency elicits altered social behaviour, as shown by an increased anxiety and a reduced neuronal connectivity.
a. In the forced swim test (FST) *Lyl-1*-deficient mice (n+10) showed no difference in depressive-like behaviour when compared to WT mice (n=10; unpaired *t*-test).
b. *Lyl-1*-deficient mice (n=10) displayed increased anxiety in the elevated plus maze (EPM) relative to controls (n=10; unpaired *t*-test).
c. *Lyl-1*-deficient mice (n=10) and WT mice (n=10) spent similar time self-grooming (unpaired *t*-test).
d. Three-chamber test: While WT mice (n=10) spent more time in the chamber housing a stranger mouse (dotted bars) than in the chamber containing an empty cage (solid bars), *Lyl-1*-deficient mice (n=10) had no preference for either chamber. Striped bars indicate time spent in the centre region of the three-chamber box (unpaired *t*-test).
e. WT mice (n=10) spent more time in the chamber housing an unfamiliar mouse (dotted bars) than in a chamber housing a familiar mouse (solid bars). *Lyl-1*-deficient mice (n=10) preferred interacting with the familiar mouse and spent less time with an unfamiliar mouse. Striped bars indicate time spent in the centre region of the three-chamber box (unpaired *t*-test).
f. *Lyl-1*-deficient (n=10) and WT mice (n=10) have similar olfactory avoidance time (unpaired *t*-test).
g. In novel object recognition test, *Lyl-1*-deficient (n=10) and WT mice (n=10) had normal recognition memory for a pre-exposed object (plain histogram) presented 24 h before the test, so that they spent more time with the novel (dotted histogram), unfamiliar object (unpaired *t*-test).
h. Discrimination index: the normalized ratio of time spent with the familiar object divided by time spent with the novel object showed no difference between *Lyl-1*-deficient (n=10) and WT mice (n=10) for novel object recognition ability (unpaired *t*-test). Data are mean ± s.e.m. *n* is the number of mice. $p<0.05$ (*), $p<0.01$ (**), and n.s.; not significant.
i. Seed-based analysis of the ACC of WT (n=3; left) and *Lyl-1*-deficient mice (n=3; right) at P42. The colour scale on the right indicates the *correlation coefficient r*. The regions that showed lower FC in the *Lyl-1*-deficient group are indicated on corresponding coronal section of the Franklin and Paxinos anatomical mouse brain atlas (right panel) depicting cortex (CTX), caudate putamen (CP), ACC, hippocampal field (HPF), thalamus (TH), hypothalamus (HY) and amygdala (Amy).
j. The comparison of the connectivity changes based on the correlated (positive–red spectrum) and anticorrelated (negative–blue spectrum) nodal activities, indicates lower FC in *Lyl-1*-deficient mice (n=3; right) compared to WT (n=3 left) mice at P42.
k. 3D representations of all correlated ($|r|>0.1$) connections in WT and *Lyl-1*-deficient groups highlights the reduction of the ACC functional connectivity in the *Lyl-1*-deficient group along with a pronounced loss of positively correlated brain regions. Analysed regions include: ACC: anterior cingulate cortex area; AI: agranular insular area; IL: infralimbic cortex; ORB: orbital area; rAcc: right nucleus accumbens; lAcc: left nucleus accumbens; rAmy: right amygdala; rvHPF: right ventral hippocampus; lvHPF: left ventral hippocampus; lAmy: left amygdala; TH: thalamus; DG: dentate gyrus; lAH: left anterior hypothalamus; lRSP: left retrosplenial area; vRSP: ventral retrosplenial area; rRSP: right retrosplenial area.

Decreased spine density and spiking activity in cinguli gyrus pyramidal cells in Lyl-1-deficient mice

As microglia are involved in synaptic pruning *(Paolicelli et al., 2011; Zhan et al., 2014),* we quantified spine density in pyramidal neurons of the ACC following Golgi-cox staining. In *Lyl-1*-deficient mice, the overall spine density was reduced ***(Fig. 7a)***, but the number of dendritic endpoints in apical or basal parts of pyramidal neurons remained unchanged ***(Fig. 7b)***. To directly test whether reduced cortical connectivity and spine density of pyramidal

neurons of *Lyl-1*$^{LacZ/LacZ}$ mice alters prefrontal activity levels, we recorded single-unit discharges from the anterior cingulate cortex of awake *Lyl-1*$^{LacZ/LacZ}$ and control animals ***(Fig. 7c-e)***. Pyramidal neurons were identified based on broad kinetics of their spike waveforms and the formation of excitatory synaptic connections in the local network ***(Fig. S5)***. *Lyl-1*$^{LacZ/LacZ}$ pyramidal neurons discharged at significantly reduced frequency (median: 3.4 Hz, SD: 3.8 Hz, n=92 pyramidal neurons from 3 mice) compared to WT neurons (median: 4.7 Hz, SD: 5.5 Hz, n=47 neurons from 3 mice; p=0.026, *U(137)=1724*, Mann-Whitney U test; ***Fig. 7c, d***). Furthermore, *lyl-1* deficiency resulted in reduced synchrony of pyramidal cell discharges in relation to ongoing theta (4-12 Hz) oscillations in the local field potential (LFP). These rhythmic activities provide a temporal reference frame for prefrontal discharges during behaviour *{O'Neill, 2013 #7244}*. Fewer pyramidal neurons aligned their spiking activity with ongoing theta oscillations (89 vs. 34%, $p=2*10^{10}$, Fisher's exact test, oscillation coupling assessed using Rayleigh's test for circular uniformity, $p<0.05$; ***Fig. 7e***). Moreover, analysis of the pairwise phase consistency of single-unit discharges revealed that the strength of spike-LFP_{theta} association was significantly reduced in *Lyl-1*$^{LacZ/LacZ}$ mice (n=42 and 31 coupled neurons from 3 control and *Lyl-1*$^{LacZ/LacZ}$ mice, respectively, U(71)=486, p=0.033, Mann-Whitney U-test; ***Fig. 7e***). These findings could not be explained by a general loss of oscillatory power since spectral analysis revealed comparable oscillation power densities across multiple frequency bands (theta (4-12 Hz): U(6)=6, p=0.333, beta (15-30 Hz): U(6)=7, p=0.443, gamma (30-100 Hz): U(6)=7, p=0.443, n=4 *Lyl-1*$^{LacZ/LacZ}$ and control mice, Mann-Whitney U-tests; ***Fig. 7e)***. Thus, *Lyl-1* deficiency impairs the firing rate and temporal organization of neuronal discharges in the anterior cingulate cortex.

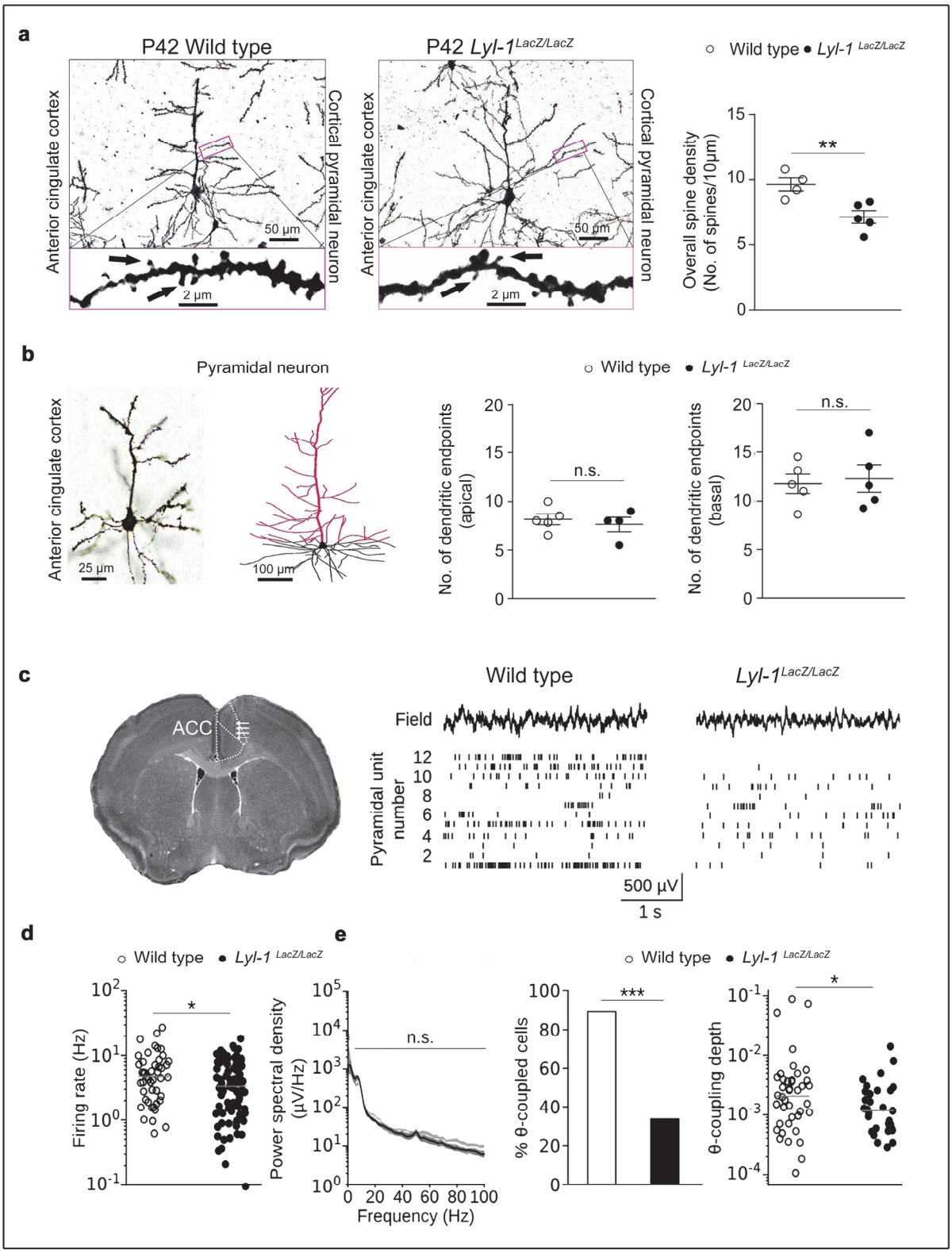

Figure 7: Decreased dendritic spine density and impaired neuronal activity in pyramidal neurons from the anterior cingulate cortex of Lyl-1-deficient mice.

a. Representative bright field images of Golgi-stained WT (left) and *Lyl-1*-deficient (right) cortical pyramidal neurons. Insets show dendrites and dendritic spines at higher magnification. Scatter-plot of overall dendritic spine density (far right).

b. Quantification of dendritic endpoints in the apical and basal portion of pyramidal neurons from anterior cingulate cortex of WT and *Lyl-1*-deficient mice (right). Apical and basal segment of cortical

pyramidal neuron are depicted as bright field image (far left) and schematic drawing (middle). Circles indicate number of mice analysed. At least 12 neuronal branches from 4 different neurons were analysed per animal. Unpaired *t*-test, data are mean ± s.e.m. . p<0.01 (**), and n.s.; not significant.
c. Single-unit recording from anterior cingulate cortex area (ACC). Left, histological identification of the recording probe placement in the ACC (arrows). Right, local field potential (top) and action potentials of simultaneously recorded pyramidal units (bottom) in Lyl-1-competent (left) and deficient (right) mice revealed reduced spike rates in *Lyl-1*$^{LacZ/LacZ}$ mice.
d. Quantification of pyramidal neuron discharge rates. n=3 mice per group. Mann-Whitney U-test. Horizontal bars indicate median.
e. Power spectral density analysis indicated comparable oscillatory power levels (left) but reduced coupling of pyramidal discharges to ongoing theta (4-12 Hz) oscillations. In *Lyl-1*$^{LacZ/LacZ}$ mice, fewer pyramidal cells phase-lock to theta (middle, Fisher's exact test) at reduced phase-locking depth (right, Mann-Whitney U-test). Horizontal bars indicate median. *p<0.05; **p<0.01; ***p<0.001.

DISCUSSION

Overall, we identified Lyl-1 as a marker for primitive YS-derived MΦ progenitors and microglia. We also showed that Lyl-1 controls microglia development and that a defective Lyl-1 expression impairs neurodevelopmental processes leading to behavioural defects associated with impaired social interaction and anxiety.

So far, Lyl-1 is the first marker that discriminates MΦ progenitors from the primitive and transient definitive/EMP-derived YS waves. From our results, it appears that during normal YS development, Lyl-1 controls the size of the MΦ^{Prim} progenitor pool and/or the duration of its production, which is thought to be transient *(McGrath et al., 2015b)*. This novel finding may translate into a better understanding of the mechanisms underlying the differences between the two MΦ waves, possibly leading to a significant advance in investigations of other HSC-independent lineages. This will be particularly relevant to the Embryonic Stem Cells/iPS field in which the production of definitive cells types is complicated by the poor discrimination between primitive and definitive populations. Interestingly, recent evidence also pointed to Lyl-1 expression in progenitors of the primitive erythroid lineage, as well as its role in the maintenance of this lineage *(Chiu et al., 2018).*

When analysing the contribution of Lyl-1^{+} MΦ progenitors, we focused on the developing brain, and found that right from the onset of its development, microglia maintain Lyl-1 expression and share with MΦ^{Prim} progenitors a low level of *cMyb* expression. While fate mapping analyses were instrumental to firmly ascribe a YS origin to microglia (Ginhoux et al., 2013; Gomez Perdiguero et al., 2015; Kierdorf et al., 2013; Schulz et al., 2012), this strategy could not ascertain which YS progenitor wave contributes to microglia (McGrath et al., 2015b). Indeed, several features prevent an independent/specific targeting of only one MΦ

progenitors wave in these fate map analyses performed at the initial stages of YS hematopoiesis: 1- the similar phenotype of the primitive and transient definitive MΦ progenitors *(Bertrand et al., 2005b)*; 2- the short time-span separating the two YS waves (E7.25 and E8.25), 3- the duration of the inducing treatment and 4- the high range of development stages of individual embryos within a litter at these early developmental stages *(Downs and Davies, 1993)*. Using *ex vivo* approaches whereby the potential and expression pattern was examined in individually staged embryos, we found that Lyl-1 expression discriminates $M\Phi^{Prim}$ from EMP-derived $M\Phi^{T\text{-}Def}$ progenitors, and also marks the entire embryonic microglia. We may therefore consider that microglia could develop from Lyl-1^+ $M\Phi^{Prim}$ progenitors.

Such model is supported by the low level of *cMyb* expression expressed by both Lyl-1^+ $M\Phi^{Prim}$ progenitors and Lyl-1^+ microglia: The intact microglia pool in *cMyb*-deficient mice *(Kierdorf et al., 2013; Schulz et al., 2012)* also suggests that microglia originate from primitive progenitors rather than EMP-derived $M\Phi^{T\text{-}Def}$ progenitors. Similar evidence was obtained from zebrafish where the fate of $M\Phi^{Prim}$ progenitors can be more easily traced than in mammals as they arise from a location distinct from other hematopoietic progenitors (Ferrero et al., 2018; Herbomel et al, 2001). This model is also supported by the recently reported presence of a normal microglia pool in mice lacking the ligand for cKit (Stem Cell Factor or steel factor), despite an impaired development of EMPs, which led to a depletion of tissue resident macrophages in various tissues (skin, liver, lung), but not in the brain *(Azzoni et al., 2018)*.

E12 and P0-P3 were identified as key stages of microglia development impacted by *Lyl-1* deficiency. These time points correspond to the end of "early" (E9-E12) and "pre-microglia" (E14-P9) stages of the recently defined stepwise microglia development program *(Matcovitch-Natan et al., 2016)*. Considering the sustained expression of Lyl-1 in microglia during adulthood, and the down-regulation of genes essential for microglia function in Lyl-1 mutants at E12 and P0-P3, Lyl-1 deregulation might contribute to various neurodegenerative/neuroinflammatory diseases and possibly support the development of brain tumours. Such involvement of Lyl-1 in the regulation of brain homeostasis was suggested by its deregulation uncovered through the analyses of a database cumulating dataset reports for various pathological models of brain myeloid cells *(Friedman et al., 2018)*. Moreover, Lyl-1 expression was also reported in human microglia from healthy adult frontal cortex *(Wehrspaun et al., 2015)* and a few data highlight the relevance of Lyl-1 deregulation

in human neurodevelopmental and neurodegenerative diseases *(Colangelo et al., 2002; McCallum et al., 2016; Thomas et al., 2006)*.

Based on the gene expression pattern of *Lyl-1*-deficient microglia, a major contribution of Lyl-1 to neuropsychiatric disorders like ASD and social anxiety disorder can be assumed. ASD has a very strong developmental component, which forms the basis for atypical neurological development and functioning *(Salter and Stevens, 2017)* and is often accompanied by social anxiety disorder *(Bejerot et al., 2014)*. In addition, as seen from rsfMRI analyses of *Lyl-1*-deficient mice, significant connectivity disturbances of the ACC were uncovered. Interestingly, a similar reduced connectivity of the ACC was observed at baseline in patients suffering from social anxiety disorder patients while after therapy, social anxiety disorder patients demonstrated significantly increased connectivity with the ACC *(Doruyter et al., 2016)*. Similarly, a hypo-connectivity of the ACC was also reported for ASD patients *(Di Martino et al., 2014; Zhou et al., 2016b)*. As a consequence of hypo-connectivity, an impaired network activity can be expected when we assume that brain areas, which are functionally connected in the resting-state, form intrinsic networks that are synergistically activated in performing the network's typical function. Morphological analyses and electrophysiological *in-vivo* recordings from the ACC further supported rsfMRI data. We observed that *Lyl-1* deficiency resulted in reduced spine density, most probably due to increased microglial phagocytosis. In line with a limited number of potentially functional synapses, *Lyl-1*-deficient mice displayed a compromised firing rate and diminished temporal organization of neuronal discharges in pyramidal neurons of the ACC.

Enhanced synaptic pruning and the associated defective behaviour described here, likely stem from *Lyl-1* deficiency at stage P0-P3, the later key developmental stage regulated by Lyl-1. This phase in development leads to synaptic pruning and neural maturation *(Matcovitch-Natan et al., 2016)* and fits with the general emerging concept that activated microglia shape synaptic function in ASD during development *(Salter and Stevens, 2017)*. The long-term consequences of *Lyl-1* inactivation at E12 remain to be determined because this early time-point is not related to any major regulation of synapse number and function.

Altogether, using a multi-disciplinary approach combining developmental hematopoiesis and molecular and behavioural neuroscience, our findings reveal *Lyl-1* to be a key factor regulating microglial and brain development as well as normal brain function during adulthood.

MATERIALS AND METHODS

Ethic statement. Mice were housed in the animal facilities of Institut Gustave Roussy ("Plate-forme d'évaluation préclinique", animal facility licence # E 94-076-11). All animal experiments were conducted in compliance with French regulations (Transposition of Directive 2010/63), under authorized project #5798-2016062214256796 approved by officially accredited Ethical committee n°26, and with the national guidelines of the German animal protective law for the use of laboratory animals, with permission of the responsible local authorities for the University Medical Center Freiburg (Regierungspräsidium Freiburg, permit numbers: G-11/50).

Mice and embryos. We used the following mouse strains: 1- C57BL/6 mice from Harlan or Charles Rivers Laboratories, France, referred to as wild type (WT); 2- *Lyl-1*^{LacZ} mice, in which an in-frame insertion of the β-Galactosidase reporter encoding gene *LacZ* replaced the HLH domain and the entire 3' end of the *Lyl-1* gene, were genotyped as described before *(Capron et al., 2006).* *Lyl-1*$^{LacZ/LacZ}$ males were crossed with WT or *Lyl-1*$^{LacZ/LacZ}$ females to respectively generate *Lyl-1*$^{WT/LacZ}$ or *Lyl-1*$^{LacZ/LacZ}$ embryos. This breeding scheme avoided the possible detection of FDG/Lyl-1 expression in maternally derived MΦ *(Bertrand et al., 2005b)* in the expression analyses performed in early *Lyl-1*$^{WT/LacZ}$ embryos; 3- *Cx3cr1*^{GFP} mice *(Jung et al., 2000).* *Cx3cr1*$^{GFP/GFP}$ males were crossed with C57BL/6 to generate *Cx3cr1*$^{WT/GFP}$ mice/embryos or to *Lyl-1*$^{LacZ/LacZ}$ females to generate *Cx3cr1*$^{WT/GFP}$*:Lyl-1*$^{WT/LacZ}$ mice/embryos. 4-The *Cx3cr1*$^{GFP/GFP}$*:Lyl-1*$^{LacZ/LacZ}$ double mutant strain was developed from *Cx3cr1*$^{WT/GFP}$*:Lyl-1*$^{WT/LacZ}$ crosses. *Cx3cr1*$^{WT/GFP}$*:Lyl-1*$^{WT/LacZ}$ and *Cx3cr1*$^{WT/GFP}$*:Lyl-1*$^{LacZ/LacZ}$ mice/embryos were obtained by crossing *Cx3cr1*$^{GFP/GFP}$*:Lyl-1*$^{LacZ/LacZ}$ males to C57BL/6 or *Lyl-1*$^{LacZ/LacZ}$ females, respectively. To exclude maternal/placental cell contamination, the *Cx3cr1* transgene was always inherited from the male parent.

The day of vaginal plug observation was considered as E0.5. Pregnant females were sacrificed by cervical dislocation. Pre-somite embryos were staged according to Downs et al.*(1993).* From E8 to E10.5, embryos were staged by somite counting and thereafter according to morphological landmarks.

For behavioural, fMRI and electrophysiological studies only male mice were used. The sample size was based on previous experiments and published data. No statistical

methods were used to determine sample sizes.

Tissues preparation and cell counts. YS (E7.5-E10.5) were dissected as described before *(Bertrand et al., 2005a).* To perform cytometry analyses of the developing brain, two different protocols were applied:

1- For analyses performed at early stages and for kinetic studies (E9 to E14), the whole brain embryos were dissected and dissociated as previously described *(Alliot et al., 1999)* and further cleaned from surrounding tissues. To obtain the kinetics evolution of microglia number from E9 to E14, the numbers of microglia per brain were estimated by reporting the percentage of microglia obtained from flow cytometry analysis, gating on $CD45^+CD11b^+F4/80^+$ cells, to the total numbers of cells by per brain, counted after whole brain mechanical dissociation.

2- From E12 to adult stages, microglia were recovered following Percoll (P1644, Sigma) separation, according to *(Mildner et al., 2007)*. After Percoll purification, 100 µl of the cell suspension was used for cell counting and the rest was used for flow cytometry analysis. To estimate the number of microglia per brain, the percentage of $CD11b^+CD45^{lo}F4/80^+$ microglia was reported to the cell count recorded for the corresponding sample.

In vitro culture.

Organ culture: YS explants were placed into plates containing "Complete OptiMEM medium", i.e. OptiMEM with Glutamax (51985-042), 1% Penicillin-streptomycin, 0.1% β-mercaptoethanol (all from ThermoFisher) and 10% foetal calf serum (FCS; Hyclone). YS explants were maintained in organ culture at 37°C, 5% CO_2 for 1 day and are referred to as OrgD1-YS.

Clonogenic assay: Cells were plated in triplicate at $3x10^3$ cells/mL in Methocult® M3234 (StemCell Technologies Inc.) supplemented with Stem Cell factor (50ng/mL), EPO (3U/mL), IL-3 (10 ng/mL), all from Peprotech, IL-6 (10 ng/mL**,** a gift from Sam Burstein, Maryville IL, USA), CSF-1 (10 ng/mL) and TPO (10ng/mL, provided by Kirin Brewery, Tokyo, Japan). Cultures were maintained in a humidified incubator at 37°C, 5% CO_2 and colonies were scored at day 5 for primitive erythrocytes (Ery^P) and day 7 for the other progenitors types.

Flow cytometry, FACS-Gal, proliferation and apoptosis assays. See ***Table S1*** for the list of antibodies and dyes used throughout this study. CD31, F4/80, CD45, CD11b and cKit

antibodies were used to characterize myeloid cells. Dead cells were excluded by adding 1 μg/mL 7-amino actinomycin or DAPI (Sigma) before acquisition. Acquisitions were performed on a Canto II cytometer and cell sorting using FACS-Aria III or Influx (All from BD Biosciences). Data were analysed using FlowJo (Treestar) software.

FACS-Gal assay: this assay *(Fiering et al., 1991; Guo and Wu, 2008)* used as a reporter for Lyl-1 expression, allows the flow cytometry characterization of cells that display a β-Gal activity, using its fluorescent substrate (Fluorescein di-β-galactopyranoside (FDG) F1179; Molecular probe; Thermo Fisher).

Apoptosis assays: For apoptosis analysis, microglia were stained with anti-CD45-PECy7, anti-CD11b-APC-eFluor®780 and anti-F4/80-APC, washed and incubated with Annexin V-FITC. 7AAD was added before acquisition.

Proliferation assay (BrdU incorporation): Pregnant WT and *Lyl-1$^{LacZ/LacZ}$* females were injected with BrdU (10μM) 12 days after plug detection and sacrificed 2 hours later. Microglia were isolated and stained with CD45-PECy7, CD11b-APC-eFluor®780 and F4/80-PE antibodies. Cells were fixed, permeabilised and treated with DNase (1 hour at 37°C) according to kit instruction (BD Pharmingen No. 552598) and BrdU incorporation was revealed using anti-BrdU-APC.

Brain imaging.

E12 brain imaging: To assess microglia morphology in E12 embryos, the midbrain was dissected from *Cx3cr1$^{WT/GFP}$:Lyl-1$^{WT/WT}$* and *Cx3cr1$^{WT/GFP}$:Lyl-1$^{LacZ/LacZ}$* embryos, sectioned through the midline. After fixation in 4% paraformaldehyde (PFA) overnight at 4°C, whole midbrains were washed in phosphate-buffered saline (PBS)/0.1M glycine and incubated in 15% sucrose in PBS overnight at 4°C. Midbrains were then washed with PBS+0.1% Tween, and incubated with blocking buffer (PBS+10% FCS) for 90 min at room temperature (RT). Midbrains were subsequently immuno-labelled with F4/80-APC overnight at 4°C. After washing, they were incubated in PBS+DAPI (1 mg/mL) for 3 min at RT and washed. Finally, midbrains were placed in the central well of glass-bottom culture dishes (P35G-1.5-10-C; MatTek, USA) filled with PBS+10% FCS. After appropriate orientation of the sample, the well was covered with a 12 mm coverslip glass. Image stacks were collected using a Leica SP8 confocal microscope. Images were processed using Imaris x 64 (version 7.7.2; Bitplane) and Photoshop 8.0 (Adobe Systems, San Jose, CA) software. To unsure an unbiased choice of the

cells imaged, taking into account possible changes in cell distribution induced by *Lyl-1* deficiency, we always acquired cells in similar positions regarding the landmark set in the midbrain flat mount, as shown in ***Fig. S3b***.

Histology: Histology was performed as described recently *(Goldmann et al., 2015)*. Brains were removed and fixed in 4% buffered formalin. Samples were embedded in paraffin before staining with Hematoxylin-Eosin, Mac-3 for activated macrophages/microglia, CD3 for T cells, APP for indication of axonal damage and Iba-1 for microglia. For β-galactosidase staining, tissues were directly frozen unfixed in Tissue-Tek on dry ice. Cryosections were post fixed in 0.2% glutaraldehyde. Tissue sections were analysed using an Olympus BX-61 microscope in combination with the cell-P software (Olympus).

Immunofluorescence: After transcardial perfusion with PBS, brains were fixed in 4% PFA and embedded. Cryosections (14 µm) were obtained as described previously *(Blank et al., 2016).* Sections were blocked with PBS+5% bovine serum albumin and permeabilised with 0.1% Triton-X100 in blocking solution. Primary antibodies were added overnight at a dilution of 1:500 for Iba-1, 1:100 for CD68 and 1:250 for CD34 at 4°C. Secondary antibodies were added as follows: Alexa-Fluor®488: 1:500, Alexa-Fluor®555: 1:500 and Alexa-Fluor®568: 1:500 for 2h at RT. Nuclei were counterstained with DAPI. The various brain areas were analysed using a conventional fluorescence microscope (Olympus BX-61), and confocal images acquired with Fluoview FV 1000 (Olympus).

Three-dimensional reconstruction of microglia: Free-floating 30 µm cryosections from P42 brain were stained overnight with anti-Iba-1 (1:500) at 4°C, followed by Alexa-®568 secondary antibody (1:500) for 2h at 20–25°C. Nuclei were counterstained with DAPI. Imaging was performed on an Olympus Fluoview1000 confocal laser-scanning microscope using a 20×0.95 NA objective. *Z-stacks* with 1.1 µm steps in the *z* direction, 1,024×1,024 pixel resolution, were recorded and analysed using Imaris software (Bitplane).

Golgi-Cox Staining: The Golgi-Cox staining was performed as described before *(Zaqout and Kaindl, 2016)*. Freshly dissected brains were immersed in staining solution for 10 days and in protection solution for 7 days, all in the dark. Samples were embedded in 2% agarose and coronal sections (300µm) were cut on a vibratome. For staining, all sections were incubated in 16% ammonia solution to develop the impregnation, fixed in 5% sodium thiosulfate, dehydrated in ethanol, cleared in xylol and mounted on slides. To examine spine distribution, the first 40–70 µm of randomly chosen first-order branches of dendrites from pyramidal

neurons in the anterior cingulate cortex were imaged.

RT-qPCR analyses. Total RNA was extracted from sorted $CD11b^{+}F4/80^{+}CD45^{low}$ microglia using Trizol (ThermoFisher). After cDNA synthesis using a SuperScript™ VILO™ Master Mix reverse transcriptase (Invitrogen), quantitative PCR was performed using SYBR Premix Ex TaqII (Tli RNase H Plus, Takara Bio). Reference genes were *Actin*, *Hprt* and *Tubulin*. Gene expressions were normalized to the value obtained from E12 WT microglia and relative gene expression levels were determined by the ΔΔCt method. Gene expression was considered undetectable if Ct values were >35 cycles. The sequences of the primers used are provided in ***Table S2.***

RNA-sequencing. Total RNA was extracted from FACS sorted microglia cells using Picopure RNA extraction kit (Life Technologies) according to manufacturer's protocol. The SMARTer Ultra Low Input RNA Kit for Sequencing v4 (Clontech Laboratories, Inc., Mountain View, CA, USA) was used to generate first strand cDNA from 500 to 750 pg total RNA. Double stranded cDNA was amplified by LD PCR (11 cycles) and purified via magnetic bead clean-up. Library preparation was carried out as described in the Illumina Nextera XT Sample Preparation Guide (Illumina, Inc., San Diego, CA, USA). 150 pg input cDNA were tagmented (tagged and fragmented) by the Nextera XT transposome. The products were purified and amplified via a limited-cycle PCR program to generate multiplexed sequencing libraries. For the PCR step 1:5 dilutions of index 1 (i7) and index 2 (i5) primers were used. The libraries were quantified using the KAPA SYBR FAST ABI Prism Library Quantification Kit (Kapa Biosystems, Inc., Woburn, MA, USA). Equimolar amounts of each library were pooled, and the pools were used for cluster generation on the cBot with the Illumina TruSeq SR Cluster Kit v3. The sequencing run was performed on a HiSeq1000 instrument using the indexed, 50 cycles single-read (SR) protocol and the TruSeq SBS v3 Reagents according to the Illumina HiSeq 1000 System User Guide. Image analysis and base calling resulted in .bcl files, which were converted into fastq files with the CASAVA1.8.2 software. Library preparation and RNA-seq were performed at the Genomics Core Facility "KFB - Center of Excellence for Fluorescent Bioanalytics" (University of Regensburg, Regensburg, Germany; www.kfb-regensburg.de). Fastq Files were quality controlled using FastQC *(Andrews, 2010)* and reads were mapped to the GRCm38 mouse genome using the Star aligner *(Dobin et al., 2013)*. Read counts were obtained by the featureCounts package and differential gene expression analysis was performed using the limma/voom pipeline in R *(Law et al., 2014; Phipson et al., 2016; Ritchie*

et al., 2015). Heatmaps were generated using the R library heatmap.3 *(Zhao et al., 2014)*.

Accession numbers: All sequencing data are available at GEO Submission (GSE128378).

Behavioural tests.

Testing was performed between the hours of 18:00 and 20:00 corresponding to the beginning of the dark cycle for all assays. Behavioral testing was completed in the following order with one test per day: Repet. Behavior, 3 chambers test, EPM, NOR, olf. avoidance, FST.

Forced swim test (FST): FST was used to assess depressive-like behaviour in mice at P42 as previously described *(Blank et al., 2016)*. In brief, a glass transparent cylinder (height: 18cm, diameter: 19cm) was filled with water (~25 °C) up to 12 cm. Mice were placed in the centre of the filled cylinder and the behaviour was recorded for 10 min for each mouse used in the study. The time of swimming activity was interrupted when animals were passive and afloat. A passive behaviour is considered as sign of helplessness and despair. The first 2min of recording were regarded as an acclimation period, whereas subsequent 8 minutes were evaluated for immobility as a sign of depressive-like behaviour *(Porsolt et al., 1977)*.

Elevated plus maze (EPM): EPM was used to assess the anxiety-like phenotype. The platform consisted of 4 cross-aligned 6 cm wide and 30 cm long arms, with two arms on the same axis enclosed in 30 cm high walls. The EPM platform was elevated 50 cm from its base. The EPM test relies on a basic conflict between exploring a novel area and aversion to an open space. A decrease in time spent in open area (non-walled arms of elevated plus maze) is considered as a sign of increase in anxiety-like behaviour in mice. The anxiety-like behaviour (time spent on open arms) was monitored for 5 min in the EPM and analysed with the movement-tracking software *Biobserve* (*Viewer 2*, BIOBSERVE GmbH, Bonn, Germany).

Repetitive behaviour: Self-grooming behaviour was examined by placing mice in a clean empty cage. They were left for habituation for 10min and consecutively video-recorded for 10 min. Cumulative time spent in full-body grooming was measured with a stopwatch.

Three-chamber social interaction test: Mice were tested for voluntary social interaction in a three-chamber apparatus. The arena was divided into left, middle and right chambers (20×40×22cm) by two semi-transparent partitions with a small rectangular opening (5×3cm) in the bottom centre, through which a test mouse could travel between the three chambers. A quarter cylindrical wired cage (radius: 10 cm, height: 10.5 cm) was placed at each back corner of the left and right chambers. A P42 test mouse was first placed in the centre of the

middle chamber and left to habituate for 10 min in the absence of stranger mice in the wired cages (empty–empty session). Subsequently, a stranger mouse was introduced into one of the two-wired cages. Then, the test mouse was placed in the centre of the middle chamber and allowed to freely explore all three chambers for 10 min (stranger–empty session). Finally, after a novel stranger mouse was placed in another wired cage that had served as the empty cage in the previous sessions, the test mouse was again allowed to freely explore for 10 min (familiar–stranger session). Movement of the test mouse was recorded by a charge-coupled device camera and analysed online with *Biobserve* (*Viewer 2*, BIOBSERVE GmbH, Bonn, Germany) tracking software. The open arena, partitions, wired cages and weights were cleaned with 70% ethanol and wiped with paper towels before the next trial. Time spent in close interaction with each wired cage was recorded.

Olfactory avoidance test: An olfactory avoidance test was performed as described previously *(Kaneko-Goto et al., 2013; Kobayakawa et al., 2007)* with some modifications. To habituate the mice to the experimental environment, individual mice were placed in a cage (31×25×12.5cm) identical to the test cage for 30min and then transferred to a new cage. In the trial, mice were transferred to the test cage, where a filter paper (2×2cm) scented with 40 µl of non-dehydrogenated 2,4,5-trimethylthiazole (nTMT; Tokyo Chemical) was introduced. This test was performed under the weak-light condition (<5 lux) and the test cage was divided into two halves. Avoidance times were measured during a 10min test period and defined by subtracting the time spent in the section with nTMT-scented filter paper from the time spent in the section without filter paper.

Novel object recognition test: To evaluate recognition memory, a novel object recognition test was performed as described previously *(Bevins and Besheer, 2006; Breton-Provencher et al., 2009)*. First, mice were familiarized with the test cage (31×25×12.5cm) for 10 min and then returned to their home cage. One hour later, in the habituation phase, two identical objects (metal nuts) were placed on both sides of the test cage. The time spent exploring each object was recorded for 10 min. We considered the animal to be exploring when its mouth, nose, or paws were in direct contact with the object. The mice were then returned to their home cages. 24 hours later, in the test phase, two different objects were presented: the familiar object and a novel object (metal bolt). The time exploring each object was recorded for 10 min. The two objects with distinct features were easily distinguishable from each other by non-olfactory cues such as vision or touch.

Resting state functional magnetic resonance imaging. Prior to rsfMRI experiments animals were anesthetized using 1.5% isoflurane (Forene; Abbvie Deutschland GmbH & Co. KG, Wiesbaden, Germany), in 1.2L oxygen/min and reducing respiratory rate to 60–80 breaths per minute. Preparation for the scans included stereotactic fixation of the head, attachment of physiological monitoring devices covering ECG, respiration rate, body core temperature and pO_2 and placing a subcutaneous (s.c.) catheter. To induce sedation, a medetomidine (MD, Domitor, Pfizer, Karlsruhe, Germany) bolus s.c. injection of 0.3 mg per kg body weight in 100 µl 0.9% sodium chloride solution was applied. The animals were then placed within the MRI system and 15 min after the MD bolus injection, a continuous s.c. MD infusion of 0.6mg per kg body weight at 200 µl per hour was applied to the animals while reducing the isoflurane concentration to 0.8%. This sedation scheme was kept constant throughout the rsfMRI sessions, which were started after the animals reached a stable condition. The total scanning time ranged from 60 to 70min. All acquisitions were performed with a 7 T small horizontal bore animal scanner (Biospec 70/20, Bruker, Ettlingen, Germany), a mouse head cryocoil (MRI CryoProbe, Bruker, Ettlingen, Germany) and ParaVision 5.1 (Bruker, Ettlingen, Germany). For rsfMRI data acquisition, a single shot Gradient Echo based echo planar imaging (EPI) sequence was used with an echo time (TE) of 10 ms and a repetition time (TR) of 1700 ms. The whole mouse brain (excluding the cerebellum and olfactory bulb) was covered using 12 axial slices with a slice thickness of 0.7 mm, a field of view (FOV) of 19.2×12.0 mm^2 and an acquisition matrix of 128×80. Thus, obtained image resolution was 0.15×0.15×0.7 mm^3. 200 volumes were recorded with slice acquisition in interlaced fashion for each run. High resolution T2-weighted morphological reference images were acquired using a RARE sequence (TE/TR=50ms/6514ms), 48 slices of 0.3 mm thickness, sampling in interlaced fashion, and 2 averages at RARE factor of 4. An acquisition matrix of 256×196 and a FOV of 1.3×1cm^2 led to a spatial resolution of 0.051×0.051×0.3 mm^3.

Independent component, functional connectivity and correlation analyses. Independent component analysis of co-registered/normalized rsfMRI data using GIFTv3.0b (http://mialab.mrn.org/ *(Calhoun et al., 2001)*) with the infomax algorithm and ICASSO (20 repetitions) revealed 50 independent components (ICs). Stable ICs (Iq>0.85, i.e. 44 ICs) showing substantial overlap with brain regions of interest as defined by the Allen Mouse Brain Atlas *(Lein et al., 2007)* were included in partial correlation analysis (16 IC's time

courses, spearman rank correlation *(Mechling et al., 2016)*, p>0.05) to find their functional connectivity (FC) matrix. To find the voxel wise whole brain correlation of the ACC, we used the IC representing the ACC as a seed region for a whole brain seed-to-voxel partial correlation (spearman rank correlation, |r|>0.1).

Single-unit and LFP recording. WT and *Lyl-1*$^{LacZ/LacZ}$ (8-14 week old) were anesthetized with isoflurane (induction: 3%, maintenance: 1-1.5%). A craniotomy was performed to implant a fixed stereotrode array (3 mice), a tetrode microdrive (2 mice), or a 32-channel silicon probe (Cambridge Neurotech, 3 mice) mounted on a microdrive into the anterior cingulate cortex (stereotaxic coordinates: 0.7 mm anterior, 0.38-0.45 mm lateral and 1.5-1.9 mm ventral of bregma). Two screws in the bone over the cerebellum served as ground and reference. Post-operative analgesia was achieved by s.c. injection of buprenorphine (0.05-0.1 mg/kg body weight, 3x daily for 2 days) in combination with carprofen (4-5 mg/kg body weight, every 24h for 2 days).

After at least 5 days of recovery, recording commenced using a 32-channel tethered acquisition system (RHD2000, Intan Technologies) routed through a commutator to ensure free movement of the animals. Wide-band neural signals were recorded at 30 kHz while the animal explored a novel environment (square box or elongated open arena) for 10-20 min. In case of microdrives, the electrodes were slowly advanced by ~200 µm after the recording session to establish recordings from a new set of units. Single-unit activity was acquired from 6 mice (3 WT, 3 *Lyl-1*$^{LacZ/LacZ}$) during 11 sessions in total. Individual sessions were separated by one day. From an additional set of one WT and one *Lyl-1*$^{LacZ/LacZ}$ mouse, we recorded LFPs without single-unit acquisition.

After recording, the animals were intracardially perfused with ice-cold PBS (~1 min) followed by 4% PFA (~10 min). Frontal sections (100 µm) were taken with a vibratome, stained with 4', 6'-diamino-2-phenylindole, and analysed using an epifluoresence microscope to visualize electrode locations. Only animals with electrode positioning in the cingulate cortex 1 or 2 were accepted for analysis.

Spike sorting and data analysis. Local referencing was obtained by subtracting a channel without apparent unit activity or a common average of 10 randomly chosen channels from each electrode. Epochs containing movement artefacts were visually identified and discarded

before further analysis. The signals were band-pass filtered (0.3-6 kHz) for spike detection. Automated clustering was performed using Mountainsort *(Chung et al., 2017)* with automated cluster curation (settings: isolation >0.95, noise overlap <0.05, peak noise <30). Clusters containing spikes within a 1ms refractory period were considered multi-unit activity and not analysed further. To distinguish pyramidal units from GABAergic neurons, we quantified the trough-to-peak duration, asymmetry index defined as the difference in the height of the peak following the trough and the peak preceding the trough divided by the sum of both measures, and firing frequency for each isolated unit *(Sirota et al., 2008).* Plotting these three parameters resulted in two apparent clusters, which were visually separated in putative pyramidal cells and GABAergic interneurons. Action potentials of putative pyramidal cells (n=139) displayed a long trough-peak duration (median: 0.48ms, SD: 0.10ms), negative asymmetry index (median: 0.38, SD: 0.20) and low average firing rate (median: 4.2Hz, SD: 12.4Hz), significantly different from putative GABAergic interneurons (n=12) with narrower spike waveforms (median trough-peak duration: 0.22ms, SD: 0.04ms, $p=7*10^{-8}$, Mann-Whitney U-test), larger asymmetry index (median: 0.21, SD: 0.16, $p=1*10^{-7}$, Mann-Whitney U-test), and higher firing rate (median: 32.8Hz, SD: 24.2Hz, $p=3*10^{-7}$, Mann-Whitney U-test). To corroborate our classification, we identified excitatory synaptic connections from cross-correlograms (binwidth 1ms) of the spike trains of simultaneously recorded single units *(Dupret et al., 2013)*. To account for random cofiring, we defined a threshold as exceeding three standard deviations of the time-lag period ranging from -50 ms to -10 ms. An excitatory interaction was scored if cofiring in one of the 1-3 ms timelag bins exceeded the threshold. Excitatory connections (n=35) were only detected for single units of the putative pyramidal neuron cluster, confirming our classification method ***(Figure S5)***. GABAergic interneurons were not analysed further due to their low number in the recorded sample. Average spike rate was statistically compared between groups using a non-parametric Mann-Whitney U-test. Oscillatory power was assessed from the LFP recorded on one channel. Power spectral density was obtained using the *psd* function of the Python package matplotlib.mlab with a window size of 500 ms (overlap 333 ms) zero-padded to 10s. To determine spike-oscillation coupling, the raw signal was filtered in the theta frequency range (4-12Hz, 2nd-order Butterworth filter) applied in forward and reverse direction. The instantaneous phase of the theta wave at each time point of spiking was extracted using Hilbert transformation. Oscillation coupling was tested using Rayleigh's test for circular

uniformity applied to the phase angle distribution ($p<0.05$). To quantify the strength of spike-oscillation coupling, we measured pairwise phase consistency *P (Vinck et al., 2010)* as $P = \frac{\pi - 2D}{\pi}$ (1), where *D* is the pairwise circular distances $D = \frac{2}{n(n-1)} \sum_{i=1}^{n-1} \sum_{k=(i+1)}^{n} d(\theta_j, \theta_k)$ (2) where *d* is the angular distance between the phase angle of two spikes, *Θj* and *Θk* are the theta phase angles of spikes *j* and *k* of a neuron, and *N* is the total number of spikes. All single-unit and LFP analysis was performed in Python2.7.

Statistical analysis. Unless otherwise stated, data were analyzed using GraphPad six statistical software. We first tested the distribution of the data with the Shapiro-Wallis test for normality. Data that were normally distributed was analyzed using an unpaired two-tailed *t*-test for analysis of experiments involving two groups. Data with a non-normal distribution were analyzed by using the non-parametric test Mann-Whitney when comparing two groups. Mean effects ± 95% confidence intervals were derived to reflect the differences that were consistent with statistically meaningful differences. Statistical tests were performed using Prism six software (GraphPad Software). Measurements from different mice were considered biological repeats to determine sample size. Data points were considered outliers and excluded if they were two standard deviations away from the mean. Statistical significance is indicated with the exact p-value or as *p < 0.05, **p < 0.01, and ***p < 0.001.

Acknowledgements.

The authors thank Julien Y. Bertrand for critical reading of the manuscript. We are grateful to the staff of Animal Facility at Gustave Roussy (PFEP, UMS AMMICa UMS 3655/US23, directed by Dr P Gonin) and at Freiburg University for animal care, the staff of the imaging facility at Gustave Roussy (PFIC, UMS AMMICa UMS 3655/US23, directed by Corinne Laplace-Builhe).

Author Information.

The authors declare no competing financial interests.

Correspondence should be addressed to I.G. (Isabelle.Godin@gustaveroussy.fr) or M.P. (marco.prinz@uniklinik-freiburg.de).

SUPPLEMENTARY INFORMATION

Supplementary Figures

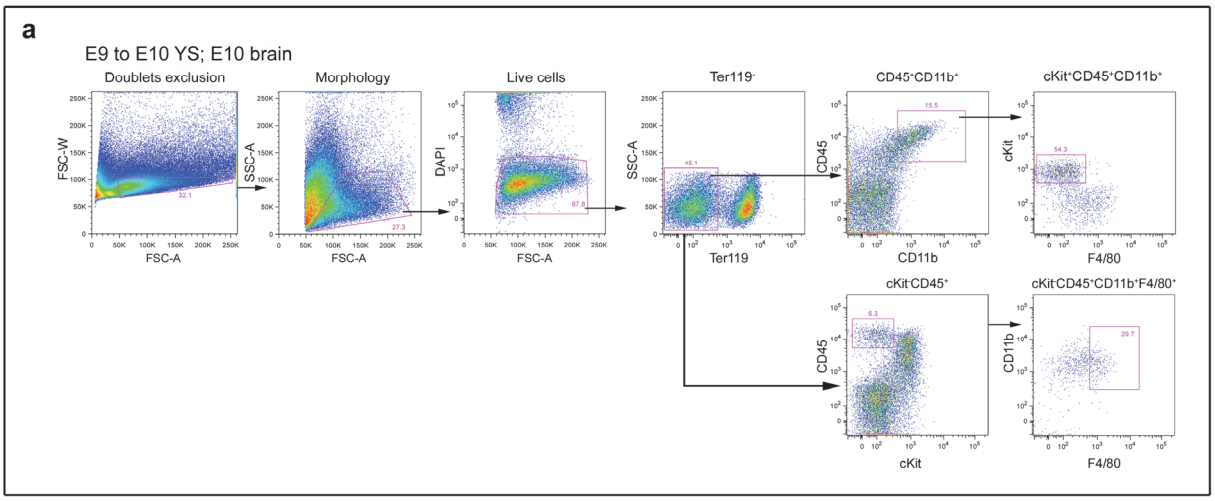

Supplementary Figure 1: Gating strategy used for embryonic MΦ progenitors analyses.
a. Gating strategy used to analyse FDG^{+}/Lyl-1^{+} expression in MΦ progenitors from E9 and E9.5 YS from WT, *Lyl-1$^{WT/LacZ}$* and *Lyl-1$^{lacZ/LacZ}$* embryos ***(Fig.1c)*** and in MΦ progenitors and mature MΦ from E10 WT and *Lyl-1$^{lacZ/LacZ}$* YS and brain ***(Fig. 1d)***.

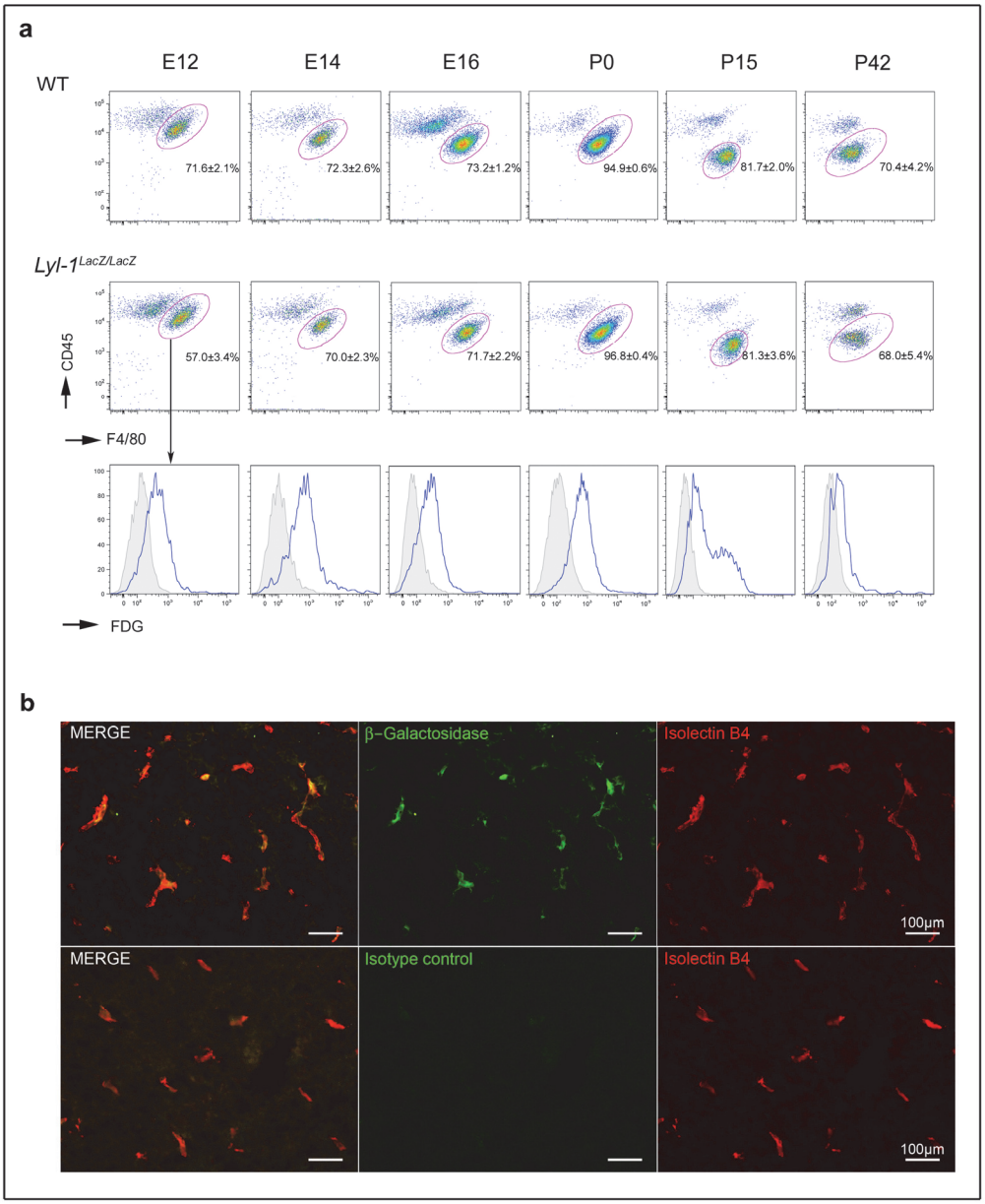

Supplementary Figure 2: Microglia express Lyl-1 from embryonic stages to adulthood.

b. FDG/Lyl expression in WT and *Lyl-1*$^{LacZ/LacZ}$ brain from E12 to adult stages. In *Lyl-1*$^{LacZ/LacZ}$ mutants, the entire microglia population is FDG^{+}/Lyl-1^{+}, but Lyl-1 expression level decreases in the adult, with a clear transition occurring at P15. Plain grey histograms indicate non-specific background β-Gal activity/FDG levels in WT samples.

c. β-Galactosidase immuno-labelling of the brain of E14 *Lyl-1*$^{WT/LacZ}$ embryos. Top: Microglia, characterised by Isolectine B4 expression (red), also display β-Gal/Lyl-1 expression (green). Lower panel shows the β-Gal isotype control.

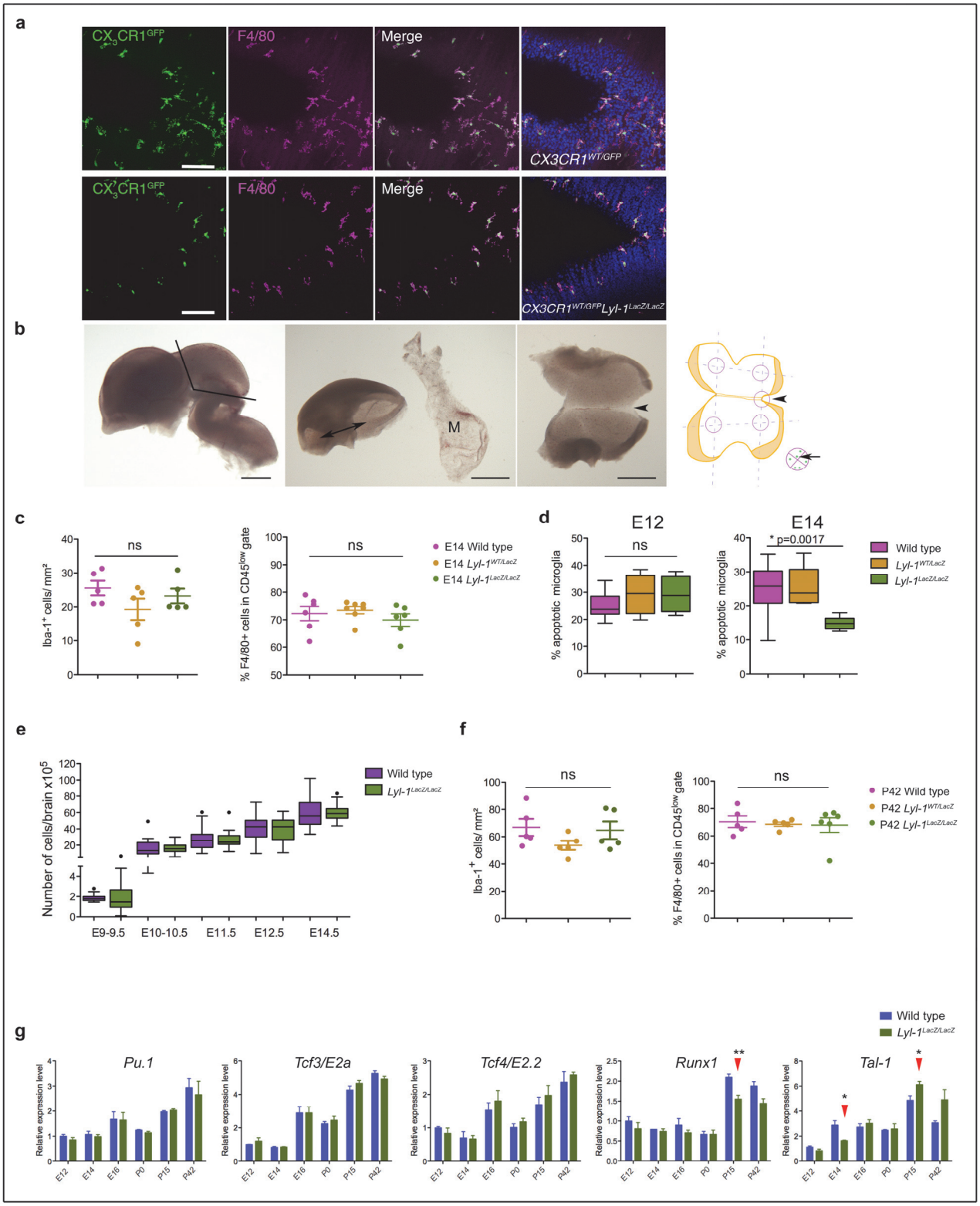

Supplementary Figure 3: Lyl-1 deficiency leads to transient reductions of the microglia pool at E12 and P0-P3.

a. Confocal imaging of the midbrain of *Cx3cr1*$^{WT/GFP}$ and *Cx3cr1*$^{WT/GFP}$*:Lyl-1*$^{LacZ/LacZ}$ embryos at E12 pointed to morphological changes in double mutant microglia. Microglia were identified by *Cx3cr1*-driven GFP expression and F4/80 immuno-staining (Bar=100 µm).

b. The midbrain was dissected from *Cx3cr1*$^{WT/GFP}$*:Lyl-1*$^{WT/WT}$ and *Cx3cr1*$^{WT/GFP}$*:Lyl-1*$^{LacZ/LacZ}$ embryos (left). After removal of the meningeal layer (M), the midbrain was sectioned along the midline (middle left) and flat mounted (middle right). To unsure an unbiased choice, cells were always acquired in the

same location (right) using the midline (arrowhead) and lateral thickening as landmarks, the cell closest to the middle of the frame (arrow) being acquired (Bar=1mm).

c. Counting of Iba-1-labelled microglia cell on midbrain sections (left) and cytometry analyses of $CD11b^{+}F4/80^{+}CD45^{low}$ microglia from Percoll purified brain (right) show no genotype-related difference in microglia amount at E14.

d. Annexin V-7AAD quantification of apoptosis levels in $CD11b^{+}F4/80^{+}CD45^{low}$ microglia at E12 and E14. No significant genotype-associated modification of microglia apoptosis level was observed in E12 microglia (right). At E14 (left), the apoptosis level was significantly lower in *Lyl-1*$^{LacZ/LacZ}$ compared to WT and *Lyl-1*$^{WT/LacZ}$ brains, which may account for the recovery of microglia population size after E12.

e. *Lyl-1* deficiency does not lead to modifications of cells recovery from E9 to E14 whole brains.

f. In adults, both Iba-1^{+} cell counting on midbrain sections (left) and cytometry analyses (right) evidenced no genotype-associated difference in microglia pool size in WT and *Lyl-1*$^{WT/LacZ}$ brains.

g. Quantitative RT-PCR analyses: $CD11b^{+}F4/80^{+}CD45^{low}$ microglia was isolated at sequential development stages. Bar graphs show the kinetic of expression of a selected set of genes that are not significantly modified in *Lyl-1* mutants at E12 and P0-P3, but may be so at post-natal stages. Gene expression was normalized to the mean expression value in WT E12 microglia (n=3). Error bars indicate s.e.m.

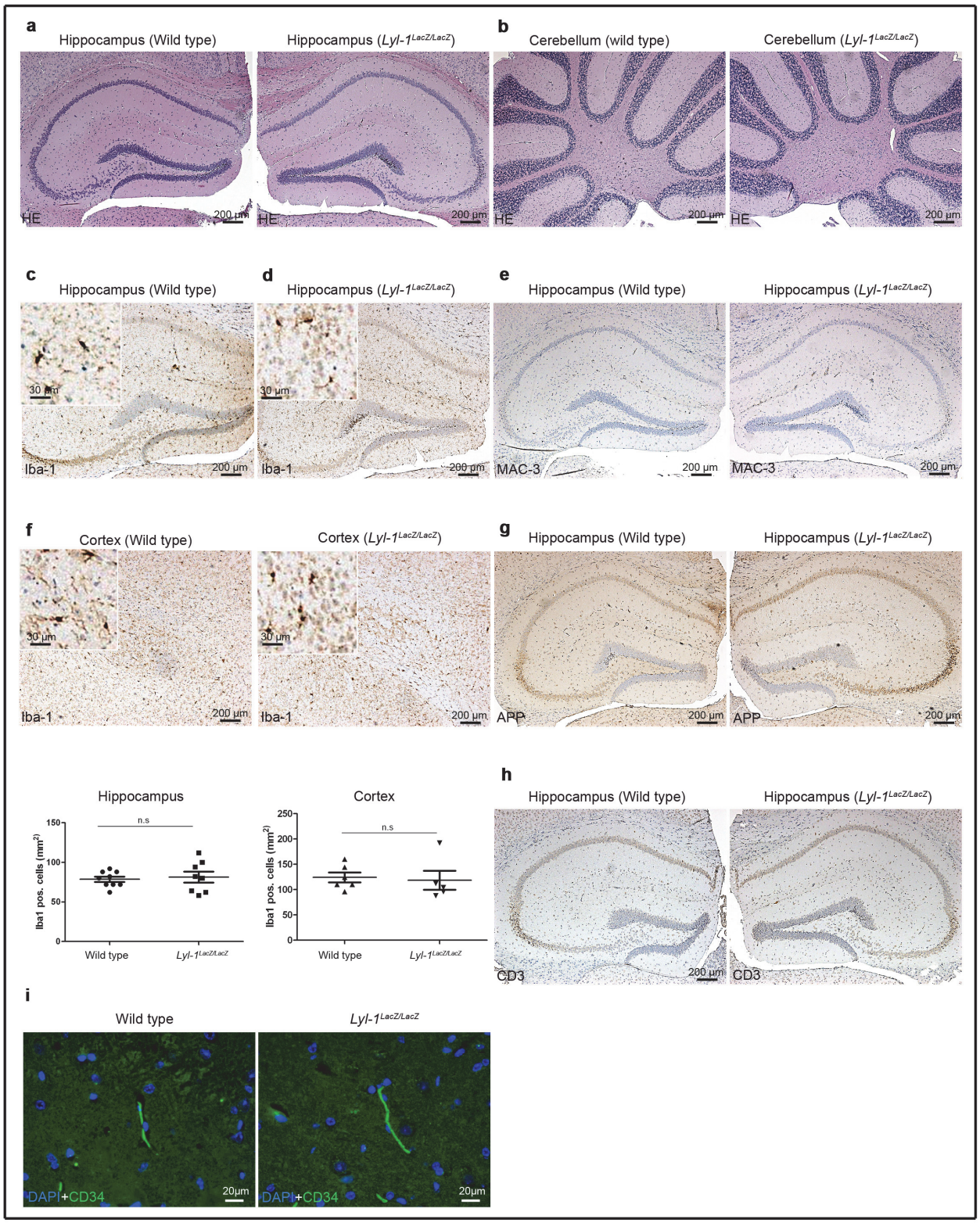

Supplementary Figure 4: Histological analysis of WT and Lyl-1-deficient brain sections.
a-i Histological staining of brain sections from adult WT (left) and *Lyl-1*$^{LacZ/LacZ}$ (right) mice. Overall structure of hippocampal dentate gyrus (DG) (a) and cerebellum (b) revealed by Haematoxylin-Eosine (HE) staining. Iba-1 staining of microglia in the DG (c, d) and cortex (f). Number of Iba-1^{+} ramified parenchymal microglia in the DG and cortex (f: lower panel). Each symbol represents data from one mouse. Four to five sections per mouse were examined. Iba-1^{+} microglia quantification is expressed as mean ± s.e.m. Significant differences were determined by an unpaired *t* test (n.s., non-significant). MAC-3 staining of MΦ in DG (e). Amyloid precursor protein (APP) staining for axonal damage (g). CD3

staining of T lymphocytes (h). Labelling of $CD34^+$ endothelia (green) and nuclei by DAPI (blue) in the cortical area (h). Labelling of endothelia (CD34, green) and nuclei (DAPI, blue) in the hippocampal area (i).

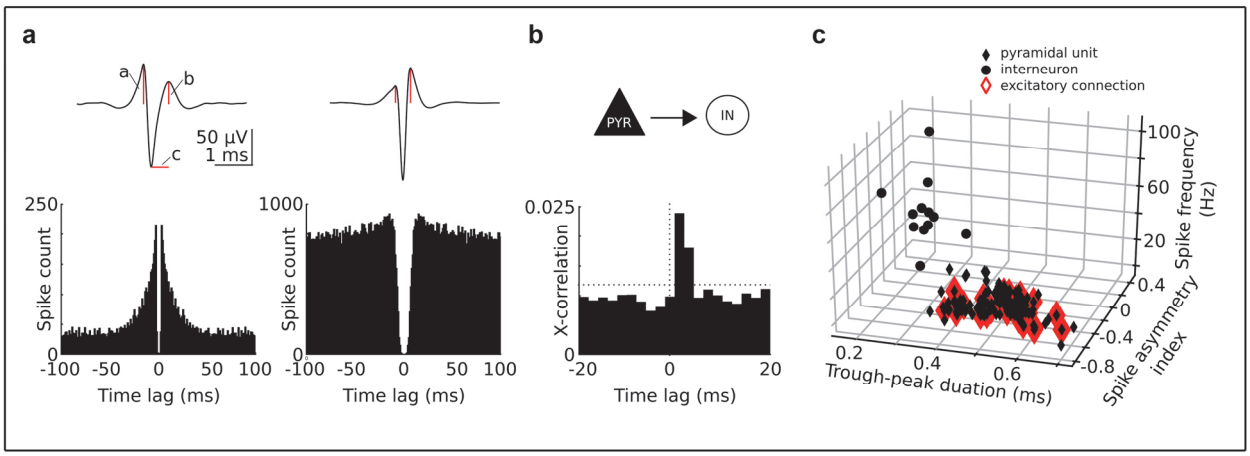

Supplementary Figure 5: Identification of pyramidal units in awake mice.

a. Filtered waveforms (0.8-5 kHz, top) and auto-correlograms (bottom) of a putative pyramidal neuron (left) and interneuron (right). To separate both neuron types based on spike shape, two measures were used: Asymmetry index defined as (b-a)/(b+a) and trough to peak latency.

b. Cross (X)-correlation of spike trains of two neurons reveals a sharp peak in spike transmission probability at short (~1-3 ms) latency, indicative of an excitatory synaptic connection.

c. Classification of recorded neurons as pyramidal and interneuronal, based on spike shape measures and firing frequency. Note that excitatory synaptic interactions originated only from the putative pyramidal cluster (bottom right), confirming their glutamatergic nature.

Supplementary table 1: list of antibodies and fluorescent stains used throughout this study

Antibody name	***Clone***	***Supplier/Reference***	***Fluorochrome/ Chromogen***
Ter119	TER-119	Biolegend; 116205 Biolegend; 116208 eBioscience 17-5921-82	FITC PE APC
Mac3	M3/84	BD Pharmingen; 550292	DAB
CD3	CD3-12	Biorad; 1477	DAB
APP (amyloid precursor protein)	22C11	Merck; 348	DAB
β-galactosidase	Polyclonal	Abcam; 9361	
F4/80	BM8 CI:A3-1 BM8 BM8	eBioscience; 53-4801-82 Biolegend; 122606 eBioscience; 12-4801-82 Biolegend ; 123116	Alexa fluor 488 FITC PE APC
GR-1	RB6-8C5 RB6-8C5 RB6-8C5	BD-Pharmingen; 553127 Biolegend; 108416 Biolegend , 108437	FITC PE-Cy7 BV510
CD45	30-F11 30-F11 30-F11 30-F11	BD-Pharmingen; 553081 BD-Pharmingen; 553082 eBioscience; 25-0451-82 Biolegend; 103124	PE PE-Cy5 PE-Cy7 Alexa fluor 647
CD31	MEC13.3 390 MEC13.3 MEC13.3 MEC13.3	Biolegend; 102514 Biolegend; 102408 Biolegend; 102419 Biolegend; 102516 BD-Pharmingen; 583089	Alexa fluor 488 PE PE-Cy5.5 Alexa fluor 647 BV510
Iba-1	NCNP24	WACO, Japan; 019-19741	Purified
CD68	clone FA-11	Biolegend; 137001	Purified
CD34	clone MEC14.7	Biolegend; 19321	Purified
CKit	2B8 2B8 2B8	Biolegend; 05824 BD-Pharmingen; 553358 Biolegend ; 105825	Alexa fluor 488 APC APC-Cy7
CD11b	M1/70	eBioscience; 45-0112-82 Biolegend; 101215 Biolegend; 101212 eBioscience; 47-0112-82	PE-Cy5.5 PE-Cy7 APC APC-eFluor 780
Sca-1	D7	Biolegend; 108113	PE-Cy7
Annexin V	NA	Biolegend; B206040	FITC
Anti-Brdu	B44	BD-Pharmingen; 51-23619L	APC
7AAD	NA	BD-Pharmingen; 51-68981E	Dye

Supplementary Table 2: Primers used in this study

Gene		***Sequence***
Actin	Primer forward:	5’- CTTCTTTGCAGCTCCTTCGT-3’
	Primer reverse:	5’- ATCACACCCTGGTGCCTAG-3’
Hprt	Primer forward:	5’- TGATTATGGACAGGACTGAAAGA-3’
	Primer reverse:	5’- AGCAGGTCAGCAAAGAACTTATAG-3’
Tubulin	Primer forward:	5’- GGGTGGAGGCACTGGCT-3’
	Primer reverse:	5’- GTCAGGATATTCTTCCCGGATCT-3’
c-Maf	Primer forward:	5'- CTGCCGCTTCAAGAGGGTGCAGC -3'
	Primer reverse:	5'- GATCTCCTGCTTGAGGTGGTC -3'
Lyl-1	Primer forward:	5'- TGGACTGACAAACCTGACCA-3'
	Primer reverse:	5'- TGGACCCCACGGATAGAATG-3'
Tal-1/Scl	Primer forward:	5'- CATGTTCACCAACAACAACCG-3'
	Primer reverse:	5'- GGTGTGAGGACCATCAGAAATCTC-3'
Runx1	Primer forward:	5'- CTCCGTGCTACCCACTCACT-3'
	Primer reverse:	5'- ATGACGGTGACCAGAGTGC-3'
Meis1	Primer forward:	5'-TGAAGTAGGAAGGGAGCCAG-3’
	Primer reverse:	5'-GCCTACTCCATCCATACCCC-3’
Lmo2	Primer forward:	5'-ATGTCCTCGGCCATCGAAAG-3’
	Primer reverse:	5'-CGGTCCCCTATGTTCTGCTG-3’
PU.1	Primer forward:	5'- GCTATACCAACGTCCAATGCA-3'
	Primer reverse:	5'-TGTGCGGAGAAATCCCAGTA-3'
Tcf3/E2A	Primer forward:	5'-GGGCTCTGACAAGGAACTGA-3’
	Primer reverse:	5'-AGTCCTGAGCCTGCAAACTG-3’
Tcf4/E2.2	Primer forward:	5'-GCCTCTTCACAGTAGTGCCAT-3’
	Primer reverse:	5'-TCCCTGTTGTAGTCGGCAGT-3’
Csfr1	Primer forward:	5'-GCAGTACCACCATCCACTTGTA-3'
	Primer reverse:	5'-GTGAGACACTGTCCTTCAGTGC-3'
Cx3cr1	Primer forward:	5’ - AGTTCCCTTCCCATCTGCTC-3’
	Primer reverse:	5’ - GCCACAATGTCGCCCAAATA-3’
Irf8	Primer forward:	5'- CGGGGCTGATCTGGGAAAAT-3'
	Primer reverse:	5'- CACAGCGTAACCTCGTCTTC-3'
CMyb	Primer forward:	5’-AGCGTCACTTGGGGAAAACT-3’
	Primer reverse:	5’- AGTCGTCTGTTCCGTTCTGT-3’

2.2 RNA-seq analysis of YS MΦ progenitors

Aim of the study:

From our previous results, we found that Lyl-1 appears to be a specific marker for $M\Phi^{Prim}$ progenitors in the YS and that Lyl-1 disruption alters the development of $M\Phi^{Prim}$ progenitors as well as microglia development, leading in the adult to impaired social interactions. We aimed to determine firstly the specific features of $M\Phi^{Prim}$ progenitors and secondly to assess the function of Lyl-1 during the development of these progenitors. To do so, we applied RNA-seq analysis (see material and methods chapter) on sorted YS MΦ A1 progenitors ($CD45^+CD11b^+cKit^+$) at E9, when the YS only contains these $M\Phi^{Prim}$ progenitors and at E10, when the YS contains both $M\Phi^{Prim}$ progenitors and $M\Phi^{T\text{-}Def}$ progenitors from the transient definitive wave.

Results:

General information

The MA plot showed the expression distribution of whole transcriptome data **(Supplemental Figure 1)**. The samples exhibited similar expression scale, mainly ranging from 1e-01 to 1e05. The PCA plot **(Figure 1)** pointed to a clear-cut separation of E9 samples from E10 samples, irrelevant to their genotype. Furthermore, WT and *Lyl-1*$^{lacZ/lacZ}$ samples were also distinct from each other. The clear separation of E9 and E10 samples may reflects the differences between $M\Phi^{Prim}$ progenitors and $M\Phi^{T\text{-}Def}$ progenitors, which are present at higher levels in E10 YS, possibly together with a developmental maturation of $M\Phi^{Prim}$ progenitors along the MΦ lineage.

I will present the results in two parts. The first will deal with the features that are different in E9 vs. E10 YS MΦ progenitors, first in a WT context and next in *Lyl-1*$^{LacZ/LacZ}$ mutants. In the 2nd part, I will discuss the function of Lyl-1 in the regulation of MΦ progenitors development by analyzing the gene modifications observed at E9 (*Lyl-1*$^{lacZ/lacZ}$ vs. WT), as well as at E10.

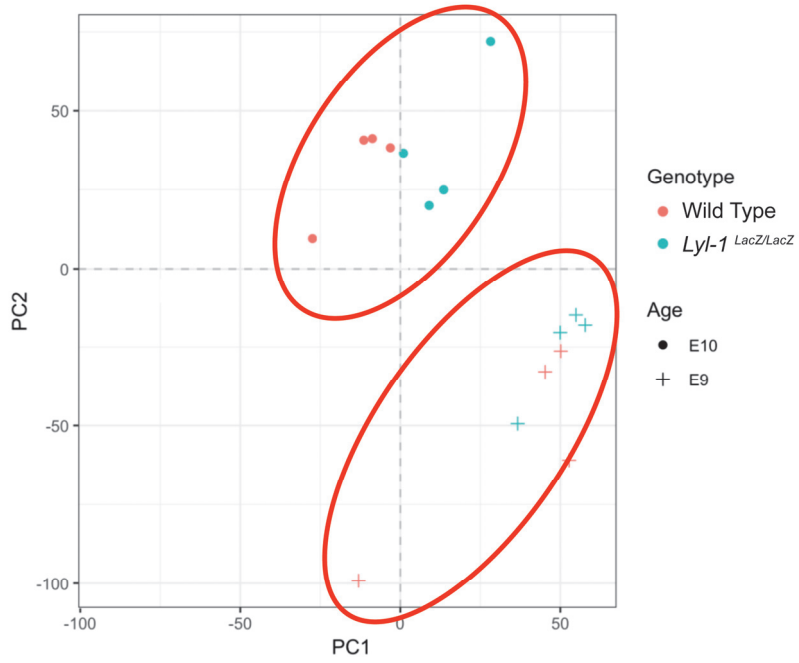

Figure 1: General information of PCA.
PCA plot of E9 and E10 MΦ A1 progenitors. Red color represents *Lyl-1*$^{lacZ/lacZ}$ samples, Blue represents WT sample; + represents E9 and solid circle represents E10.

2.2.1: E9 and E10 MΦ progenitors display marked differences in gene expression

The Volcano plot **(Figure 2A)** indicates that WT E9 and E10 MΦ A1 progenitors differ by the expression of 726 genes. Amongst these differentially expressed genes (DEG), 176 were up-regulated at E9 and 550 at E10. The heatmap **(Figure 2B)** showed that E9 and E10 progenitors segregated into two distinct groups, indicating a good homogeneity of the replicates.

We first compared our data with data obtained by other scientists also investigating hematopoietic cells development from the early YS. Mass *et al.* identified the gene signature for EMP and embryonic MΦ through bulk RNA-seq data comparisons (Mass et al., 2016). A gene signature of 91 genes was obtained from CD45^{low} cKit^{+} AA4.1^{+} EMPs purified from E9-E10.25 YS and FL. The signature for embryonic MΦ (73 genes) was obtained from CD45^{+}CD11b^{+}F4/80^{+} cells collected from the YS, head, liver, limbs and caudal part of E10.25-E10.5 embryos.

We thus overlapped the differentially expressed genes (DEGs) characterizing WT E9 and E10

WT MΦ progenitors with both the EMPs and MΦ signatures obtained in this study using the Venny software. Interestingly, none of the genes enriched in E9 MΦ progenitors were present in the EMPs **(Figure 2C)** or MΦ **(Figure 2D)** signatures. In contrast, 25 DEGs enriched in WT E10 MΦ progenitors overlapped with this EMPs signature, accounting for 27.5% of this signature. At E10, 26 enriched DEGs were found within Mass *et al.* mature MΦ signature, which accounts for 35.6% of this signature.

These results suggest that EMP-derived E10 MΦ A1 progenitors retain some EMPs signature, while already upregulating genes that will characterize their mature progeny. But, we must also consider that a contamination our E10 MΦ A1 progenitors samples with EMP if they express CD11b. This possibility has to be considered for EMP because CD11b has been shown to be expressed outside the MΦ lineage during development, for example in HSC (Hills et al., 2011; Morrison et al., 1995). Nevertheless, the main results here is that at E9 MΦ progenitors are clearly distinct from both EMP and MΦ progenitors from E10 YS, which reflects their primitive status.

Using Gene Set Enrichment Analysis (GSEA) to compare E9 and E10 WT MΦ progenitors, we found that E10 MΦ progenitors samples were enriched in genes targeted by the transcription factor GATA1 **(Figure 2E)**. *Gata1* is an important regulator of the generation and differentiation of erythroid cells during development, as mentioned in **chapter1.4.3**. Surprisingly, genes related to erythrocyte development appeared overexpressed in E10 WT samples, such as *Gata1*, *Gata2* and *Klf1*, and so were hemoglobin coding genes, both embryonic (*Hbb-bh1*, *Hba-x,* and *Hbb-y*) and definitive (*Hba-a2*, *Hba-a1,* and *hbb-bt*) ones **(Figure 2C)**.

Previous research extensively focused on the mutual antagonism between *Gata1* and *Pu.1/Spi1* during the commitment erythroid and MΦ lineages (see (Graf and Enver, 2009) for a review). *Gata1* is required for the generation of erythroid cells and the forced expression of *Gata1* in myeloid cells is sufficient to reprogram them into erythroid cells. Reversely, the enforced expression of *Pu.1/Spi1* in an erythroid-megakaryocytic cell line could convert erythroid cells into myeloid ones by repressing *Gata1* (Graf and Enver, 2009). *Pu.1/Spi1* is absolutely required for the commitment and maturation of the myeloid lineage. Accordingly, our RNA-seq data showed that at both E9 and E10, *Pu.1/Spi1* exhibits a similar high expression level compared to *Gata1*, as indicated by their relative TPM (Transcripts per

Million Kilobases) expression levels. The higher expression of *Pu.1/Spi1* and low level of *Gata1* expression in E9 MΦ progenitors, compared to E10, may be related to the monopotent status of primitive MΦ progenitors, while E10 MΦ A1 progenitors may retain some gene expression pattern that characterize their EMP ancestor **(Figure 2G)**.

This is consistent with the observation from Monteiro *et al.,* who found that *Pu.1/Spi1* is highly expressed in the anterior lateral mesoderm (ALM) of zebrafish embryos, which gives rise to primitive macrophages (Herbomel et al., 1999) and that *Gata1* expression is inhibited by *Pu.1/Spi1* (Monteiro et al., 2011). In contrast, EMP that maintain both erythroid and myeloid lineage potentials (Graf and Enver, 2009), highly express both *Gata1* and *Pu.1/Spi1* (Bertrand et al., 2007; Monteiro et al., 2011).

Hemoglobin genes are traditionally thought to be exclusively expressed in cells from the erythroid lineage, but several data suggest that they may also be expressed by many other cell types such as epithelial cells (Straub et al., 2012), neurons (Biagioli et al., 2009) and MΦ (Liu et al., 1999; Matcovitch-Natan et al., 2016). Consistent with the higher expression level of embryonic hemoglobin genes found in MΦ progenitors at E10, Mass *et al.* also that *Hba-x*, *Hbb-bh1* and *Hbb-y* were highly expressed in E10.25-10.5 MΦ (Mass et al., 2016). Hagemeyer *et al.* also found that *Hba-x* and *Hbb-y* are highly enriched in embryonic F4/80^{hi} MΦ from all tissues, reflecting their common origin with erythrocytes from the EMP (Hagemeyer et al., 2016). Matcovitch-Natan *et al.* also showed through the bulk RNA-sequencing of YS MΦ, that *Hba-x* and *Hbb-y* were highly enriched in E10.5 to E13.5 MΦ. In contrast, the expression of these two genes was 10 times lower in early embryonic microglia (E10.5-E14.5) than in YS MΦ and no expression was detected in microglia at E16.5. These observation strongly suggest that microglia does not originate from the MΦ progenitors that express hemoglobin genes (Matcovitch-Natan et al., 2016). The expression of hemoglobin genes by MΦ progenitors from the YS at E10 and subsequent stages is thus clearly evidenced, but whether these genes are transcribed and play a role during MΦ development would requires further investigation.

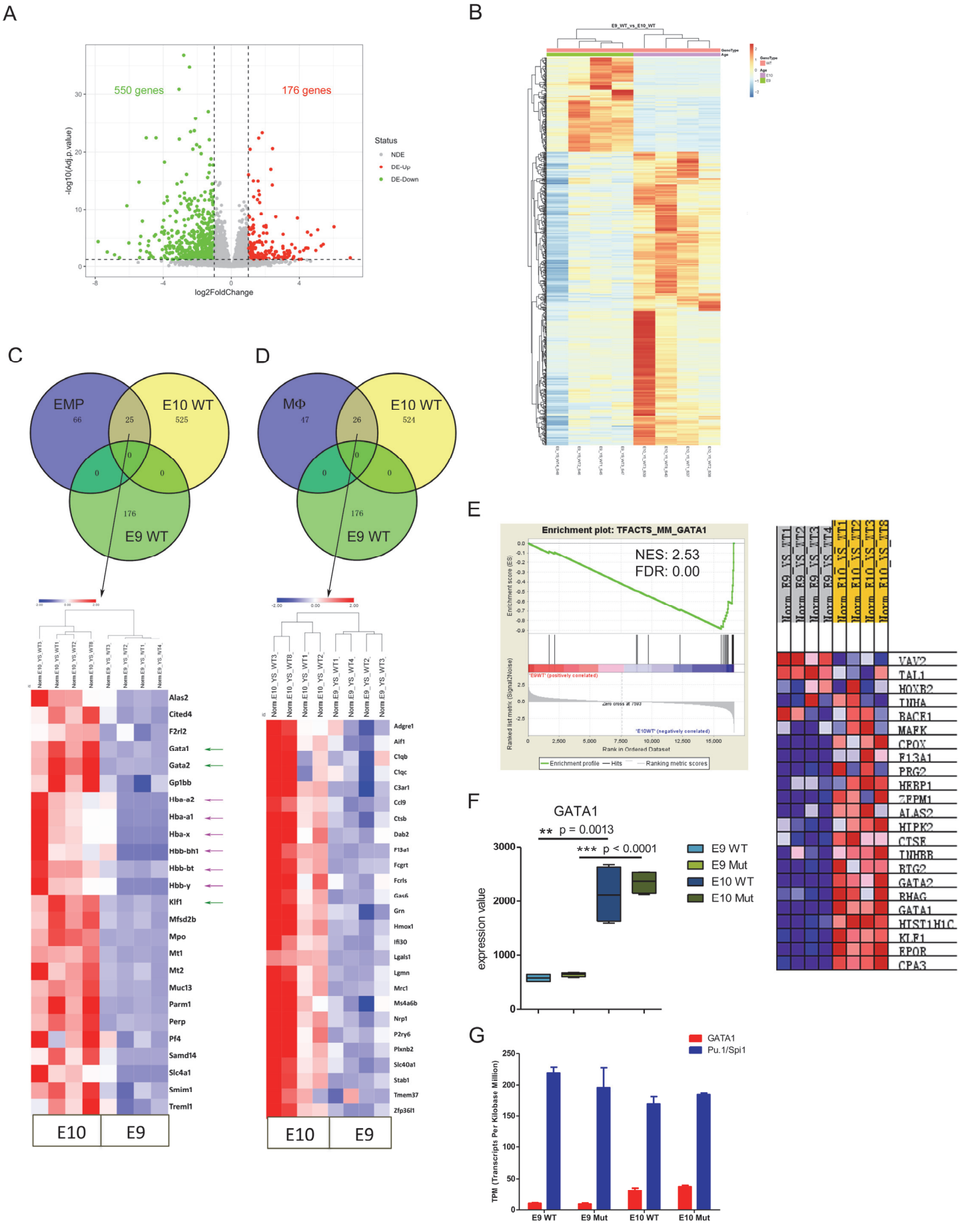
A
550 genes
176 genes
Status
NDE
DE-Up
DE-Down
-log10(Adj.p.value)
log2FoldChange
B
E9_WT_vs_E10_WT
C
EMP
66
25
E10 WT
525
0
0
0
176
E9 WT
D
MΦ
47
26
E10 WT
524
0
0
0
176
E9 WT
Alas2
Cited4
F2rl2
Gata1
Gata2
Gp1bb
Hba-a2
Hba-a1
Hba-x
Hbb-bh1
Hbb-bt
Hbb-y
Klf1
Mfsd2b
Mpo
Mt1
Mt2
Muc13
Parm1
Perp
Pf4
Samd14
Slc4a1
Smim1
Treml1
E10
E9
Adgre1
Aif1
C1qb
C1qc
C3ar1
Ccl9
Ctsb
Dab2
F13a1
Fcgrt
Fcrls
Gas6
Grn
Hmox1
Ifi30
Lgals1
Lgmn
Mrc1
Ms4a6b
Nrp1
P2ry6
Plxnb2
Slc40a1
Stab1
Tmem37
Zfp36l1
E10
E9
E
Enrichment plot: TFACTS_MM_GATA1
NES: 2.53
FDR: 0.00
Enrichment score (ES)
Ranked list metric (Signal2Noise)
Rank in Ordered Dataset
Enrichment profile
Hits
Ranking metric scores
VAV2
TAL1
HOXB2
TNFA
RACE1
MAFK
CPOX
F13A1
PRG2
HBBP1
ZFPM1
ALAS2
HIPK2
CTSE
TNFRB
BTG2
GATA2
RHAG
GATA1
HIST1H1C
KLF1
EPOR
CPA3
F
GATA1
** p = 0.0013
*** p < 0.0001
expression value
E9 WT
E9 Mut
E10 WT
E10 Mut
G
GATA1
Pu.1/Spi1
TPM (Transcripts Per Kilobase Million)
E9 WT
E9 Mut
E10 WT
E10 Mut

Figure: 2: Differential expressed genes between E9 WT and E10 WT MΦ A1 progenitors.
Comparison with EMP and mature MΦ data set from (Mass et al., 2016).
A. Volcano plot: differentially expressed genes. Red and green dots indicate genes with statistically significant changes in gene expression. (*P*-value <0.05, absolute fold change≥2.0) (NDE: not deregulated genes; DE-Up: up-regulated genes; DE-Down: down-regulated genes).
B. Heatmap showing expression profiles of DEGs identified by the volcano plot. Heat map displays transformed log2-expression values from red to blue via white.
C. Upper panel: Venn diagram showing overlap of genes that are differentially expressed in E9 (green) and E10 (Yellow) WT MΦ progenitors with "EMPs" signature genes (Blue). Lower panel: Heatmap showing expression profiles of overlapping genes identified by the Venn diagram. Heatmap displays transformed log2-expression values from red to blue via white.
D. Venn diagram showing overlap patterns of genes that are differentially expressed in E9 (green) and E10 (Yellow) WT MΦ progenitors with embryonic MΦ signature (Blue). Lower panel: Heatmap showing expression profiles of overlapping genes identified by the Venn diagram. Heatmap displays transformed log2-expression values from red to blue via white.
E. GSEA analysis showing a GATA1 targeting genes enrichment in E10 WT MΦ A1 progenitors compared to E9 WT.
F. Read counts of GATA1 expression level in E9 and E10 WT and *Lyl-1*$^{lacZ/lacZ}$ MΦ A1 progenitors
G. Relative expression level of GATA1 and Pu.1/Spi1 in different E9 and E10 WT and *Lyl-1*$^{lacZ/lacZ}$ MΦ A1 progenitor as indicated by TPM (Transcripts Per Million Kilobases).

Using the Ingenuity Pathway analysis (IPA), 38 canonical pathways enriched in E9 vs. E10 WT MΦ progenitors were identified, 8 of them with an absolute Z score ≥ 2 **(Figure 3A)**. This analysis revealed that E9 progenitors are active in Eicosanoid signaling whereas they are inhibited in inflammatory related signaling involving pattern recognition receptors in recognition of bacteria and viruses, TNFR1 and TGF-β signaling pathways.

In top network analysis **(Figure 3B)**, the DEGs were overrepresented in *Cell-To-Cell Signaling and Interaction, Hematological System Development and Function* and *Immune Cell Trafficking* with an enrichment score of 33, among the network. MHC-II complex related molecules, especially CD74, were overrepresented at E9 WT YS MΦ A1 progenitors, while TNFα pathway, which forms a core center in the network, was down-regulated. Moreover, consistent with IPA results, the GSEA analysis **(Figure 3D)** pointed also to an enrichment in inflammatory related signaling pathways at E10 MΦ progenitors. These inflammatory signals comprised TGFβ and Toll like receptors signaling pathways, as well as the downstream activation of NFκB signaling. These results strongly suggest that E10 MΦ progenitors are more involved in the regulation inflammatory processes than E9 MΦ^{Prim} progenitors.

Previous results have suggested that IFNβ is required for the maturation of tissue resident

MΦ, since the population of resident MΦ is reduced in IFNβ$^{-/-}$ mice (Deonarain et al., 2003). In our RNA-seq results, E9 MΦ^{Prim} progenitors are enriched in type I interferon IFNβ signaling, as well as in type II IFNγ response genes **(Figure 3D)**, suggesting IFNβ and IFNγ may be involved in MΦ^{Prim} development and function. IFNγ, a pro-inflammatory cytokine secreted in the uterus mainly by trophoblasts during early pregnancy, then by uterine NKs in the maternal endometrium, is very important for successful pregnancy. Endometrial IFNγ is first detected at E6.5, it reaches a peak at E10 and then declines in normal mice (Murphy et al., 2009). IFNγ has been shown to induce the expression of MHC class II related genes through Ciita (Muhlethaler-Mottet et al., 1998). This is in frame with the higher expression level of MHC class II related genes in E9 MΦ^{Prim} progenitors, even though few information on the regulation and function of interferons from YS MΦ is available.

We further compared the MHC-II expression levels in E9 and E10 MΦ progenitors using flow cytometry and we confirmed that it was significantly higher at E9 than at E10 **(Supplementary Figure 2)**, but it is still expressed at a low level. This is consistent with a previous report which indicates a significantly increase of MHC-II genes at the RNA level led only to a slight increase at the protein level (van de Laar et al., 2016).

Besides its function as part of the MHC-II complex, CD74 is also a receptor for MΦ migration inhibitory factor (MIF), which is very important for MΦ survival and innate immunity (Calandra and Roger, 2003). MIF has been previously shown to activate the production of eicosanoid (Mitchell RA, 1999; Sun et al., 2013). This might explain the active state of eicosanoid signaling pathway in E9 MΦ A1 progenitors.

In addition, IPA function prediction indicated that compared to E10, phagocytosis was reduced in E9 MΦ progenitors **(Figure 3C**).

A

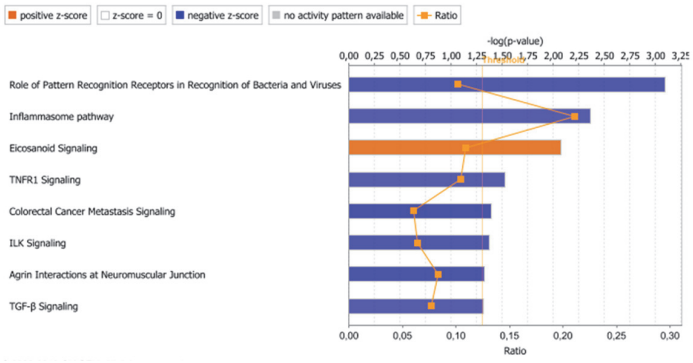

B

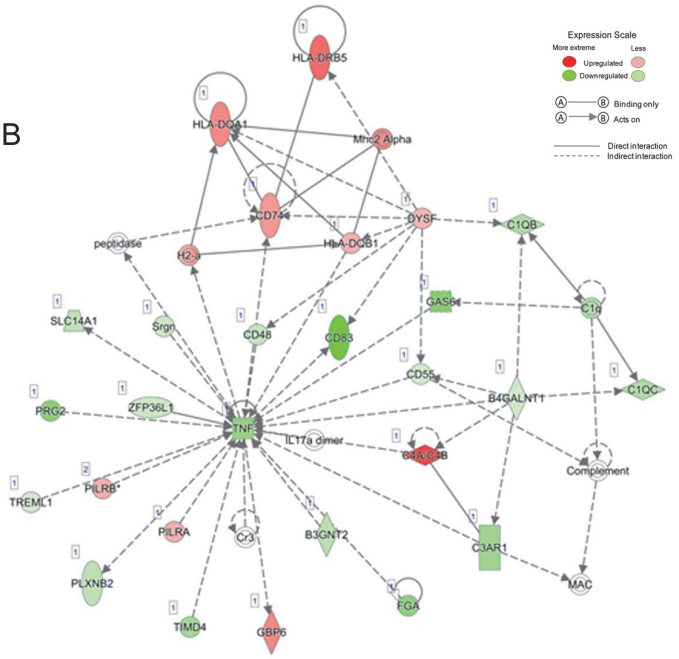

C

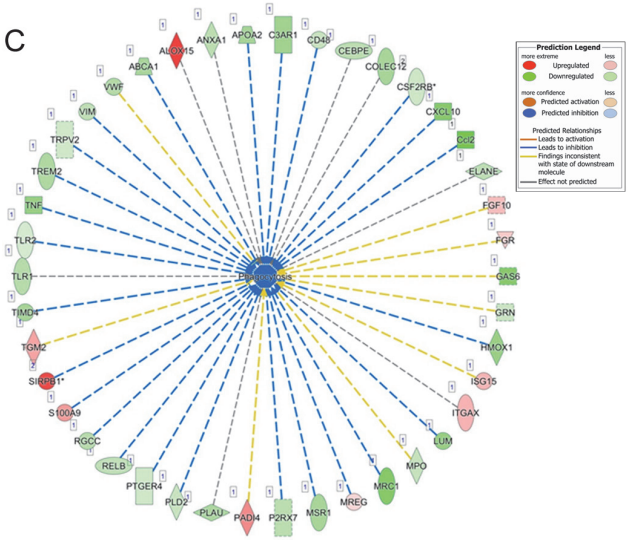

D

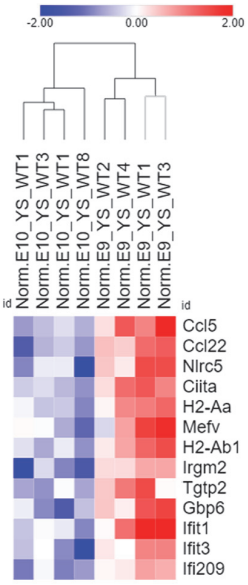

E

Toll receptor signaling

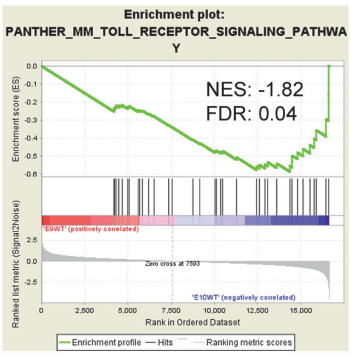

NFKB activation

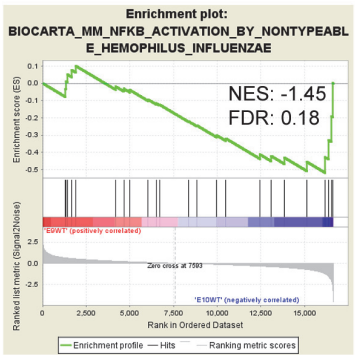

TNFa signaling pathway

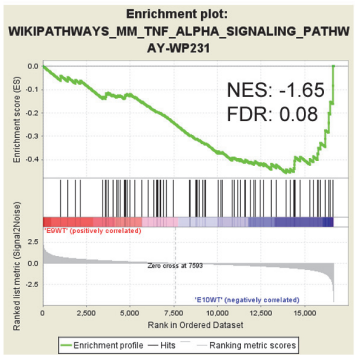

TGFBETA receptor signaling

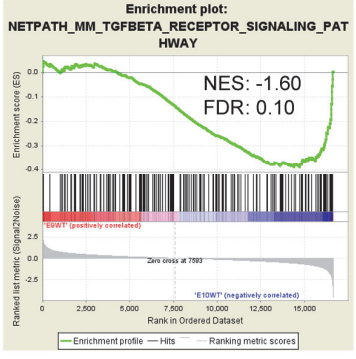

TGFBETA signaling

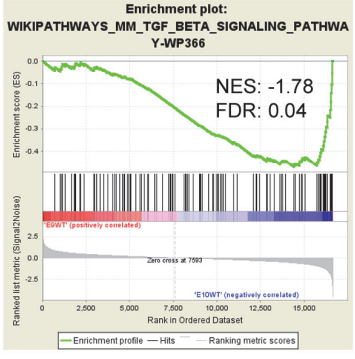

Cytokines and inflammation

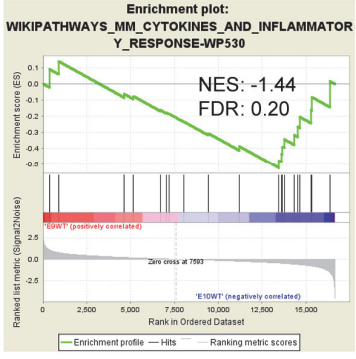

Figure 3: Enrichment pattern between WT E9 and E10 MΦ A1 progenitors.
A: Top canonical pathway enrichment analysis: E9 WT MΦ A1 progenitors have low expression level of genes involved in inflammatory signaling pathways. Bars: minus log of the p-value of each canonical pathway; threshold line (orange): p-value of 0.05. Yellow line with square: ratio between the number of genes from the dataset in a given pathway that meet the cutoff criteria and the total number of genes of that pathway.
B: Network representing the molecular relationships of DEGs between in E9 vs. E10 WT MΦ progenitors.
C. IPA function prediction: phagocytosis in reduced at E9 WT compared to E10.
D. Heatmap showing the expression profiles of DEGs related to IFNγ and IFNβ response, identified by g:Profiler. The heatmap displays transformed log2-expression values from red to blue via white.
E. GSEA enrichment analysis: inflammatory signaling pathways in WT MΦ progenitors at E9 and E10.

When we compared E9 and E10 MΦ progenitors from *Lyl-1*$^{lacZ/lacZ}$ samples, we observed 1085 DEGs, including 452 up-regulated at E9 (red dots) and 633 (green dots) up-regulated at E10 **(Figure 4A).** The heatmap showed that E9 and E10 *Lyl-1*$^{lacZ/lacZ}$ samples categorized into 4 distinct clusters according to their expression level and stage **(Figure 4B)**.

To compare with the WT data, the mutant DEGs were overlapped with the "EMPs" (91 genes) and MΦ signatures (73 genes) described by Mass *et al.*, using Venny (Mass et al., 2016). Consistently with the observation obtained from WT samples, the genes enriched at E9 were identified neither in "EMPs" **(Figure 4C)** nor in MΦ signatures **(Figure 4D).** Similarly, we found that 26 DEGs (27.5%) enriched in E10 *Lyl-1*$^{lacZ/lacZ}$ progenitors were common with those in the "EMPs" signature, and that 16 DEGs (21.9%) overlapped with genes with the MΦ signature. Again, E10 *Lyl-1*$^{lacZ/lacZ}$ progenitors had an increased *Gata1* expression level and were enriched in *Gata1* targeting genes **(Figure 4E)** compared to E9 *Lyl-1*$^{lacZ/lacZ}$ progenitors.

In IPA analysis, 84 canonical pathways enriched in E9 vs. E10 DEGs were identified, 8 of them with an absolute Z score ≥ 2 **(Figure 5A)**. Compared to E10, E9 *Lyl-1*$^{lacZ/lacZ}$ progenitors were inhibited in inflammatory related signaling such as TREM1 signaling, neuro inflammation signaling pathways and iNOS signaling. IPA function prediction indicated that phagocytosis was also down regulated at E9 in *Lyl-1*$^{lacZ/lacZ}$ progenitors as it was for the WT ones **(Figure 5C**). Network analysis **(Figure 5B)** also indicated that the DEGs were overrepresented in *Cell Morphology, Hematological System Development and Function and Hematopoiesis* with a score of 35 (Top1 network).

In the network, *Gata1* was again overrepresented at E10 and had a broad connection with

the genes in the network, suggesting it has an important role in regulating the network, consistent with the previous GSEA analysis.

A

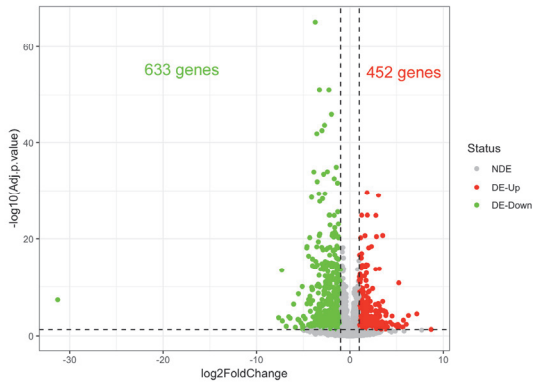
633 genes
452 genes
Status
NDE
DE-Up
DE-Down
-log10(Adj.p.value)
log2FoldChange

B

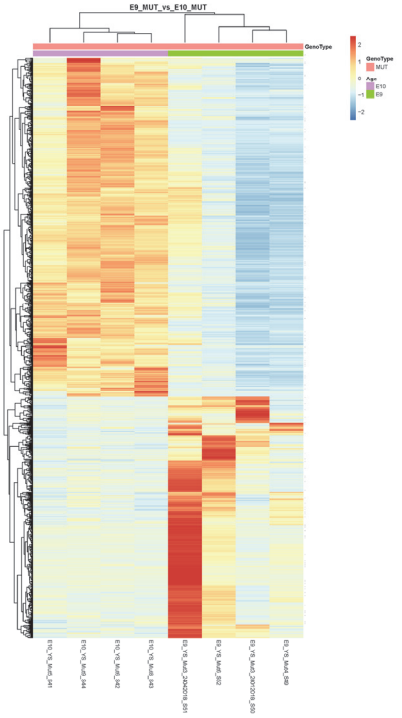
E9_MUT_vs_E10_MUT
GenoType
Age

C

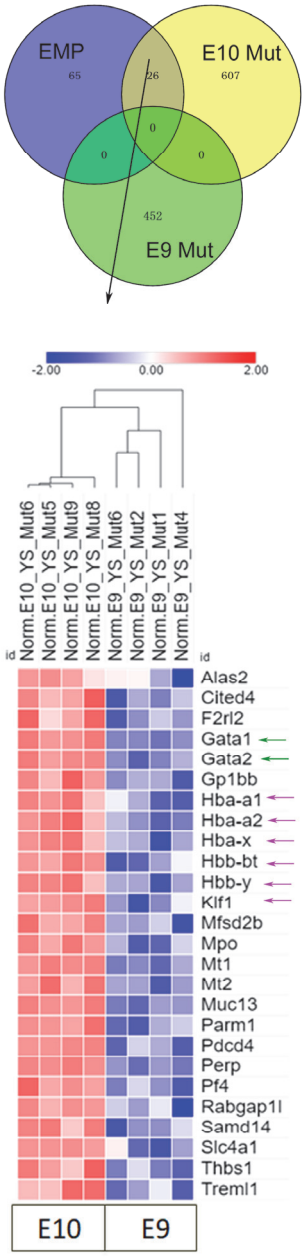
EMP
65
E10 Mut
607
E9 Mut
452
26
0
0
0
-2.00
0.00
2.00
Norm.E10_YS_Mut6
Norm.E10_YS_Mut5
Norm.E10_YS_Mut9
Norm.E10_YS_Mut8
Norm.E9_YS_Mut6
Norm.E9_YS_Mut2
Norm.E9_YS_Mut1
Norm.E9_YS_Mut4
id
Alas2
Cited4
F2rl2
Gata1
Gata2
Gp1bb
Hba-a1
Hba-a2
Hba-x
Hbb-bt
Hbb-y
Klf1
Mfsd2b
Mpo
Mt1
Mt2
Muc13
Parm1
Pdcd4
Perp
Pf4
Rabgap1l
Samd14
Slc4a1
Thbs1
Treml1
E10
E9

D

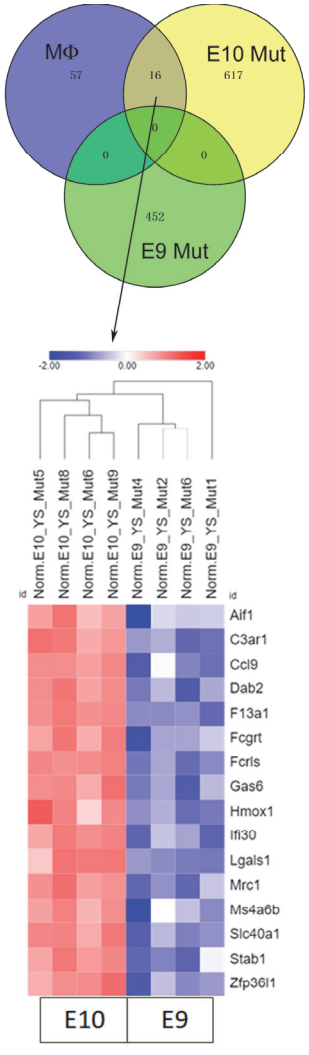
MΦ
57
E10 Mut
617
E9 Mut
452
16
0
0
0
-2.00
0.00
2.00
Norm.E10_YS_Mut5
Norm.E10_YS_Mut8
Norm.E10_YS_Mut6
Norm.E10_YS_Mut9
Norm.E9_YS_Mut4
Norm.E9_YS_Mut2
Norm.E9_YS_Mut6
Norm.E9_YS_Mut1
id
Aif1
C3ar1
Ccl9
Dab2
F13a1
Fcgrt
Fcrls
Gas6
Hmox1
Ifi30
Lgals1
Mrc1
Ms4a6b
Slc40a1
Stab1
Zfp36l1
E10
E9

E

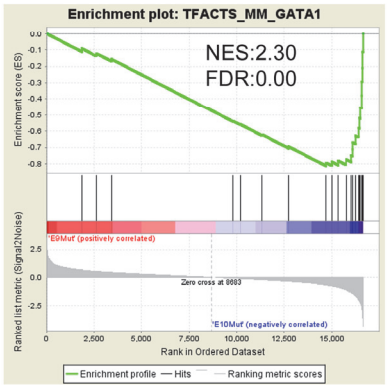
Enrichment plot: TFACTS_MM_GATA1
NES:2.30
FDR:0.00
Enrichment score (ES)
'E9Muf (positively correlated)
Zero cross at 8003
'E10Muf (negatively correlated)
Ranked list metric (Signal2Noise)
Rank in Ordered Dataset
Enrichment profile
Hits
Ranking metric scores

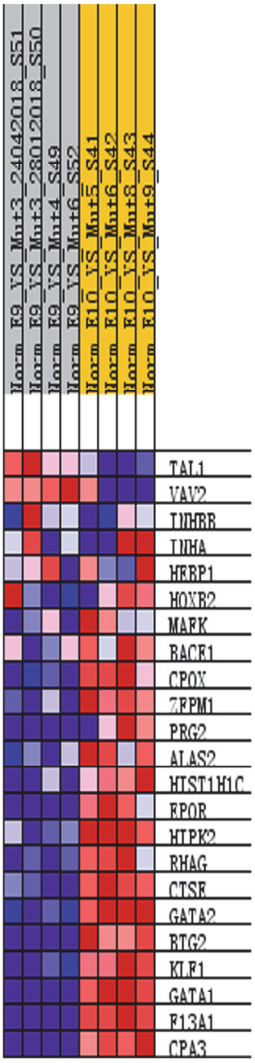
Norm_E9_YS_Mut3_24042018_S51
Norm_E9_YS_Mut3_28012018_S50
Norm_E9_YS_Mut4_S49
Norm_E9_YS_Mut6_S52
Norm_E10_YS_Mut5_S41
Norm_E10_YS_Mut6_S42
Norm_E10_YS_Mut8_S43
Norm_E10_YS_Mut9_S44
TAL1
VAV2
INHBB
INHA
HERP1
HOXB2
MARK
RACE1
CPOX
ZFPM1
PRG2
ALAS2
HIST1H1C
EPOR
HIPK2
RHAG
CTSE
GATA2
BTG2
KLF1
GATA1
F13A1
CPA3

Figure 4: Differential expressed genes between *Lyl-1*$^{lacZ/lacZ}$ E9 and E10 MΦ A1 progenitors. Comparison with EMP and mature MΦ data set (Ref (Mass et al., 2016)**).**
A. Volcano plot: differentially expressed genes. Red and green dots indicate genes statistically up- and down-regulated respectively (*P*-value <0.05, absolute fold change≥2.0). **B.** Heatmap showing expression profiles of DEGs identified by the volcano plot. Heatmap displays transformed log2-expression values from red to blue via white.
C. Upper panel: Venn diagram: overlap of genes with "EMPs" signature genes (Blue) with thoses differentially expressed at E9 (green) and E10 (Yellow). Lower panel: Heatmap showing expression profiles of overlapping genes identified by the Venn diagram. Heatmap displays transformed log2-expression values from red to blue via white.
D. Venn diagram: overlap patterns of genes that share a MΦ signature and are differentially expressed in E9 and E10 *Lyl-1*$^{lacZ/lacZ}$ MΦ A1 progenitors. Lower panel: Heatmap: expression profiles of overlapping genes identified by the Venn diagram. Heatmap displays transformed log2-expression values from red to blue via white.
E. GSEA analysis showing a GATA1 targeting genes enrichment in E10 *Lyl-1*$^{lacZ/lacZ}$ MΦ A1 progenitors compared to E9 *Lyl-1*$^{lacZ/lacZ}$.

The top 2 network pointed to a down-regulated pattern of TNFα which forms a core of the network, suggesting a weaker inflammatory signaling in E9. Similarly to the IPA results obtained from WT, the GSEA pathway analysis **(Figure 5D)** also indicated that E10 *Lyl-1*$^{lacZ/lacZ}$ progenitors were enriched in inflammatory signaling pathways, compared to E9 progenitors. These inflammatory signaling pathways comprised TGFβ and Toll like receptors signaling pathways, as well as the downstream activation of NFκB signaling. Even if *Lyl-1*$^{lacZ/lacZ}$ E9 and E10 progenitors had more DEGs than their WT counterparts , they shared a similar enrichment pattern for transcription factors and genes involved in inflammatory signaling.

Together with the results obtained from WT samples **(Figures 2, 3)**, the comparison of E9 and E10 *Lyl-1*$^{lacZ/lacZ}$ progenitors confirms that E9 progenitors are clearly distinct from both EMP and E10 MΦ progenitors, which reflects their primitive status. In both WT and *Lyl-1*$^{lacZ/lacZ}$ embryos, E9 MΦ^{Prim} progenitors appear to express low levels of *Gata1*, higher MHC-II related complexes and to be less involved in inflammatory signaling pathways compared to MΦ$^{T\text{-}Def}$ progenitors.

A

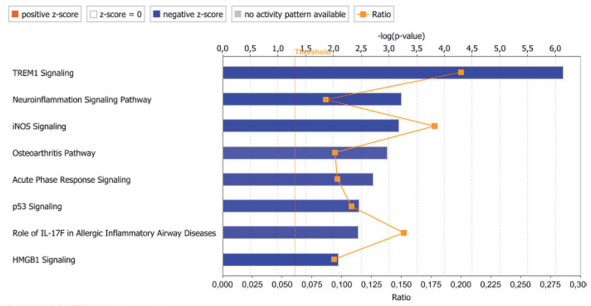

C

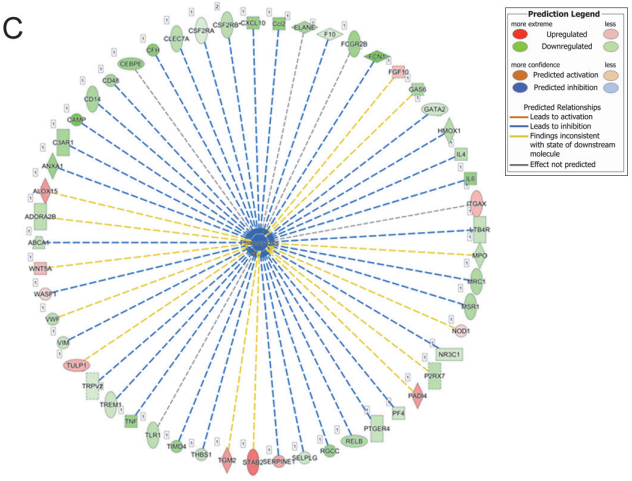

B

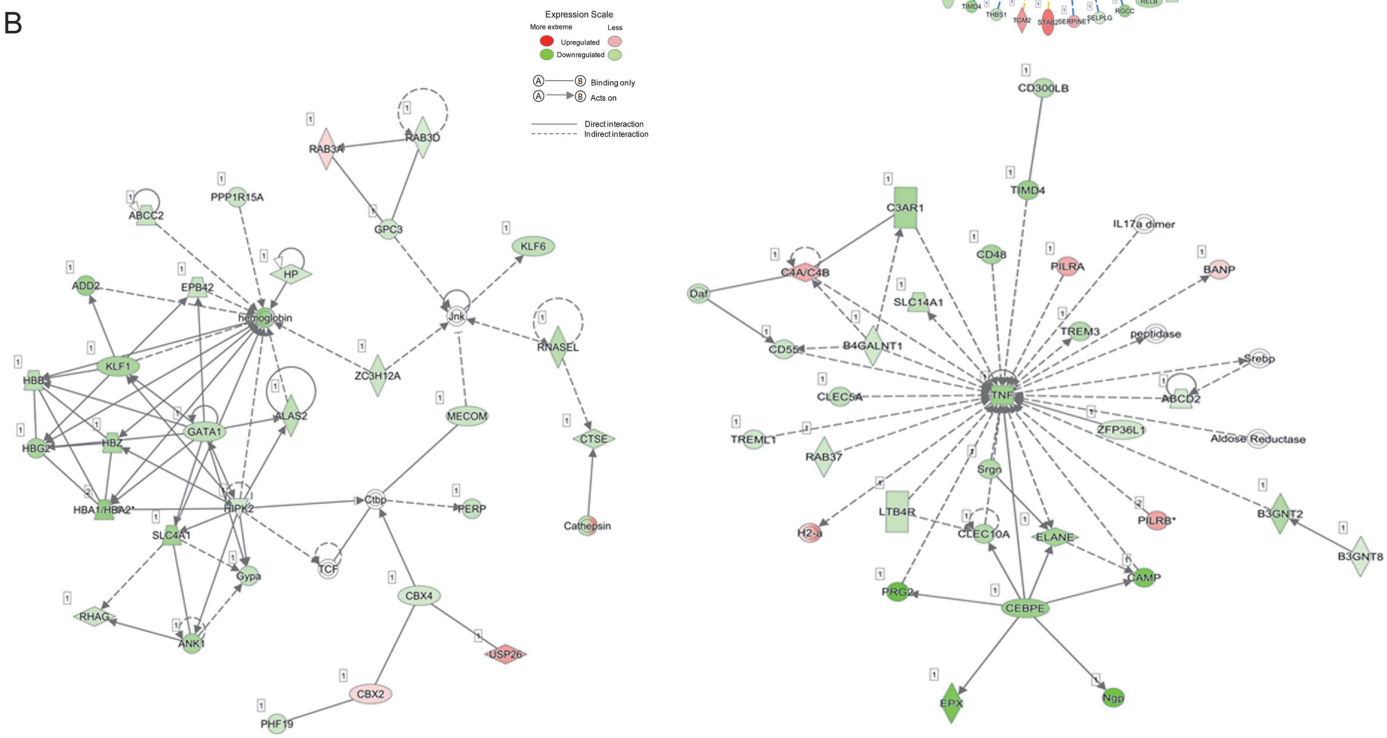

D

Toll like receptor

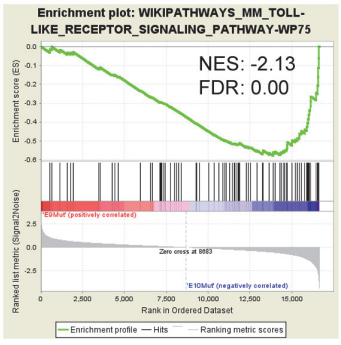

NFKB signaling

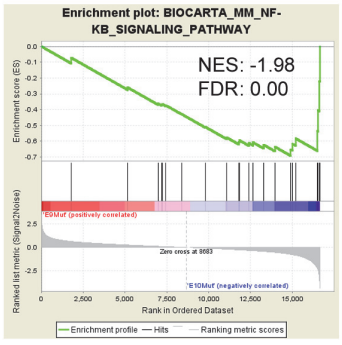

TNFa signaling pathway

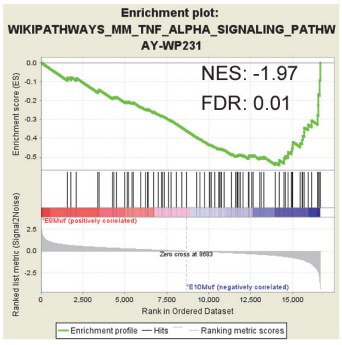

TGFBETA receptor signaling

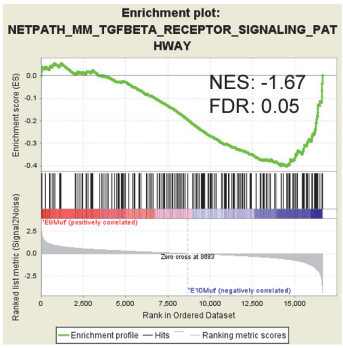

TGFBETA signaling

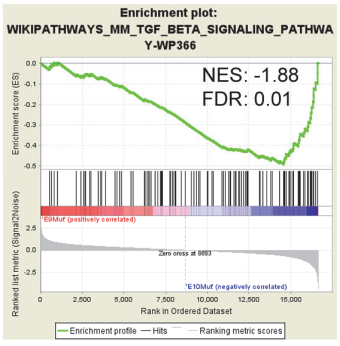

Cytokines and inflammation

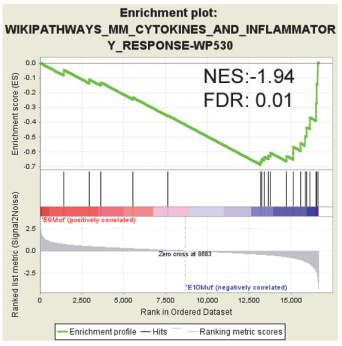

Figure 5: Enrichment pattern between *Lyl-1*$^{lacZ/lacZ}$ E9 and E10 progenitors.
A: Top canonical pathway enrichment analysis indicates a lower expression level of genes involved in inflammatory signaling pathways at E9. Bars: minus log of the p-value of each canonical pathway. Threshold line (orange): p-value of 0.05. Yellow line with square: ratio between the number of genes from the dataset in a given pathway that meet the cutoff criteria and the total number of genes of that pathway.
B: Network representing the molecular relationships between genes differentially expressed in at E9 to E10.
C. IPA function prediction of phagocytosis.
D. GSEA enrichment analysis of inflammatory signaling pathways.

2.2.2: The difference of expression between E9 WT and *Lyl-1*$^{lacZ/lacZ}$ MΦ progenitors

As shown by the volcano plot **(Figure 6A**), at E9, WT and *Lyl-1*$^{lacZ/lacZ}$ MΦ progenitors differed by the expression of 99 genes. Amongst them, 34 were significantly up-regulated in WT samples and 65 in *Lyl-1*$^{lacZ/lacZ}$ samples **(Figure 6B**). In IPA analysis, 53 canonical pathways were identified as enriched in the DEGs, 9 of them with an absolute Z score ≥ 1 **(Figure 6C)**. This analysis indicated that E9 WT MΦ progenitors were more active in inflammatory signaling pathways, such as IL-6 signaling, in acute phase response signaling and NF-κb signaling than the *Lyl-1*$^{lacZ/lacZ}$ ones, while *Lyl-1*$^{lacZ/lacZ}$ MΦ progenitors were more active in LXR/RXR activation pathways.

The top 1 of over-represented networks were *Connective Tissue Development and Function, Tissue Morphology and Cell Morphology networks*, with an enrichment score of 34. *Lyl-1*$^{lacZ/lacZ}$ MΦ progenitors were enriched in PI3K complex related signaling pathways. Interestingly some genes related to neurotransmitter function, such as *Gabra2* and *Gabrb1* were also enriched in *Lyl-1*$^{lacZ/lacZ}$ progenitors **(Figure 6D)**. On the other hand, compared to the WT, mutant progenitors had a reduced SMAD7 signaling.
The top 2 enriched networks, with a score of 29, was related to *Cell-To-Cell Signaling and Interaction, Hematological System Development and Function and Tissue Morphology*. This network has several core hubs. One of them was IL1R related signaling pathway, which is down-regulated in *Lyl-1*$^{lacZ/lacZ}$ MΦ progenitors. IL1R signaling is involved in the extensive microglia proliferation that occurs after microglia depletion. Proliferating microglia highly express IL-1R, and the treatment with an IL-1R antagonist during the repopulation phase following microglia depletion impairs this proliferation (Bruttger et al., 2015). Signaling

through IL1R might also control microglia proliferation at embryonic stages. Our previous results showing that Lyl-1 mutant microglia at E12 have a reduced proliferating rate compared to WT **(see results part 1)** might thus be due to a defective IL-1R signaling.

Another core hubs in the top 2 enriched network, such as *Ccr7* and MHC-II related molecular complexes (*H2-Aa*) were also down-regulated in *Lyl-1*$^{lacZ/lacZ}$ E9 MΦ progenitors, suggesting that Lyl-1 may regulates the expression level of *H2-Aa*.

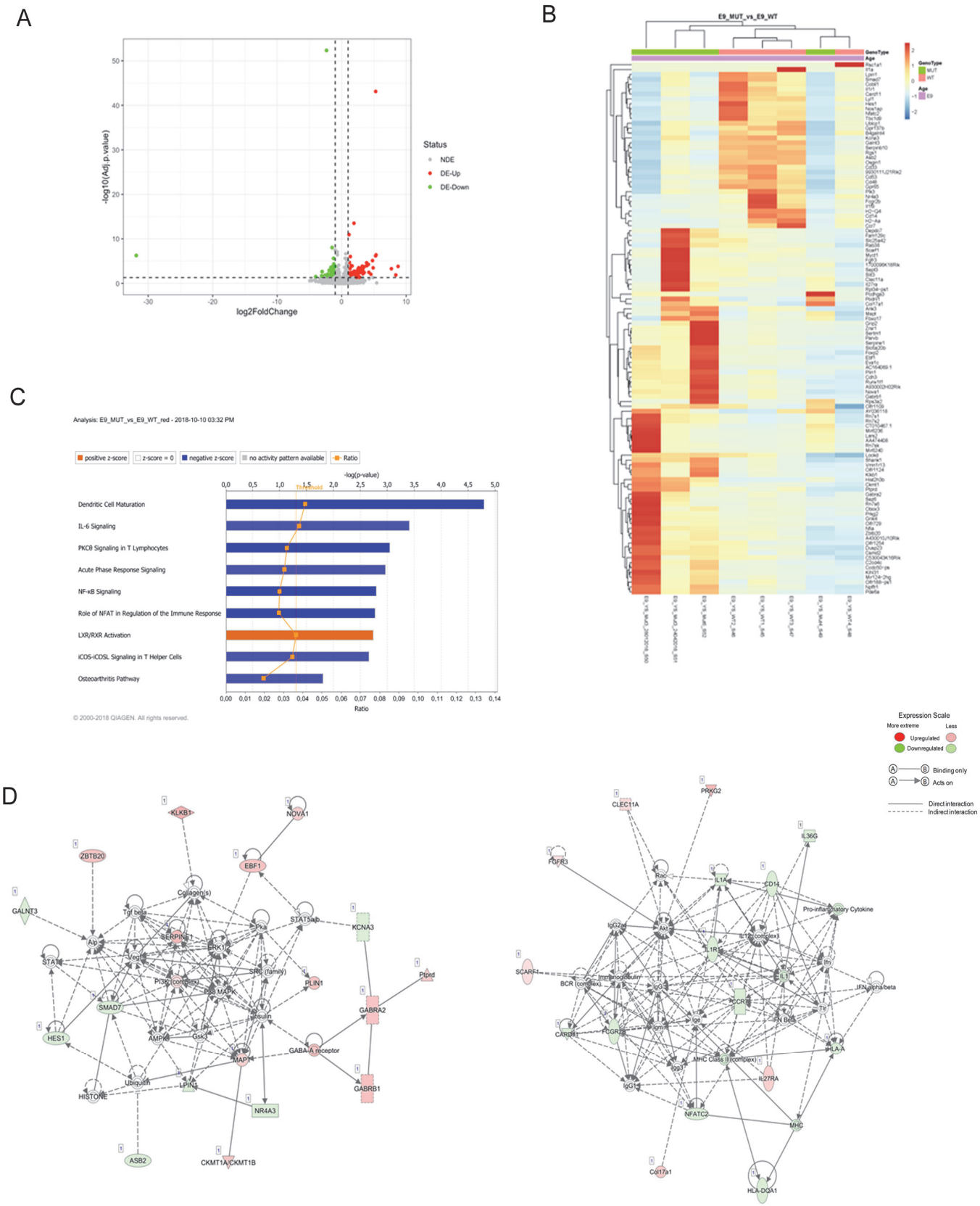

Figure 6: Enrichment pattern between E9 *Lyl-1*$^{lacZ/lacZ}$ and WT MΦ A1 progenitors.

A. Volcano plot: differentially expressed genes. Red and green dots indicate genes with statistically

significant changes in gene expression. (*P*-value <0.05, absolute fold change≥2.0) (NDE: not deregulated genes; DE-Up: up-regulated genes; DE-Down: down-regulated genes).
B Heatmap: expression profiles of DEGs identified by the volcano plot. Heatmap displays transformed log2-expression values from red to blue via white.
C. Top canonical pathway enrichment analysis indicated a low expression level of genes involved in inflammatory signaling pathways *Lyl-1*$^{lacZ/lacZ}$ MΦ progenitors. Bar length indicate the minus log of the p-value of each canonical pathway. Threshold line (orange): p-value of 0.05. Yellow line with square: ratio between the number of genes from the dataset in a given pathway that meet the cutoff criteria and the total number of genes of that pathway.
D. Network representing the molecular relationships between genes differentially expressed in *Lyl-1*$^{lacZ/lacZ}$ and WT MΦ progenitors.

GSEA analysis focusing on transcription factor **(Figure 7A)** revealed that WT MΦ progenitors were enriched in *Pu.1/Spi1* targeting genes compared to *Lyl-1*$^{lacZ/lacZ}$ ones. Since *Pu.1/Spi1* is an important regulator of MΦ lineage commitment, these results suggest that Lyl-1 regulates genes responsible for MΦ identity.

Compared to *Lyl-1*$^{lacZ/lacZ}$, WT MΦ progenitors were also highly enriched in the GO terms *inflammatory response*, *immune response* and *cellular response to lipopolysaccharide*. Indeed, half of the top 20 enriched GO terms were related to inflammatory signaling and immune response **(**in red in **Figure 7B)**. For example, E9 WT progenitors were enriched in NFκB1 targeting genes Consistent with the previously described IPA results, these data point to deficient inflammatory signaling pathway in *Lyl-1*$^{lacZ/lacZ}$ MΦ progenitors compared to the WT ones **(Figure 7C)**.

A

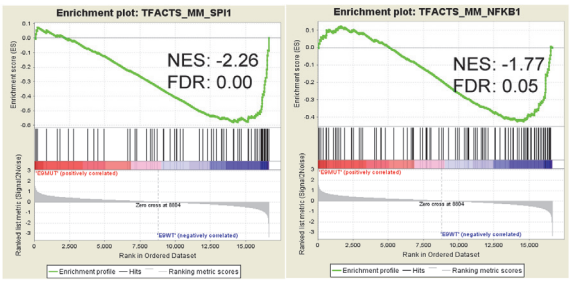
Enrichment plot: TFACTS_MM_SPI1
NES: -2.26
FDR: 0.00
Enrichment plot: TFACTS_MM_NFKB1
NES: -1.77
FDR: 0.05

B

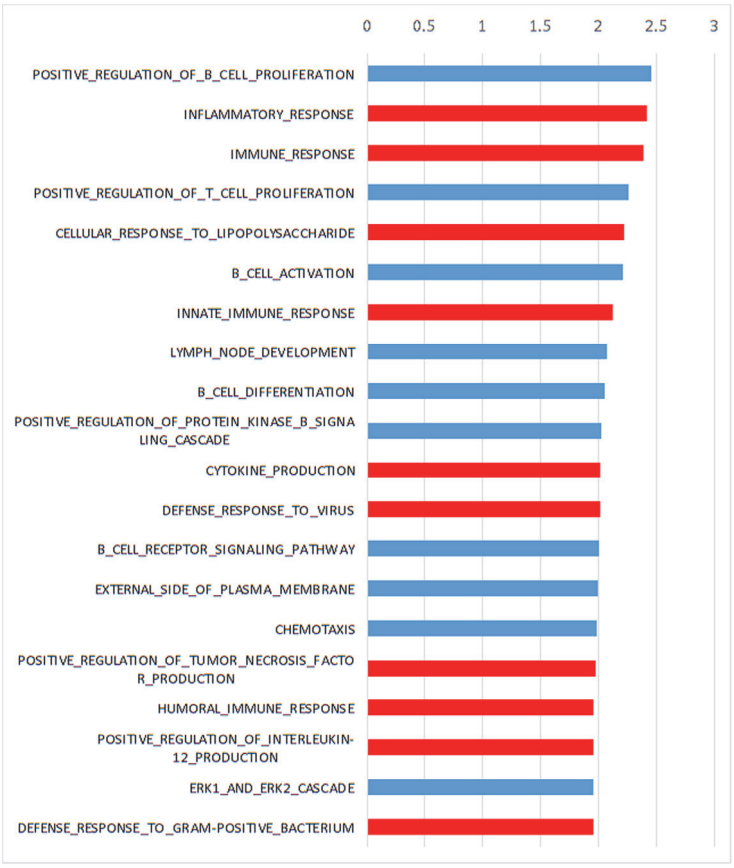
0
0.5
1
1.5
2
2.5
3
POSITIVE_REGULATION_OF_B_CELL_PROLIFERATION
INFLAMMATORY_RESPONSE
IMMUNE_RESPONSE
POSITIVE_REGULATION_OF_T_CELL_PROLIFERATION
CELLULAR_RESPONSE_TO_LIPOPOLYSACCHARIDE
B_CELL_ACTIVATION
INNATE_IMMUNE_RESPONSE
LYMPH_NODE_DEVELOPMENT
B_CELL_DIFFERENTIATION
POSITIVE_REGULATION_OF_PROTEIN_KINASE_B_SIGNALING_CASCADE
CYTOKINE_PRODUCTION
DEFENSE_RESPONSE_TO_VIRUS
B_CELL_RECEPTOR_SIGNALING_PATHWAY
EXTERNAL_SIDE_OF_PLASMA_MEMBRANE
CHEMOTAXIS
POSITIVE_REGULATION_OF_TUMOR_NECROSIS_FACTOR_PRODUCTION
HUMORAL_IMMUNE_RESPONSE
POSITIVE_REGULATION_OF_INTERLEUKIN-12_PRODUCTION
ERK1_AND_ERK2_CASCADE
DEFENSE_RESPONSE_TO_GRAM-POSITIVE_BACTERIUM

C

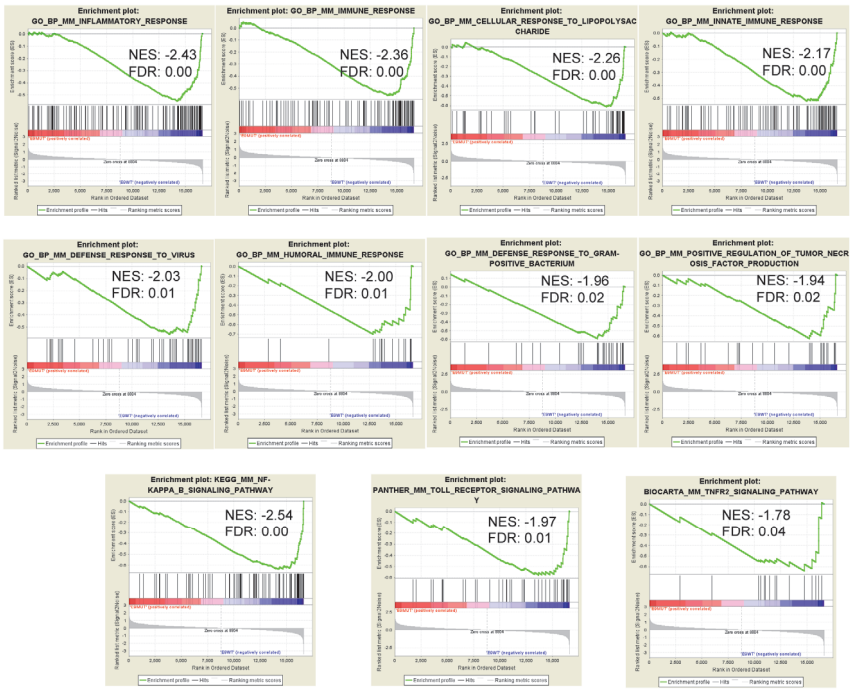
Enrichment plot: GO_BP_MM_INFLAMMATORY_RESPONSE
NES: -2.43
FDR: 0.00
Enrichment plot: GO_BP_MM_IMMUNE_RESPONSE
NES: -2.36
FDR: 0.00
Enrichment plot: GO_BP_MM_CELLULAR_RESPONSE_TO_LIPOPOLYSACCHARIDE
NES: -2.26
FDR: 0.00
Enrichment plot: GO_BP_MM_INNATE_IMMUNE_RESPONSE
NES: -2.17
FDR: 0.00
Enrichment plot: GO_BP_MM_DEFENSE_RESPONSE_TO_VIRUS
NES: -2.03
FDR: 0.01
Enrichment plot: GO_BP_MM_HUMORAL_IMMUNE_RESPONSE
NES: -2.00
FDR: 0.01
Enrichment plot: GO_BP_MM_DEFENSE_RESPONSE_TO_GRAM-POSITIVE_BACTERIUM
NES: -1.96
FDR: 0.02
Enrichment plot: GO_BP_MM_POSITIVE_REGULATION_OF_TUMOR_NECROSIS_FACTOR_PRODUCTION
NES: -1.94
FDR: 0.02
Enrichment plot: KEGG_MM_NF-KAPPA_B_SIGNALING_PATHWAY
NES: -2.54
FDR: 0.00
Enrichment plot: PANTHER_MM_TOLL_RECEPTOR_SIGNALING_PATHWAY
NES: -1.97
FDR: 0.01
Enrichment plot: BIOCARTA_MM_TNFR2_SIGNALING_PATHWAY
NES: -1.78
FDR: 0.04

Figure 7: GSEA analysis of enrichment in E9 *Lyl-1*$^{lacZ/lacZ}$ compared to E9 WT MΦ A1 progenitors.
A. GSEA transcription factor targets enrichment plot indicates an enrichment in Pu.1/Spi1 and NFκB1 targeted genes in E9 WT progenitors.
B. Summary of the top 20 GSEA enrichment GO terms in E9 WT, the bar length indicating the absolute value of NES and the red color representing the GO term relating to inflammatory signaling.
C. GSEA plot of inflammatory signaling enriched in E9 WT MΦ A1 progenitors.
NES: Normalized enrichment score; FDR: False discovery rate.

We also compared *Lyl-1*$^{lacZ/lacZ}$ and WT MΦ progenitors at E10, to better identify the defects induced by the mutation, independently of the maturation process that occurs between E9 and E10.

At E10, 96 genes were found differentially expressed as shown by the volcano plot **(Figure 8A)**, with 52 overexpressed in the WT and 44 in *Lyl-1*$^{lacZ/lacZ}$ progenitors **(Figure 8B)**. In the IPA analysis, 26 canonical pathways enriched in the DEGs were identified **(Figure 8C)**. This analysis indicated that E10 *Lyl-1*$^{lacZ/lacZ}$ MΦ A1 progenitors are inhibited in immune response pathways, such as icos-icol signaling in T helper cells and role of NFAT in regulation of immune response.
The top 1 enriched network, with an enrichment score of 37, was related to *Cell-To-Cell Signaling and Interaction, Hematological System Development and Function and Immune Cell Trafficking* network. Compared to E10 *Lyl-1*$^{lacZ/lacZ}$ progenitors, E9 progenitors had a lower expression of MHC-II complex related genes, such as *H2-Aa*, and a higher expression of *Fcgr2b* and *Il27ra* **(Figure 8D)**.

To better understand the influence of Lyl-1 on MΦ progenitor development, taking into account the maturation that occur between E9 and E10, we overlapped the WT and *Lyl-1*$^{lacZ/lacZ}$ DEGs identified at E9 and E10. Only 16 DEGs were common to both stages **(Figure 9A)**, suggesting that Lyl-1 plays different functions during different developmental stage. Compared to the WT samples, 8 genes were down-regulated and 7 genes were up-regulated in *Lyl-1*$^{lacZ/lacZ}$ progenitor at both stages **(Figure 9B)**. One gene, *Fcgr2b*, showed opposite deregulation during development since it was first down-regulated in the mutant at E9, but expressed at higher levels than in the WT at E10, suggesting a context dependent expression pattern. Because few research have focused on this early stage of MΦ progenitors development, the function of these 16 genes remains largely un-annotated.

A

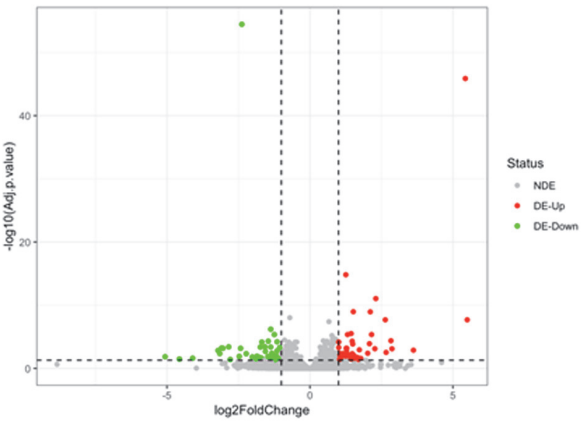
-log10(Adj.p.value)
log2FoldChange
Status
NDE
DE-Up
DE-Down

B

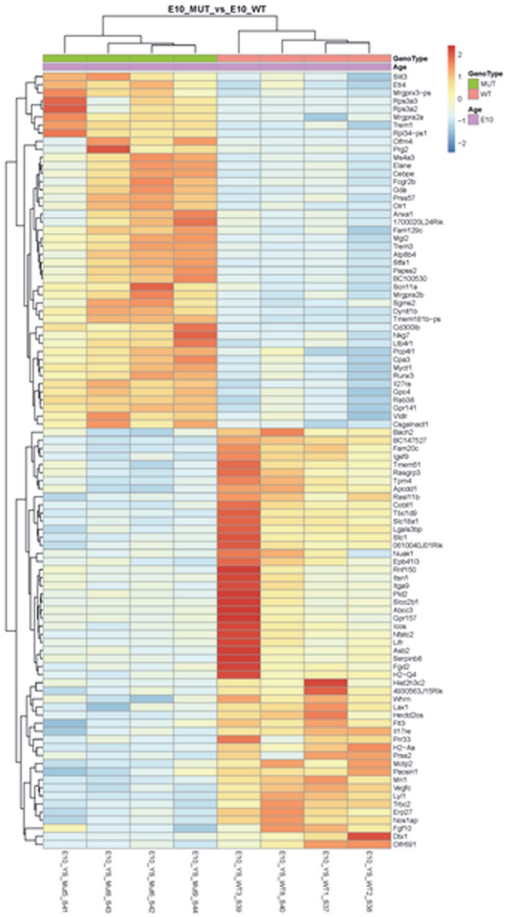
E10_MUT_vs_E10_WT
GenoType
Age
MUT
WT
E10

C

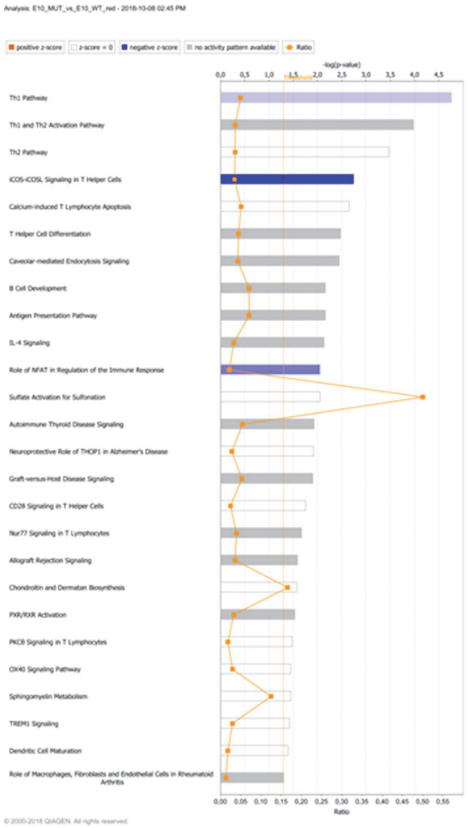
positive z-score
negative z-score
no activity pattern available
Ratio
Th1 Pathway
Th1 and Th2 Activation Pathway
Th2 Pathway
ICOS-ICOSL Signaling in T Helper Cells
Calcium-induced T Lymphocyte Apoptosis
T Helper Cell Differentiation
Caveolar-mediated Endocytosis Signaling
B Cell Development
Antigen Presentation Pathway
IL-4 Signaling
Role of NFAT in Regulation of the Immune Response
Sulfate Activation for Sulfonation
Autoimmune Thyroid Disease Signaling
Neuroprotective Role of THOP1 in Alzheimer's Disease
Graft-versus-Host Disease Signaling
CD28 Signaling in T Helper Cells
Nur77 Signaling in T Lymphocytes
Allograft Rejection Signaling
Chondroitin and Dermatan Biosynthesis
PXR/RXR Activation
PKCθ Signaling in T Lymphocytes
OX40 Signaling Pathway
Sphingomyelin Metabolism
TREM1 Signaling
Dendritic Cell Maturation
Role of Macrophages, Fibroblasts and Endothelial Cells in Rheumatoid Arthritis
-log(p-value)
Ratio

D

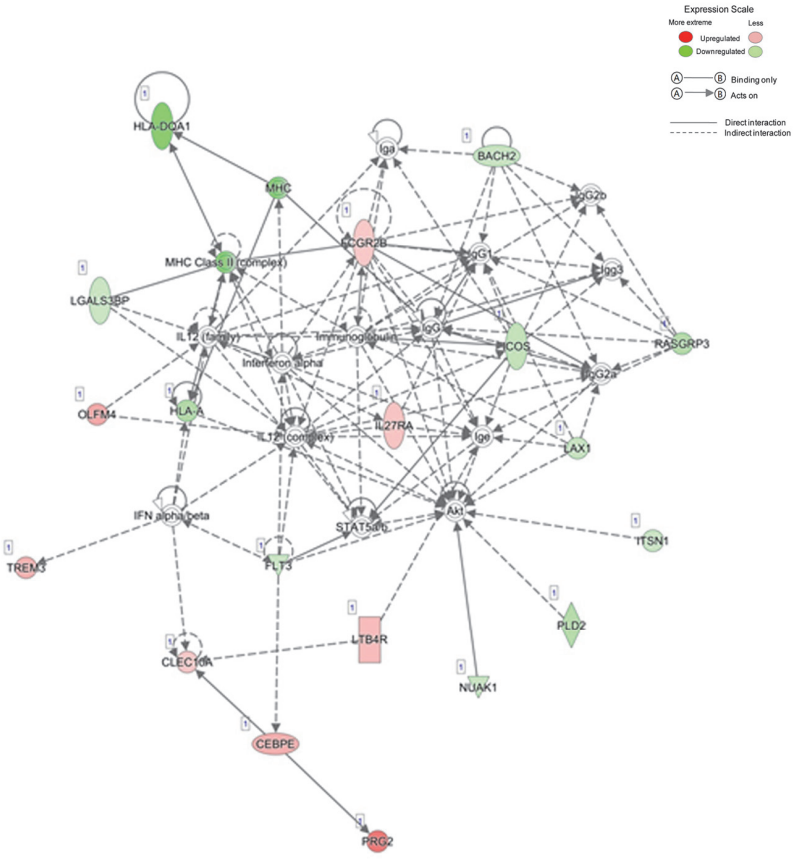
Expression Scale
More extreme
Less
Upregulated
Downregulated
Binding only
Acts on
Direct interaction
Indirect interaction
HLA-DQA1
MHC
MHC Class II (complex)
LGALS3BP
OLFM4
HLA-A
IFN alpha beta
TREM3
Ig
BACH2
IgG2b
FCGR2B
IgG1
Igg3
IL12 (family)
Immunoglobulin
IgG
COS
RASGRP3
Interferon alpha
IgG2a
IL12 (complex)
IL27RA
Ige
LAX1
Akt
STAT5a/b
ITSN1
PLY3
PLD2
LTB4R
CLEC10A
NUAK1
CEBPE
PRG2

Figure 8: Enrichment pattern in E10 *Lyl-1*$^{lacZ/lacZ}$ and WT MΦ progenitors.

A. Volcano plot: differentially expressed genes. Red and green dots indicate genes with statistically significant changes in expression levels. (*P*-value <0.05, absolute fold change≥2.0) (NDE: not deregulated genes; DE-Up: up-regulated genes; DE-Down: down-regulated genes).

B Heatmap: expression profiles of DEGs identified by the volcano plot. Heatmap displays transformed log2-expression values from red to blue via white.

C. Top canonical pathway enrichment analysis of E10 *Lyl-1*$^{lacZ/lacZ}$ and WT MΦ progenitors indicated a low expression level of genes involved in inflammatory signaling pathways in *Lyl-1*$^{lacZ/lacZ}$ progenitors. Bars length: minus log of the p-value of each canonical pathway. Threshold line (orange): p-value of 0.05. Yellow line with square: ratio between the number of genes from the dataset in a given pathway that meet the cutoff criteria and the total number of genes of that pathway.

D. Network representing the molecular relationships between *Lyl-1*$^{lacZ/lacZ}$ and WT MΦ progenitors DEGs at E10.

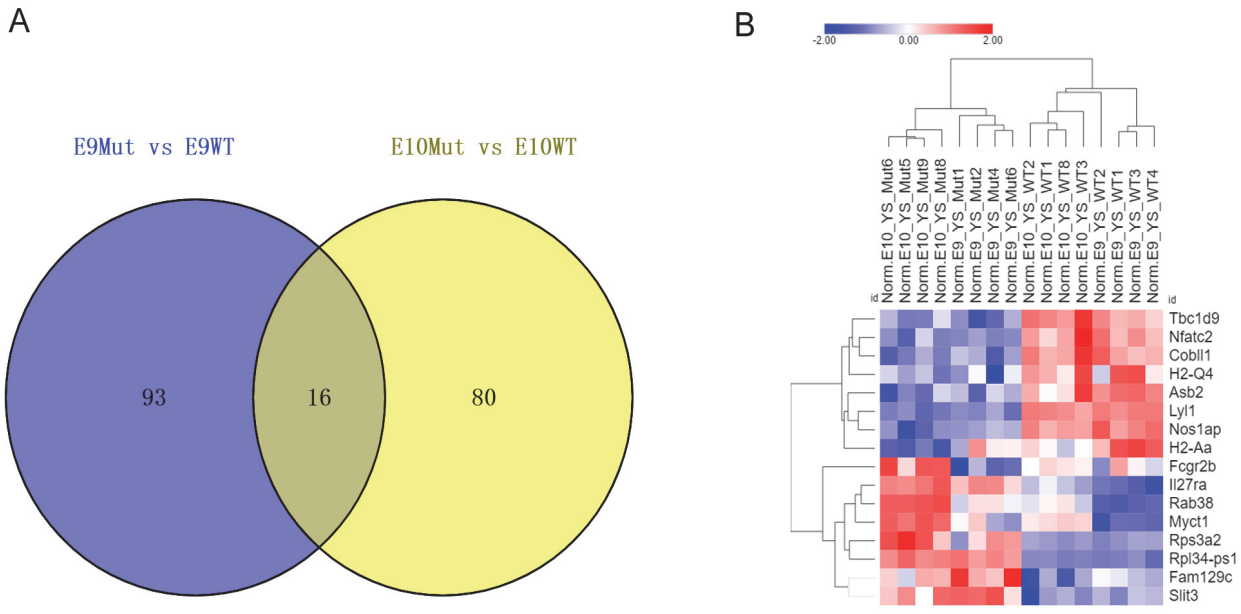

Figure 9: 16 WT vs. *Lyl-1*$^{lacZ/lacZ}$ DEGs common to E9 and E10 progenitors.

A. Venn diagram: overlap of genes that are differentially expressed in E9 WT vs. E9 *Lyl-1*$^{lacZ/lacZ}$ (blue) and E10 WT vs. E10 *Lyl-1*$^{lacZ/lacZ}$ (yellow).

B. Heatmap: expression profiles of overlapping genes identified by the Venn diagram. Heatmap displays transformed log2-expression values from red to blue via white.

2.2.3 : Are E9 MΦ^{Prim} progenitors primed to express microglia enriched genes?

We previously found that Lyl-1 was a marker of YS MΦ^{Prim} progenitors and of microglia **(See results part 1 chapter 2.1.1)**. We thus investigated whether E9 MΦ^{Prim} progenitors already showed a transcriptome biased to microglia features. To do so, we compared the DEGs between E9 and E10 WT MΦ progenitors identified here with those from published results related to the development of YS MΦ progenitors and microglia.

Such a RNA-seq analysis, from Matcovitch-Natan *et al.*, indicated that the development of microglia involves several shifts of gene expression patterns from E10.5 YS MΦ progenitors to adult. Using K-means clustering method, they identified 7 clusters during microglia development. Among these, a cluster of 373 genes was highly enriched in the YS compared to other microglia development stages (Matcovitch-Natan et al., 2016).

We thus compared the DEGs we identified in E9 vs. E10 WT MΦ with those belonging to this YS cluster. 50 genes which were up-regulated in E10 WT belonged to this cluster, which accounted for 9% of the up-regulated genes in E10 WT and 13.4% of genes in the YS cluster.

In contrast, only 5 genes up-regulated in E9 WT were found in this YS cluster **(Figure 10A)**, which accounts less than 3% of up-regulated genes in E9 WT and less than 1.5% genes in YS cluster. This data suggest that a similar expression pattern of genes exists between E9 WT and microglia other than E10 WT MΦ. Indeed, we compared the genes in YS cluster in our E9 WT and E10 WT MΦ progenitors, the expression pattern in E9 MΦ progenitors showed similar low expression pattern as embryonic Microglia **(Figure 10B)**.

Embryonic microglia display a tissue specific transcriptional program compared to other tissue resident MΦ and progenitors, including a down-regulation of the mannose receptor (*CD206/Mrc1*) and the T-cell immunoglobulin and mucin domain containing 4 (*Timd4*) and an up-regulation of the transcriptional repressors *Sall1* and *Sall3* (Lavin et al., 2014; Mass et al., 2016). In the DEGs identified between E9 and E10 WT progenitors, we found a significantly decreased of *CD206/Mrc1* and *Timd4* expression levels and a significant increase of *Sall3* but not of *Sall1* (slightly increased but not statistically significantly) expression in E9 MΦ^{Prim} progenitors **(Figure 10C)**. Compared to *Sall3*, *Sall1* is expressed at low levels during early embryonic stage (Mass et al., 2016) and it seems more important to maintain microglia identity in the adult than during embryonic stages (Buttgereit et al., 2016). The expression pattern of *CD206/Mrc1*, *Timd4* and *Sall3* suggests that E9 MΦ^{Prim} progenitors already show a partial bias to microglia expression pattern.

On the other hand, we observed that E10 MΦ progenitors had an increased expression of transcriptional regulators specific to other tissue resident MΦ, such as *Id3* for Kupffer cells (Mass et al., 2016) and *Runx3* for Langerhans cells (Fainaru et al., 2004) **(Figure 10B)**. All the information gathered here point to E9 $M\Phi^{Prim}$ progenitors as the source of embryonic microglia and also favor the hypothesis that most other tissue resident MΦ derive from EMP progenitors. These results suggest that the first stage of microglia development is already started in $M\Phi^{Prim}$ progenitors in E9 YS.

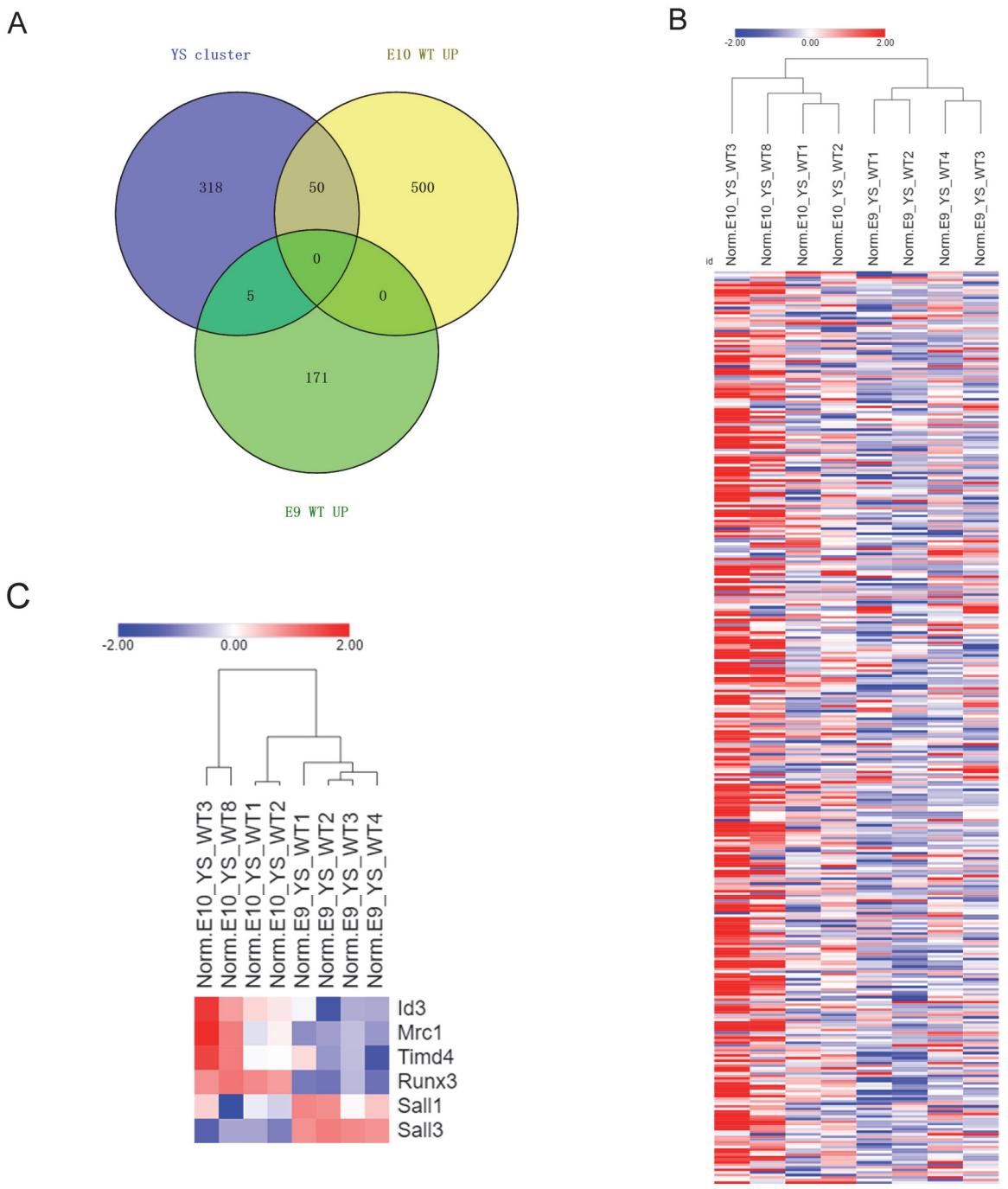

Figure 10: **Gene expression pattern of WT E9 YS MΦ^{Prim} progenitors compared to E10 YS MΦ$^{Prim+T-Def}$ progenitors.**

A. E10 YS MΦ$^{Prim+T-def}$ progenitors display a YS MΦ cluster expression pattern compared to E9 YS MΦ^{Prim} progenitors. Venn diagram showing overlap patterns of genes that are differentially expressed in E9 YS MΦ^{Prim} progenitors compared to E10 YS MΦ$^{Prim+T-def}$ progenitors with YS MΦ cluster.

B. Heatmap comparison of YS cluster genes (Matcovitch-Natan et al., 2016) expression pattern in E9 YS MΦ^{Prim} and E10 YS MΦ$^{Prim+T-def}$ progenitors. Heatmap displays transformed log2-expression values from red to blue via white.

C. E9 YS MΦ^{Prim} progenitors showed an embryonic microglia specific signature compared to E10 YS MΦ$^{Prim+T-def}$ progenitors. The heatmap shows the expression profiles of few DEGs that mark embryonic

tissue resident MΦ development. Heatmap displays transformed log2-expression values from red to blue via white.

Moreover, we had discovered that in *Lyl-1*$^{LacZ/LacZ}$ embryos, E12 microglia was defective, with both a decreased cell number and morphological defects **(see results part 1 chapter 2.1.4)**. We wanted to know whether these defects could already be suggested by microglia related biased DEGs in early YS E9 MΦ^{Prim} progenitors.

IPA analysis showed that a subset of the DEGs between E9 MΦ^{Prim} progenitors and E9 *Lyl-1*$^{lacZ/lacZ}$ was related to brain formation and neuron development **(Figure 11A)**. From a developmental point of view, the brain rudiment just starts the neurogenesis process from E9 (Reemst et al., 2016), this observation suggested Lyl-1 gene invalidation in early MΦ progenitors would influence neural development of microglia related function. In GSEA analysis, we observed that E9 *Lyl-1*$^{lacZ/lacZ}$ MΦ progenitors were enriched in synaptic related function, such as *regulation of synaptic transmission*, *pre-synaptic membrane* and *excitatory synapse* **(**Red bar in **Figure 11B)**. The individual enrichment plots are shown in **Figure 11C.**

As microglia is involved in synaptic pruning *(Paolicelli et al., 2011; Zhan et al., 2014)*, our previous results from adult stage have found that in Lyl-1 deficient microglia shows an increased activated phenotype, and the overall spine density of pyramidal neurons was significantly reduced in *Lyl-1*$^{LacZ/LacZ}$ mice. Based on this pre-microglia timing, this probably represents microglia progenitors that already start to shift into a microglia related gene expression pattern with roles in synaptic pruning and neural maturation, already from the E9 stage, and that Lyl-1 is one of the transcription factors which governs this transition.

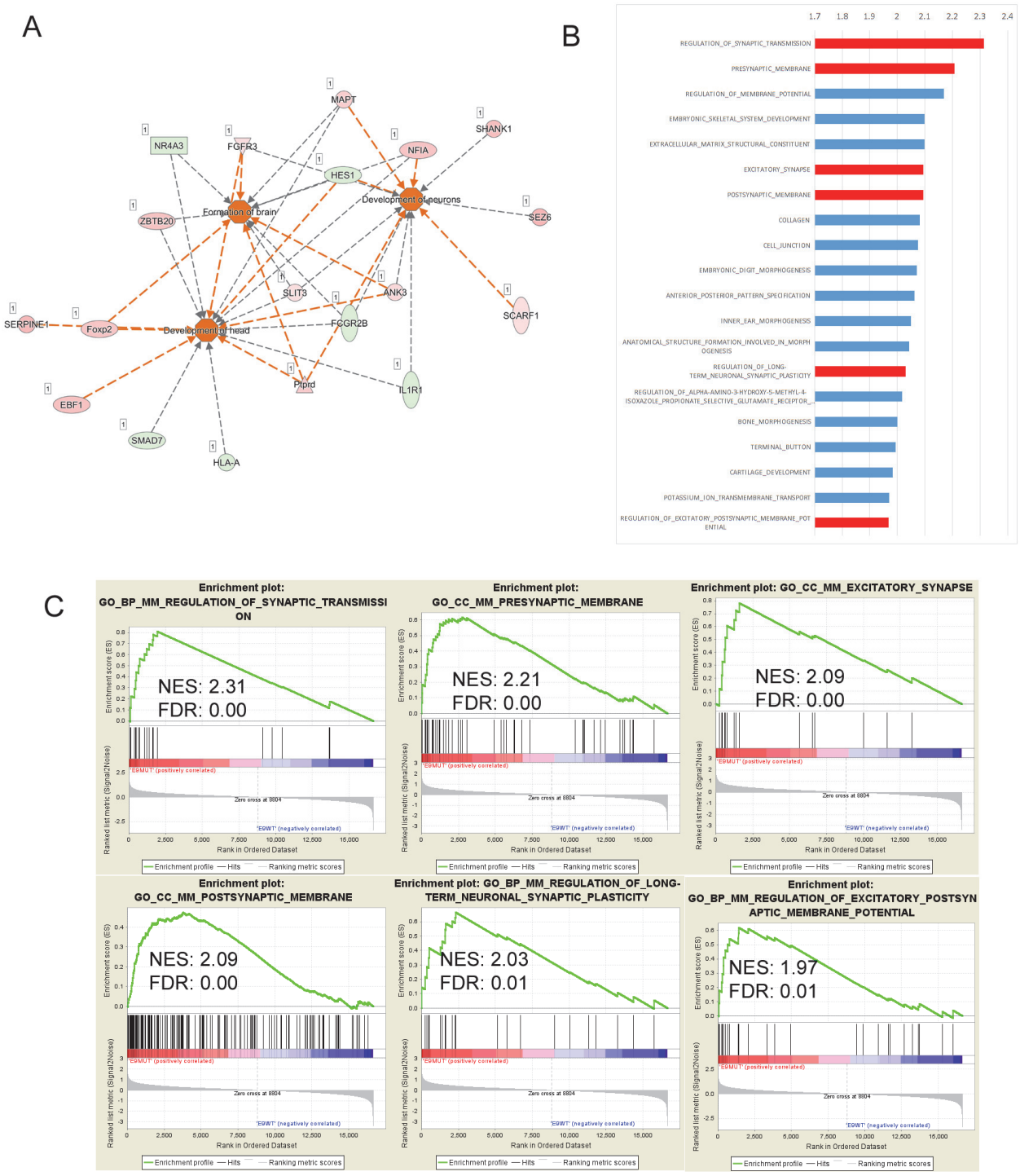

Figure 11: E9 *Lyl-1*$^{lacZ/lacZ}$ MΦ A1 progenitors are enriched in neurogenesis and synaptic regulation related function compared to E9 WT.

A. IPA functional analysis of DEGs enriched in E9 Lyl-1$^{lacZ/lacZ}$ MΦ A1 progenitors predicted them enriched in neurogenesis related function;

B. Top 20 GSEA enrichment GO term in E9 *Lyl-1*$^{lacZ/lacZ}$. Bar length indicates the absolute value of NES and the red color represents the GO term relating to synaptic regulation.

C. GSEA plot of GO term related to synaptic regulation enriched in E9 *Lyl-1*$^{lacZ/lacZ}$ MΦ progenitors. NES: Normalized enrichment score; FDR: False discovery rate.

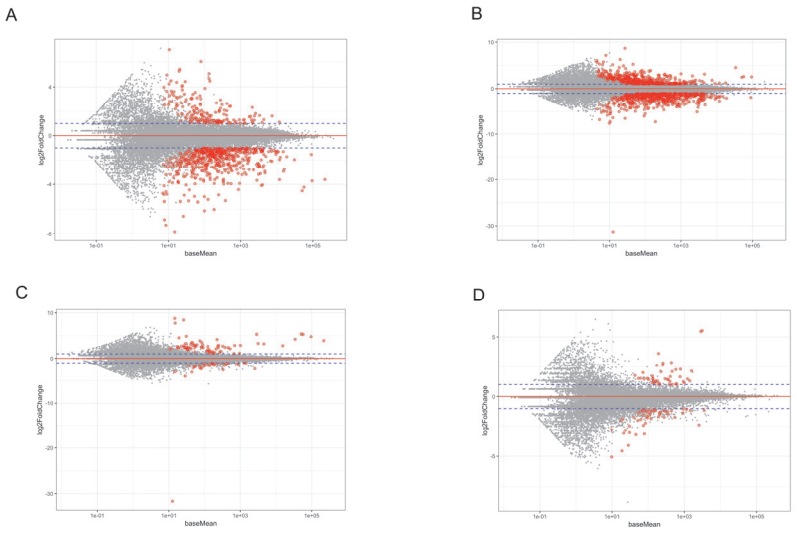

Supplemental Figure 1: MA plots show a similar expression scale of whole transcriptome data between E9/10 WT and *Lyl-1*$^{LacZ/LacZ}$ YS MΦ progenitors.
The samples exhibited similar expression scale, mainly ranging from 1e-01 to 1e05 (X axis). Each dot represents a gene. Gray dots: genes with Padj > 0.05. Red dots: genes with Padj < 0. 05. Y axis: MA plot of log2 fold change of normalized counts between two comparisons. A: E9 WT vs. E10 WT; B: E9 *Lyl-1*$^{LacZ/LacZ}$ vs. E10 *Lyl-1*$^{LacZ/LacZ}$; C: E9 *Lyl-1*$^{LacZ/LacZ}$ vs. E9 WT; D: E10 *Lyl-1*$^{LacZ/LacZ}$ vs. E10 WT.

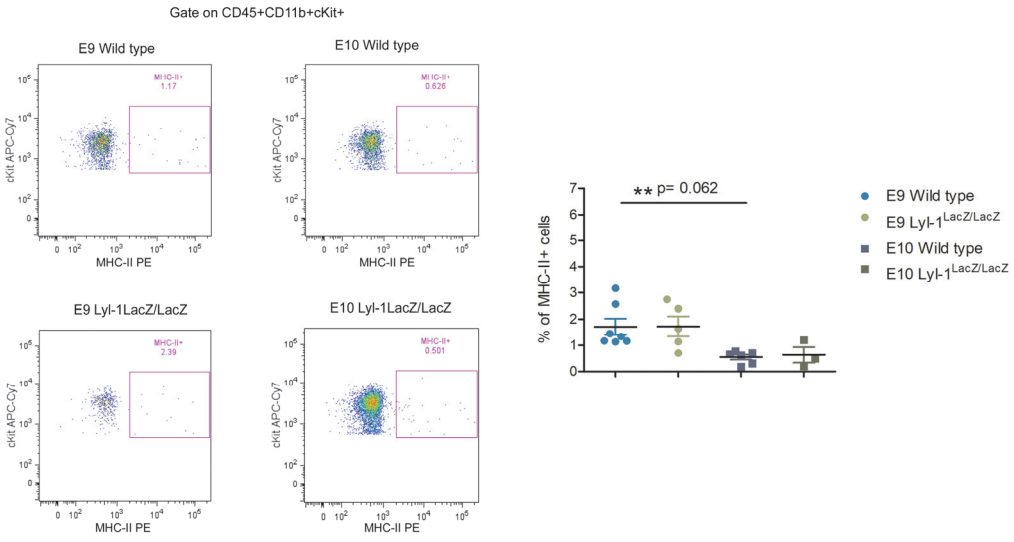

Supplementary Figure 2： MHC-II expression level in is significatnly higher in E9 compared to E10 YS MΦ progenitors.
Left: MHC-II expression level in E9/E10 wild type and *Lyl-1*$^{LacZ/LacZ}$.
Right: Statistical analysis of the percentage of MHC-II expressing cell in MΦ A1 progenitors.

Supplemental table1：GSEA related information for the figures.

NAME: related to Figure 2	SIZE	ES	NES	NOM p-val	FDR q-val	FWER p-val	RANK AT MAX	LEADING EDGE
TFACTS_MM_GATA1	23	-0.884	-2.526	0	0	0	1045	tags=74%, list=6%, signal=79%
NAME: related to Figure 3 E9 WT vs. E10 WT	**SIZE**	**ES**	**NES**	**NOM p-val**	**FDR q-val**	**FWER p-val**	**RANK AT MAX**	**LEADING EDGE**
PANTHER_MM_TOLL_RECEPTOR_SIGNALING_PATHWAY	38	-0.585	-1.820	0.000	0.036	0.227	2286	tags=29%, list=14%, signal=33%
WIKIPATHWAYS_MM_TGF_BETA_SIGNALING_PATHWAY-WP366	109	-0.473	-1.769	0.000	0.042	0.388	2237	tags=23%, list=13%, signal=26%
WIKIPATHWAYS_MM_TNF_ALPHA_SIGNALING_PATHWAY-WP231	82	-0.457	-1.653	0.001	0.082	0.852	2731	tags=23%, list=16%, signal=28%
NETPATH_MM_TGFBETA_RECEPTOR_SIGNALING_PATHWAY	208	-0.391	-1.604	0.000	0.105	0.956	2237	tags=19%, list=13%, signal=21%
BIOCARTA_MM_NFKB_ACTIVATION_BY_NONTYPEABLE_HEMOPHILUS_INFLUENZAE	23	-0.518	-1.455	0.053	0.183	1	466	tags=17%, list=3%, signal=18%
WIKIPATHWAYS_MM_CYTOKINES_AND_INFLAMMATORY_RESPONSE-WP530	20	-0.524	-1.440	0.063	0.199	1	3184	tags=50%, list=19%, signal=62%
NAME: related to Figure 4E	**SIZE**	**ES**	**NES**	**NOM p-val**	**FDR q-val**	**FWER p-val**	**RANK AT MAX**	**LEADING EDGE**
TFACTS_MM_GATA1	23	-0.813	-2.300	0	0	0	1944	tags=70%, list=12%, signal=79%
NAME: related to Figure 5 E9 Mut vs. E10 Mut	**SIZE**	**ES**	**NES**	**NOM p-val**	**FDR q-val**	**FWER p-val**	**RANK AT MAX**	**LEADING EDGE**
WIKIPATHWAYS_MM_TOLL-LIKE_RECEPTOR_SIGNALING_PATHWAY-WP75	86	-0.579	-2.135	0	0.001	0.001	2749	tags=38%, list=17%, signal=46%
BIOCARTA_MM_NF-KB_SIGNALING_PATHWAY	22	-0.692	-1.981	0	0.005	0.024	1740	tags=32%, list=10%, signal=35%
WIKIPATHWAYS_MM_TNF_ALPHA_SIGNALING_PATHWAY-WP231	82	-0.542	-1.969	0	0.005	0.030	2452	tags=28%, list=15%, signal=33%
WIKIPATHWAYS_MM_CYTOKINES_AND_INFLAMMATORY_RESPONSE-WP530	20	-0.689	-1.940	0	0.006	0.052	3467	tags=75%, list=21%, signal=95%
WIKIPATHWAYS_MM_TGF_BETA_SIGNALING_PATHWAY-WP366	109	-0.492	-1.879	0	0.009	0.132	2061	tags=26%, list=12%, signal=29%
NETPATH_MM_TGFBETA_RECEPTOR_SIGNALING_PATHWAY	208	-0.402	-1.670	0	0.046	0.852	2134	tags=20%, list=13%, signal=23%
NAME: related to Figure 7A E9 Mut vs. E9 WT	**SIZE**	**ES**	**NES**	**NOM p-val**	**FDR q-val**	**FWER p-val**	**RANK AT MAX**	**LEADING EDGE**
TFACTS_MM_SPI1	73	-0.580	-2.264	0	0	0	2511	tags=44%, list=15%, signal=51%
TFACTS_MM_NFKB1	111	-0.424	-1.771	0	0.05340364	0.238	2039	tags=32%, list=12%, signal=36%
NAME: related to Figure 7C upper panel E9 Mut vs. E9 WT	**SIZE**	**ES**	**NES**	**NOM p-val**	**FDR q-val**	**FWER p-val**	**RANK AT MAX**	**LEADING EDGE**
GO_BP_MM_INFLAMMATORY_RESPONSE	158	-0.551	-2.4324	0	0	0	2386	tags=44%, list=14%, signal=50%
GO_BP_MM_IMMUNE_RESPONSE	120	-0.563	-2.3604	0	0	0	2462	tags=45%, list=15%, signal=52%
GO_BP_MM_CELLULAR_RESPONSE_TO_LIPOPOLYSACCHARIDE	53	-0.613	-2.2634	0	4.28E-04	0.002	1796	tags=51%, list=11%, signal=57%
GO_BP_MM_INNATE_IMMUNE_RESPONSE	102	-0.521	-2.1724	0	0.00138	0.009	2875	tags=41%, list=17%, signal=49%
GO_BP_MM_DEFENSE_RESPONSE_TO_VIRUS	50	-0.562	-2.0252	0.002	0.00980	0.097	3026	tags=48%, list=18%, signal=58%
GO_BP_MM_HUMORAL_IMMUNE_RESPONSE	17	-0.702	-1.9997	0	0.01178	0.142	3811	tags=82%, list=23%, signal=107%
GO_BP_MM_DEFENSE_RESPONSE_TO_GRAM-POSITIVE_BACTERIUM	35	-0.589	-1.9554	0.0022	0.01518	0.254	2645	tags=66%, list=16%, signal=78%
GO_BP_MM_POSITIVE_REGULATION_OF_TUMOR_NECROSIS_FACTOR_PRODUCTION	27	-0.624	-1.9374	0	0.01798	0.307	2645	tags=52%, list=16%, signal=62%
NAME: related to Figure 7C lower panel E9 Mut vs. E9 WT	**SIZE**	**ES**	**NES**	**NOM p-val**	**FDR q-val**	**FWER p-val**	**RANK AT MAX**	**LEADING EDGE**
KEGG_MM_NF-KAPPA_B_SIGNALING_PATHWAY	81	-0.640	-2.544	0	0	0	2386	tags=42%, list=14%, signal=49%
PANTHER_MM_TOLL_RECEPTOR_SIGNALING_PATHWAY	38	-0.576	-1.975	0	0.00990	0.06	2944	tags=42%, list=18%, signal=51%
BIOCARTA_MM_TNFR2_SIGNALING_PATHWAY	17	-0.643	-1.781	0.004	0.04124	0.458	1873	tags=41%, list=11%, signal=46%
NAME: related to Figure 11 E9 Mut vs. E9 WT	**SIZE**	**ES**	**NES**	**NOM p-val**	**FDR q-val**	**FWER p-val**	**RANK AT MAX**	**LEADING EDGE**
GO_BP_MM_REGULATION_OF_SYNAPTIC_TRANSMISSION	18	0.8095	2.314	0	9.6E-04	0.001	1924	tags=72%, list=12%, signal=82%
GO_CC_MM_PRESYNAPTIC_MEMBRANE	48	0.6164	2.207	0	2.8E-03	0.006	2739	tags=52%, list=16%, signal=62%
GO_CC_MM_EXCITATORY_SYNAPSE	15	0.7814	2.094	0	4.5E-03	0.029	1596	tags=60%, list=10%, signal=66%
GO_CC_MM_POSTSYNAPTIC_MEMBRANE	158	0.4745	2.093	0	3.8E-03	0.029	3779	tags=46%, list=23%, signal=59%
GO_BP_MM_REGULATION_OF_LONG-TERM_NEURONAL_SYNAPTIC_PLASTICITY	23	0.6655	2.030	0	5.2E-03	0.075	2308	tags=57%, list=14%, signal=66%
GO_BP_MM_REGULATION_OF_EXCITATORY_POSTSYNAPTIC_MEMBRANE_POTENTIAL	27	0.6189	1.967	0.00210	1.0E-02	0.203	1413	tags=44%, list=8%, signal=48%

Supplemental table 2：IPA related information for the figures.

Ingenuity Canonical Pathways related to figure 3 (E10 Mut vs. E10 WT)	-log (p-value)	zScore	Ratio	Molecules
Role of Pattern Recognition Receptors in Recognition of Bacteria and Viruses	3.1	-2.121	0.102	CCL5,TLR1,C1QB,LIF,C3AR1,C1QC,IL18,C5AR1,TNF,OAS3,RNASEL,TLR2,NLRC4
Inflammasome pathway	2.36	-2.000	0.211	IL18,CTSB,NLRC4,P2RX7
Eicosanoid Signaling	2.07	2.000	0.109	CYSLTR1,PLA2G4B,FPR2,PLA2G7,PTGER4,PLBD1,ALOX15
TNFR1 Signaling	1.53	-2.000	0.104	JUN,TNFAIP3,PAK6,TNF,NFKBIA
Colorectal Cancer Metastasis Signaling	1.39	-2.324	0.06	MMP25,JUN,MMP9,VEGFA,TLR1,MRAS,PTGER4,FZD9,MMP19,FZD1,TNF,RHOB,MMP8,MMP28,TLR2
ILK Signaling	1.37	-2.121	0.0638	JUN,VIM,MYH14,FN1,MMP9,DSP,VEGFA,TNF,RHOB,BMP2,RPS6KA4,KRT18
Agrin Interactions at Neuromuscular Junction	1.33	-2.236	0.0833	JUN,PAK6,PKLR,MRAS,ITGA4,ERBB3
TGF-β Signaling	1.32	-2.000	0.0769	JUN,MRAS,FOXH1,RUNX3,VDR,HNF4A,BMP2
Ingenuity Canonical Pathways related to figure 5 (E9Mut vs. E10Mut)	**-log (p-value)**	**zScore**	**Ratio**	**Molecules**
TREM1 Signaling	5.78	-2.840	0.217	TLR1,MPO,NOD1,ITGAX,CASP1,IL6,Naip1 (includes others), CD83,FCGR2B,NLRP10,NLRP3,TNF,CCL2,TREM1,CXCL3
Neuroinflammation Signaling Pathway	2.8	-2.858	0.0947	MMP9,HLA-DQA1,TLR1,IFNGR2,IL6,IRAK3,Naip1 (includes others), FZD1,TNF,HLA-DRB5,SLC1A3,GABRB1,HLA-DOA,HLA-DQB1,CXCL10, IL4,CASP1,PLA2G4F,GABRA2,HMOX1,P2RX7,PLA2G4C,NLRP3,PTGS2,CCL2,MAPK13,IKBKE
iNOS Signaling	2.8	-2.646	0.182	LY96,IFNGR2,CD14,MAPK13,LBP,NFKBIA,IRAK3,IKBKE
Osteoarthritis Pathway	2.38	-2.065	0.098	MMP9,VEGFA,DDIT4,CASP1,CASR,BMP2,FZD9,P2RX7,FN1,SMAD7,ANKH,FZD1,TNF,PTGS2,FZD6,ITGA4,SDC4,HES1,CASP4,RUNX2
Acute Phase Response Signaling	2.35	-2.309	0.104	OSM,KLKB1,LBP,IL6,NFKBIA,HMOX1,C4A/C4B,FN1,HP,NR3C1,TNF,MAPK13,IL1A,SERPINA1,SERPINE1,VWF,IKBKE
p53 Signaling	2.07	-2.333	0.112	PERP,DRAM1,BBC3,SERPINE2,CDKN1A,PLAGL1,GADD45B,GADD45A,THBS1,HIPK2,COQ8A,HDAC9
Role of IL-17F in Allergic Inflammatory Airway Diseases	2.35	-2.236	0.171	RPS6KA5,CXCL10,CCL2,IL6,CCL4,IGF1,RPS6KA4
HMGB1 Signaling	1.75	-2.887	0.0985	OSM,IFNGR2,IL4,RHOC,LIF,IL13,IL6,TNF,RHOB,CCL2,MAPK13,IL1A,SERPINE1
Ingenuity Canonical Pathways related to figure 6 (E9 Mut vs. E9 WT)	**-log (p-value)**	**zScore**	**Ratio**	**Molecules**
Dendritic Cell Maturation	4.8	-1.342	0.0412	FGFR3,CCR7,HLA-A,FCGR2B,HLA-DQA1,IL1A,IL36G
IL-6 Signaling	3.41	-1.000	0.0382	FGFR3,IL1R1,CD14,IL1A,IL36G
PKCθ Signaling in T Lymphocytes	3.04	-1.342	0.0316	FGFR3,CARD11,HLA-A,NFATC2,HLA-DQA1
Acute Phase Response Signaling	2.97	-1.000	0.0305	IL1R1,KLKB1,IL1A,SERPINE1,IL36G
NF-κB Signaling	2.8	-1.342	0.0279	FGFR3,CARD11,IL1R1,IL1A,IL36G
Role of NFAT in Regulation of the Immune Response	2.77	-1.342	0.0275	FGFR3,HLA-A,FCGR2B,NFATC2,HLA-DQA1
LXR/RXR Activation	2.74	2.000	0.0364	IL1R1,CD14,IL1A,IL36G
iCOS-iCOSL Signaling in T Helper Cells	2.65	-1.000	0.0345	FGFR3,HLA-A,NFATC2,HLA-DQA1
Osteoarthritis Pathway	1.8	-1.000	0.0196	FGFR3,SMAD7,IL1R1,HES1
Ingenuity Canonical Pathways related to figure 8 (E10 Mut vs. E10 WT)	**-log (p-value)**	**zScore**	**Ratio**	**Molecules**
Th1 Pathway	4.76	-0.447	0.0492	HLA-A,ICOS,NFATC2,HLA-DQA1,RUNX3,IL27RA
Th1 and Th2 Activation Pathway	3.98	ND	0.0357	HLA-A,ICOS,NFATC2,HLA-DQA1,RUNX3,IL27RA
Th2 Pathway	3.47	ND	0.037	HLA-A,ICOS,NFATC2,HLA-DQA1,RUNX3
iCOS-iCOSL Signaling in T Helper Cells	2.75	-2	0.0345	HLA-A,ICOS,NFATC2,HLA-DQA1
Calcium-induced T Lymphocyte Apoptosis	2.66	ND	0.0517	HLA-A,NFATC2,HLA-DQA1
T Helper Cell Differentiation	2.48	ND	0.0448	HLA-A,ICOS,HLA-DQA1
Caveolar-mediated Endocytosis Signaling	2.44	ND	0.0435	HLA-A,ITSN1,ITGA9
Antigen Presentation Pathway	2.16	ND	0.0714	HLA-A,HLA-DQA1
B Cell Development	2.16	ND	0.0714	HLA-A,HLA-DQA1
IL-4 Signaling	2.13	ND	0.0337	HLA-A,NFATC2,HLA-DQA1
Sulfate Activation for Sulfonation	2.05	ND	0.5	PAPSS2,
Role of NFAT in Regulation of the Immune Response	2.05	-1	0.022	FCGR2B,HLA-A,NFATC2,HLA-DQA1
Autoimmune Thyroid Disease Signaling	1.93	ND	0.0541	HLA-A,HLA-DQA1
Neuroprotective Role of THOP1 in Alzheimer's Disease	1.92	ND	0.028	HLA-A,PRSS57,PRSS2
Graft-versus-Host Disease Signaling	1.91	ND	0.0526	HLA-A,HLA-DQA1
CD28 Signaling in T Helper Cells	1.75	ND	0.0242	HLA-A,NFATC2,HLA-DQA1
Nur77 Signaling in T Lymphocytes	1.66	ND	0.0392	HLA-A,HLA-DQA1
Allograft Rejection Signaling	1.59	ND	0.0357	HLA-A,HLA-DQA1
Chondroitin and Dermatan Biosynthesis	1.58	ND	0.167	CSGALNACT1,
PXR/RXR Activation	1.53	ND	0.0333	PAPSS2,ABCC3
PKCθ Signaling in T Lymphocytes	1.47	ND	0.019	HLA-A,NFATC2,HLA-DQA1
Sphingomyelin Metabolism	1.46	ND	0.125	SGMS2,
OX40 Signaling Pathway	1.46	ND	0.0303	HLA-A,HLA-DQA1
TREM1 Signaling	1.42	ND	0.029	FCGR2B,TREM1
Dendritic Cell Maturation	1.39	ND	0.0176	FCGR2B,HLA-A,HLA-DQA1
Role of Macrophages, Fibroblasts and Endothelial Cells in Rheumatoid Arthritis	1.3	ND	0.0129	NFATC2,PRSS2,CEBPE,VEGFC

ID related to Fig 3	Analysis	Molecules in Network	Score	Focus Molecules	Top Diseases and Functions
1	E10_MUT_vs_E10_WT	Akt,BACH2,CEBPE,CLEC10A,FCGR2B,FLT3,HLA-A,HLA-DQA1,ICOS,IFN alpha/beta,IL12 (complex),IL12(family),IL27RA,ITSN1,IgG,IgG1,IgG2a,IgG2b,Iga,Ige,Igg3,Immunoglobulin, Interferon alpha,LAX1,LGALS3BP,LTB4R,MHC,MHC Class II (complex) ,NUAK1, OLFM4, PLD2,PRG2,RASGRP3,STAT5a/b,TREM3	37	19	Cell-To-Cell Signaling and Interaction, Hematological System Development and Function, Immune Cell Trafficking
ID related to Fig 5	**Analysis**	**Molecules in Network**	**Score**	**Focus Molecules**	**Top Diseases and Functions**
1	E9_MUT_vs_E10_MUT	ABCC2,ADD2,ALAS2,ANK1,CBX2,CBX4,CTSE,Cathepsin,Ctbp,EPB42,GATA1,GPC3,Gypa,HBA1/HBA2,HBB,HBG2,HBZ,HIPK2,HP,Jnk,KLF1,KLF6,MECOM,PERP,PHF19,PPP1R15A,RAB3A ,RAB3D,RHAG,RNASEL,SLC4A1,TCF,USP26,ZC3H12A,hemoglobin	35	30	Cell Morphology, Hematological System Development and Function, Hematopoiesis
2	E9_MUT_vs_E10_MUT	ABCD2,Aldose Reductase,B3GNT2,B3GNT8,B4GALNT1,BANP,C3AR1,C4A/C4B, CAMP, CD300LB,CD48,CD55,CEBPE,CLEC10A,CLEC5A,Daf,ELANE,EPX,H2-a,IL17a dimer,LTB4R , Ngp,PILRA,PILRB,PRG2, RAB37,SLC14A1,Srebp,Srgn, TIMD4,TNF,TREM3,TREML1, ZFP36L1, peptidase	33	29	Cell-To-Cell Signaling and Interaction, Hematological System Development and Function, Immune Cell Trafficking
ID related to Fig 6	**Analysis**	**Molecules in Network**	**Score**	**Focus Molecules**	**Top Diseases and Functions**
1	E9_MUT_vs_E9_WT	AMPK,ASB2,Alp,CKMT1A/CKMT1B,Collagen(s),EBF1,ERK1/2,GABA-A receptor, GABRA2, GABRB1,GALNT3,Gsk3,HES1,HISTONE,Insulin,KCNA3,KLKB1,LPIN1,MAPT,NOVA1,NR4A3,P 38 MAPK,PI3K (complex),PLIN1,Pka,Ptprd,SERPINE1,SMAD7,SRC (family),STAT, STAT5a/b, Tgf beta, Ubiquitin,Vegf,ZBTB20	34	18	Connective Tissue Development and Function, Tissue Morphology, Cell Morphology
2	E9_MUT_vs_E9_WT	Akt,BCR (complex),CARD11,CCR7,CD14,CLEC11A,Col17a1,FCGR2B,FGFR3,HLA-A,HLA-DQA1,IFN Beta,IFN alpha/beta,IL1,IL12 (complex),IL1A,IL1R1,IL27RA,IL36G, Ifn,IgG, IgG1, IgG2a,Ige,Igg3,Igm,Immunoglobulin,MHC,MHC Class II (complex),NFATC2,PRKG2,Pro-inflammatory Cytokine,Rac,SCARF1,Tlr	29	16	Cell-To-Cell Signaling and Interaction, Hematological System Development and Function, Tissue Morphology
ID related to Fig 8	**Analysis**	**Molecules in Network**	**Score**	**Focus Molecules**	**Top Diseases and Functions**
1	E10_MUT_vs_E10_WT	Akt,BACH2,CEBPE,CLEC10A,FCGR2B,FLT3,HLA-A,HLA-DQA1,ICOS,IFN alpha/beta,IL12 (complex),IL12 (family),IL27RA,ITSN1,IgG,IgG1,IgG2a,IgG2b, Iga,Ige,Igg3,Immunoglobulin, Interferon alpha, LAX1,LGALS3BP,LTB4R,MHC,MHC Class II (complex),NUAK1,OLFM4, PLD2,PRG2,RASGRP3,STAT5a/b,TREM3	37	19	Cell-To-Cell Signaling and Interaction, Hematological System Development and Function, Immune Cell Trafficking

Materials and methods

Mice and embryos

Mice were housed in the animal facilities of Institut Gustave Roussy ("Plate-forme d'évaluation préclinique", animal facility licence #E94-076-11). All animal experiments were conducted in compliance with French regulations (Transposition of Directive 2010/63), under authorized project #5798-2016062214256796 approved by officially accredited Ethical committee n°26. C57BL/6J mice from Harlan or Charles Rivers Laboratories, France, referred to as wild type (WT). *Lyl-1*^{LacZ} mice (on a C57BL/6J/Ly5.2 background), genotyped as described before (Capron et al., 2006) were to generate *Lyl-1*$^{LacZ/LacZ}$ embryos. The day of vaginal plug observation was considered as E0.5.

Tissues preparation and cell sorting

Pregnant females were sacrificed by cervical dislocation and embryos were staged by somite counting. YS at E9 or E10 were dissected as described previously (Bertrand et al., 2005a). Ter119^{-}CD45^{+}CD11b^{+}ckit^{+} MΦ A1 progenitors were sorted from WT or *Lyl-1*$^{lacZ/LacZ}$ YS at E9 or E10, using BD Aria III. Sorted cells were dry-pelleted at 1500rpm for 5mins at 4°C and the samples were stored in 200ul Trizol at -80 °C until RNA extraction.

RNA-purification and RNA-sequencing

Total RNA was extracted from FACS sorted MΦ progenitors using Trizol methods. The RNA concentration and the quality of the samples were determined using Agilent Bioanalzyer. The sequencing was performed by the genomic facility on a HiSeq2000 instrument, using single-read sequencing (50 bp; >30 MIO-reads per run).

Data analysis

The pre-processing of RNA-seq data was performed by Dr. Guillaume Meurice at the bioinformatics platform of the Gustave Roussy Institute. Briefly, a quality check was conducted using FastQC (Andrews, 2010) and reads were mapped to the GRCm38 mouse genome (release M17) using the Star aligner (Dobin et al., 2013). The interpretation of transcript quantification was done by multiQC (salmon) (Patro et al., 2017). DESeq2 package was applied to normalize the data and to identify differential genes expression. Principal component analysis (PCA), MA-plots, heatmaps and volcano plots were also generated using

DESeq2. Genes with an absolute fold change above 2 and Padj value/false discovery rate below 0.05 were selected as different expressed genes (DEGs). Heatmaps for selected gene sets were visualized using online website Morpheus (Broad Institute). Venn diagrams were constructed using the Venny software (http://bioinfogp.cnb.csic.es/tools/venny/). Gene enrichment assay was done by Ingenuity Pathway Analysis (IPA) or GSEA (Broad Institute) or online g:Profiler software.

PCA analysis was used to reduce the dimension of our dataset, with the first principal component being the mathematical combination of measurements that account for the largest amount of variability in the data (Reich et al., 2008). The second component finds the coefficients that maximize variance orthogonally to the first component.

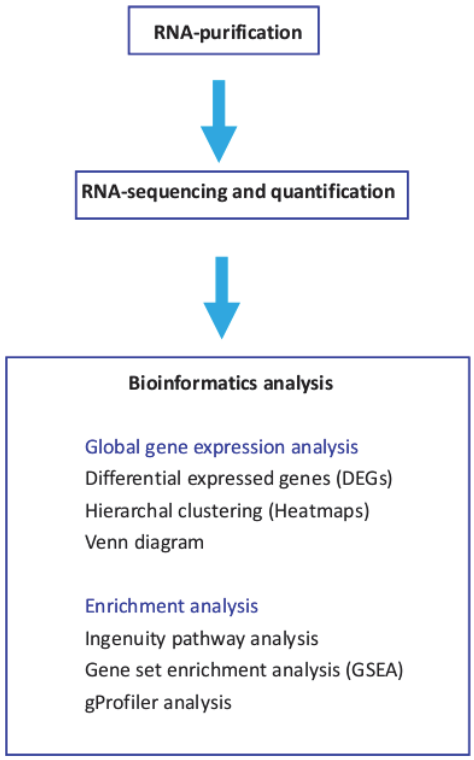

Figure 12: Chart illustrating the general analysis used in this study.

GSEA analysis

Gene Set Enrichment Analysis (GSEA) is a powerful analytical method for interpreting the characteristic of transcriptome data (Subramanian et al., 2005) as shown in **Figure 13**.

GSEA has several advantages compared basic transcriptome analyses. Firstly, basic DEGs analyses always select genes that are highly modified, for example fold change above 2, this

may neglect a lot of genes which are slightly changed but important during some process, such as development. On the other hand, GSEA, using knowledge-based gene sets to define ranked gene list and this would help to pinpoint previously ignored data, for example, if many genes in your transcriptome belonging to one specific gene set are changed, even slightly, this could lead to some interesting discovery.

Secondly, the DEGs are simply identified through change in expression levels by a per gene statistic method, the genes are distinguished into either differentially expressed or non-differentially expressed genes according to a selected threshold. The GSEA will also sort the genes in a per gene statistic approach ranking them according to the largest differences in expression levels between two phenotypes, but without a selection using a cutoff. This allows to evaluate the enrichment in a more balanced way, as the contribution of each genes is taken into consideration.

To compare given sets of gene, the GSEA sofware locates the distribution of the members of the gene sets along pre-ranked transcriptome data and calculates the enrichment significance of certain gene sets: if the gene set mainly falls at either the top (over-expressed) or bottom (under-expressed), it is thought to be related to the phenotype differences, on the contrary, if the genes in a given set are distributed randomly across the list, they are not significantly associated with any phenotypic differences. The false discovery rate below 0.25, which indicates the results is likely to be valid 3 out of 4 times, is considered to mark a significant enrichment. The detailed parameter of each GSEA plot used in this research can be found in **Supplemental table1：GSEA related information for the figures.**

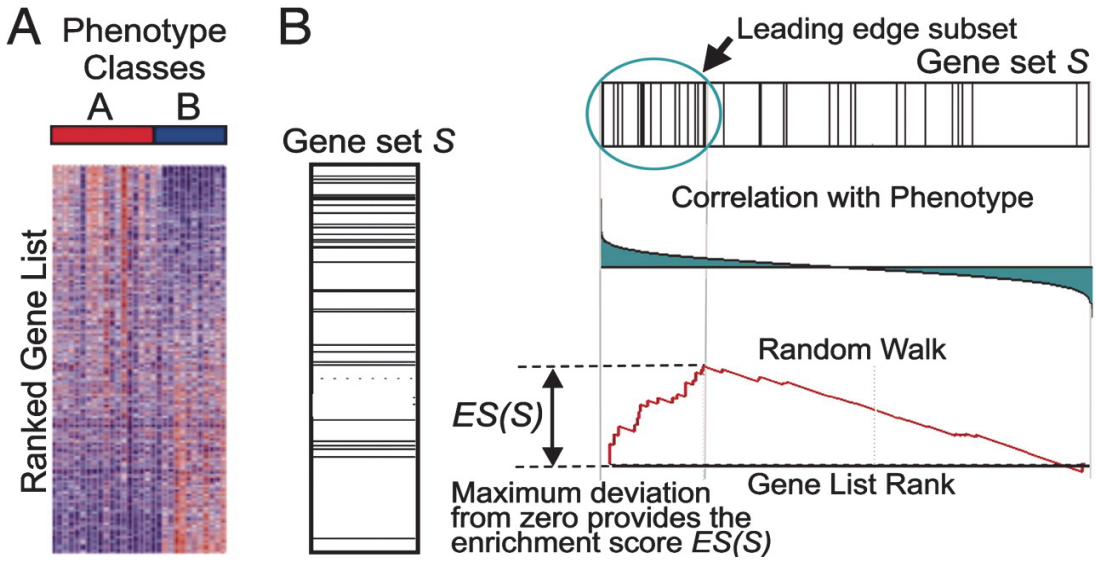

Figure 13：Overview illustrating the GSEA method.
(A) An expression data set sorted by correlation with phenotype, the corresponding heatmap, and the "gene tags", i.e., location of genes from a set S within the sorted list. (B) Plot of the running sum for S in the dataset, including the location of the maximum enrichment score (ES) and the leading-edge subset. From (Subramanian et al., 2005).

IPA-analysis

Differentially expressed genes, characterized by a fold change greater than 2 and a false discovery rate below than 0.05 (FDR < 0.05), were analyzed using the IPA software (Ingenuity Systems, Redwood City, CA, USA; www.ingenuity.com). The canonical pathway analysis was used to identify the significantly modified biological functions and pathways. Functions and pathways with P-value <0.05 (Fischer's exact test) were considered to be statistically significant. The calculated activation z-score was used to predict activation or inhibition states based on verified findings which are accessible through the Ingenuity Knowledge Base. Those pathways with a z-score $\geqslant$ 2 or $\leqslant$ –2 were considered to be significantly activated or inhibited. Diseases and Biological Functions analysis were used to reveal enriched functions among the dataset relating to Diseases and Disorders, Molecular and Cellular Functions or Physiological System Development and Function.

The significance of the association between the dataset and the functional class or canonical pathway was expressed as negative log p-value using Fisher's exact test. The molecular relationships between gene products were represented in a network generated from information contained in the Ingenuity Pathways Knowledge Base. Gene networks were generated by overlaying the filtered genes in our dataset onto global molecular networks and algorithmically generated based on their connectivity. By default, genes that were up-regulated in the dataset are shown in red and genes that were down-regulated are shown in green. The detailed parameter of each IPA plot used in this research can be found in **Supplemental table 2：IPA related information for the figures.**

2.3 Lyl-1 function during HSC development

The transcription factor Lyl-1*,* a close relative of Tal-1/SCL, is involved in translocations leading to pediatric T-cell acute lymphoblastic leukemia. The disruption of *Lyl-1* HLH domain or the deletion of the full coding sequence leads to an impaired hematopoietic repopulation ability of adult HSC. Our team previously observed that Lyl-1 and Tal-1/SCL expression patterns overlap, notably in newly generated AGM HSC. Since then, many RNA-seq or single RNA-seq data have confirmed the expression of *Lyl-1* in AGM or FL HSCs. However, the function of Lyl-1 during HSC development remains undefined.

Here, we make use of *Lyl-1*$^{lacZ/LacZ}$ mice, which lack a functional HLH domain but harbor the reporter gene LacZ, to investigate the role of Lyl-1 during the development of HSC. Previous results from the team had shown that AGM HSC were normally generated in *Lyl-1*$^{lacZ/LacZ}$ mice. I started to develop these 3 years ago. I found that Lyl-1 invalidation leads to a two-fold decrease of the HSC pool size rapidly after their generation, due to an elevated apoptosis level. This reduction of HSC pool was maintained in *Lyl-1* mutants during the subsequent development steps, in the fetal liver at E12 and E14, with no further defects of HSC proliferation and survival. Notably, the increased HSC apoptosis was specific to the generation stage, revealing that the final size of the HSC pool is determined at the initial stage of HSC generation. We are still investigating what signals (inflammatory signal/cytokines or MΦ?) influence the survival at AGM the stage and are impaired in Lyl-1 mutants.

Lyl-1 mutation reveals that the size of the HSC pool is set at the AGM stage

Deshan Ren, Shoutang Wang, Anna-Lila Kaushik, Claudia Santos, Gabriel Matherat, Yann Lécluse, William Wainchenker, Hana Raslova, Isabelle Plo, Isabelle Godin

Abstract

Lyl-1, a basic helix-loop-helix (bHLH) transcription factor paralog to Tal-1/SCL, is involved in translocations leading to pediatric T-cell acute lymphoblastic leukemia. The disruption of *lyl-1* HLH domain or the deletion of the full coding sequence leads to a reduction of the hematopoietic stem cells (HSC) population in the adult. While Tal-1/SCL requirement for HSC generation during ontogeny is well established, Lyl-1 function during developmental hematopoiesis is still unknown. Using *Lyl-1*$^{LacZ/LacZ}$ mice that lack a functional HLH domain, we previously observed that Lyl-1 and Tal-1/SCL expression patterns overlap, notably in newly generated HSC. Analyzing HSC development in Lyl-1-deficient embryos, we found that while HSC were normally generated, the pool size rapidly underwent a two-fold decrease due to an elevated apoptosis level. This reduction of HSC pool was maintained in *Lyl-1* mutants during the subsequent development steps, with no impairment of HSC proliferation, survival and expansion. Notably, the increased HSC apoptosis was specific to the generation stage, revealing that the final size of the HSC pool is determined at this stage. Lyl-1 function during HSC development thus appears distinct from- and complementary to-that of Tal-1/SCL. While Tal-1/SCL is required for HSC generation, Lyl-1 regulates HSC pool size.

Introduction

The basic helix-loop-helix (bHLH) transcription factors, *Tal-1/Scl (Begley et al., 1989)* and *Lyl-1 (Chen et al., 1990; Mellentin et al., 1989)* are paralogous genes that were first identified in chromosomal translocation leading to pediatric T-cell acute lymphoblastic leukemia (T-ALL). These genes belong a hematopoietic transcriptional complex, which regulates the various hematopoiesis features, such as cell fate decision, Hematopoietic Stem Cell (HSC) maintenance and differentiation *(Wilson et al., 2011)*. The regulation of these pleiotropic functions relies on the nature of the partners present/active within the complex at a given time and on the availability of target genes *(Pina and Enver, 2007)*. More

recently, gene dosage within this complex also emerged as an essential regulator.

This can be exemplified by the relative importance of Lyl-1 and Tal-1/Scl in the control of HSC self-renewal. While Lyl-1 invalidation led to an impaired competitive long term reconstitution (LTR) ability of adult HSC *(Capron et al., 2006; Souroullas and Goodell, 2011),* the importance of Tal-1/Scl in adult HSC self-renewal was less clear: LTR ability of adult *Tal-1/Scl* -deficient HSC was not impaired *(Curtis et al., 2004; Mikkola et al., 2003),* while shRNA-mediated decreased expression of Tal-1/Scl in HSC impaired the reconstitution capacity *(Brunet de la Grange et al., 2006)*. In fact, it appeared that the two transcription factors collaborate to maintain adult HSC self-renewal ability, as HSC deficient of both *Lyl-1* and *Tal-1/Scl* cannot reconstitute lethally irradiated recipients. Interestingly, while a single *Lyl-1* allele is sufficient to restore HSC function, a single *Tal-1/Scl* allele cannot achieve this rescue *(Souroullas et al., 2009).*

Besides its regulatory function of adult hematopoietic homeostasis, the hematopoietic complex has been shown to be active from the earliest step of hematopoietic development *(Pimanda et al., 2007b; Pina and Enver, 2007; Wilson et al., 2009)* hence the importance of defining the expression and function of the partners involved. In contrast to Tal-1/Scl, which function during developmental hematopoiesis has been extensively characterized *(Curtis et al., 2012)*, the role played by Lyl-1 in this process is currently unknown.

During vertebrate ontogeny, independents hematopoietic progenitors generation waves cooperate initially to rapidly provide the embryo with differentiated blood cells in the "HSC-independent hematopoiesis" phase and later, to produce the HSC pool that will be responsible for lifelong maintenance of hematopoiesis *(Cumano and Godin, 2007).* Erythroid and myeloid cells are generated in the yolk sac (YS), first from monopotent progenitors, in the primitive wave as soon as embryonic day (E) 7.25, and later (from E8.5) from erythro-myeloid progenitors (EMP) in the transient definitive wave *(McGrath and Palis, 2005).* HSC, characterized by their long term multilineage reconstituting (LTR) activity are generated one day later in the aorta region, called para-aortic splanchnopleura (P-Sp) from E9 to E10 (Godin et al., 1995) and aorta, gonads and mesonephros (AGM) from E10.5 to E11.5 *(Cumano and Godin, 2007; Kieusseian et al., 2012)*.

Targeted deletion of either the complete *Tal-1/Scl* sequence *(Shivdasani et al., 1995)* or its bHLH domain *(Robb et al., 1995)* leads to the absence of both extra- and intra-embryonic hematopoiesis *(Porcher et al., 1996; Robb et al., 1995)*, thus demonstrating *Tal-1/Scl* requirement for the generation of hematopoietic progenitors in both the YS and P-Sp/AGM.

In contrast, targeting *Lyl-1* bHLH domain *(Capron et al., 2006)* or its whole coding sequence *(Souroullas and Goodell, 2011)* does not lead to embryonic lethality. However, a function for Lyl-1 during the developing hematopoietic system was suggested in a previous study showing that Tal-1/Scl and Lyl-1 expression patterns during ontogeny *(Giroux et al., 2007)* are mostly overlapping, both transcription factors being expressed in the developing vasculature, in AGM-HSC and in hematopoietic cells within the fetal liver (FL).

We show here that Lyl-1 is required for the maintenance of a proper sized HSC pool in the AGM. While the generation of HSC appeared normal in the AGM of *Lyl-1*$^{LacZ/LacZ}$ embryos, functional analyses performed *in vitro* and *in vivo* showed that these AGM-HSC were functionally impaired, as shown by a 2-3 fold reduction of HSC pool size, accompanied by an increase level of apoptosis. Surprisingly, the 2-3 fold reduction of the HSC pool size appeared maintained in E12 and E14 FL of *Lyl-1*$^{LacZ/LacZ}$ embryos, without any modification of the apoptosis level, nor decrease of the proliferation rate compared to wild type embryos. These data concur with earlier data reporting a 2-3 fold reduction of the HSC pool in both E14 FL *(Capron et al., 2006)* and adult bone marrow *(Souroullas et al., 2009)* of *Lyl-1*$^{LacZ/LacZ}$, again without changes in the apoptosis and proliferation *(Capron et al., 2006; Souroullas et al., 2009; Zohren et al., 2012)*. The constant reduction of the size of the HSC pool observed upon Lyl-1 invalidation at the different stages of hematopoietic development suggests that the size of the HSC pool is set at the earliest stages of HSC development and is maintained throughout the lifespan of mice.

Results

2.3.1 AGM-HSC express Lyl-1, but do not depend on Lyl-1 for their generation

Native AGM-HSC, characterized by a CD45$^{-/lo}$ckit^{+}CD31^{+}CD41$^{+/lo}$AA4.1^{+} phenotype at E10, are located within Hematopoietic Intra-Aortic Cluster (HIAC*) (Bertrand et al., 2005a; Godin et al., 1995; Yokomizo and Dzierzak, 2010)*. Our previous confocal microscopy analyses established that Lyl-1, as well as Tal-1/SCL is expressed by CD45$^{-/lo}$ckit^{+}CD31^{+}CD41$^{+/lo}$ in E10 *Lyl-1$^{WT/LacZ}$* embryos ***(Figure 1A left panel,*** *from (Giroux et al., 2007))*. Lyl-1 expression in the HIAC was also evidenced through X-Gal staining ***(Figure 1A right panel)***. Beside X-Gal staining, β-Galactosidase (β-Gal) activity that reports Lyl-1 expression can be detected in cytometry analyses in FACS-Gal assay whereby β-Gal activity is revealed using its fluorescent substrate FDG *(Fiering et al., 1991; Guo and Wu, 2008).*

To further characterize Lyl-1-expressing progenitors, single FDG+/Lyl-1+ and FDG-/Lyl-1- cells were sorted from E10 *Lyl-1$^{WT/LacZ}$* AGM and their differentiation potential was tested *in vitro*. Most hematopoietic progenitors belonged to the FDG^{+} population ***(Figure 1B)***. At E10-10.5, when the number of Hematopoietic Stem and Progenitor Cells (HSPC) culminates *(Godin et al., 1999; Yokomizo and Dzierzak, 2010)*, the AGM contains two types of progenitors, YS-derived erythro-myeloid progenitors (EMP) present in the systemic circulation and newly generated HSPC *(Bertrand et al., 2005a).* To precise the type of progenitors (EMP vs. HSPC) that display a β-Gal activity/Lyl-1 expression, the progeny of single cells was analyzed after 14 days of OP9 culture (n=3). Nearly all (32/35) FDG^{+}/Lyl-1^{+} single progenitor cell produced erythroid, myeloid and lymphoid progenies, thus displaying the multipotent potential that characterizes HSPC. In contrast, all colonies derived from single FDG^{-}/Lyl-1^{+} progenitors (9/9), which were less frequent, lacked a lymphoid progeny, thus qualifying as EMP. Both cytological observations and *in vitro* assays correlate to show that AGM-HSPC express Lyl-1.

We next quantified by flow cytometry AGM-HSPC from E10 (30-35 Somite pairs (S)) Wild Type (WT), *Lyl-1$^{WT/LacZ}$* and *Lyl-1$^{LacZ/LacZ}$* embryos and found that the percentage of cells harboring an AGM-HSC phenotype (CD45$^{-/lo}$ckit^{+}CD31^{+}CD41$^{+/lo}$AA4.1^{+}) was similar for the 3 genotypes ***(Figure 1C; Sup. Figure 1A, B)***. Since the AGM cellularity was identical in the 3 genotypes, it appears that Lyl-1 inactivation does not modify the amount of HSPC present in native E10 AGM. The independency of Lyl-1 for HSPC generation was also evidenced through the organ culture of the P-Sp/AGM presumptive territory, called Splanchnopleura

(Sp) that allows mesoderm commitment toward a HSC fate (Cumano et al., 2001; Ganuza et al., 2018). Sp explants were isolated at E8 (0-5S) ***(Sup. Figure 1C)***, i.e. prior to the establishment of blood connections, in order to avoid a contamination by YS cells *(McGrath et al., 2003)*. After three days in organ culture, the number of newly generated hematopoietic progenitors was quantified by limiting dilution assay (LDA). The number of HSPC recovered from Sp-explants was similar in the three genotypes ***(Sup. Figure 1C)***. This confirmed that *Lyl-1* deficiency does not impair HSC generation. Accordingly, the expression levels of the major genes involved in HSC generation (*Runx1*, *Tal1/Scl*, *Lmo2*, *cMyb* and *Meis1*) were not significantly modified in E10 AGM HSPC, except for a decreased *Meis1* expression level ***(Sup. Figure 1D)***.

Figure 1

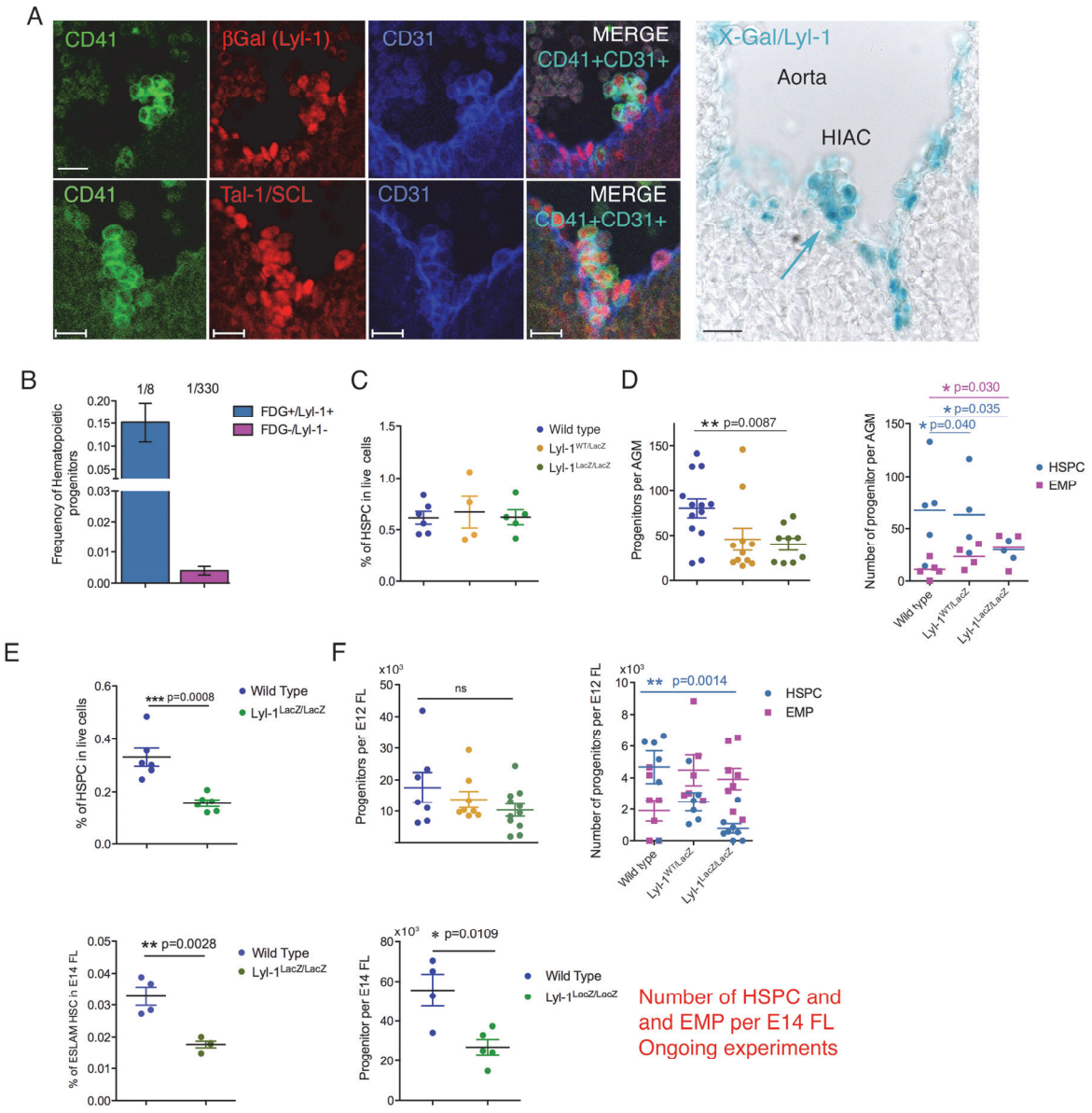

Figure 1: AGM-HSC express Lyl-1, but do not depend on it for their generation

A: HSPC in the aorta wall express Lyl-1. Left: Confocal immuno-labeling of AGM consecutive sections from E10 *lyl-1*$^{LacZ/LacZ}$ embryos showing β-Gal-Lyl-1 (Top) and Tal-1/SCL (Bottom) expression. Both factors are similarly expressed by CD31+CD41+ HSCs within the HIAC (Reprints from *(Giroux et al., 2007)*). Right: X-gal staining of E10 *Lyl-1*$^{WT/LacZ}$ embryo. A β-Gal activity reporting Lyl-1 expression is detected in endothelial cell lining the Aorta and in the Hematopoietic Intra-Aortic Cluster (HIAC) that characterize HSC emergence. Bars: 20 µM.

B: Percentage of single FDG^{+}/Lyl-1^{+} and FDG^{-}/Lyl-1^{-} cells sorted from AGM that gave rise to a hematopoietic progeny (n=3; p=0.0257).

C: Flow cytometry quantification of HSPC in E10 AGM, based on the AA4.1^{+}CD31^{+}c-Kit^{+} CD41^{low} CD45$^{-/low}$ phenotype that characterizes HSPC at this stage. See ***Sup. Figure 1A*** for the gating strategy.

D: Left panel: The number of HSPC present in E10-10.5 (30-37 somites) AGM, quantified by LDA, is reduced two folds in *Lyl-1*$^{LacZ/LacZ}$ and *Lyl-1*$^{WT/LacZ}$ compared to WT embryos.

Right panel: Distribution of EMP and HSPC in WT, *Lyl-1*$^{WT/LacZ}$ and *Lyl-1*$^{LacZ/LacZ}$ AGM. The frequency of HSPC is decreased in *Lyl-1*$^{LacZ/LacZ}$ compared to *Lyl-1*$^{WT/LacZ}$ and WT AGM. An increased number of EMP is also recovered

from *Lyl-1*$^{LacZ/LacZ}$ compared to WT AGM.

E: Flow cytometry quantification of HSC within E12 and E14 FL. The HSC pool is reduced two folds in the FL of *Lyl-1*$^{WT/LacZ}$ embryos at both E12 (LSK-SLAM cells, upper panel) and E14 (ESLAM cells, lower panel).

F: Left panel: The number of progenitors in WT, *Lyl-1*$^{WT/LacZ}$ and *Lyl-1*$^{LacZ/LacZ}$ E12 FL (Upper panel) and E14 FL (Lower panel) quantified by LDA, show no obvious genotype-associated difference at both stages.

Right panel: Distribution of EMP and HSPC in WT, *Lyl-1*$^{WT/LacZ}$ and *Lyl-1*$^{LacZ/LacZ}$ E12 FL (Upper panel) and E14 FL (Lower panel), point to a 2-3 fold decrease of HSPC at E12, while EMP yield is unmodified… Ongoing experiments at E14.

Supplementary Figure 1

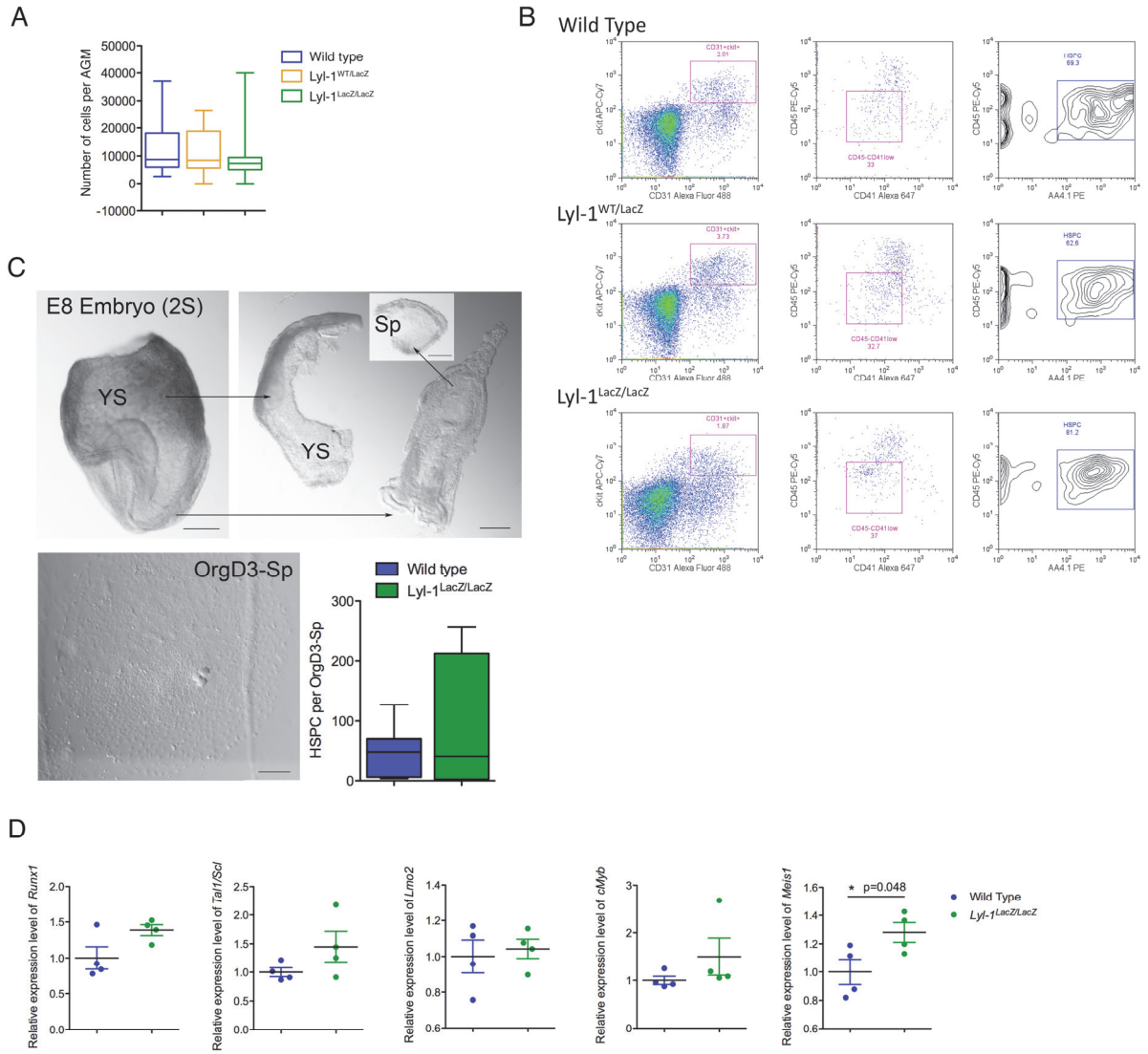

Supplementary Figure 1:

A: Cellularity of E10 AGM isolated from WT, *Lyl-1*$^{WT/LacZ}$ and *Lyl-1*$^{LacZ/LacZ}$: The cellularity of E10 (30-35S) AGM is identical in the 3 genotypes (n=12, 12, 12; E12 FL: n=7, 10, 11 for WT, *Lyl-1*$^{WT/LacZ}$ and *Lyl-1*$^{LacZ/LacZ}$, respectively); Tuckey box plot; unpaired t-test).

B: Flow cytometry analysis used to quantify HSPC in E10 AGM: Quantification of AA4.1^{+}CD31^{+}c-Kit^{+} CD41^{low} CD45$^{-/low}$ HSPC from E10 AGM from WT, *Lyl-1*$^{WT/LacZ}$ and *Lyl-1*$^{LacZ/LacZ}$ embryos, related to figure 1C.

C: Mesoderm commitment to HSPC is not impaired in Lyl-1 mutant embryos: Left panel: Procedure for the analysis of mesoderm commitment to HSC generation. The P-Sp/AGM presumptive territory, called splanchnopleura (Sp) is separated from the embryo before the 4-5S stage and maintained in organ culture for

2-3 days (Bar=200µm). The quantification of HSPC generated from the explanted Sp, analyzed using limiting dilution assay showed no genotype-associated differences (WT: n=7; *Lyl-1*$^{LacZ/LacZ}$: n=4; Tuckey box plot; unpaired t-test).
D: RT-qPCR analysis of the relative expression of levels of transcription factors involved in HSC generation process.

2.3.2 Lyl-1 invalidation leads to a 2-3 fold decrease of the HSC pool in E10 AGM and in E12 and E14 FL

To assess whether AGM-HSPC were functionally impaired, as a possible explanation for the reduced HSC pool size observed in E14 FL in previous studies *(Capron et al., 2006)*, we first quantified hematopoietic progenitors using LDA, and observed a two- to four-fold reduction of HSPC in E10-10.5 *Lyl-1*$^{WT/LacZ}$ and *Lyl-1*$^{LacZ/LacZ}$ AGM compared to WT ***(Figure 1D left)***. To determine the type of progenitors (EMP or HSPC) affected by *Lyl-1* invalidation, WT and mutant AGM cells were seeded at clonal conditions and the progeny analyzed after 10 days in OP9 culture ***(Figure 1D right)***. The frequency of multipotent clones was significantly decreased in *Lyl-1*$^{LacZ/LacZ}$ AGM compared to *Lyl-1*$^{WT/LacZ}$ and WT AGM). The frequency of EMP recovered from *Lyl-1*$^{LacZ/LacZ}$ AGM appeared significantly increased compared to WT. Such increased production of EMP concomitant to a decreased HSPC production might be the consequence of a premature differentiation of HSPC resulting from Lyl-1 deficiency. This possibility was ruled out since clonogenic assay did not show any increase in the clonogenic potential of E10 AGM cell from *Lyl-1*$^{LacZ/LacZ}$ embryos ***(Sup. figure 2A)***. Alternatively, a subset of cell classified as EMP may correspond to HSPC unable to produce a B-lymphoid progeny, since it was previously reported that *Lyl-1* bHLH disruption leads to an impaired B-lymphoid differentiation, including a partial block after the pro-B stage *(Capron et al., 2006)*. However, even if most progenitors classified as EMP were HSPC with impaired B-lymphoid differentiation, the decrease in HSPC number in *Lyl-1*$^{LacZ/LacZ}$ AGM would still remain highly significant.

We next performed *in vivo* reconstitution experiments, using Rag2$^{-/-}\gamma c^{-/-}$ immuno-deficient mice (Colucci et al., 1999) as appropriate recipients for early HSC, which poorly express MHC-I and are therefore prone to NK-mediated elimination upon engraftment into immune-competent recipient before E11.5 *(Cumano et al., 2001; Kieusseian et al., 2012)*. To evaluate the extent of a possible deficit in HSC in *Lyl-1*$^{LacZ/LacZ}$ AGM, recipient mice were engrafted with serially diluted AGM cells from WT, *Lyl-1*$^{WT/LacZ}$ and *Lyl-1*$^{LacZ/LacZ}$ embryos and analyzed 5-6 month post-transplantation for multi-lineage reconstitution ***(Table 1)***. The frequency of repopulating units, evaluated using ELDA software *(Hu and Smyth, 2009)* was

reduced 2-3 folds in *Lyl-1*$^{LacZ/LacZ}$ AGM compared to WT, while *Lyl-1*$^{WT/LacZ}$ AGM had an intermediate phenotype. Of note, the estimated frequency of repopulating units obtained in our reconstitution scheme (Rag2$^{-/-}\gamma c^{-/-}$ recipient) for WT-AGM was consistent with those obtained by other using immune-deficient NSG recipients in E10.5 AGM LTR experiments *(Vo et al., 2018)*.

The impact of Lyl-1 deficiency at later stages of HSC development was similarly estimated, focusing on E12 and E14 FL. Cytometry quantification pointed to a 2-fold reduction of HSC in the FL at both E12 (Lineage-negative Sca-1^{+}cKit^{+} (LSK) CD201^{+} *(Kim et al., 2006)*) and E14 (CD150^{+} CD48^{-} (SLAM) CD201^{+} cells, or ESLAM *(Benz et al., 2012)*) ***(Figure 1E; Sup. figure 2B,C)***.

In LDA assays ***(Figure 1F)***, while the overall progenitors production was not significantly modified, the cytometry analysis of colonies retrieved from wells seeded with WT and *Lyl-1*$^{LacZ/LacZ}$ FL at clonal concentrations, revealed a 2-3 fold reduction in multipotent progenitors at E12 (Analyses of E14 FL are ongoing).

In *in vivo* LTR assay, HSC (E12: LSK CD201^{+}; E14: ESLAM) were sorted from WT and *Lyl-1*$^{LacZ/LacZ}$ FL at E12 and transplanted into immuno-competent Ly5.1 recipients at doses of 300, 100 and 33 HSC per recipient, together with 2 x 10^5 helper cells (Ly5.1 x Ly5.2). (LTR tests are ongoing).

Table 1: Lyl-1-deficiency leads to a decreased number of reconstitution units.

	Wild type	*Lyl-1*$^{WT/LacZ}$	*Lyl-1*$^{LacZ/LacZ}$
1 AGM	1/5	0/5	0/8
3 AGM	2/6	2/5	1/6
6 AGM	2/6	2/5	1/6
9 AGM	5/6	2/6	2/5
Estimated repopulating cell frequency	1/8.08	1/14.59	1/23.69 (p= 0.0482)
Frequency upper limit	1/4.51	1/6.73	1/9.23
Frequency lower limit	1/14.8	1/32.4	1/62.2

LDA analysis of long-term reconstitution capacity of WT, Lyl-1$^{WT/LacZ}$ and Lyl-1$^{LacZ/LacZ}$ AGM-HSC (E10-10.5). Upper panel: Number of reconstituted Rag$^{-/-}\gamma C^{-/-}$ recipients depending on the number of AGM per recipient engrafted. Lower panel: Estimation of number of repopulating units calculated by the ELDA algorithm. Statistically significant differences in frequency are indicated by the p-value (pairwise $\chi 2$ test). In a goodness of fit, a p-value of 0.94 indicated a good fit (score test of heterogeneity: p=0.95).

2.3.3 Lyl-1 invalidation leads to an increased level of apoptosis at the AGM stage only

To identify the mechanism leading to the 2-3 fold diminution of the HSPC pool size, we analyzed the levels of proliferation ***(Figure 2A)*** and apoptosis ***(Figure 2B)*** in HSPC from WT and *Lyl-1*$^{LacZ/LacZ}$ E10 AGM, E12 FL and E14 FL using respectively *in vivo* BrdU incorporation and AnnexinV-7AAD assays. Interestingly, we did not observe any decrease in the proliferation levels. Instead, it was increased and only in E14 FL, possibly to compensate the reduced HSC pool size. The only feature that might explain the reduction of the HSPC population was therefore the increased level of apoptotic HSPC, which was only observed at the AGM stage.

We therefore analyzed the expression of apoptosis-related gene in E10 AGM HSPC (cKit^{+}CD31^{+}CD41^{low}CD45$^{-/low}$) ***(Sup. figure 2D)***, some of which being known to be expressed in E10.5 AGM (*Bclx and Bcl2*) (Orelio et al., 2004). There was no increase in the expression of the pro-apoptotic genes *Noxa* and *Bmf*. Amongst anti-apoptosis genes, the expression levels of *Bclxl,Mcl1,* and *Pim1* were unmodified, while a two-fold decrease was observed for *Bcl2* ***(Figure 2C)***. This is in frame with previous observation involving Bcl2 in the early steps of HSC development (Orelio et al., 2004). Interestingly, Bcl2 was previously shown to be regulated by Lyl-1 in a T-ALL context (Ferrando et al., 2002). Bcl2 also appears to be a direct target of Lyl-1, which over-expression can rescue the B-Lymphoid differentiation defect in *Lyl-1*$^{LacZ/LacZ}$ bone marrow *(Souroullas et al., 2009)*.

Ongoing work and planned studies: Because the AGM-HSC generation process is unaffected in Lyl-1 mutant, the HSC defect we observed (reduced number through increased apoptosis, appear to stem from a later development stage of HSC maturation. From E10 to E11, native HSC evolve from a CD45-negative to a CD45+ phenotype *(Bertrand et al., 2005a; Rybtsov et al., 2011; Zhou et al., 2016a)*. We therefore stated analyzing the HSC compartment at E11, first by quantifying this compartment in the WT and Lyl-1 Mutant, then by comparing the distribution of T1 "pre-HSC" ($CD31^{+}c\text{-}Kit^{+}CD45^{-}CD41^{low}CD201^{high}$) and T2 ($CD31^{+}c\text{-}Kit^{+}CD45^{+}CD201^{high}$) *(Zhou et al., 2016a)* HSC at E11, when both subsets co-exist. These data will tell us whether the diminution of the HSC pool already starts at a later stage of AGM-HSC development, if we find a diminished number of T2 HSC. We will also assess the apoptosis level in these two populations to see if the increased apoptosis level observed at E10 in $CD31^{+}ckit^{+}CD41^{low}CD45^{low/-}$ HSPC is maintained at E11, and also present in T2 HSPC.

Confronting our data to those from other lab (Table 2) pointed to a striking persistence of HSC defects in *Lyl-1*$^{LacZ/LacZ}$ embryos whatever the development stage investigated. Indeed, a 2-3 fold decreased of the HSC pool was also observed in both E14 FL *(Capron et al., 2006)* and adult BM *(Capron et al., 2006; Souroullas et al., 2009; Zohren et al., 2012)*, without concomitant modification of the apoptosis and proliferation levels at these stages.

Figure 2

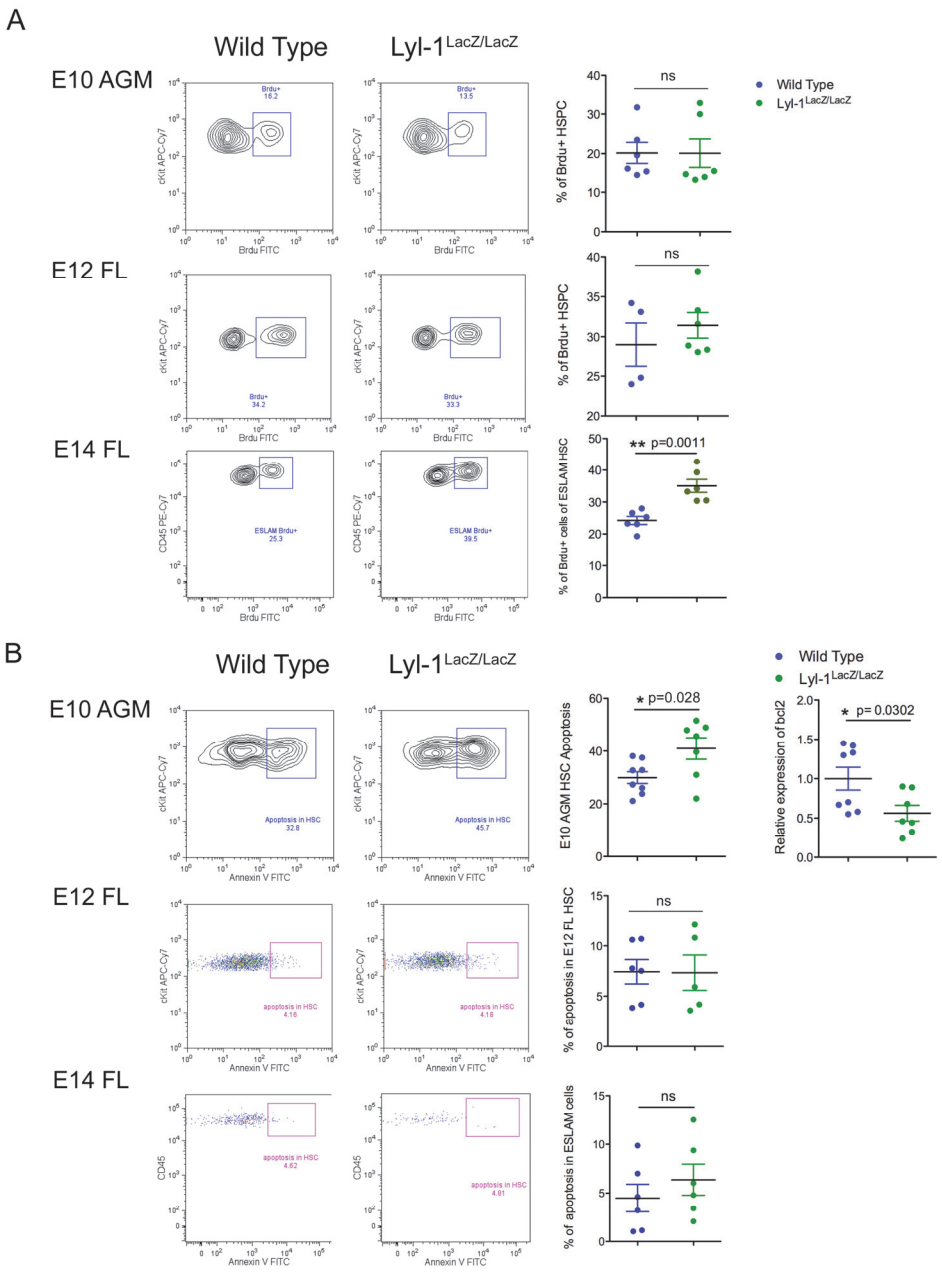

Figure 2: Comparison of proliferation and apoptosis levels in HSPC from E10 AGM, E12 FL and E14 FL in WT and *Lyl-1$^{LacZ/LacZ}$* embryos.

A: Flow cytometry quantification of the proliferation rate in HSPC from E10 AGM, E12 FL and E14 FL from in WT and *Lyl-1$^{LacZ/LacZ}$* embryos. The proliferation rate is unchanged in the mutant except in E14 FL.

B: Flow cytometry quantification of apoptosis level in HSPC from E10 AGM, E12 FL and E14 FL from in WT and *Lyl-1$^{LacZ/LacZ}$* embryos. The level of apoptosis is elevated in the mutant only in E10 HSPC. Upper right: the expression level of the anti-apoptotic gen Bcl2 is diminished in HSPC at E10.

C: Quantitative RT-PCR analyses of apoptosis regulating genes ***(See sup. Figure 2D)*** points to the anti-apoptotic gene Bcl2 as being expressed at a lower level in *Lyl-1$^{LacZ/LacZ}$* AGM-HSPC (WT: n=8; *Lyl-1$^{LacZ/LacZ}$*: n=7).

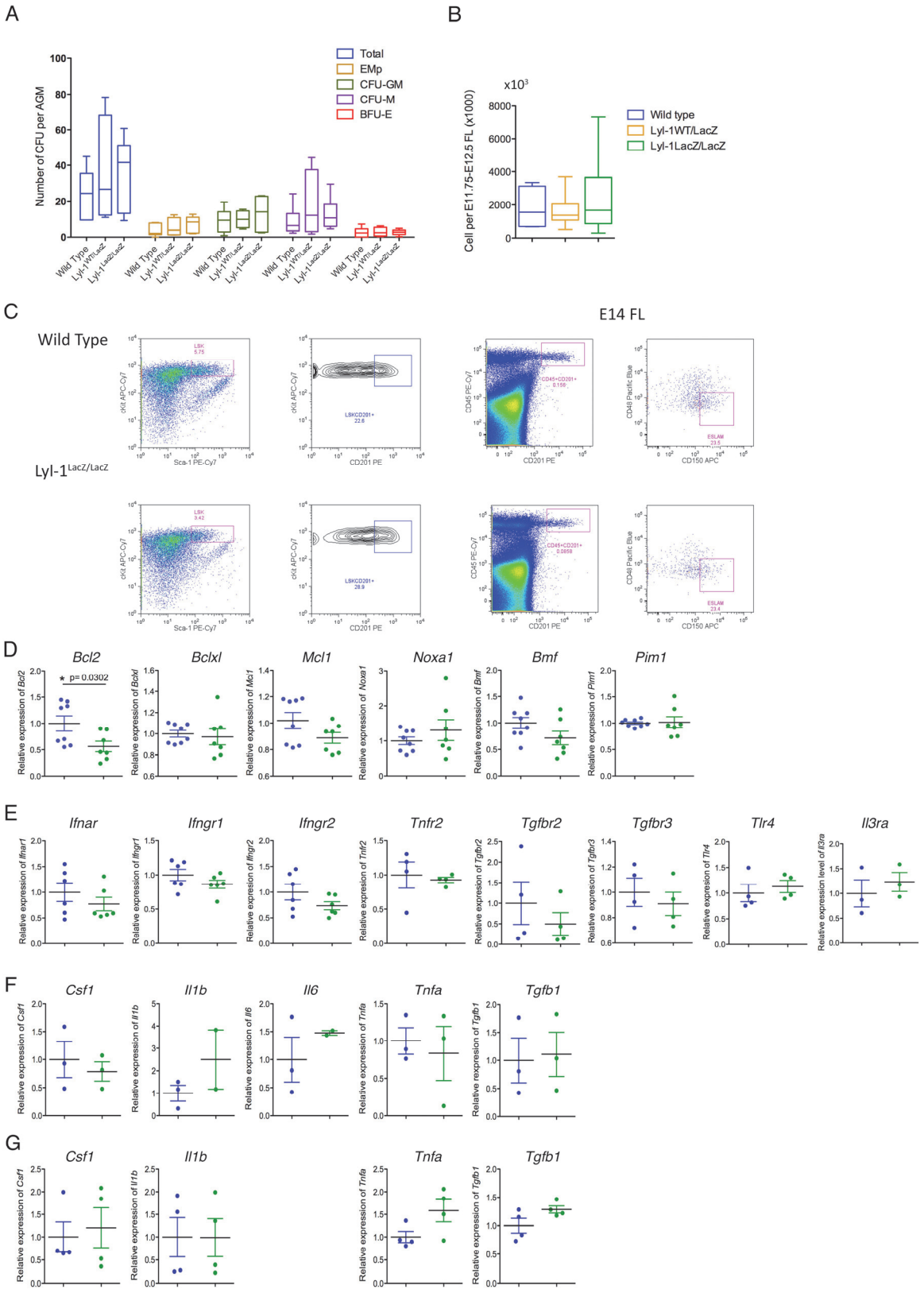

Supplementary Figure 2:

A: Lyl-1 deficiency does not lead to a premature differentiation of AGM HSPC. Clonogenic assays performed with E10 AGM cells mostly detect YS-derived progenitors present in the systemic circulation (Godin et al., 1999). No genotype-associated significant difference in the number of colonies was observed in clonogenic assays performed with E10 AGM cells from WT, *Lyl-1*$^{WT/LacZ}$ and *Lyl-1*$^{LacZ/LacZ}$ embryos (WT: n=6; *Lyl-1*$^{WT/LacZ}$: n=4;

Lyl-1$^{LacZ/LacZ}$: n=6).

B: Cellularity of FL isolated from E12 and E14 FL from WT, *Lyl-1*$^{WT/LacZ}$ and *Lyl-1*$^{LacZ/LacZ}$.

The cellularity of E12 FL (left) and E14 (Right) was identical in the 3 genotypes (E12 FL: n=7, 10, 11 for WT, *Lyl-1*$^{WT/LacZ}$ and *Lyl-1*$^{LacZ/LacZ}$, respectively; n=17 for WT, n=13 for *Lyl-1*$^{LacZ/LacZ}$, E14 FL); Tuckey box plot; unpaired t-test).

C: Flow cytometry analysis used to quantify HSPC in E12 and E14 FL.

Quantification of HSC in the FL of E12 (left: LSK SLAM cells) and E14 (right: ESLAM cells) from WT, *Lyl-1*$^{WT/LacZ}$ and *Lyl-1*$^{LacZ/LacZ}$ embryos, related to figure 1E.

D: RT-qPCR analysis of the relative expression of levels of pro- (*Noxa* and *Bmf*) and anti- (*Bcl2, Bclxl*, *Mcl1 and Pim1)* apoptotic genes in WT and *Lyl-1*$^{LacZ/LacZ}$ AGM-HSPC (WT: n=8; *Lyl-1*$^{LacZ/LacZ}$: n=7).

Table 2: Summary of the modification of HSC compartment in Lyl-1$^{LacZ/LacZ}$ mutant, analyzed by flow cytometry and in vitro an in vivo assays. Comparison with the data from the literature (in gray)

Stage Localization	HSC Phenotype	% HSC	Proliferation	Apoptosis	Limiting Dilution assay	Long-term reconstruction	Reference
E10 AGM	CD31^{+}ckit^{+}CD41^{low}CD45$^{low/-}$	*No difference;*	*No difference*	*2 fold Increase*	*2-3 fold decrease*	*2-3 fold decrease*	Our observation
E12 FL	LSK CD201+	*2 fold decrease*	*No difference*	*No difference*	*2-3 fold decrease*	*Ongoing*	Our observation
E14 FL	ESLAM: CD45+CD201+CD150+CD48-	*2 fold decrease*	*2 fold increased*	*No difference*	*Ongoing*	*ND*	Our observation
E14 FL	Lin-Sca1+cKit+	*2 fold decrease*	*No difference*	*No difference* Mentioned-Not shown	ND	ND	(Capron et al., 2006)
Adult BM	Lin-Sca1+cKit+	*2 fold decrease*	*No difference*	*No difference* Mentioned-Not shown	ND	*2 fold decrease*	(Capron et al., 2006)
Adult BM	LSK-Flt3neg	*30% decrease*	*No difference*	*No difference*	ND	ND	(Zohren et al., 2012)
Adult BM	Whole BM	ND	ND	ND	ND	*2 fold decrease*	(Souroullas et al., 2009)

Apoptosis levels in cells with a HSC phenotype was determined in flow cytometry by Annexin V-7AAD labeling in all mentioned studies.
Proliferation rate was quantified by BrdU incorporation by cells with a HSC phenotype in all studies, except for adult bone marrow (BM) in the study by Capron et al, 2006, where Hoechst 33342-Pyronin-Y was used instead.

2.3.4 Are modifications of inflammatory signaling responsible for the HSC defect in Lyl-1$^{LacZ/LacZ}$ mutants?

The proper development of blood cells during ontogeny depends on shear mechanical forces and sterile inflammation and thus shares similarities with stress hematopoiesis. In search of the factors that may influence the setting of AGM pool size, we first focused on inflammatory signaling which has been involved in AGM-HSC generation process (See *(Clapes et al., 2016; Espin-Palazon et al., 2014)* for reviews). We therefore analyzed the expression levels of inflammatory receptors on purified AGM HSPC ***(Sup. Figure 2E)***, as well as inflammatory cytokines in the whole AGM ***(Sup. Figure 2F)*** or, more specifically, in the macrophage population ***(Sup. Figure 2G)***. Indeed, embryonic macrophages have been involved in inflammatory-mediated regulation of AGM HSC production in zebrafish, mouse and human embryos *(Li et al., 2014; Sawamiphak et al., 2014; Travnickova et al., 2015)*, through the production of pro-inflammatory mediators. This latest point appears particularly important taking into account the previously described regulatory function of Lyl-1 over the production and differentiation of primitive macrophages. Similarly, this analysis performed on the whole AGM may uncover changes in expression levels of inflammatory mediators secreted by other AGM cell types, such as mesenchymal cells (IL-1 *(Orelio et al., 2008))* or, more importantly, endothelial cells (IL-1 *(Orelio et al., 2008),* TGF1β *(Monteiro et al., 2016)*). Indeed, endothelial cells express Lyl-1 and the blood vessels of Lyl-1 mutant mice have a reduced pericyte coverage and increased permeability, as well as a defective endothelial cells maturation *(Pirot et al., 2010; Pirot et al., 2014)*, so that Lyl-1 deficient endothelial cells may play a role in the HSC phenotype observed, independently of their function in AGM-HSC emergence, since this process appears unaffected in *Lyl-1$^{LacZ/LacZ}$* embryos.

We first focused on the HSC receptors reported to be involved to the answer to inflammatory signaling, such as IFNα and IFNγ receptors (*Ifnar1*, *Ifngr1* and 2) *(Kim et al., 2016; Li et al., 2014)*, TNFα receptor *Tnfr2 (Espin-Palazon et al., 2014)*, Toll-like receptor 4 *(He et al., 2015)*, and the Interleukin (IL)-receptor 3 *(Robin et al., 2006)*. However, no overt modification of the expression of receptors for inflammatory-related signals was observed in *Lyl-1$^{LacZ/LacZ}$* HSPC

(Sup. Figure 2E).

Our first investigation on the expression level of the mediators of inflammatory response did not uncover changes in expression levels in the whole AGM or embryonic macrophages ***(Sup. Figure 2F, G)***. However, these analyses are incomplete and we are currently complementing them to reach an appropriate number of tests (IL1β, IL6, IL3, IFNα, IFNβ and TNFα, in whole AGM and/or MΦ samples) and to extend them by analyzing the expression level of IRF2, a negative regulator of IFNα signaling, which was reported to increase HSPC production in zebrafish *(Li et al., 2014)*, and IRF8 which is expressed by YS-derived MΦ *(Hagemeyer et al., 2016).*

Material and methods

Mice and embryos

Ethic statement. Mice were housed in the animal facilities of Institut Gustave Roussy ("Plate-forme d'évaluation préclinique", animal facility licence # E 94-076-11). All animal experiments were conducted in compliance with French regulations (Transposition of Directive 2010/63), under authorized project #5798-2016062214256796 approved by officially accredited Ethical committee n°26.

Mouse strains: We used the following mouse strains:

1- C57BL/6J mice from Harlan or Charles Rivers Laboratories, France, referred to as wild type (WT). These mice bear the Ly5.2 allele of the pan-hematopoietic marker CD45.

2- *Lyl-1^{LacZ}* mice (on a C57BL/6J/Ly5.2 background), genotyped as described before *(Capron et al., 2006). Lyl-1$^{LacZ/LacZ}$* males were crossed with C57Bl/6J or *Lyl-1$^{LacZ/LacZ}$* females to generate *Lyl-1$^{WT/LacZ}$* or *Lyl-1$^{LacZ/LacZ}$* embryos. The day of vaginal plug observation was considered as E0.5.

3- The C57BL/6J congenic line bearing the Ly5.1 allele of the pan-hematopoietic marker CD45 was used as recipient for *in vivo* long-term reconstitution assays.

4- F1 mice resulting from the cross of C57BL/6J Ly5.1 males to C57BL/6J Ly5.2 females were used to provide carrier bone marrow cells in for *in vivo* long-term reconstitution assays.

4- Rag2$^{-/-}\gamma c^{-/-}$ immuno-deficient mice (Colucci et al., 1999) bearing the Ly5.1 allele were used as recipients in the reconstitution experiments.

Embryos: Pregnant females were sacrificed by cervical dislocation. Pre-somite embryos were staged according to Downs et al.*(1993).* E8 to E11 embryos were staged by somite counting and thereafter according to morphological landmarks. Sp-explants, E10-11 AGM and E12-E14 FL were dissected as described before *(Bertrand et al., 2005a; Kieusseian et al., 2012)*.

In vitro culture

Clonogenic assay: Cells were plated in triplicate at 3.10^3 cells/ml in methocult® M3234 (StemCell Technologies Inc.) supplemented Stem Cell factor (50ng/mL), EPO (3U/mL), IL-3 (10 ng/mL), all from Peprotech, IL-6 (10 ng/mL, a gift from Sam Burstein, Maryville IL, USA), CSF-1 (10 ng/mL) and TPO (10ng/mL, provided by Kirin Brewery, Tokyo, Japan). Cultures

were maintained in a humidified incubator at 37°C, 5% CO_2 and colonies were scored at day 7.

Limiting dilution assay: Cells were distributed in plates containing OP9 stroma (kindly given by S.-I. Nishikawa and T. Nakano, Riken-Kobe, Japan) in 48 wells per dilution (AGM, E12 and E14 FL: 300/100/30 cells/well, Sp-explants after organ culture: 100/30/10 cells/well). Cells were cultured in "Complete OptiMEM medium", i.e. OptiMEM with Glutamax (51985-042), 100U/ml penicillin, 100µg/ml streptomycin, $5x10^{-5}$M 2-mercapoethanol (all from ThermoFisher) and 10% fetal calf serum (FCS; Hyclone), supplemented with 50 ng/ml Stem Cell Factor, 5U/ml EPO, 0.5 ng/ml GM-CSF, 20 ng/ml Il-7 (All from Peprotech) and 10 ng/ml Flt-3 ligand (a generous gift from Celldex therapeutics, Needham MA, USA). Cultures were maintained in a humidified incubator at 37°C, 5% CO_2 and wells negative for hematopoietic cell growth were recorded at day 10 and progenitors frequency was determined following the Poisson distribution.

To determine the frequency of EMP and HSPC, AGM of FL cells were seeded at clonal conditions (96-144 wells per genotype), as determined using LDA (e.g. for WT-AGM, progenitor frequency: 1/200 (1/211.88±1/34.78; n=13); seeding for clonal analysis: 50 cells/well). We ensured that more than 37% of the wells did not contain a hematopoietic progeny, confirming a clonal origin. After 10 days, the progeny of each well was analyzed by flow cytometry. Cells that differentiated only into erythroid and myeloid cells were classified as EMP, while those that also gave rise to a B-lymphoid progeny were classified as HSPC.

Organ culture: Sp-Explants were placed into plates containing "Complete OptiMEM medium", and maintained in organ culture at 37°C, 5% CO_2 for 3 days to allow HSC commitment, as described before and are thereafter referred to as OrgD3-Sp *(Cumano et al., 1996; Cumano et al., 2001)*.

In vivo long-term reconstitution (LTR) assay

$Rag2^{-/-}\gamma c^{-/-}$Ly5.1 recipient mice were sub-lethally irradiated (6.5 Gy; X-Ray source, Xrad 320). Cells from WT, *Lyl-1*$^{WT/LacZ}$ or *Lyl-1*$^{LacZ/LacZ}$ AGM, bearing the Ly5.2 allele of CD45, were injected, at serial dilutions (1-3-6-9 embryo-equivalents per recipient). For the reconstitution assays involving HSC from E12 FL, lethally irradiated (9 Gy; X-Ray source, Xrad 320) C57BL/6 Ly5.1

were injected intravenously in the retro-orbital sinus with sorted LSKCD201$^+$ cell suspension, at serial dilutions (300, 100 or 33 cells per recipient), together with a carrier cell dose of 2x10^5 total BM cells from F1 animals (Ly5.1 x Ly5.2). Recipient mice received antibiotic-treated drinking water for 1 month post-irradiation.

In LTR assays, donor-derived contribution was followed in peripheral blood cells 45 days and 3 month post-transplantation. After 5 to 6 months, recipient mice were sacrificed and the BM, spleen and thymus were analyzed by flow cytometry. Mice were considered reconstituted when the % donor-derived granulocytes in bone marrow was ≥ 1%.

The ELDA online software (WEHI bioinformatics) http://bioinf.wehi.edu.au/software/elda/ was used to quantify of the reconstituting units *(Hu and Smyth, 2009)*. The 95% confidence interval for the frequency of repopulating units was indicated by the upper and lower limits. The goodness of fit tests was used to assess how well the data fit the single-hit model (one repopulating unit gives a positive signal): 1 indicates a good fit, <1 an heterogeneity in donor cells, and >1 a multi-hit model, i.e. a hypersensitivity of recipients mice to a dose of donor cells; p values were calculated by the ELDA algorithm.

Imaging

Beta-Galactosidase staining: After PBS wash, dissected embryos were fixed in PBS, 0.2% paraformaldehyde, 0.1M PIPES pH6.9, 2mM $MgCl_2$, 5mM EGTA for 30 minutes at room temperature, and washed in PBS. Embryos were incubated overnight at 37°C with X-Gal staining solution (5-bromo-4-chloro-3-indoyl β-D-galactopyranoside: 1mg/mL), 5 mM Potassium Ferricyanide, 5 mM potassium Ferrocyanide, 2mM $MgCl_2$, 0.02% Nonidet P-40, 0.01% Na Deoxycholate, in PBS, as previously described *(Giroux et al., 2007)*.

Flow cytometry, FACS-Gal, proliferation and apoptosis assays.

Single-cell suspensions, treated with purified anti-CD16/32, were stained with the appropriate combination of antibodies (See ***Supplementary Table 1*** for the list of antibodies and dyes used throughout this study). Dead cells were excluded by adding 1 μg/mL 7-amino actinomycin (7AAD) or DAPI (both from Sigma) before acquisition. Acquisitions were

performed on a Canto II cytometer and cell sorting using FACS-Aria III or Influx (All from BD Biosciences). Data were analysed using FlowJo (Treestar) software.

FACS-Gal assay: this assay (Fiering et al., 1991; Guo and Wu, 2008) used as a reporter for Lyl-1 expression, allows the flow cytometry characterization of cells that display a β-Gal activity, using its fluorescent substrate (Fluorescein di-β-galactopyranoside (FDG) F1179; Molecular probe; Thermo Fisher).

Proliferation assay (BrdU incorporation): Pregnant WT and *Lyl-1*$^{LacZ/LacZ}$ females were injected with BrdU (10μM) 10, 12 or 14 days after plug detection, to analyse respectively E10 AGM-HSC or E12 and E14 FL-HSC and sacrificed 2 hours later. AGM or FL were isolated, dissociated and stained with the antibody cocktail appropriate for HSC detection. Cells were fixed, permeabilised and treated with DNase (1 hour at 37°C) according to kit instruction (BD Pharmingen No. 552598) and BrdU incorporation was revealed using anti-BrdU-APC.

Apoptosis assays: For apoptosis analysis, AGM or FL were isolated, dissociated and stained with the antibody cocktail appropriate for HSC detection, washed and incubated with Annexin V-FITC. 7AAD was added before acquisition.

Acquisitions were performed on FACS-Sort or Canto II cytometers and cell sorting using FACS-Diva (Becton Dickinson). Data were analyzed using FlowJo (Treestar) software.

RT-qPCR

Total RNA was extracted from sorted HSPC using Trizol (ThermoFisher). After cDNA synthesis using a SuperScript™ VILO™ Master Mix reverse transcriptase (Invitrogen), quantitative PCR was performed using SYBR Premix Ex TaqII (Tli RNase H Plus, Takara Bio). Reference genes were *Actin*, *Hprt* and *SDHA*. Gene expressions were normalized to the value obtained from WT samples and relative gene expression levels were determined by the ΔΔCt method. Gene expression was considered undetectable if Ct values were >35 cycles. The sequences of the primers used are provided in ***Supplementary Table 2.***

Statistical analysis

Statistical tests were performed using Prism six software (GraphPad Software). Statistical significance (p-value) was analyzed using unpaired Student's t-test. Significant modifications

compared to WT, were shown by asterisks and exact p-value (*p $\leq$ 0.05, **p $\leq$ 0.01, and ***p < 0.001). Absent marks or ns indicate no significant modification compared to WT control. The LDA algorithm ELDA performed statistical analysis on the limiting dilution reconstitution experiments.

Supplementary table 1: Antibodies and fluorescent stains used throughout this study

Antibody name	*Clone*	*Supplier/Reference*	*Fluorochrome/ Chromogen*
β-galactosidase	Polyclonal	Abcam; 9361	
CD16⁄32(Fc block)	93	Biolegend; 101301	
Ter119	TER-119	Biolegend; 116205 Biolegend; 116208 eBioscience; 17-5921-82	FITC PE APC
CD3	145-2C11	BD-Pharmingen; 553062 BD-Pharmingen; 553064	FITC PE
CD4	Gk1.5	BD-Pharmingen; 553729 BD-Pharmingen; 561829	FITC PE
CD8a	53-6.7	BD-Pharmingen; 553031 BD-Pharmingen; 100707	FITC PE
CD19	6D5 1D3	Biolegend; 115507 BD-Pharmingen; 550992	PE APC
B220/CD45R	RA3-6B2	eBioscience; 11-0452-82 Biolegend; 103208	FITC PE
GR-1	RB6-8C5 RB6-8C5 RB6-8C5	BD-Pharmingen; 553127 Biolegend; MA1-83934 eBioscience; 108416	FITC PE PE-Cy7
Sca-1	D7	Biolegend; 108113	PE-Cy7
cKit	2B8 2B8	BD-Pharmingen; 553358 Biolegend ; 105825	APC APC-Cy7
CD45	30-F11 30-F11	BD-Pharmingen; 553082 eBioscience; 25-0451-82	PE-Cy5 PE-Cy7
CD31	MEC13.3 390 MEC13.3	Biolegend; 102514 Biolegend; 102408 BD-Pharmingen; 583089	Alexa fluor 488 PE BV510
CD41	Mwreg30	BD-Pharmingen; 553848 Invitrogen; C29332	Alexa fluor 488 Alexa fluor 647
AA4.1	AA4.1	eBioscience; 12-5892-82	PE
CD150	TC15-12F12.2	Biolegend; 115909	APC
CD48	HM48-1	Biolegend; 103418	Pacific Blue
CD201⁄EPCR	1560	Miltenyi Biotec; 130-106-585 Miltenyi Biotec; 130-106-586	PE APC

CD11b	M1/70	Biolegend; 101212	APC
CD45.1	A20	eBioscience; 45-0453-82	Pecy5.5
CD45.2	104	eBioscience 47-0454-82	APC-efluor780
Annexin-V	NA	Biolegend; B206040	FITC
Anti-Brdu	B44	BD-Pharmingen;51-23619L	FITC
7AAD	NA	BD-Pharmingen; 51-68981E	Dye
DAPI	NA		Dye

Supplementary Table 2: Primers used in this study

Gene		***Sequence***
Actin	Primer forward:	5′- CTTCTTTGCAGCTCCTTCGT-3′
	Primer reverse:	5′- ATCACACCCTGGTGCCTAG-3′
Hprt	Primer forward:	5′- TGATTATGGACAGGACTGAAAGA-3′
	Primer reverse:	5′- AGCAGGTCAGCAAAGAACTTATAG-3′
SDHA	Primer forward:	5'-AAGTTGAGATTTGCCGATGG-3′
	Primer reverse:	5'-TGGTTCTGCATCGACTTCTG-3′
Tal-1/Scl	Primer forward:	5'- CATGTTCACCAACAACAACCG-3'
	Primer reverse:	5'- GGTGTGAGGACCATCAGAAATCTC-3'
Runx1	Primer forward:	5'- CTCCGTGCTACCCACTCACT-3'
	Primer reverse:	5'- ATGACGGTGACCAGAGTGC-3'
Meis1	Primer forward:	5'-TGAAGTAGGAAGGGAGCCAG-3′
	Primer reverse:	5'-GCCTACTCCATCCATACCCC-3′
Lmo2	Primer forward:	5'-ATGTCCTCGGCCATCGAAAG-3′
	Primer reverse:	5'-CGGTCCCCTATGTTCTGCTG-3′
IFNAR	Primer forward:	5'- GACAACTACACCCTAAAGTGGAG-3'
	Primer reverse:	5'- GCTCTGACACGAAACTGTGTTTT-3'
IFNGR1	Primer forward:	5'- CTGGCAGGATGATTCTGCTGG -3′
	Primer reverse:	5'- GCATACGACAGGGTTCAAGTTAT -3′
IFNGR2	Primer forward:	5'- CTTCCAGCAATGACCCAAGAC -3′
	Primer reverse:	5'- TCCAGCAACCTATGCCAAGAG -3′
CSF1R	Primer forward:	5'-GCAGTACCACCATCCACTTGTA-3'
	Primer reverse:	5'-GTGAGACACTGTCCTTCAGTGC-3'
TNFR2	Primer forward:	5′ - TCCCCAAGCAAGAGTCATGG -3′
	Primer reverse:	5′ - CGATGCAGGTGACGTTGAC -3′
TGFBR2	Primer forward:	5'- CCCCATTTGGTTCCAAGGTG -3'
	Primer reverse:	5'- AGCACTCGGTCAAAGTCTC -3'
cMyb	Primer forward:	5′-AGCGTCACTTGGGGAAAACT-3′
	Primer reverse:	5′- AGTCGTCTGTTCCGTTCTGT-3′
TGFBR3	Primer forward:	5′-CAGCATTTGTGATCGGAGC-3′
	Primer reverse:	5′- TCTGAGTGCTCCCTATGCTG-3′

TLR4	Primer forward:	5’-CAGCAAAGTCCCTGATGACA-3’
	Primer reverse:	5’- CCTGGGGAAAAACTCTGGAT-3’
IL3RA	Primer forward:	5'- CTGGCATCCCACTCTTCAGAT-3'
	Primer reverse:	5'- GGTCCCAGCTCAGTGTGTA-3'
Bcl2	Primer forward:	5'- TTGTGGCCTTCTTTGAGTTCGGTG -3'
	Primer reverse:	5'- CTTCAGAGACAGCCAGGAGAAATC -3'
Bclxl	Primer forward:	5’-GGAAAGCGTAGACAAGGAGATG -3’
	Primer reverse:	5’-CCCGTAGAGATCCACAAAAGTG -3’
Pim1	Primer forward:	5'- GAGGATTCTTCTGGCAGGTG-3'
	Primer reverse:	5'- GGTAGCGATGGTAGCGAATC-3'
Mcl1	Primer forward:	5'-GGTGCCTTTGTGGCCAAACACTTA-3'
	Primer reverse:	5'- ACGTGGAAGAACTCCACAAACCCA-3'
Bmf	Primer forward:	5'-AGTTCCATCGGCTTCATACG-3'
	Primer reverse:	5'-GACTGCATTCCTGGTGATCC -3'
Noxa1	Primer forward:	5'-ACTTTGTCTCCAATCCTCCG -3'
	Primer reverse:	5'-GAAGTCGCAAAAGAGCAGGA -3'
IL1β	Primer forward:	5'-GAAATGCCACCTTTTGACAGTG-3'
	Primer reverse:	5'-TGGATGCTCTCATCAGGACAG-3'
IL6	Primer forward:	5'-CTCTGGGAAATCGTGGAAAT-3'
	Primer reverse:	5'-CCAGTTTGGTAGCATCCATC-3'
TNFα	Primer forward:	5'- GCCACCACGCTCTTCTGT-3'
	Primer reverse:	5'- TGAGGGTCTGGGCCATAG -3'
TGFβ1	Primer forward:	5'- GAGCCCGAAGCGGACTACTA-3'
	Primer reverse:	5'- TGGTTTTCTCATAGATGGCGTTG-3'

3. Conclusion and general perspectives

3.1 The function of Lyl-1 during YS MΦ development

Both $M\Phi^{Prim}$ and $M\Phi^{T\text{-}Def}$ originate from the YS before the generation of HSC. By now, there is no available marker to distinguish them, except by their kinetics of appearance (Bertrand et al., 2005b). Previously, by making use of the LacZ reporter present in *Lyl-1^{lacZ}* mice, Shoutang Wang showed that Lyl-1 expression marks the MΦ progenitors generated during the primitive wave, but not those produced in the 2nd transient definitive (EMP-derived) ones. Consistent with this finding, single-cell RNA-seq analyses performed on E7.75 embryos in other groups have demonstrated that primitive progenitors express Lyl-1 (Chiu et al., 2018; Scialdone et al., 2016). 20 years ago, our team first came up with the hypothesis that brain microglia originate from YS MΦ progenitors (Alliot et al., 1999) and later, this hypothesis was confirmed by a fate mapping model using an inducible reporter for Runx1, which is expressed by early progenitors in the YS (Ginhoux et al., 2010). To reinforce our observation, we also detected Lyl-1 expression in the embryonic microglia using the FDG staining as a reporter for Lyl-1 expression.

Thus, here we provide a potential marker that discriminates $M\Phi^{Prim}$ from $M\Phi^{T\text{-}Def}$ progenitors. Due to the limitation of LacZ reporter which only reports Lyl-1 expression in *Lyl-1$^{WT/LacZ}$* embryos and not in a wild type context, new mouse models as Lyl-1 indicator, such as Lyl-1^{Tomato} and Lyl-1^{CreERT}, would be further required to better analyse the distribution of Lyl-1 expressing cells. By crossing new mouse models with the CX3CR1^{GFP} or other reporter models such as Rosa26-Stop^{fl}-YFP, we would be able to monitor the contribution of $M\Phi^{Prim}$ and $M\Phi^{T\text{-}Def}$ to different tissue resident MΦ. Indeed, primitive MΦ progenitors may also contributes to other tissue resident MΦ, it will be interesting to analysis the contribution of Lyl-1^{Tomato} expressing or Lyl-1^{CreERT} lineage-traced MΦ to the tissue resident MΦ pool in various tissues which harbours YS-derived resident macrophages, as determined by various fate map analyses (see chapter 1.3.1, and reference (Epelman et al., 2014b) for a review). By injecting TAM around E6.5 to the Lyl-1^{CreERT} fate-mapping system could help us delineate the contribution of $M\Phi^{Prim}$ to other tissue resident MΦ in the adult. Complementary to the gene indicator mouse strains, a Lyl-1^{loxp} mouse model would also be better to characterise the tissue-cell and temporal specific functions of Lyl-1 than the former *Lyl-1$^{LacZ/LacZ}$* mouse strain.

So far, the molecular differences between MΦ^{Prim} and MΦ$^{T\text{-}Def}$ progenitors have not been investigated and the mechanism underlying Lyl-1 function during MΦ^{Prim} development needs to be precisely analysed. To answer these questions, we performed a RNA-seq analysis on sorted MΦ progenitors at E9 (which contains mainly MΦ^{Prim} progenitors) and MΦ progenitors at E10 (which have both MΦ^{Prim} and MΦ$^{T\text{-}Def}$ progenitors) from both WT and *Lyl-1*$^{LacZ/LacZ}$ embryos.

Interestingly, we found several different features between MΦ^{Prim} and E10 progenitors from the WT YS. Firstly, in MΦ^{Prim} progenitors, we find a higher expression level of genes related to MHC-II complexes and interferon signalling genes, such as *Cd74*, *H2-Aa*, *Ifit1* and *Ifit3*, that possibly reveals functional differences from later progenitors. Besides its function as a member of MHC-II complexes, CD74 has been identified as MIF receptor (Calandra and Roger, 2003)**.** Further analysis of the expression level of CD74 and its potential function in MΦ^{Prim} progenitors would be important. On the contrary, at E10, MΦ progenitors have a higher expression level of genes that were previously thought specifically expressed by erythroid cells. For example, they express high level of *Gata1*, a transcription factor required for erythrocyte development. Moreover, we observed high expression level of genes coding for hemoglobin, such as *Hba-x* and *Hbb-y* in MΦ$^{T\text{-}Def}$ progenitors, possibly revealing their EMP ontogeny. Interestingly, more and more researchers have found that those hemoglobin genes are more ubiquitous expressed than previously thought, with an expression in other lineage than the erythroid one, where they could play yet unknown functions (Biagioli et al., 2009; Lim et al., 2019; Straub et al., 2012). Several groups of researchers have also found a high expression level of hemoglobin genes in several embryonic MΦ (Hagemeyer et al., 2016; Mass et al., 2016; Matcovitch-Natan et al., 2016). It will be interesting to investigate their function in MΦ$^{T\text{-}Def}$ development, if they are transcribed into protein in these cells.

Moreover, our RNA-seq analysis revealed that the embryonic microglia-specific gene *Sall3* is already significantly expressed at higher levels in E9 MΦ^{Prim} progenitors than in E10 YS MΦ progenitors (Mass et al., 2016). Further analysis of Sall3 expression pattern on MΦ progenitors from the two YS waves and on their mature MΦ progeny would be important to know whether Sall3 also discriminates the two waves of MΦ. I have to admit that it is difficult to fully reveal the YS wave-specific signature due to the mixed existence of MΦ^{Prim}

and MΦ$^{T\text{-}Def}$ progenitors at E10. Further transcriptome analyses on sorted YS MΦ progenitors from Lyl-1^{Tomato} positive and Lyl-1^{Tomato} negative and single cell RNA-seq analysis on early YS MΦ progenitors would be required to fully decipher the ontogeny and developmental difference between MΦ^{Prim} and MΦ$^{T\text{-}Def}$.

Beside being a marker that distinguishes MΦ^{Prim} and MΦ$^{T\text{-}Def}$ progenitors, Lyl-1 also regulates the development of MΦ^{Prim}. *Lyl-1$^{LacZ/LacZ}$* embryos harbour more MΦ progenitors in the YS and in the developing brain at the colonization stage than the corresponding WT. This was evidenced by the test of YS cells in clonogenic assay, which only detect progenitors but not mature cells, and also by the flow cytometry analysis of the distribution of A1 to A3 progenitors in the YS and brain. Specifically, there is more A1 MΦ progenitors than A3 mature MΦ in Lyl-1 mutants. These data suggested Lyl-1 possibly regulates the maturation process of MΦ^{Prim} and microglia in normal conditions. Consistent with this, GSEA analysis also show that Pu.1/Spi1 target genes are enriched in WT compared to *Lyl-1$^{LacZ/LacZ}$* MΦ^{Prim} progenitors. Lyl-1 also seems regulates the inflammatory signalling in MΦ^{Prim} progenitors during normal development, as inflammatory signalling related pathways are down regulated in *Lyl-1$^{LacZ/LacZ}$* MΦ^{Prim} progenitors compared to WT.

Of note, RNA-seq analysis on MΦ^{Prim} progenitors at E9 from WT and *Lyl-1$^{LacZ/LacZ}$* already indicated the deregulation of genes involved in neuronal development, Lyl-1 invalidation leading to the enrichment of neurogenesis and synaptic regulation related genes. This may give us some lead to interpret the neuronal disorder observed at later stages.

To make the best use of our RNA-seq data, we still need to dig deeper by comparing with the already available RNA-seq data generated by recent progress on MΦ microglia research. For example, Matcovitch-Natan *et al.* analysed microglia sequential development from E10.5 YS and brain MΦ/microglia till adult stage. However, in E10.5 YS they analysed CX3CR1^{GFP+} mature MΦ (Matcovitch-Natan et al., 2016), and not, as we did, MΦ progenitors. It would be important to re-analysis our RNA-seq data together with their data (GEO accession number GSE79819) using methods such as Kmeans clustering to identify YS MΦ progenitors specific

gene clusters during microglia development, which will finally help to decipher the whole transcriptomic landscape evolution during microglia development. Mass *et al.* traced the tissue resident MΦ specification using RNA-seq and scRNA-seq starting from E9 YS "EMP" ($CD45^{low}$ $cKit^{+}$ $AA4.1^{+}$), E9.5 pre-MΦ ($CD45^{+}CD11b^{+}cKit^{-}F4/80^{-}$) that might correspond to A2 MΦ progenitors, E10.25 MΦ ($CD45^{+}CD11b^{+}F4/80^{+}$) to resident MΦ of different tissues from later developmental stage, but they also did not consider the MΦ progenitor population (Mass et al., 2016). Their "EMP" may also contain some $MΦ^{Prim}$ progenitors. But it seems that our RNA-seq data suggested $CD45^{low}$ $cKit^{+}$ $AA4.1^{+}$ may contain more EMP than $MΦ^{Prim}$ progenitors, since only up-regulated genes in E10 MΦ progenitors share some common genes with their "EMP" signature. With our RNA-seq data, it would be possible to redefine the signatures for "EMP", MΦ progenitor, and pre-MΦ/MΦ. Our RNA-seq data on E10 YS MΦ progenitors will also provide information about the missing developmental gap between EMP to MΦ by combining analysis of our RNA-seq data together with their published data (GSE81774).

3.2 The function of Lyl-1 during microglia development

Microglia are important for neuronal growth and synapse formation, thus their proper branching and morphology are very important during development (Gumusoglu et al., 2017) and homeostasis (Davalos et al., 2005; Nimmerjahn et al., 2005). Our confocal analysis on E12 embryonic microglia showed significantly reduced branching and ramifications in the *Lyl-1*$^{LacZ/LacZ}$ brain compared to the WT and a similar reduction of branches was also observed in the newborn microglia. So, it would be important to identify the downstream genes regulated by Lyl-1 that are involved in the control of the microglia branching process, by performing RNA-seq on E12 and P0 WT and Lyl-1 KO microglia. We cannot exclude that the defect observed in E12 could also result from a delay in the maturation process of microglia, since microglia will become ramified after maturation (Pont-Lezica et al., 2011). Following the evolution of morphology of microglia at later stages (E14, E16 and P0) in confocal analysis would allow to check whether this hypothesis is correct.

The result of the BrdU assay performed at E12 showed that Lyl-1 regulates the proliferation rate of microglia. The microglia pool was smaller in *Lyl-1*$^{LacZ/LacZ}$ brain than in the WT due to a

reduced proliferation rate. Of note, IL1R signaling is required for extensive microglia proliferation after microglia depletion (Bruttger et al., 2015). Consistent with this, our RNA-seq results indicated that Lyl-1 could positively regulate the expression level of IL1R in E9 $M\Phi^{Prim}$ progenitors. Such a regulation could be a possible explanation for reduced proliferation rate in *Lyl-1*$^{LacZ/LacZ}$ microglia, since E9 *Lyl-1*$^{LacZ/LacZ}$ MΦ progenitors have a reduced IL1R expression level compared to the WT. Proper microglia morphology (Nimmerjahn et al., 2005; Stence et al., 2001) and proliferation rate (Gomez-Nicola et al., 2013; Li et al., 2013) are both very important for maintain brain homeostasis. Further deep RNA-seq analysis on E12 microglia from both WT and Lyl-1-deficient embryos would provide more information about the genes regulating microglia morphology and also genes involved in microglia proliferation.

Microglia regulate the size of the neural precursor cell pool in the developing cerebral cortex (Cunningham et al., 2013). They also regulate the development of astrocytes (Antony et al., 2011). Moreover, they are responsible for the elimination of excess synapses during brain maturation. Proper microglia distribution and cell density in the developing brain is very important for appropriate neuronal connection and brain development (Antony et al., 2011; Hammond et al., 2018). Mice lacking the chemokine receptor Cx3cr1 exhibit a transient reduction of microglia pool during the early postnatal period leading to a deficit in synaptic pruning and to neuropsychiatric disorders *(Zhan et al., 2014)*. Interestingly, our collaborators on microglia function and neural development have found that the inactivation of Lyl-1 in microglia leads to abnormal microglia function and behavior defects in newborn and adult stages. Specifically, the microglia pool in our *Lyl-1*$^{LacZ/LacZ}$ mouse model also went through a transient reduction of microglia pool in both E12 and newborn brain. More interestingly, the expression level of Lyl-1 in Cx3cr1 deficient E12 microglia is not modified, but the expression level of Cx3cr1 in *Lyl-1*$^{LacZ/LacZ}$ E12 microglia is significantly reduced, which suggesting Lyl-1 could be a potential regulator of Cx3cr1. In adult mice, functional analysis of microglia such as monitoring their daily surveying behaviour and response to external stimuli (Nimmerjahn et al., 2005) would also help us to understand the response behaviour in normal and Lyl-1 invalidation situation and possibly deciphers their role in neuronal related diseases. Further

analysis on genes controlling microglia pool size during development would be essential to understand how the neurodevelopmental disorders arise early in life. Also, we could understand better the molecular pathway underlying the maturation process of microglia during development by sorting the microglia progeny of $M\Phi^{Prim}$ progenitors "lineage traced" by Lyl-1^{CreERT} fate-mapping at different developmental times and compared this population to its counterpart derived from Lyl-1^{Tomato} positive $M\Phi^{Prim}$ progenitors.

3.3 The function of Lyl-1 during the HSC development

In a previous study, our confocal imaging has detected Lyl-1 and Tal1/Scl expression in newly generated AGM-HSC at E10 (Giroux et al., 2007). Results obtained by many others scientists by different methods also show that Lyl-1 is expressed by AGM HSC. RNA-seq results from McKinney-Freeman *et al.* also showed that Lyl-1 is highly expressed in E11.5 AGM HSC and FL HSCs (McKinney-Freeman et al., 2012). Later, RNA-seq analysis from Solaimani Kartalaei *et al.* also confirmed that Lyl-1 is expressed by E10.5 AGM HSC (Solaimani Kartalaei et al., 2015). Recent single cell RNA-seq data again evidence Lyl-1 expression in AGM HSC (Baron et al., 2018; Bergiers et al., 2018) as well as in early FL HSC at single cell levels (Zhou et al., 2016a). Although the expression of Lyl-1 in HSC from E10 AGM and early stages of FL development is now well established, the function of Lyl-1 during HSC development remains poorly defined. In this study, we aimed to answer some questions regarding the function of Lyl-1 during HSC development.

To determine whether Lyl-1 influences the generation of AGM HSC, we used *in vitro* culture of P-Sp/AGM presumptive territory explanted before circulation and flow cytometry analysis. We did not observe significantly changes in the output of AGM HSC in *Lyl-$1^{LacZ/LacZ}$* AGM or in *in vitro* culture of the P-Sp/AGM presumptive territory. Further quantitative RT-PCR analysis of hematopoietic transcription factors expression in AGM HSC did not identify significant changes of the expression level of genes involved in AGM HSC generation. Altogether, these results clearly show that Lyl-1 does not influence the EHT process and the initial steps of HSC generation during development.

To test the influence of Lyl-1 invalidation on AGM HSC, we first applied LDA assay on AGM

HSC. We found that Lyl-1 invalidation leads to a significant 2-4 folds reduction of the HSPCs output compared to WT. Because a block in the differentiation of B-cell was observed by other scientists in E14 FL and adult HSC (Capron et al., 2006), we had to consider that this reduction of HSPC could be influenced by the defect of B-cell differentiation, since the detection of B-cell, together with erythroid and myeloid cells from clonal colonies allows us to quantify HSPC *in vitro*. The reduction of HSPC pool could be confirmed by the following reasons: the reported block of B-cell differentiation mainly impairs the maturation from pro-B to pre-B /immature B-cells, all of them expressing CD19. Here, in the LDA analysis, we use CD19 as a marker for the B-cell lineage. Even if there is a defect in the maturation from pro B to pre-B cell, we could still detect the B-cell lineage capability in pro-B cell. Secondly, even if the B cell lineage was totally blocked, we should expect more EMP progenitors, which is not the case here.

To further reinforce our results, we used the LDA-LTR system to test the HSC function *in vivo*, by engrafting E10 AGM cells from WT, *Lyl-1*$^{WT/\,LacZ}$ and *Lyl-1*$^{LacZ/LacZ}$ at 1, 3, 6 and 9 AGM per Rag2$^{-/-}\gamma c^{-/-}$ recipient. Here, we used a chimerism rate of myeloid cells above 1% as an indicator for successful HSC engraftment, because all the mature B- and T-cell will be from donor HSCs, since Rag2$^{-/-}\gamma c^{-/-}$ lack mature B and T cell. Also, previous LTR assay performed by other scientists did not find any significantly influence of Lyl-1 invalidation on the myeloid lineage (Capron et al., 2006; Souroullas et al., 2009). The repopulation unit for WT was 1/8.08 and the frequency for *Lyl-1*$^{LacZ/LacZ}$ was 2-3 folds reduced in *Lyl-1*$^{LacZ/\mathrm{LacZ}}$ AGM compared to WT, while *Lyl-1*$^{WT/\mathrm{LacZ}}$ AGM had an intermediate phenotype. Of note, the estimated frequency of repopulating units obtained in our reconstitution experiments for WT-AGM was consistent with those obtained by others using immune-deficient NSG recipients in E10.5 AGM LTR experiments (Vo et al., 2018). Thus, combining the *in vivo* and *in vitro* results together, the data indicated that Lyl-1 invalidation leads to a 2-3 folds decrease of functional HSC in E10 AGM.

Next, we analyzed the apoptosis and proliferation levels in AGM HSC. The proliferation rate was not modified in WT and *Lyl-1*$^{LacZ/LacZ}$ AGM HSC, while the apoptosis level was significantly increased in *Lyl-1*$^{LacZ/LacZ}$ AGM HSC compared to the WT. Consistent with our observation, Lyl-1 was also suggested to be involved in the regulation of apoptosis, since Tal1/Scl null HSCs

expressing a single allele of Lyl-1 (Lyl1$^{+/-}$;Tal1/Scl$^{-/-}$) could engraft normally in LTR assays and can maintain long-term hematopoiesis, while Lyl1$^{-/-}$;Tal1/Scl$^{-/-}$ HSCs die due to rapid apoptosis (Souroullas et al., 2009).

To evaluate the consequence of the apoptosis in AGM HSC, we further analyzed the size of the HSC pool in the FL at E12 and E14 by flow cytometry and LDA. The information gathered here revealed that the HSC pool was decreased by two-fold in *Lyl-1$^{LacZ/LacZ}$* compared to WT embryos, at both the E12 and E14 stages. Cell proliferation and apoptosis were not significantly modified in both WT and *Lyl-1$^{LacZ/LacZ}$* FL at E12. The apoptosis level remained low and comparable in WT and *Lyl-1$^{LacZ/LacZ}$* E14 FL, while the proliferation rate was increased, possibly compensate for the loss of some committed multipotent progenitors, as we have less CD150^{+}CD48^{+} progenitors in *Lyl-1$^{LacZ/LacZ}$* FL.

Confronting our data to those from other teams pointed to a striking persistence of HSC defects in *Lyl-1$^{LacZ/LacZ}$* mouse whatever the development stage investigated. Indeed, a 2-3 fold decreased of the HSC pool was also observed in both E14 FL (Capron et al., 2006) and adult BM (Capron et al., 2006; Souroullas et al., 2009; Zohren et al., 2012), without concomitant modification of the apoptosis and proliferation levels at these stages. Together, these results indicate that Lyl-1 controls the pool size of HSCs. The abnormal apoptosis of HSC, which only occurs at the AGM stage, can therefore lead to a life-long defect in HSC pool size. This observation also suggests the size of the HSC pool is set at the AGM stage. This maybe is not the best model to investigate the influence of early AGM stage defect to the long term whole HSC pool since *Lyl-1$^{LacZ/LacZ}$* is a knockout model in whole tissue. Further specific knockout of Lyl-1 using stem cell specific deletion tools, such as Hlf-Cre (Yokomizo et al., 2019) and with the Lyl-1^{loxp} model will give final interpretation of our results.

Since an increased apoptosis level was only observed in E10 AGM HSC, we analyzed the expression level of several apoptosis related genes. We tested several anti- and pro-apoptotic genes and found that only the expression level of bcl2 was modified, with a significant decrease in *Lyl-1$^{LacZ/LacZ}$* HSC. This could probably account for the increased apoptosis in *Lyl-1$^{LacZ/LacZ}$* HSC. This is consistent with observation from a previous report, which showed Bcl2 is involved in the survival of AGM HSCs (Orelio et al., 2004). Moreover, Bcl2 was

previously shown to be increased in T-ALL context and possibly regulated by Lyl-1 (Ferrando et al., 2002). Bcl2 also predicted to be a direct target of Lyl-1 (Wilson et al., 2011), which could stop the cell intrinsic apoptosis in Lyl1$^{-/-}$; Tal1/Scl$^{-/-}$ HSCs (Souroullas et al., 2009).

Recent studies have shown inflammatory signal and some factors are important for early embryonic HSC formation (Clapes et al., 2016; Hayashi et al., 2019) and survival (Azzoni et al., 2018). At least, RNA-seq data from our E9 MΦ progenitors suggested that Lyl-1 regulates inflammatory related signalling. After analyzing several reported inflammatory signaling pathways involved in HSC development, we did not find overt modification of the expression of these inflammatory-related signals in *Lyl-1*$^{LacZ/LacZ}$ HSPC at E10. However, we cannot exclude that other factors that we did not check yet are involved in AGM HSC survival. Another thing needs to be pointed out is that, whether inflammatory signaling is also involved in HSC survival is still unknown. Recently, Kit ligand (Kitl) was suggested to be important for the survival and maturation of AGM HSC, but not proliferation. Of note, Kitl KO AGM HSPCs share a similar phenotype with our *Lyl-1*$^{LacZ/LacZ}$ HSPCs: no modification of the proliferation rate but an increased in the apoptosis level (Azzoni et al., 2018).
Further deep analysis of other factors which are involved in AGM HSC survival such as Kitl expression level in AGM local microenvironment would be essential to determine whether the apoptosis in *Lyl-1*$^{LacZ/LacZ}$ AGM HSPCs is cell intrinsic or extrinsic. This could be achieved by further RNA-seq/scRNA-seq and real-time PCR analysis on both whole AGM and AGM HSPCs from WT and *Lyl-1*$^{LacZ/LacZ}$ embryos.

Of note, mature bloods cell are generated by the differentiation of bone marrow HSC in the adult hematopoietic system, while the embryonic hematopoietic system develops in a totally reverse program (Hofer et al., 2016). It starts with lineage-restricted progenitors in the primitive wave, then EMP progenitors appear, and finally HSC generation is initiated. The molecular mechanisms of this reverse progression of hematopoietic ontogeny remain unexplained. It will be interesting to known the genes controlling the developmental process, especially epigenetic factors which are thought to control the multipotentcy of hematopoietic progenitors (Noble, 2015; Vo et al., 2018). This will help us better understand

the epigenetic shift from primitive wave, then transient definitive wave to definitive wave. This could be achieved by newly adapted single cell ATAC-seq (Cusanovich et al., 2018), and provide more clues about different features within each hematopoietic wave.

In conclusion, we first analyzed the function of Lyl-1 during developmental hematopoiesis with special focus on YS MΦ and AGM HSC development. Using RNA-seq analysis we first compared the molecular features between $M\Phi^{Prim}$ and $M\Phi^{T\text{-}Def}$ progenitors and interpret the function of Lyl-1 during YS MΦ development. In the development of HSCs, Lyl-1 seems to specifically regulate apoptosis in AGM HSC and to control the HSC pool size in late embryonic and adult stage.

4 Résumé

Résumé

Les étapes du développement de l'hématopoïèse chez l'embryon

Chez les mammifères adultes, les cellules sanguines sont composées de divers types de cellules qui se déplacent dans les vaisseaux sanguins pour atteindre les différents tissus, où elles fournissent l'oxygène (érythrocytes), produisent les plaquettes nécessaires aux processus de coagulation (mégacaryocytes) ou forment une première barrière contre les pathogènes (macrophages et neutrophiles). Les défenses spécifiques contre ces pathogènes et l'élimination des cellules anormales sont assurées par les cellules de la lignée lymphoïde (lymphocytes B, T et cellules NK). Ces cellules sanguines sont constamment régénérées par des progéniteurs produits par une population rare de cellules de la moelle osseuse, les cellules souches hématopoïétiques (CSH), caractérisée par leur capacité à fournir tous les type de cellules sanguines et à maintenir leur propre population par auto-renouvellement. La caractérisation phénotypique et fonctionnelle de ces progéniteurs a conduit à l'isolement des CSH et ont fait du système hématopoïétique un modèle en biologie des cellules souches (Laurenti and Gottgens, 2018).

Bien que les CSH adultes résident dans la moelle osseuse des mammifères adultes, elles ne sont pas générées dans ce tissu, mais proviennent d'une population produite *de novo* pendant l'ontogenèse. Pendant l'ontogenèse, la production des cellules hématopoïétiques diffère de celle présentée par les modèles hiérarchiques d'hématopoïèse décrits chez l'adulte. Ce processus implique trois sites anatomiques principaux: le sac vitellin (SV), extra-embryonnaire, la région aorta-gonade-mésonéphros (AGM), intra-embryonnaire et le foie foetal (FF) (Cumano and Godin, 2007). Le SV constitue le premier site d'hématopoïèse de l'embryon, l'AGM est le site de génération de CSH, tandis que FF fournit le micro-environnement nécessaire à l'expansion du contingent de CSH, ainsi qu'à leur différenciation (Khan *et al.*, 2016).

Au cours de l'ontogenèse, la génération des progéniteurs hématopoïétiques s'établit en trois vagues successives distinctes limitées dans le temps et dans l'espace, chacune produisant ses propres progéniteurs. Le développement hématopoïétique commence par une hématopoïèse dite "indépendante des CSH" (Palis, 2016), qui se déroulent dans les îlot sanguins du SV.

Celui-ci produit les deux premières vagues de progéniteurs hématopoïétiques, appelées respectivement vague primitive et vague "transitoire-définitive". Ces deux vagues ont en commun la capacité de produire des cellules de la lignée érythro-myéloïde, mais elles diffèrent principalement par le type de progéniteur qui leur donne naissance. Ces progéniteurs sont monopotents pour la vague primitive, alors que dans la vague transitoire-définitive, les cellules matures dérivent d'un progéniteur érythro-myéloïde tel qu'il existe chez l'adulte. La troisième vague est la vague définitive, qui génère des CSH dans la région de l'aorte (appelée splanchnopleure para-aortique (P-Sp) au jour embryonnaire (E) 9, puis AGM à E10). Ces CSH, qui se forme à partir des cellules endothéliales de la paroi de l'aorte via un processus appelé transition endothélio-hématopoïétique (EHT), sont multipotentes et possédent l'activité de reconstitution à long terme (RLT) qui caractérise l'auto-renouvellement ds CSH. Au cours du développement, les progéniteurs issus des trois vagues migrent séquentiellement vers le FF qu'ils colonisent, puis certains d'entre eux colonisent le thymus, la rate et enfin, la fin de la gestation, la moelle osseuse.

La vague primitive débute dans les îlots sanguins du SV à partir de E7 avant la jonction de la circulation sanguine entre le SV et le compartiment intra-embryonnaire (McGrath *et al.*, 2003). Cette vague produit des progéniteurs à potentiel érythroïde, mégacaryocytaire et macrophagique (MΦ) (Palis *et al.*, 2001; Palis *et al.*, 1999). Après la jonction de la circulation entre le SV et l'embryon proprement dit qui a lieu à E8.25 (Ji *et al.*, 2003 ; McGrath *et al.*, 2003), ces précurseurs et leurs descendants entrent dans le flux sanguin et se mélangent rapidement avec les progéniteurs (et leurs descendants matures) dérivés de la vague transitoire-définitive, puis définitives (Kingsley *et al.*, 2004). Les progéniteurs érythrocytaires primitifs produisent de grosses cellules érythrocytaires nucléées exprimant la globine βH1, qui diffèrent des érythrocytes définitifs des 2ème et 3ème vagues, qui sont petits, énucléés et expriment uniquement les globines adultes. D'autres études indiquent que l'érythropoïèse primitive, la mégakaryopoïèse et la MΦ se développent indépendamment de cMyb. Bien que l'érythropoïèse primitive et définitive ait été bien caractérisée, on sait peu de choses sur les différences qui existent entre les mégakaryocytes et les macrophages (MΦ) primitifs et définitifs, quant à leur

développement et leurs fonctions spécifiques. Contrairement aux progéniteurs issus des vagues transitoires-définitives et définitives, qui donnent naissance MΦ par l'intermédiaire de progéniteurs intermédiaires bi-potents (granulo-monocytaires ou GM), dans la vague primitive les macrophages (MΦ) sont produits par des progéniteurs monopotents (Tober *et al.*, 2007).

La 2ème vague d'hématopoïèse du SV donne naissance à des progéniteurs érythro-myéloïdes (EMP) à partir de E8.0 (Palis, 2016). Cette vague est plus complexe que la première, car les EMP ont un potentiel multilignage et produisent des cellules sanguines matures par des voies de différenciation similaires à celles de l'adulte. Pourtant, les progéniteurs de cette vague n'ont pas de potentiel de reconstitution à long terme et ont donc été appelés "transitoire-définitifs". Cette vague est donc distincte de la vague primitive, qui est également transitoire mais est aussi dépourvue de progéniteurs multipotents, mais également de la troisième vague, par son absence de capacité de maintien à long terme (McGrath *et al.*, 2015a). Les progéniteurs de la 2ème vague donnent naissance à des érythrocytes définitifs, des mégacaryocytes, des MΦ, mais également des granulocytes, qui vont maturer et se différencier principalement dans le FF, après sa colonisation. Cependant, les différences entre les progéniteurs MΦ primitifs et ceux issus des EMPs ne sont toujours pas claires, et mon projet de thèse abordera cette question.

La troisième vague d'hématopoïèse s'amorce dans le compartiment intra- embryonnaire, dans un site qui contient l'aorte en développement, les gonades et le mésonéphros (AGM). Ce site est appelé d'abord Splanchnopleure Para-aortique (P-Sp) à E9 et il se développe en AGM après E10. Les CSH, caractérisées par leur capacité à reconstituer à long terme tous les lignages hématopoïétiques d'adultes irradiés, sont générées dans cette région P-Sp/AGM. Une fois générées, ces cellules migrent vers le FF où leur nombre augmente considérablement. Enfin, à la fin de la gestation, les CSH migrent vers la moelle osseuse, où elles seront responsables de l'hématopoïèse adulte. Les expériences de reconstitution à long terme (RLT) *in vivo* ont confirmé que seuls les progéniteurs de la 3ème vague pouvaient fournir des CSH qui confèrent un potentiel de reconstitution à long terme (Cumano *et al.*, 1996 ; Cumano *et al.*, 2001 ; Ganuza *et al.*, 2018). Les CSH de l'AGM sont caractérisées par un niveau d'expression élevé de cKit, un niveau bas de CD41, et une expression faible à

négative de CD45. Elles expriment également plusieurs marqueurs, dont l'expression est commune avec les cellules endothéliales, comme CD31, CD34, tie2 et AA4.1 (Bertrand *et al.*, 2005a).

Aux stades précoces de leur génération (E10), les CSH n'expriment pas encore les molécules du MHC-I et ne peuvent donc pas greffer dans des receveurs adultes normaux. Cependant, elles peuvent effectuer une RLT multilignage lorsqu'elles sont transférées dans des souris $Rag2^{-/-}\gamma c^{-/-}$ immunodéficientes (dépourvues de cellules tueuses naturelles NK, ainsi que des cellules lymphoïdes B et T (Kieusseian *et al.,* 2012)) ou des receveurs nouveaux-nés (Arora *et al.*, 2014). Peu après E10.5, dans l'AGM ou après leur migration vers le FF, les CSH acquièrent un phénotype CD45+ et MHC-1+ et la capacité d'effectuer la RLT chez un receveur adulte normal (Kieusseian et al., 2012; Arora *et al.*, 2014).

Comme la circulation sanguine entre le SV et l'embryon est établie juste après la formation de la première vague primitive (McGrath *et al.*, 2003), les progéniteurs des trois vagues sont mélangés dans le flux sanguin et se trouvent dans le SV, l'AGM, le FF et d'autres tissus comme le placenta (McKinney- Freeman *et al.*, 2009), rendant difficile la détermination de la contribution de chaque vague à l'hématopoïèse.

Le développement des macrophages et leur contribution à la microglie

Les macrophages sont présents dans tous les tissus où ils forment la population de MΦ résidents. Ils jouent des rôles comprenant la régulation du développement, le maintien de l'homéostasie et la surveillance immunitaire des pathogènes (Wynn *et al.*, 2013). Pendant longtemps, les MΦ adultes ont été considéré comme continuellement reconstitués par les CSH de la moelle osseuse par des intermédiaires monocytaires. Cependant, ce point de vue a été modifié par plusieurs travaux qui ont démontré que dans la plupart des tissus adultes, les MΦ résidents étaient générés pendant le développement embryonnaire et qu'ils pouvaient se renouveler localement sans l'apport de monocytes dérivés des CSH de la moelle osseuse (Sieweke and Allen, 2013).

Les études de cartographie du destin cellulaire ("fate mapping") ont fourni beaucoup d'informations sur l'ontogenèse des MΦ résidents des différents tissus. Par exemple, le consensus actuel est que la microglie (MΦ résidents du système nerveux) dérive

exclusivement de progéniteurs du SV (Ginhoux *et al.*, 2010; Gomez Perdiguero *et al.*, 2015). Néanmoins, ce type de modèle impliquant une induction lors de stades précoces du développement embryonnaire présente des défauts inévitables en ce qui concerne l'efficacité et la précision du traçage de la lignée, car certains des facteurs ciblés, tels que Runx1, Tie2 et cKit, ne sont pas des spécifiques d'une vague de progéniteurs, étant exprimés par tous les progéniteurs pendant le développement. De plus, contrairement aux affirmations antérieures, des recherches récentes sur le système Cre-loxP inductible ont montré qu'une activité Cre significative persiste dans les cellules sanguines de souris pendant 72 h après l'injection de Tamoxifène (Senserrich *et al.*, 2018). Une telle activité prolongée de la recombinaison *in vivo* est une source potentielle de mauvaise interprétation, particulièrement dans l'analyse des processus dynamiques du développement aux premiers stades de l'embryogenèse.

Comme mentionné précédemment, les deux vagues de progéniteurs hématopoïétiques du SV ont la capacité de donner naissance à MΦ dans un court laps de temps et, jusqu'à présent, aucun marqueur immuno-phénotypique ne peut distinguer les deux progéniteurs MΦ des 2 vagues (Bertrand *et al.*, 2005b). Les progéniteurs des deux vagues maturent en 3 étapes (de la population A1 vers la population A3) à partir d'un phénotype CD11b+CD31+CD45^{+}cKit^{+} (A1) par la perte progressive de CD31 et cKit (A2) puis ils deviennent des MΦ matures (A3) par une expression accrue des marqueurs CX3CR1 et F4/80.

Même s'il existe certains désaccords sur l'origine de plusieurs populations de MΦ résidents des tissus, tous s'accordent sur un fait: la microglie du cerveau des embryons dérive exclusivement des progéniteurs du SV. Cependant, la contribution des progéniteurs MΦ primitifs et de ceux dérivés des EMP de la deuxième vague fait encore l'objet de débats. Différents modèles de contribution de l'hématopoïèse du SV à la microglie ont été proposés. Le premier correspond aux résultats de (Gomez Perdiguero *et al.*, 2015). Combinant des modèles de souris inductibles Tie2cre et Csf1r inductibles, les auteurs ont proposé que les EMP sont à l'origine de la grande majorité des MΦ résidant dans les tissus, y compris la microglie. Le deuxième modèle, proposé par (Hoeffel *et al.*, 2015), considère que la plupart des MΦ résidents dérivent des EMP cMyb+ du SV tardifs alors que la microglie

proviendrait d'"EMP précoces" sans intermédiaire monocytique. Ces "EMPs précoces" correspondent très probablement aux progéniteurs des MΦ primitifs, car ils partagent un phénotype commun avec les EMP, mais ne se différencient pas en MΦ via des intermédiaires monocytiques (Bertrand *et al.*, 2005b). Le dernier modèle correspond à l'observation obtenue par (Sheng *et al.*, 2015) en utilisant le modèle cKit-cre inductible pour suivre la progénie des progéniteurs cKit à différents stades. L'induction à E7.5 à E9.5 conduit au marquage de toute la microglie et d'une partie des cellules de Langerhans (MΦ de la peau). Au contraire, l'induction à E8.5 provoque le marquage des MΦ résidents des autres tissus. Néanmoins, dans toutes ces expériences de cartographie, seul un sous-ensemble de microglie a été marqué chez l'adulte, ce qui laisse ouverte la possibilité qu'il puisse y avoir d'autres sources de progéniteurs microgliaux. En effet, des recherches sur le poisson zèbre ont montré qu'il existe deux progéniteurs de microglie distincts chez ce poisson (Ferrero *et al.*, 2018; Xu *et al.*, 2015). Chez le poisson zèbre, les trois vagues d'hématopoïèse sont plus facile à distinguer que chez les mammifères en raison de la séparation spatio-temporelle des progéniteurs pendant le développement (Bertrand *et al.*, 2007). Les résultats montrent que les progéniteurs MΦ primitifs donnent naissance à la microglie embryonnaire, mais que celle de l'adulte provient de progéniteurs issus de la vague définitive (Ferrero *et al.*, 2018; Xu *et al.*, 2015). Plus récemment, la découverte de 2 sous-populations de microglie (microglie canonique, Hoxb8-négative et microglie Hoxb8-positive) a ajouté un nouveau niveau de complexité aux études relative à l'ontogenèse de la microglie (De *et al.*, 2018). En effet, il est difficile jusqu'à présent de séparer les progéniteurs des trois vagues hématopoïétiques à l'aide de marqueurs de surface, en raison du chevauchement de leurs stades de génération et d'un phénotype immunitaire similaire (Bertrand *et al.*, 2005a ; Bertrand *et al.*, 2005b ; Inlay *et al.*, 2014 ; Lee *et al.*, 2016 ; McGrath *et al.,* 2015a ; McGrath *et al.*, 2015b).

Ces résultats discordants sur l'ontogenèse de la microglie à partir des modèles de souris inductibles actuellement disponibles pour cartographier les destinées cellulaires, révèle la difficulté de marquer in utero des populations hématopoïétiques spécifiques qui apparaissent toutes dans une fenêtre temporelle très étroite pendant le développement (Bertrand *et al.*, 2005b ; Ferrero *et al.*, 2018). Ainsi, une meilleure compréhension de la

signature moléculaire limitée à chaque vague de progéniteurs hématopoïétiques et l'identification de nouveaux marqueurs spécifiques pour chaque vague sont nécessaires pour aborder pleinement le processus d'ontogenèse de la microglie.

Le facteur de transcription Lyl-1

Les différentes propriétés des progéniteurs hématopoïétiques sont contrôlées par un réseau d'une dizaine de facteurs de transcription incluant Tal-1/Scl, Lmo2 et Runx1/AML1 qui constituent des régulateurs majeurs du développement hématopoïétique de l'embryon (Pina *et al.,* 2007 ; Moignard *et al.,* 2013), et qui sont également fréquemment impliqués dans des translocations aboutissant au développement de leucémies aigües pédiatriques (LAL-T) (Ferrando *et al.*, 2002). Lyl-1, qui partage de grandes similitudes avec Tal-1/Scl appartient également à ce réseau. Mais, contrairement à Tal-1/Scl, dont le rôle dans le développement du système hématopoïétique a été très étudié (il est indispensable à la production des progéniteurs hématopoïétiques de l'embryon), les fonctions de Lyl-1 durant l'ontogenèse sont encore inconnues (Curtis, 2012 *;* Wilson *et al.,* 2010).

Lyl-1, un facteur de transcription appartenant à la famille des facteurs de transcription bHLH de classe II, a été identifié pour la première fois en 1989 dans la translocation chromosomique t(7;19) conduisant à des LAL-T (Mellentin *et al.*, 1989). Environ 10 % des LAL-T pédiatriques et 25 % de celles de l'adulte sont associés à des altérations génétiques du Lyl-1 (Pui *et al.*, 2004). Lyl-1 est un proche parent de Tal1/Scl, puisque ces 2 facteurs présentent plus de 80 % de similarité dans leur domaine bHLH, et sont également impliqués dans la leucémogenèse (Curtis *et al.*, 2012 ; Ferrando *et al.*, 2002).

L'analyse des cellules hématopoïétiques des souris "knock-in" Lyl-1^{LacZ} (Capron *et al*., 2006), où la partie de l'exon 4 qui code le domaine HLH a été remplacée par le gène codant pour la β-galactosidase (β-Gal), a montré une expression de Lyl-1 dans les CSH du FF. De plus, les CSH *Lyl-1$^{LacZ\ /LacZ}$* montrent un déficit de potentiel de maintenance (Capron *et al.,* 2006 ; Souroullas *et al*., 2009). Une analyse comparative des patrons d'expression de Lyl-1 et de Tal1/Scl au cours du développement hématopoïétique a suggéré qu'ils ont des fonctions redondantes, ainsi que des rôles distincts pendant le développement embryonnaire et la vie postnatale (Giroux *et al.*, 2007 ; Pirot *et al.*, 2010 ; Visvader *et al.*, 1991). En effet,

l'expression de Tal1/Scl (Silver et Palis, 1997) et de Lyl-1 a été observée dans le système cardiovasculaire, dans les îlots sanguins du SV à E7.5, mais également dans les CSH de l'AGM (Giroux *et al.*, 2007). Comme indiqué ci-dessus, les souris Knockout de *Tal1/Scl* meurent in utero en raison de l'absence complète d'érythropoïèse primitive (Robb *et al.*,1995) suggèrant un rôle critique dans l'hématopoïèse du SV. Des données récentes d de séquençage sur cellule unique d'embryons précoces ont montré que les cellules érythroïdes primitives exprimaient à la fois *Tal1/Scl* et *Lyl-1*. De plus, l'expression du Lyl-1 pourrait remplacer celle du Tal1/Scl dans les cellules érythroïdes primitives lorsque son expression est significativement réduite (Chiu *et al.*, 2018). La perte de *Tal1/Scl* entraîne l'absence de tous les progéniteurs hématopoïétiques, ce qui montre que ce facteur est aussi essentiel à la genèse des CSH (Robb *et al.*, 1995; Shivdasani *et al.*,1995). Cependant, Tal1/Scl n'est pas nécessaire pour le maintien des CSH postnatales, car l'élimination conditionnelle de Tal1/Scl dans les CSH adultes n'a aucun impact sur leur activité RLT (Curtis *et al.*, 2004 ; Mikkola *et al.*, 2003).

Les deux lignées de souris knock-out pour *Lyl-1* présentent un nombre réduit de CSH dans le foie fœtal et la moelle osseuse adulte (Capron *et al*., 2006; Souroullas et Goodell, 2011), ce qui suggère que *Lyl-1* est essentiel au maintien des CSH. L'étude des CSH des souris double mutantes conditionnelles *Lyl-1:Tal1/Scl* a révélé qu'un seul allèle de *Lyl-1* était suffisant pour maintenir l'hématopoïèse à partir de CSH *Tal1/Scl* nulles, alors qu'une perte rapide de CSH était observée lorsque *Tal1/Scl* et *Lyl-1* étaient tous deux supprimés, en raison d'une augmentation significative de l'apoptose (Souroullas *et al.*, 2009), confirmant *l'*importance du rôle du *Lyl-1* dans le maintien des CSH adultes. Ces résultats suggèrent que *Lyl-1* et *Tal1/Scl* partagent un certain chevauchement mais aussi des fonctions distinctes dans la formation et le maintien des CSH. Malgré les similitudes dans l'expression de *Lyl-1* et de *Tal1/Scl* dans l'hématopoïèse, il est clair que les deux gènes exercent des fonctions distinctes dans l'hématopoïèse embryonnaire. Bien que *Lyl-1* soit dispensable pour le développement précoce de la souris, son rôle précis dans l'hématopoïèse embryonnaire précoce n'a pas été bien étudié.

Un ensemble d'analyses fonctionnelles pratiquées dans notre équipe pour déterminer le rôle de Lyl-1 dans le développement des progéniteurs hématopoïétiques de l'embryon a permit de montrer que l'invalidation de Lyl-1 conduisait à deux effets distincts, affectant d'une part

le développement des macrophages du SV et et de la microglie embryonnaire et, d'autre part, celui des CSH de l'embryon. Les résultats que j'ai obtenus lors de l'étude des fonctions de *Lyl-1* dans le développement de l'hématopoïèse embryonnaire sont présentés ci-dessous, tout d'abord ceux concernant le rôle de Lyl-1 lors du développement des progéniteurs MΦ du SV et de la microglie, puis ceux qui concernent la régulation par Lyl-1 du développement des CSH.

Le développement des macrophages et de la microglie est régulé par Lyl-1.

Chacune des deux vagues hématopoïétiques qui se produisent dans le SV produit une population de progéniteurs MΦ, de sorte que le SV abrite à la fois des progéniteurs MΦ primitifs ($MΦ^{Prim}$), qui dérivent de progéniteurs MΦ monopotents, et des MΦ définitifs transitoires ($MΦ^{T\text{-}Def}$), qui proviennent de la différenciation des EMP. Cependant, en raison de leur phénotype similaire et du chevauchement de leur génération, leur contribution exacte aux populations de MΦ résidents, en particulier à la microglie, n'est toujours pas claire. Dans nos travaux antérieurs, nous avons trouvé en utilisant le gène rapporteur lacZ des souris *Lyl-1*^{lacZ}, que l'expression de Lyl-1 marquait spécifiquement les progéniteurs $MΦ^{Prim}$ du SV de E9, mais aussi la microglie de l'embryon. De plus, nous avons montré que l'inactivation de Lyl-1 entraînait une augmentation de la production de progéniteurs $MΦ^{Prim}$ dans le SV, puis une diminution transitoire de la population microgliale à E12 et chez le nouveau-né. Mon apport dans cette étude a été de montrer que l'inactivation de Lyl-1 provoquait également dans la microglie des embryons *Lyl-1*$^{LacZ/LacZ}$, des changements morphologiques catacyérisés par une réduction du nombre et de l'extension des ramifications par rapport à la microglie de témoins sauvages, et ceci aux deux stades impactés par la mutation.

Pour élargir cette étude, nous avons procédé des comparaisons en séquençage ARN afin de : 1- Définir les caractéristiques des progéniteurs MΦ des vagues primitive et définitive-transitoire pour mieux comprendre les différences existant entre les progéniteurs $MΦ^{Prim}$ et $MΦ^{T\text{-}Def}$, et 2- Identifier les différences d'expression génique qui sous-tendent les défauts observés chez les embryons mutants.

Pour cela, nous avons procédé au séquençage ARN des progéniteurs $MΦ^{Prim}$ triés à partir de

SV sauvages ou *Lyl-1*$^{lacZ/LacZ}$ à E9, lorsque seuls les progéniteurs MΦ^{Prim} sont présents. Les progéniteurs MΦ ont été triés à partir de SV de E10, qui contiennent à la fois des progéniteurs MΦ^{Prim} et MΦ$^{T\text{-}Def}$. Les données obtenues ont montré que le patron d'expression génique des progéniteurs MΦ^{Prim} de E9 était clairement distinct de celui obtenu à E10, œ qui reflète leurs natures primitives. Par rapport à ceux de E10, dans un contexte sauvage ou mutant, les progéniteurs MΦ^{Prim} de E9 expriment un niveau plus élevé de gènes du complexe majeur d'histocompatibilité MHC-II tels que *Cd74*, *H2-Aa* et ils expriment déjà des gènes spécifiques de la microglie, tels que *Sall3*. Les progéniteurs MΦ de E10 présentent eux, des niveaux plus élevés de gènes caractéristiques des EMP tels que *Gata1* et les gènes de l'hémoglobine, comme *Hba-x* et *Hbb-y*. De façon intéressante, à E10, les progéniteurs MΦ expriment des gènes spécifiques des MΦ résidents d'autres tissus que la microglie tels que *Id3* et *Runx3*, ce qui marque leur origine à partir d'EMP. De plus, l'invalidation de Lyl-1 influence certaines voies de signalisation inflammatoires. Elle conduit également à une activation anormale des gènes de la microglie impliqués dans la régulation synaptique.

Lyl-1 régule développement des CSH embryonnaires

Dans une étude précédente, nous avions détecté l'expression de Lyl-1 et de Tal1/Scl dans les CSH nouvellement générées, dans l'AGM à E10 (Giroux *et al.*, 2007). Les données de RNA-seq obtenues par plusieurs groupes montrent également l'expression de Lyl-1 par les CSH de l'AGM à E10 et E11,5, mais également dans celles du FF. Bien que l'expression de Lyl-1 dans les CSH de l'AGM du FF soit maintenant bien établie, la fonction du Lyl-1 pendant le développement de ces CSH reste mal définie et nous avons cherché à répondre à cette questions.

Pour déterminer si Lyl-1 influence la production de CSH AGM, nous avons utilisé une culture *in vitro* du territoire présomptif de la P-Sp/AGM suivi d'une analyse en cytométrie de flux. Nous n'avons pas observé de changements significatifs dans la génération des CSH *Lyl-1*$^{LacZ/LacZ}$ dans ces cultures. De même, le nombre de CSH présentes dans l'AGM à E10 est semblable à celui des témoins sauvages. Enfin, l'analyse en RT-PCR n'a pas permis

d'identifier de changements significatifs du niveau d'expression des facteurs de transcriptions impliqués dans la génération des CSH. L'ensemble de ces résultats montre clairement que Lyl-1 n'influence pas le processus d' EHT et les premières étapes de la génération de CSH pendant le développement.

Pour tester l'influence de l'invalidation du Lyl-1 sur le devenir des CSH de l'AGM, nous avons analysé leur devenir lors de culture en dilution limite (TDL). Nous avons constaté que l'invalidation du Lyl-1 entraînait une réduction significative de 2 à 4 fois de nombre de cellule souches et progénitrices par rapport au sauvage. Pour renforcer ces résultats, nous avons pratiqué des expériences de reconstitution à long terme en dilution limite pour tester fonctionnellement les CSH *in vivo*. Des cellules d' AGM (sauvage, *Lyl-1*$^{WT/LacZ}$ et *Lyl-1*$^{LacZ/LacZ}$) ont été greffées à 1, 3, 6 et 9 AGM par receveur Rag2$^{-/-}\gamma c^{-/-}$. L'analyse du nombre d'animaux reconstitués pour chaque dose de greffe a montré une réduction de 2-3 fois du nombre d'unité de reconstitution pour les greffons d'AGM *Lyl-1*$^{LacZ/LacZ}$ comparativement au sauvage, tandis que *Lyl-1*$^{WT/LacZ}$ AGM avait un phénotype intermédiaire. Il est à noter que la fréquence estimée des unités de reconstitution obtenues dans nos expériences correspondait pour l'AGM sauvage à celle obtenue par d'autres personnes utilisant également des receveurs immunodéficients (NGS) dans les greffes d'AGM de E10.5 (Vo et al., 2018). Ainsi, en combinant les résultats *in vivo* et *in vitro*, les données indiquent que l'invalidation du Lyl-1 entraîne une diminution de 2 à 3 fois de la quantité de CSH fonctionnelle dans l'AGM de E10.

Ensuite, nous avons analysé les niveaux d'apoptose et de prolifération des CSH de l'AGM. Le taux de prolifération n'était pas modifié dans les CSH sauvages et *Lyl-1*$^{LacZ/LacZ}$ AGM, tandis que le taux d'apoptose était significativement plus élevé dans les CSH de l'AGM *Lyl-1*$^{LacZ/LacZ}$ que dans l'équivalent sauvage. Conformément à notre observation, il a également été suggéré que le Lyl-1 est impliqué dans la régulation de l'apoptose, puisque les CSH *Tal1/Scl* nulles exprimant un seul allèle de Lyl-1 (*Lyl1*$^{+/-}$*; Tal1/Scl*$^{-/-}$) peuvent maintenir une hématopoïèse à long terme lors de greffes alors que, en l'absence de Lyl-1, les CSH *Tal1/Scl*$^{-/-}$ meurent rapidement par apoptose (Souroullas *et al.*, 2009).

Pour évaluer les conséquences de la diminution du nombre de CSH dans l'AGM des mutants, nous avons analysé la taille du pool de CSH dans le FF à E12 et E14 par cytométrie

de flux et culture en TDL. Cette analyse arévélé que la population de CSH des embryons *Lyl-1*$^{LacZ/LacZ}$ était réduite d'un facteur deux par rapport à celle d'embryons sauvages aux deux stades (E12 et E14), sans modification du niveau d'apoptose, et sans augmentation du niveau de prolifération. Au contraire, le taux de prolifération est augmenté dans le FF *Lyl-1*$^{LacZ/LacZ}$ à E14, peut- être pour compenser la perte de certains progéniteurs multipotents engagés.

La comparaison de nos données avec celles d'autres équipes a révélé une persistance frappante du défauts de la taille de la population de CSH chez les souris *Lyl-1*$^{LacZ/LacZ}$ quel que soit le stade de développement étudié. En effet, une diminution de 2 à 3 fois du stock de CSH a également été observée dans la FF de E14 (Capron *et al.*, 2006) et dans la moelle osseuse adulte (Capron et al., 2006; Souroullas et al., 2009; Zohren et al.,2012), sans modification concomitante des niveaux d'apoptose et de prolifération aux deux stades. Ensemble, ces résultats indiquent que Lyl-1 contrôle la taille de la population de CSH. L'apoptose accrue des CSH, qui ne se produit qu'au stade de l'AGM, peut donc entraîner un défaut à vie dans la taille du contingent de CSH. Cette observation suggère également que cette taille du contingent de CSH est fixée au stade de l'AGM.

Comme une augmentation du taux d'apoptose des CSH n'a été observée que dans le l'AGM de E10, nous avons analysé le taux d'expression de plusieurs gènes anti- et pro-apoptotiques et constaté que seul le niveau d'expression de *Bcl2* était modifié, avec une diminution significative dans les CSH d'AGM *Lyl-1*$^{LacZ/LacZ}$, ce qui pourrait expliquer l'augmentation de l'apoptose. Ce résultat concorde avec les observations d'un rapport précédent, qui montrait que Bcl2 est impliqué dans la survie des CSH de l'AGM (Orelio *et al.*, 2004). De plus, il a déjà été démontré que l'expression de *Bcl2* était augmentée dans le contexte des leucémies aigües lymphoblastiques T, possiblement à la suite d'une régulation par Lyl-1, qui est impliqué dans des translocation conduisant à ce type de leucémie (Ferrando *et al.*, 2002). Bcl2 a également identifié comme une cible potentielle directe de Lyl-1 (Wilson *et al.*, 2011).

En conclusion, nous avons d'abord analysé la fonction de Lyl-1 pendant l'ontogenèse de l'hématopoïèse en nous concentrant particulièrement sur le développement des MΦ du SV et celui des CSH de l'AGM. En utilisant l'analyse des séquences d'ARN, nous avons d'abord

comparé les caractéristiques moléculaires des progéniteurs $M\Phi^{Prim}$ et $M\Phi^{T\text{-}Def}$ et caractérisé la fonction de Lyl-1 pendant le développement des MΦ du SV. Lyl-1 semble réguler la production. La fonction spécifique des progéniteurs $M\Phi^{Prim}$ semble différente de celle exercée par les $M\Phi^{T\text{-}Def}$ et ceux issus des CSH, comme le montrent nos résultats de RNA-seq qui demandent à être développés. En ce qui concerne le développement des CSH, Lyl-1 semble réguler spécifiquement l'apoptose dans les CSH immédiatement après leur génération, ce qui contrôle la taille du contingent de CSH aux stades embryonnaires et jusque dans la vie adulte.

5 References

Ajami, B., Bennett, J.L., Krieger, C., Tetzlaff, W., and Rossi, F.M. (2007). Local self-renewal can sustain CNS microglia maintenance and function throughout adult life. Nature neuroscience *10*, 1538-1543.

Alliot, F., Godin, I., and Pessac, B. (1999). Microglia derive from progenitors, originating from the yolk sac, and which proliferate in the brain. Brain Res Dev Brain Res *117*, 145-152.

Andrews, S. (2010). FastQC A Quality Control tool for High Throughput Sequence Data.

Angers, S., and Moon, R.T. (2009). Proximal events in Wnt signal transduction. Nature reviews. Molecular cell biology *10*, 468-477.

Antony, J.M., Paquin, A., Nutt, S.L., Kaplan, D.R., and Miller, F.D. (2011). Endogenous microglia regulate development of embryonic cortical precursor cells. Journal of neuroscience research *89*, 286-298.

Arora, N., Wenzel, P.L., McKinney-Freeman, S.L., Ross, S.J., Kim, P.G., Chou, S.S., Yoshimoto, M., Yoder, M.C., and Daley, G.Q. (2014). Effect of developmental stage of HSC and recipient on transplant outcomes. Developmental cell *29*, 621-628.

Azzoni, E., Frontera, V., McGrath, K.E., Harman, J., Carrelha, J., Nerlov, C., Palis, J., Jacobsen, S.E.W., and de Bruijn, M.F. (2018). Kit ligand has a critical role in mouse yolk sac and aorta-gonad-mesonephros hematopoiesis. EMBO reports *19*.

Baron, C.S., Kester, L., Klaus, A., Boisset, J.C., Thambyrajah, R., Yvernogeau, L., Kouskoff, V., Lacaud, G., van Oudenaarden, A., and Robin, C. (2018). Single-cell transcriptomics reveal the dynamic of haematopoietic stem cell production in the aorta. Nature communications *9*, 2517.

Batsivari, A., Rybtsov, S., Souilhol, C., Binagui-Casas, A., Hills, D., Zhao, S., Travers, P., and Medvinsky, A. (2017). Understanding Hematopoietic Stem Cell Development through Functional Correlation of Their Proliferative Status with the Intra-aortic Cluster Architecture. Stem cell reports *8*, 1549-1562.

Begley, C.G., Aplan, P.D., Denning, S.M., Haynes, B.F., Waldmann, T.A., and Kirsch, I.R. (1989). The gene SCL is expressed during early hematopoiesis and encodes a differentiation-related DNA-binding motif. Proc Natl Acad Sci *86*, 10128-10132.

Bejerot, S., Eriksson, J.M., and Mortberg, E. (2014). Social anxiety in adult autism spectrum disorder. Psychiatry Res *220*, 705-707.

Bennett, F.C., Bennett, M.L., Yaqoob, F., Mulinyawe, S.B., Grant, G.A., Hayden Gephart, M., Plowey, E.D., and Barres, B.A. (2018). A Combination of Ontogeny and CNS Environment Establishes Microglial Identity. Neuron *98*, 1170-1183 e1178.

Benz, C., Copley, M.R., Kent, D.G., Wohrer, S., Cortes, A., Aghaeepour, N., Ma, E., Mader, H., Rowe, K., Day, C., *et al.* (2012). Hematopoietic stem cell subtypes expand differentially during development and display distinct lymphopoietic programs. Cell stem cell *10*, 273-283.

Bergiers, I., Andrews, T., Vargel Bolukbasi, O., Buness, A., Janosz, E., Lopez-Anguita, N., Ganter, K., Kosim, K., Celen, C., Itir Percin, G., *et al.* (2018). Single-cell transcriptomics reveals a new dynamical function of transcription factors during embryonic hematopoiesis. eLife *7*.

Bertrand, J.Y., Cisson, J.L., Stachura, D.L., and Traver, D. (2010). Notch signaling distinguishes 2 waves of definitive hematopoiesis in the zebrafish embryo. Blood *115*, 2777-2783.

Bertrand, J.Y., Giroux, S., Golub, R., Klaine, M., Jalil, A., Boucontet, L., Godin, I., and Cumano, A. (2005a). Characterization of purified intraembryonic hematopoietic stem cells as a tool to define their site of origin. Proceedings of the National Academy of Sciences of the United States of America *102*, 134-139.

Bertrand, J.Y., Jalil, A., Klaine, M., Jung, S., Cumano, A., and Godin, I. (2005b). Three pathways to mature macrophages in the early mouse yolk sac. Blood *106*, 3004-3011.

Bertrand, J.Y., Kim, A.D., Violette, E.P., Stachura, D.L., Cisson, J.L., and Traver, D. (2007). Definitive hematopoiesis initiates through a committed erythromyeloid progenitor in the zebrafish embryo. Development *134*, 4147-4156.

Bevins, R.A., and Besheer, J. (2006). Object recognition in rats and mice: a one-trial non-matching-to-sample learning task to study 'recognition memory'. Nat Protoc *1*, 1306-1311.

Bhatia, M., Bonnet, D., Wu, D., Murdoch, B., Wrana, J., Gallacher, L., and Dick, J.E. (1999). Bone morphogenetic proteins regulate the developmental program of human hematopoietic stem cells. The Journal of experimental medicine *189*, 1139-1148.

Biagioli, M., Pinto, M., Cesselli, D., Zaninello, M., Lazarevic, D., Roncaglia, P., Simone, R., Vlachouli, C., Plessy, C., Bertin, N*., et al.* (2009). Unexpected expression of alpha- and beta-globin in mesencephalic dopaminergic neurons and glial cells. Proceedings of the National Academy of Sciences of the United States of America *106*, 15454-15459.

Bigas, A., and Espinosa, L. (2012). Hematopoietic stem cells: to be or Notch to be. Blood *119*, 3226-3235.

Bigas, A., Guiu, J., and Gama-Norton, L. (2013). Notch and Wnt signaling in the emergence of hematopoietic stem cells. Blood cells, molecules & diseases *51*, 264-270.

Blank, T., Detje, C.N., Spiess, A., Hagemeyer, N., Brendecke, S.M., Wolfart, J., Staszewski, O., Zoller, T., Papageorgiou, I., Schneider, J*., et al.* (2016). Brain Endothelial- and Epithelial-Specific Interferon Receptor Chain 1 Drives Virus-Induced Sickness Behavior and Cognitive Impairment. Immunity *44*, 901-912.

Boehm, T., Foroni, L., Kaneko, Y., Perutz, M.F., and Rabbitts, T.H. (1991). The rhombotin family of cysteine-rich LIM-domain oncogenes: distinct members are involved in T-cell translocations to human chromosomes 11p15 and 11p13. Proc Natl Acad Sci U S A *88*, 4367-4371.

Boiers, C., Carrelha, J., Lutteropp, M., Luc, S., Green, J.C., Azzoni, E., Woll, P.S., Mead, A.J., Hultquist, A., Swiers, G*., et al.* (2013). Lymphomyeloid contribution of an immune-restricted progenitor emerging prior to definitive hematopoietic stem cells. Cell stem cell *13*, 535-548.

Boyer, S.W., Schroeder, A.V., Smith-Berdan, S., and Forsberg, E.C. (2011). All hematopoietic cells develop from hematopoietic stem cells through Flk2/Flt3-positive progenitor cells. Cell stem cell *9*, 64-73.

Breton-Provencher, V., Lemasson, M., Peralta, M.R., 3rd, and Saghatelyan, A. (2009). Interneurons produced in adulthood are required for the normal functioning of the olfactory bulb network and for the execution of selected olfactory behaviors. J Neurosci *29*, 15245-15257.

Brunet de la Grange, P., Armstrong, F., Duval, V., Rouyez, M.C., Goardon, N., Romeo, P.H., and Pflumio, F. (2006). Low SCL/TAL1 expression reveals its major role in adult hematopoietic myeloid progenitors and stem cells. Blood *108*, 2998-3004.

Bruttger, J., Karram, K., Wortge, S., Regen, T., Marini, F., Hoppmann, N., Klein, M., Blank, T., Yona, S., Wolf, Y*., et al.* (2015). Genetic Cell Ablation Reveals Clusters of Local Self-Renewing Microglia in the Mammalian Central Nervous System. Immunity *43*, 92-106.

Butovsky, O., Jedrychowski, M.P., Moore, C.S., Cialic, R., Lanser, A.J., Gabriely, G., Koeglsperger, T., Dake, B., Wu, P.M., Doykan, C.E*., et al.* (2014). Identification of a unique TGF-beta-dependent molecular and functional signature in microglia. Nature neuroscience *17*, 131-143.

Buttgereit, A., Lelios, I., Yu, X., Vrohlings, M., Krakoski, N.R., Gautier, E.L., Nishinakamura, R., Becher, B., and Greter, M. (2016). Sall1 is a transcriptional regulator defining microglia identity and function. Nature immunology *17*, 1397-1406.

Calandra, T., and Roger, T. (2003). Macrophage migration inhibitory factor: a regulator of innate immunity. Nature reviews. Immunology *3*, 791-800.

Calhoun, V.D., Adali, T., Pearlson, G.D., and Pekar, J.J. (2001). A method for making group inferences from functional MRI data using independent component analysis. Hum Brain Mapp *14*, 140-151.

Capron, C., Lecluse, Y., Kaushik, A.L., Foudi, A., Lacout, C., Sekkai, D., Godin, I., Albagli, O., Poullion, I., Svinartchouk, F*., et al.* (2006). The SCL relative LYL-1 is required for fetal and adult hematopoietic stem cell function and B-cell differentiation. Blood *107*, 4678-4686.

Cattelino, A., Liebner, S., Gallini, R., Zanetti, A., Balconi, G., Corsi, A., Bianco, P., Wolburg, H., Moore, R., Oreda, B.*, et al.* (2003). The conditional inactivation of the beta-catenin gene in endothelial cells causes a defective vascular pattern and increased vascular fragility. The Journal of cell biology *162*, 1111-1122.

Chen, Q., Cheng, J.T., Tasi, L.H., Schneider, N., Buchanan, G., Carroll, A., Crist, W., Ozanne, B., Siciliano, M.J., and Baer, R. (1990). The tal gene undergoes chromosome translocation in T cell leukemia and potentially encodes a helix-loop-helix protein. EMBO J *9*, 415-424.

Chen, S.K., Tvrdik, P., Peden, E., Cho, S., Wu, S., Spangrude, G., and Capecchi, M.R. (2010). Hematopoietic origin of pathological grooming in Hoxb8 mutant mice. Cell *141*, 775-785.

Chiaretti, S., and Foa, R. (2009). T-cell acute lymphoblastic leukemia. Haematologica *94*, 160-162.

Chiu, S.K., Saw, J., Huang, Y., Sonderegger, S.E., Wong, N.C., Powell, D.R., Beck, D., Pimanda, J.E., Tremblay, C.S., and Curtis, D.J. (2018). A novel role for Lyl1 in primitive erythropoiesis. Development *145*.

Chung, J.E., Magland, J.F., Barnett, A.H., Tolosa, V.M., Tooker, A.C., Lee, K.Y., Shah, K.G., Felix, S.H., Frank, L.M., and Greengard, L.F. (2017). A Fully Automated Approach to Spike Sorting. Neuron *95*, 1381-1394 e1386.

Ciau-Uitz, A., Monteiro, R., Kirmizitas, A., and Patient, R. (2014). Developmental hematopoiesis: ontogeny, genetic programming and conservation. Experimental hematology *42*, 669-683.

Ciau-Uitz, A., and Patient, R. (2016). The embryonic origins and genetic programming of emerging haematopoietic stem cells. FEBS letters *590*, 4002-4015.

Clapes, T., Lefkopoulos, S., and Trompouki, E. (2016). Stress and Non-Stress Roles of Inflammatory Signals during HSC Emergence and Maintenance. Frontiers in immunology *7*, 487.

Clarke, D., Vegiopoulos, A., Crawford, A., Mucenski, M., Bonifer, C., and Frampton, J. (2000). In vitro differentiation of c-myb(-/-) ES cells reveals that the colony forming capacity of unilineage macrophage precursors and myeloid progenitor commitment are c-Myb independent. Oncogene *19*, 3343-3351.

Clements, W.K., Kim, A.D., Ong, K.G., Moore, J.C., Lawson, N.D., and Traver, D. (2011). A somitic Wnt16/Notch pathway specifies haematopoietic stem cells. Nature *474*, 220-224.

Clements, W.K., and Traver, D. (2013). Signalling pathways that control vertebrate haematopoietic stem cell specification. Nature reviews. Immunology *13*, 336-348.

Colangelo, V., Schurr, J., Ball, M.J., Pelaez, R.P., Bazan, N.G., and Lukiw, W.J. (2002). Gene expression profiling of 12633 genes in Alzheimer hippocampal CA1: transcription and neurotrophic factor down-regulation and up-regulation of apoptotic and pro-inflammatory signaling. J Neurosci Res *70*, 462-473.

Colucci, F., Soudais, C., Rosmaraki, E., Vanes, L., Tybulewicz, V.L., and Di Santo, J.P. (1999). Dissecting NK cell development using a novel alymphoid mouse model: investigating the role of the c-abl proto-oncogene in murine NK cell differentiation. Journal of immunology *162*, 2761-2765.

Corrigan, P.M., Dobbin, E., Freeburn, R.W., and Wheadon, H. (2009). Patterns of Wnt/Fzd/LRP gene expression during embryonic hematopoiesis. Stem cells and development *18*, 759-772.

Cumano, A., Dieterlen-Lievre, F., and Godin, I. (1996). Lymphoid potential, probed before circulation in mouse, is restricted to caudal intraembryonic splanchnopleura. Cell *86*, 907-916.

Cumano, A., Ferraz, J.C., Klaine, M., Di Santo, J.P., and Godin, I. (2001). Intraembryonic, but not yolk sac hematopoietic precursors, isolated before circulation, provide long-term multilineage reconstitution. Immunity *15*, 477-485.

Cumano, A., and Godin, I. (2007). Ontogeny of the hematopoietic system. Annual review of immunology *25*, 745-785.

Cunningham, C.L., Martinez-Cerdeno, V., and Noctor, S.C. (2013). Microglia regulate the number of neural precursor cells in the developing cerebral cortex. The Journal of neuroscience : the official journal of the Society for Neuroscience *33*, 4216-4233.

Curtis, D.J., Hall, M.A., Van Stekelenburg, L.J., Robb, L., Jane, S.M., and Begley, C.G. (2004). SCL is required for

normal function of short-term repopulating hematopoietic stem cells. Blood *103*, 3342-3348.

Curtis, D.J., Salmon, J.M., and Pimanda, J.E. (2012). Concise review: Blood relatives: formation and regulation of hematopoietic stem cells by the basic helix-loop-helix transcription factors stem cell leukemia and lymphoblastic leukemia-derived sequence 1. Stem cells *30*, 1053-1058.

Cusanovich, D.A., Hill, A.J., Aghamirzaie, D., Daza, R.M., Pliner, H.A., Berletch, J.B., Filippova, G.N., Huang, X., Christiansen, L., DeWitt, W.S.*, et al.* (2018). A Single-Cell Atlas of In Vivo Mammalian Chromatin Accessibility. Cell *174*, 1309-1324 e1318.

Davalos, D., Grutzendler, J., Yang, G., Kim, J.V., Zuo, Y., Jung, S., Littman, D.R., Dustin, M.L., and Gan, W.B. (2005). ATP mediates rapid microglial response to local brain injury in vivo. Nature neuroscience *8*, 752-758.

De, S., Van Deren, D., Peden, E., Hockin, M., Boulet, A., Titen, S., and Capecchi, M.R. (2018). Two distinct ontogenies confer heterogeneity to mouse brain microglia. Development *145*.

Deonarain, R., Verma, A., Porter, A.C., Gewert, D.R., Platanias, L.C., and Fish, E.N. (2003). Critical roles for IFN-beta in lymphoid development, myelopoiesis, and tumor development: links to tumor necrosis factor alpha. Proceedings of the National Academy of Sciences of the United States of America *100*, 13453-13458.

Di Martino, A., Fair, D.A., Kelly, C., Satterthwaite, T.D., Castellanos, F.X., Thomason, M.E., Craddock, R.C., Luna, B., Leventhal, B.L., Zuo, X.N., and Milham, M.P. (2014). Unraveling the miswired connectome: a developmental perspective. Neuron *83*, 1335-1353.

Dobin, A., Davis, C.A., Schlesinger, F., Drenkow, J., Zaleski, C., Jha, S., Batut, P., Chaisson, M., and Gingeras, T.R. (2013). STAR: ultrafast universal RNA-seq aligner. Bioinformatics *29*, 15-21.

Doorn, K.J., Moors, T., Drukarch, B., van de Berg, W., Lucassen, P.J., and van Dam, A.M. (2014). Microglial phenotypes and toll-like receptor 2 in the substantia nigra and hippocampus of incidental Lewy body disease cases and Parkinson's disease patients. Acta Neuropathol Commun *2*, 90.

Doruyter, A., Lochner, C., Jordaan, G.P., Stein, D.J., Dupont, P., and Warwick, J.M. (2016). Resting functional connectivity in social anxiety disorder and the effect of pharmacotherapy. Psychiatry Res *251*, 34-44.

Downs, K.M., and Davies, T. (1993). Staging of gastrulating mouse embryos by morphological landmarks in the dissecting microscope. Development *118*, 1255-1266.

Dupret, D., O'Neill, J., and Csicsvari, J. (2013). Dynamic reconfiguration of hippocampal interneuron circuits during spatial learning. Neuron *78*, 166-180.

Durand, C., Robin, C., Bollerot, K., Baron, M.H., Ottersbach, K., and Dzierzak, E. (2007). Embryonic stromal clones reveal developmental regulators of definitive hematopoietic stem cells. Proc Natl Acad Sci U S A *104*, 20838-20843.

Epelman, S., Lavine, K.J., Beaudin, A.E., Sojka, D.K., Carrero, J.A., Calderon, B., Brija, T., Gautier, E.L., Ivanov, S., Satpathy, A.T.*, et al.* (2014a). Embryonic and adult-derived resident cardiac macrophages are maintained through distinct mechanisms at steady state and during inflammation. Immunity *40*, 91-104.

Epelman, S., Lavine, K.J., and Randolph, G.J. (2014b). Origin and functions of tissue macrophages. Immunity *41*, 21-35.

Espin-Palazon, R., Stachura, D.L., Campbell, C.A., Garcia-Moreno, D., Del Cid, N., Kim, A.D., Candel, S., Meseguer, J., Mulero, V., and Traver, D. (2014). Proinflammatory signaling regulates hematopoietic stem cell emergence. Cell *159*, 1070-1085.

Fainaru, O., Woolf, E., Lotem, J., Yarmus, M., Brenner, O., Goldenberg, D., Negreanu, V., Bernstein, Y., Levanon, D., Jung, S., and Groner, Y. (2004). Runx3 regulates mouse TGF-beta-mediated dendritic cell function and its absence results in airway inflammation. The EMBO journal *23*, 969-979.

Fairman, R., Beran-Steed, R.K., Anthony-Cahill, S.J., Lear, J.D., Stafford, W.F., 3rd, DeGrado, W.F., Benfield, P.A., and Brenner, S.L. (1993). Multiple oligomeric states regulate the DNA binding of helix-loop-helix peptides. Proc Natl Acad Sci U S A *90*, 10429-10433.

Ferrando, A.A., Neuberg, D.S., Staunton, J., Loh, M.L., Huard, C., Raimondi, S.C., Behm, F.G., Pui, C.H., Downing, J.R., Gilliland, D.G.*, et al.* (2002). Gene expression signatures define novel oncogenic pathways in T cell acute lymphoblastic leukemia. Cancer Cell *1*, 75-87.

Ferrero, G., Mahony, C.B., Dupuis, E., Yvernogeau, L., Di Ruggiero, E., Miserocchi, M., Caron, M., Robin, C., Traver, D., Bertrand, J.Y., and Wittamer, V. (2018). Embryonic Microglia Derive from Primitive Macrophages and Are Replaced by cmyb-Dependent Definitive Microglia in Zebrafish. Cell reports *24*, 130-141.

Fiering, S.N., Roederer, M., Nolan, G.P., Micklem, D.R., Parks, D.R., and Herzenberg, L.A. (1991). Improved FACS-Gal: flow cytometric analysis and sorting of viable eukaryotic cells expressing reporter gene constructs. Cytometry *12*, 291-301.

Finger, L.R., Kagan, J., Christopher, G., Kurtzberg, J., Hershfield, M.S., Nowell, P.C., and Croce, C.M. (1989). Involvement of the TCL5 gene on human chromosome 1 in T-cell leukemia and melanoma. Proc Natl Acad Sci U S A *86*, 5039-5043.

Frame, J.M., McGrath, K.E., and Palis, J. (2013). Erythro-myeloid progenitors: "definitive" hematopoiesis in the conceptus prior to the emergence of hematopoietic stem cells. Blood cells, molecules & diseases *51*, 220-225.

Friedman, B.A., Srinivasan, K., Ayalon, G., Meilandt, W.J., Lin, H., Huntley, M.A., Cao, Y., Lee, S.-H., Haddick, P.C.G., Ngu, H.*, et al.* (2018). Diverse Brain Myeloid Expression Profiles Reveal Distinct Microglial Activation States and Aspects of Alzheimer's Disease Not Evident in Mouse Models. Cell Reports *22*, 832-847.

Fujiwara, Y., Browne, C.P., Cunniff, K., Goff, S.C., and Orkin, S.H. (1996). Arrested development of embryonic red cell precursors in mouse embryos lacking transcription factor GATA-1. Proceedings of the National Academy of Sciences of the United States of America *93*, 12355-12358.

Fujiwara, Y., Chang, A.N., Williams, A.M., and Orkin, S.H. (2004). Functional overlap of GATA-1 and GATA-2 in primitive hematopoietic development. Blood *103*, 583-585.

Gama-Norton, L., Ferrando, E., Ruiz-Herguido, C., Liu, Z., Guiu, J., Islam, A.B., Lee, S.U., Yan, M., Guidos, C.J., Lopez-Bigas, N.*, et al.* (2015). Notch signal strength controls cell fate in the haemogenic endothelium. Nature communications *6*, 8510.

Ganuza, M., Chabot, A., Tang, X., Bi, W., Natarajan, S., Carter, R., Gawad, C., Kang, G., Cheng, Y., and McKinney-Freeman, S. (2018). Murine hematopoietic stem cell activity is derived from pre-circulation embryos but not yolk sacs. Nature communications *9*, 5405.

Gautier, E.L., Shay, T., Miller, J., Greter, M., Jakubzick, C., Ivanov, S., Helft, J., Chow, A., Elpek, K.G., Gordonov, S.*, et al.* (2012). Gene-expression profiles and transcriptional regulatory pathways that underlie the identity and diversity of mouse tissue macrophages. Nature immunology *13*, 1118-1128.

Ginhoux, F., Greter, M., Leboeuf, M., Nandi, S., See, P., Gokhan, S., Mehler, M.F., Conway, S.J., Ng, L.G., Stanley, E.R.*, et al.* (2010). Fate mapping analysis reveals that adult microglia derive from primitive macrophages. Science *330*, 841-845.

Ginhoux, F., and Guilliams, M. (2016). Tissue-Resident Macrophage Ontogeny and Homeostasis. Immunity *44*, 439-449.

Ginhoux, F., Lim, S., Hoeffel, G., Low, D., and Huber, T. (2013). Origin and differentiation of microglia. Frontiers in cellular neuroscience *7*, 45.

Giroux, S., Kaushik, A.L., Capron, C., Jalil, A., Kelaidi, C., Sablitzky, F., Dumenil, D., Albagli, O., and Godin, I. (2007). lyl-1 and tal-1/scl, two genes encoding closely related bHLH transcription factors, display highly overlapping expression patterns during cardiovascular and hematopoietic ontogeny. Gene expression patterns : GEP *7*, 215-226.

Godin, I., Dieterlen-Lièvre, F., and Cumano, A. (1995). Emergence of multipotent hemopoietic cells in the yolk sac and paraaortic splanchnopleura in mouse embryos, beginning at 8.5 days postcoitus. Proc Natl Acad Sci U S A *92*, 773-777.

Godin, I., Garcia-Porrero, J., Dieterlen-Lièvre, F., and Cumano, A. (1999). Stem cell emergence and hemopoietic activity are incompatible in mouse intraembryonic sites. The Journal of experimental medicine *190*, 43-52.

Goessling, W., North, T.E., Loewer, S., Lord, A.M., Lee, S., Stoick-Cooper, C.L., Weidinger, G., Puder, M., Daley, G.Q., Moon, R.T., and Zon, L.I. (2009). Genetic interaction of PGE2 and Wnt signaling regulates developmental specification of stem cells and regeneration. Cell *136*, 1136-1147.

Goldmann, T., Zeller, N., Raasch, J., Kierdorf, K., Frenzel, K., Ketscher, L., Basters, A., Staszewski, O., Brendecke, S.M., Spiess, A.*, et al.* (2015). USP18 lack in microglia causes destructive interferonopathy of the mouse brain. Embo J *34*, 1612-1629.

Gomez-Nicola, D., Fransen, N.L., Suzzi, S., and Perry, V.H. (2013). Regulation of microglial proliferation during chronic neurodegeneration. The Journal of neuroscience : the official journal of the Society for Neuroscience *33*, 2481-2493.

Gomez Perdiguero, E., and Geissmann, F. (2013). Myb-independent macrophages: a family of cells that develops with their tissue of residence and is involved in its homeostasis. Cold Spring Harbor symposia on quantitative biology *78*, 91-100.

Gomez Perdiguero, E., Klapproth, K., Schulz, C., Busch, K., Azzoni, E., Crozet, L., Garner, H., Trouillet, C., de Bruijn, M.F., Geissmann, F., and Rodewald, H.R. (2015). Tissue-resident macrophages originate from yolk-sac-derived erythro-myeloid progenitors. Nature *518*, 547-551.

Graf, T., and Enver, T. (2009). Forcing cells to change lineages. Nature *462*, 587-594.

Greter, M., Lelios, I., Pelczar, P., Hoeffel, G., Price, J., Leboeuf, M., Kündig, Thomas M., Frei, K., Ginhoux, F., Merad, M., and Becher, B. (2012). Stroma-Derived Interleukin-34 Controls the Development and Maintenance of Langerhans Cells and the Maintenance of Microglia. Immunity *37*, 1050-1060.

Gumusoglu, S.B., Fine, R.S., Murray, S.J., Bittle, J.L., and Stevens, H.E. (2017). The role of IL-6 in neurodevelopment after prenatal stress. Brain, behavior, and immunity *65*, 274-283.

Guo, W., and Wu, H. (2008). Detection of LacZ expression by FACS-Gal analysis. Nauture Protocole exchange.

Gupta, S., Zhu, H., Zon, L.I., and Evans, T. (2006). BMP signaling restricts hemato-vascular development from lateral mesoderm during somitogenesis. Development *133*, 2177-2187.

Hagemeyer, N., Kierdorf, K., Frenzel, K., Xue, J., Ringelhan, M., Abdullah, Z., Godin, I., Wieghofer, P., Costa Jordao, M.J., Ulas, T.*, et al.* (2016). Transcriptome-based profiling of yolk sac-derived macrophages reveals a role for Irf8 in macrophage maturation. The EMBO journal *35*, 1730-1744.

Hammond, T.R., Robinton, D., and Stevens, B. (2018). Microglia and the Brain: Complementary Partners in Development and Disease. Annual review of cell and developmental biology.

Hayashi, Y., Sezaki, M., and Takizawa, H. (2019). Development of the hematopoietic system: Role of inflammatory factors. Wiley interdisciplinary reviews. Developmental biology, e341.

He, Q., Zhang, C., Wang, L., Zhang, P., Ma, D., Lv, J., and Liu, F. (2015). Inflammatory signaling regulates hematopoietic stem and progenitor cell emergence in vertebrates. Blood *125*, 1098-1106.

Herbomel et al, P., Thisse, B., and Thisse, C. (2001). Zebrafish early macrophages colonize cephalic mesenchyme and developing brain, retina, and epidermis through a M-CSF receptor-dependent invasive process. Dev Biol *238*, 274-288.

Herbomel, P., Thisse, B., and Thisse, C. (1999). Ontogeny and behaviour of early macrophages in the zebrafish embryo. Development *126*, 3735-3745.

Hills, D., Gribi, R., Ure, J., Buza-Vidas, N., Luc, S., Jacobsen, S.E., and Medvinsky, A. (2011). Hoxb4-YFP reporter mouse model: a novel tool for tracking HSC development and studying the role of Hoxb4 in hematopoiesis. Blood *117*, 3521-3528.

Hoeffel, G., Chen, J., Lavin, Y., Low, D., Almeida, F.F., See, P., Beaudin, A.E., Lum, J., Low, I., Forsberg, E.C.*, et al.* (2015). C-Myb(+) erythro-myeloid progenitor-derived fetal monocytes give rise to adult tissue-resident

macrophages. Immunity *42*, 665-678.
Hoeffel, G., and Ginhoux, F. (2015). Ontogeny of Tissue-Resident Macrophages. Frontiers in immunology *6*, 486.
Hoeffel, G., and Ginhoux, F. (2018). Fetal monocytes and the origins of tissue-resident macrophages. Cellular immunology *330*, 5-15.
Hofer, T., Busch, K., Klapproth, K., and Rodewald, H.R. (2016). Fate Mapping and Quantitation of Hematopoiesis In Vivo. Annual review of immunology *34*, 449-478.
Hu, Y., and Smyth, G.K. (2009). ELDA: extreme limiting dilution analysis for comparing depleted and enriched populations in stem cell and other assays. Journal of immunological methods *347*, 70-78.
Ichikawa, M., Asai, T., Saito, T., Seo, S., Yamazaki, I., Yamagata, T., Mitani, K., Chiba, S., Ogawa, S., Kurokawa, M., and Hirai, H. (2004). AML-1 is required for megakaryocytic maturation and lymphocytic differentiation, but not for maintenance of hematopoietic stem cells in adult hematopoiesis. Nature medicine *10*, 299-304.
Inlay, M.A., Serwold, T., Mosley, A., Fathman, J.W., Dimov, I.K., Seita, J., and Weissman, I.L. (2014.). Identification of multipotent progenitors that emerge prior to hematopoietic stem cells in embryonic development. Stem cell reports *2*, 457-472.
Jacobson, L.O., Simmons, E.L., Marks, E.K., and Eldrdge, J.H. (1951). Recovery from radiation injury. Science. *113*, 510-511.
Ji, R.P., Phoon, C.K.L., Aristizábal, O., McGrath, K.E., Palis, J., and Turnbull, D.H. (2003). Onset of Cardiac Function During Early Mouse Embryogenesis Coincides With Entry of Primitive Erythroblasts Into the Embryo Proper. Circulation Research *92*, 133-135.
Jung, S., Aliberti, J., Graemmel, P., Sunshine, M.J., Kreutzberg, G.W., Sher, A., and Littman, D.R. (2000). Analysis of fractalkine receptor CX(3)CR1 function by targeted deletion and green fluorescent protein reporter gene insertion. Mol Cell Biol *20*, 4106-4114.
Kaneko-Goto, T., Sato, Y., Katada, S., Kinameri, E., Yoshihara, S.-i., Nishiyori, A., Kimura, M., Fujita, H., Touhara, K., Reed, R.R., and Yoshihara, Y. (2013). Goofy Coordinates the Acuity of Olfactory Signaling. The Journal of Neuroscience *33*, 12987.
Khan, J.A., Mendelson, A., Kunisaki, Y., Birbrair, A., Kou, Y., Arnal-Estape, A., Pinho, S., Ciero, P., Nakahara, F., Ma'ayan, A.*, et al.* (2016). Fetal liver hematopoietic stem cell niches associate with portal vessels. Science *351*, 176-180.
Kierdorf, K., Erny, D., Goldmann, T., Sander, V., Schulz, C., Perdiguero, E.G., Wieghofer, P., Heinrich, A., Riemke, P., Holscher, C.*, et al.* (2013). Microglia emerge from erythromyeloid precursors via Pu.1- and Irf8-dependent pathways. Nature neuroscience *16*, 273-280.
Kieusseian, A., Brunet de la Grange, P., Burlen-Defranoux, O., Godin, I., and Cumano, A. (2012). Immature hematopoietic stem cells undergo maturation in the fetal liver. Development *139*, 3521-3530.
Kim, H.G., de Guzman, C.G., Swindle, C.S., Cotta, C.V., Gartland, L., Scott, E.W., and Klug, C.A. (2004). The ETS family transcription factor PU.1 is necessary for the maintenance of fetal liver hematopoietic stem cells. Blood *104*, 3894-3900.
Kim, I., He, S., Yilmaz, O.H., Kiel, M.J., and Morrison, S.J. (2006). Enhanced purification of fetal liver hematopoietic stem cells using SLAM family receptors. Blood *108*, 737-744.
Kim, I., Yilmaz, O.H., and Morrison, S.J. (2005). CD144 (VE-cadherin) is transiently expressed by fetal liver hematopoietic stem cells. Blood *106*, 903-905.
Kim, P.G., Canver, M.C., Rhee, C., Ross, S.J., Harriss, J.V., Tu, H.C., Orkin, S.H., Tucker, H.O., and Daley, G.Q. (2016). Interferon-alpha signaling promotes embryonic HSC maturation. Blood *128*, 204-216.
Kingsley, P.D., Malik, J., Fantauzzo, K.A., and Palis, J. (2004). Yolk sac-derived primitive erythroblasts enucleate during mammalian embryogenesis. Blood *104*, 19-25.
Kobayakawa, K., Kobayakawa, R., Matsumoto, H., Oka, Y., Imai, T., Ikawa, M., Okabe, M., Ikeda, T., Itohara, S.,

Kikusui, T*., et al.* (2007). Innate versus learned odour processing in the mouse olfactory bulb. Nature *450*, 503-508.

Kodama, Y., and Sano, H. (2006). Evolution of a basic helix-loop-helix protein from a transcriptional repressor to a plastid-resident regulatory factor: involvement in hypersensitive cell death in tobacco plants. The Journal of biological chemistry *281*, 35369-35380.

Kumano, K., Chiba, S., Kunisato, A., Sata, M., Saito, T., Nakagami-Yamaguchi, E., Yamaguchi, T., Masuda, S., Shimizu, K., Takahashi, T*., et al.* (2003). Notch1 but not Notch2 is essential for generating hematopoietic stem cells from endothelial cells. Immunity *18*, 699-711.

Kumaravelu, P., Hook, L., Morrison, A.M., Ure, J., Zhao, S., Zuyev, S., Ansell, J., and Medvinsky, A. (2002). Quantitative developmental anatomy of definitive haematopoietic stem cells/long-term repopulating units (HSC/RUs): role of the aorta-gonad-mesonephros (AGM) region and the yolk sac in colonisation of the mouse embryonic liver. Development *129*, 4891-4899.

Kurotaki, D., Sasaki, H., and Tamura, T. (2017). Transcriptional control of monocyte and macrophage development. International immunology *29*, 97-107.

Laurenti, E., and Gottgens, B. (2018). From haematopoietic stem cells to complex differentiation landscapes. Nature *553*, 418-426.

Lavin, Y., Winter, D., Blecher-Gonen, R., David, E., Keren-Shaul, H., Merad, M., Jung, S., and Amit, I. (2014). Tissue-resident macrophage enhancer landscapes are shaped by the local microenvironment. Cell *159*, 1312-1326.

Law, C.W., Chen, Y., Shi, W., and Smyth, G.K. (2014). voom: Precision weights unlock linear model analysis tools for RNA-seq read counts. Genome Biol *15*, R29.

Lee, L.K., Ghorbanian, Y., Wang, W., Wang, Y., Kim, Y.J., Weissman, I.L., Inlay, M.A., and Mikkola, H.K.A. (2016). LYVE1 Marks the Divergence of Yolk Sac Definitive Hemogenic Endothelium from the Primitive Erythroid Lineage. Cell reports *17*, 2286-2298.

Lein, E.S., Hawrylycz, M.J., Ao, N., Ayres, M., Bensinger, A., Bernard, A., Boe, A.F., Boguski, M.S., Brockway, K.S., Byrnes, E.J*., et al.* (2007). Genome-wide atlas of gene expression in the adult mouse brain. Nature *445*, 168-176.

Li, T., Pang, S., Yu, Y., Wu, X., Guo, J., and Zhang, S. (2013). Proliferation of parenchymal microglia is the main source of microgliosis after ischaemic stroke. Brain : a journal of neurology *136*, 3578-3588.

Li, Y., Esain, V., Teng, L., Xu, J., Kwan, W., Frost, I.M., Yzaguirre, A.D., Cai, X., Cortes, M., Maijenburg, M.W*., et al.* (2014). Inflammatory signaling regulates embryonic hematopoietic stem and progenitor cell production. Genes & development *28*, 2597-2612.

Lim, M., Brown, H.M., Kind, K.L., Thompson, J.G., and Dunning, K.R. (2019). Hemoglobin: potential roles in the oocyte and early embryo. Biology of reproduction.

Liu, L., Zeng, M., and Stamler, J.S. (1999). Hemoglobin induction in mouse macrophages. Proceedings of the National Academy of Sciences of the United States of America *96*, 6643-6647.

Luis, T.C., Tremblay, C.S., Manz, M.G., North, T.E., King, K.Y., and Challen, G.A. (2016). Inflammatory signals in HSPC development and homeostasis: Too much of a good thing? Experimental hematology *44*, 908-912.

Lukov, G.L., Rossi, L., Souroullas, G.P., Mao, R., and Goodell, M.A. (2011). The expansion of T-cells and hematopoietic progenitors as a result of overexpression of the lymphoblastic leukemia gene, Lyl1 can support leukemia formation. Leukemia research *35*, 405-412.

Maeno, M., Mead, P.E., Kelley, C., Xu, R.H., Kung, H.F., Suzuki, A., Ueno, N., and Zon, L.I. (1996). The role of BMP-4 and GATA-2 in the induction and differentiation of hematopoietic mesoderm in Xenopus laevis. Blood *88*, 1965-1972.

Manaia, A., Lemarchandel, V., Klaine, M., Max-Audit, I., Romeo, P., Dieterlen-Lievre, F., and Godin, I. (2000). Lmo2 and GATA-3 associated expression in intraembryonic hemogenic sites. Development *127*, 643-653.

Marshall, C.J., Kinnon, C., and Thrasher, A.J. (2000). Polarized expression of bone morphogenetic protein-4 in the human aorta-gonad-mesonephros region. Blood. *96*, 3.

Mass, E., Ballesteros, I., Farlik, M., Halbritter, F., Gunther, P., Crozet, L., Jacome-Galarza, C.E., Handler, K., Klughammer, J., Kobayashi, Y.*, et al.* (2016). Specification of tissue-resident macrophages during organogenesis. Science *353*.

Mass, E., Jacome-Galarza, C.E., Blank, T., Lazarov, T., Durham, B.H., Ozkaya, N., Pastore, A., Schwabenland, M., Chung, Y.R., Rosenblum, M.K.*, et al.* (2017). A somatic mutation in erythro-myeloid progenitors causes neurodegenerative disease. Nature *549*, 389-393.

Matcovitch-Natan, O., Winter, D.R., Giladi, A., Vargas Aguilar, S., Spinrad, A., Sarrazin, S., Ben-Yehuda, H., David, E., Zelada Gonzalez, F., Perrin, P.*, et al.* (2016). Microglia development follows a stepwise program to regulate brain homeostasis. Science *353*, aad8670.

McCallum, A.P., Gallek, M.J., Ramey, W., Manziello, A., Witte, M.H., Bernas, M.J., Labiner, D.M., and Weinand, M.E. (2016). Cortical gene expression correlates of temporal lobe epileptogenicity. Pathophysiology *23*, 181-190.

McCormack, M.P., Shields, B.J., Jackson, J.T., Nasa, C., Shi, W., Slater, N.J., Tremblay, C.S., Rabbitts, T.H., and Curtis, D.J. (2013). Requirement for Lyl1 in a model of Lmo2-driven early T-cell precursor ALL. Blood *122*, 2093-2103.

McGrath, K.E., Frame, J.M., Fegan, K.H., Bowen, J.R., Conway, S.J., Catherman, S.C., Kingsley, P.D., Koniski, A.D., and Palis, J. (2015a). Distinct Sources of Hematopoietic Progenitors Emerge before HSCs and Provide Functional Blood Cells in the Mammalian Embryo. Cell reports *11*, 1892-1904.

McGrath, K.E., Frame, J.M., and Palis, J. (2015b). Early hematopoiesis and macrophage development. Seminars in immunology *27*, 379-387.

McGrath, K.E., Koniski, A.D., Malik, J., and Palis, J. (2003). Circulation is established in a stepwise pattern in the mammalian embryo. Blood *101*, 1669-1676.

McGrath, K.E., and Palis, J. (2005). Hematopoiesis in the yolk sac: more than meets the eye. Experimental hematology *33*, 1021-1028.

McKinney-Freeman, S., Cahan, P., Li, H., Lacadie, S.A., Huang, H.T., Curran, M., Loewer, S., Naveiras, O., Kathrein, K.L., Konantz, M.*, et al.* (2012). The transcriptional landscape of hematopoietic stem cell ontogeny. Cell stem cell *11*, 701-714.

McKinney-Freeman, S.L., Naveiras, O., Yates, F., Loewer, S., Philitas, M., Curran, M., Park, P.J., and Daley, G.Q. (2009). Surface antigen phenotypes of hematopoietic stem cells from embryos and murine embryonic stem cells. Blood *114*, 268-278.

McLellan, M.A., Rosenthal, N.A., and Pinto, A.R. (2017). Cre-loxP-Mediated Recombination: General Principles and Experimental Considerations. Current protocols in mouse biology *7*, 1-12.

Mechling, A.E., Arefin, T., Lee, H.L., Bienert, T., Reisert, M., Ben Hamida, S., Darcq, E., Ehrlich, A., Gaveriaux-Ruff, C., Parent, M.J.*, et al.* (2016). Deletion of the mu opioid receptor gene in mice reshapes the reward-aversion connectome. Proc Natl Acad Sci U S A *113*, 11603-11608.

Mellentin, J.D., Smith, S.D., and Cleary, M.L. (1989). lyl-1, a novel gene altered by chromosomal translocation in T cell leukemia, codes for a protein with a helix-loop-helix DNA binding motif. Cell *58*, 77-83.

Meng, Y.S., Khoury, H., Dick, J.E., and Minden, M.D. (2005). Oncogenic potential of the transcription factor LYL1 in acute myeloblastic leukemia. Leukemia *19*, 1941-1947.

Merad, M., Manz, M.G., Karsunky, H., Wagers, A., Peters, W., Charo, I., Weissman, I.L., Cyster, J.G., and Engleman, E.G. (2002). Langerhans cells renew in the skin throughout life under steady-state conditions. Nature immunology *3*, 1135-1141.

Mikkola, H.K., Klintman, J., Yang, H., Hock, H., Schlaeger, T.M., Fujiwara, Y., and Orkin, S.H. (2003).

Haematopoietic stem cells retain long-term repopulating activity and multipotency in the absence of stem-cell leukaemia SCL/tal-1 gene. Nature *421*, 547-551.

Mildner, A., Schmidt, H., Nitsche, M., Merkler, D., Hanisch, U.K., Mack, M., Heikenwalder, M., Bruck, W., Priller, J., and Prinz, M. (2007). Microglia in the adult brain arise from Ly-6ChiCCR2+ monocytes only under defined host conditions. Nat Neurosci *10*, 1544-1553.

Minegishi, N., Ohta, J., Yamagiwa, H., Suzuki, N., Kawauchi, S., Zhou, Y., Takahashi, S., Hayashi, N., Engel, J.D., and Yamamoto, M. (1999). The mouse GATA-2 gene is expressed in the para-aortic splanchnopleura and aorta-gonads and mesonephros region. Blood *93*, 4196-4207.

Mitchell RA, M.C., Peng T, Bucala R. (1999). Sustained mitogen-activated protein kinase (MAPK) and cytoplasmic phospholipase A2 activation by macrophage migration inhibitory factor (MIF). Regulatory role in cell proliferation and glucocorticoid action. J Biol Chem. *274*, 18100-18106.

Miyoshi, H., Shimizu, K., Kozu, T., Maseki, N., Kaneko, Y., and Ohki, M. (1991). t(8;21) breakpoints on chromosome 21 in acute myeloid leukemia are clustered within a limited region of a single gene, AML1. Proc Natl Acad Sci U S A *88*, 10431-10434.

Monteiro, R., Pinheiro, P., Joseph, N., Peterkin, T., Koth, J., Repapi, E., Bonkhofer, F., Kirmizitas, A., and Patient, R. (2016). Transforming Growth Factor beta Drives Hemogenic Endothelium Programming and the Transition to Hematopoietic Stem Cells. Developmental cell *38*, 358-370.

Monteiro, R., Pouget, C., and Patient, R. (2011). The gata1/pu.1 lineage fate paradigm varies between blood populations and is modulated by tif1gamma. The EMBO journal *30*, 1093-1103.

Morrison, A.S., and Heimberg, R.G. (2013). Social anxiety and social anxiety disorder. Annu Rev Clin Psychol *9*, 249-274.

Morrison, S.J., Hemmati, H.D., Wandycz, A.M., and Weissman, I.L. (1995). The purification and characterization of fetal liver hematopoietic stem cells. Proc Natl Acad Sci U S A *92*, 10302-10306.

Mucenski, M.L., McLain, K., Kier, A.B., Swerdlow, S.H., Schreiner, C.M., Miller, T.A., Pietryga, D.W., Scott, W.J.J., and Potter, S.S. (1991). A functional c-myb gene is required for normal murine fetal hepatic hematopoiesis. Cell *65*, 677-689.

Muhlethaler-Mottet, A., Di Berardino, W., Otten, L.A., and Mach, B. (1998). Activation of the MHC class II transactivator CIITA by interferon-gamma requires cooperative interaction between Stat1 and USF-1. Immunity *8*, 157-166.

Murphy, S.P., Tayade, C., Ashkar, A.A., Hatta, K., Zhang, J., and Croy, B.A. (2009). Interferon gamma in successful pregnancies. Biology of reproduction *80*, 848-859.

Nei, Y., Obata-Ninomiya, K., Tsutsui, H., Ishiwata, K., Miyasaka, M., Matsumoto, K., Nakae, S., Kanuka, H., Inase, N., and Karasuyama, H. (2013). GATA-1 regulates the generation and function of basophils. Proc Natl Acad Sci U S A *110*, 18620-18625.

Nimmerjahn, A., Kirchhoff, F., and Helmchen, F. (2005). Resting microglial cells are highly dynamic surveillants of brain parenchyma in vivo. Science *308*, 1314-1318.

Noble, D. (2015). Conrad Waddington and the origin of epigenetics. The Journal of experimental biology *218*, 816-818.

Nottingham, W.T., Jarratt, A., Burgess, M., Speck, C.L., Cheng, J.F., Prabhakar, S., Rubin, E.M., Li, P.S., Sloane-Stanley, J., Kong-A-San, J., and De Bruijn, M.F. (2007). Runx1-mediated hematopoietic stem-cell emergence is controlled by a Gata/Ets/SCL-regulated enhancer. Blood. *110*, 4188-4197.

Okuda, T., Van Deursen, J., Hiebert, S.W., Grosveld, G., and Downing, J.R. (1996). AML1, the target of multiple chromosomal translocations in human leukemia, is essential for normal fetal liver hematopoiesis. Cell. *84*, 321-330.

Orelio, C., Haak, E., Peeters, M., and Dzierzak, E. (2008). Interleukin-1-mediated hematopoietic cell regulation in

the aorta-gonad-mesonephros region of the mouse embryo. Blood *112*, 4895-4904.
Orelio, C., Harvey, K.N., Miles, C., Oostendorp, R.A., van der Horn, K., and Dzierzak, E. (2004). The role of apoptosis in the development of AGM hematopoietic stem cells revealed by Bcl-2 overexpression. Blood *103*, 4084-4092.
Orlic, D., Anderson, S., Biesecker, L.G., Sorrentino, B.P., and Bodine, D.M. (1995). Pluripotent hematopoietic stem cells contain high levels of mRNA for c-kit, GATA-2, p45 NF-E2, and c-myb and low levels or no mRNA for c-fms and the receptors for granulocyte colony-stimulating factor and interleukins 5 and 7. Proc Natl Acad Sci U S A *92*, 4601-4605.
Palis, J. (2016). Hematopoietic stem cell-independent hematopoiesis: emergence of erythroid, megakaryocyte, and myeloid potential in the mammalian embryo. FEBS letters *590*, 3965-3974.
Palis, J., Chan, R.J., Koniski, A., Patel, R., Starr, M., and Yoder, M.C. (2001). Spatial and temporal emergence of high proliferative potential hematopoietic precursors during murine embryogenesis. Proceedings of the National Academy of Sciences of the United States of America *98*, 4528-4533.
Palis, J., Robertson, S., Kennedy, M., Wall, C., and Keller, G. (1999). Development of erythroid and myeloid progenitors in the yolk sac and embryo proper of the mouse. Development. *126*, 5073-5084.
Paolicelli, R.C., Bolasco, G., Pagani, F., Maggi, L., Scianni, M., Panzanelli, P., Giustetto, M., Ferreira, T.A., Guiducci, E., Dumas, L*., et al.* (2011). Synaptic pruning by microglia is necessary for normal brain development. Science *333*, 1456-1458.
Patro, R., Duggal, G., Love, M.I., Irizarry, R.A., and Kingsford, C. (2017). Salmon provides fast and bias-aware quantification of transcript expression. Nature methods *14*, 417-419.
Phipson, B., Lee, S., Majewski, I.J., Alexander, W.S., and Smyth, G.K. (2016). Robust Hyperparameter Estimation Protects Against Hypervariable Genes And Improves Power To Detect Differential Expression. Ann Appl Stat *10*, 946-963.
Pietras, E.M., Warr, M.R., and Passegue, E. (2011). Cell cycle regulation in hematopoietic stem cells. The Journal of cell biology *195*, 709-720.
Pimanda, J.E., Donaldson, I.J., de Bruijn, M.F., Kinston, S., Knezevic, K., Huckle, L., Piltz, S., Landry, J.R., Green, A.R., Tannahill, D., and Gottgens, B. (2007a). The SCL transcriptional network and BMP signaling pathway interact to regulate RUNX1 activity. Proc Natl Acad Sci U S A *104*, 840-845.
Pimanda, J.E., Ottersbach, K., Knezevic, K., Kinston, S., Chan, W.Y., Wilson, N.K., Landry, J.R., Wood, A.D., Kolb-Kokocinski, A., Green, A.R*., et al.* (2007b). Gata2, Fli1, and Scl form a recursively wired gene-regulatory circuit during early hematopoietic development. Proc Natl Acad Sci U S A *104*, 17692-17697.
Pina, C., and Enver, T. (2007). Differential contributions of haematopoietic stem cells to foetal and adult haematopoiesis: insights from functional analysis of transcriptional regulators. Oncogene *26*, 6750-6765.
Pirot, N., Deleuze, V., El-Hajj, R., Dohet, C., Sablitzky, F., Couttet, P., Mathieu, D., and Pinet, V. (2010). LYL1 activity is required for the maturation of newly formed blood vessels in adulthood. Blood *115*, 5270-5279.
Pirot, N., Delpech, H., Deleuze, V., Dohet, C., Courtade-Saidi, M., Basset-Leobon, C., Chalhoub, E., Mathieu, D., and Pinet, V. (2014). Lung endothelial barrier disruption in Lyl1-deficient mice. American journal of physiology. Lung cellular and molecular physiology *306*, L775-785.
Pont-Lezica, L., Bechade, C., Belarif-Cantaut, Y., Pascual, O., and Bessis, A. (2011). Physiological roles of microglia during development. Journal of neurochemistry *119*, 901-908.
Porcher, C., Chagraoui, H., and Kristiansen, M.S. (2017). SCL/TAL1: a multifaceted regulator from blood development to disease. Blood *129*, 2051-2060.
Porcher, C., Swat, W., Rockwell, K., Fujiwara, Y., Alt, F.W., and Orkin, S.H. (1996). The T cell leukemia oncoprotein SCL/tal-1 is essential for development of all hematopoietic lineages. Cell *86*, 47-57.
Porsolt, R.D., Le Pichon, M., and Jalfre, M. (1977). Depression: a new animal model sensitive to antidepressant

treatments. Nature *266*, 730-732.
Prinz, M., and Priller, J. (2014). Microglia and brain macrophages in the molecular age: from origin to neuropsychiatric disease. Nature reviews. Neuroscience *15*, 300-312.
Pui, C.H., Relling, M.V., and Downing, J.R. (2004). Acute lymphoblastic leukemia. N Engl J Med *350*, 1535-1548.
Reemst, K., Noctor, S.C., Lucassen, P.J., and Hol, E.M. (2016). The Indispensable Roles of Microglia and Astrocytes during Brain Development. Frontiers in human neuroscience *10*, 566.
Reich, D., Price, A.L., and Patterson, N. (2008). Principal component analysis of genetic data. Nat Genet *40*, 491-492.
Richter, J., Traver, D., and Willert, K. (2017). The role of Wnt signaling in hematopoietic stem cell development. Critical reviews in biochemistry and molecular biology *52*, 414-424.
Ritchie, M.E., Phipson, B., Wu, D., Hu, Y., Law, C.W., Shi, W., and Smyth, G.K. (2015). limma powers differential expression analyses for RNA-sequencing and microarray studies. Nucleic Acids Res *43*, e47.
Robb, L., Lyons, I., Li, R., Hartley, L., Kontgen, F., Harvey, R.P., Metcalf, D., and Begley, C.G. (1995). Absence of yolk sac hematopoiesis from mice with a targeted disruption of the scl gene. Proceedings of the National Academy of Sciences of the United States of America *92*, 7075-7079.
Robert-Moreno, A., Guiu, J., Ruiz-Herguido, C., Lopez, M.E., Ingles-Esteve, J., Riera, L., Tipping, A., Enver, T., Dzierzak, E., Gridley, T*., et al.* (2008). Impaired embryonic haematopoiesis yet normal arterial development in the absence of the Notch ligand Jagged1. EMBO J *27*, 1886-1895.
Robin, C., and Durand, C. (2010). The roles of BMP and IL-3 signaling pathways in the control of hematopoietic stem cells in the mouse embryo. The International journal of developmental biology *54*, 1189-1200.
Robin, C., Ottersbach, K., Durand, C., Peeters, M., Vanes, L., Tybulewicz, V., and Dzierzak, E. (2006). An unexpected role for IL-3 in the embryonic development of hematopoietic stem cells. Developmental cell *11*, 171-180.
Robinson, O.J., Krimsky, M., Lieberman, L., Allen, P., Vytal, K., and Grillon, C. (2014). Towards a mechanistic understanding of pathological anxiety: the dorsal medial prefrontal-amygdala 'aversive amplification' circuit in unmedicated generalized and social anxiety disorders. Lancet Psychiatry *1*, 294-302.
Rubin, R.D., Watson, P.D., Duff, M.C., and Cohen, N.J. (2014). The role of the hippocampus in flexible cognition and social behavior. Front Hum Neurosci *8*, 742.
Ruiz-Herguido, C., Guiu, J., D'Altri, T., Ingles-Esteve, J., Dzierzak, E., Espinosa, L., and Bigas, A. (2012). Hematopoietic stem cell development requires transient Wnt/beta-catenin activity. The Journal of experimental medicine *209*, 1457-1468.
Rybtsov, S., Batsivari, A., Bilotkach, K., Paruzina, D., Senserrich, J., Nerushev, O., and Medvinsky, A. (2014). Tracing the origin of the HSC hierarchy reveals an SCF-dependent, IL-3-independent CD43(-) embryonic precursor. Stem cell reports *3*, 489-501.
Rybtsov, S., Sobiesiak, M., Taoudi, S., Souilhol, C., Senserrich, J., Liakhovitskaia, A., Ivanovs, A., Frampton, J., Zhao, S., and Medvinsky, A. (2011). Hierarchical organization and early hematopoietic specification of the developing HSC lineage in the AGM region. The Journal of experimental medicine *208*, 1305-1315.
Salter, M.W., and Stevens, B. (2017). Microglia emerge as central players in brain disease. Nat Med *23*, 1018-1027.
Sawamiphak, S., Kontarakis, Z., and Stainier, D.Y. (2014). Interferon gamma signaling positively regulates hematopoietic stem cell emergence. Developmental cell *31*, 640-653.
Schuetze, M., Rohr, C.S., Dewey, D., McCrimmon, A., and Bray, S. (2017). Reinforcement Learning in Autism Spectrum Disorder. Front Psychol *8*, 2035.
Schulz, C., Gomez Perdiguero, E., Chorro, L., Szabo-Rogers, H., Cagnard, N., Kierdorf, K., Prinz, M., Wu, B., Jacobsen, S.E., Pollard, J.W*., et al.* (2012). A lineage of myeloid cells independent of Myb and hematopoietic

stem cells. Science *336*, 86-90.

Scialdone, A., Tanaka, Y., Jawaid, W., Moignard, V., Wilson, N.K., Macaulay, I.C., Marioni, J.C., and Gottgens, B. (2016). Resolving early mesoderm diversification through single-cell expression profiling. Nature *535*, 289-293.

Senserrich, J., Batsivari, A., Rybtsov, S., Gordon-Keylock, S., Souilhol, C., Buchholz, F., Hills, D., Zhao, S., and Medvinsky, A. (2018). Analysis of Runx1 Using Induced Gene Ablation Reveals Its Essential Role in Pre-liver HSC Development and Limitations of an In Vivo Approach. Stem cell reports *11*, 784-794.

Shemer, A., Grozovski, J., Tay, T.L., Tao, J., Volaski, A., Suss, P., Ardura-Fabregat, A., Gross-Vered, M., Kim, J.S., David, E.*, et al.* (2018). Engrafted parenchymal brain macrophages differ from microglia in transcriptome, chromatin landscape and response to challenge. Nature communications *9*, 5206.

Sheng, J., Ruedl, C., and Karjalainen, K. (2015). Most Tissue-Resident Macrophages Except Microglia Are Derived from Fetal Hematopoietic Stem Cells. Immunity *43*, 382-393.

Shields, B.J., Slape, C.I., Vo, N., Jackson, J.T., Pliego-Zamora, A., Ranasinghe, H., Shi, W., Curtis, D.J., and McCormack, M.P. (2019). The NUP98-HOXD13 fusion oncogene induces thymocyte self-renewal via Lmo2/Lyl1. Leukemia.

Shivdasani, R.A., Mayer, E.L., and Orkin, S.H. (1995). Absence of blood formation in mice lacking the T-cell leukaemia oncoprotein tal-1/SCL. Nature *373*, 432-434.

Sieweke, M.H., and Allen, J.E. (2013). Beyond stem cells: self-renewal of differentiated macrophages. Science *342*, 1242974.

Silver, L., and Palis, J. (1997). Initiation of murine embryonic erythropoiesis: a spatial analysis. Blood *89*, 1154-1164.

Sirota, A., Montgomery, S., Fujisawa, S., Isomura, Y., Zugaro, M., and Buzsaki, G. (2008). Entrainment of neocortical neurons and gamma oscillations by the hippocampal theta rhythm. Neuron *60*, 683-697.

Solaimani Kartalaei, P., Yamada-Inagawa, T., Vink, C.S., de Pater, E., van der Linden, R., Marks-Bluth, J., van der Sloot, A., van den Hout, M., Yokomizo, T., van Schaick-Solerno, M.L.*, et al.* (2015). Whole-transcriptome analysis of endothelial to hematopoietic stem cell transition reveals a requirement for Gpr56 in HSC generation. The Journal of experimental medicine *212*, 93-106.

Soucie, E.L., Weng, Z., Geirsdottir, L., Molawi, K., Maurizio, J., Fenouil, R., Mossadegh-Keller, N., Gimenez, G., VanHille, L., Beniazza, M.*, et al.* (2016). Lineage-specific enhancers activate self-renewal genes in macrophages and embryonic stem cells. Science *351*, aad5510.

Souilhol, C., Lendinez, J.G., Rybtsov, S., Murphy, F., Wilson, H., Hills, D., Batsivari, A., Binagui-Casas, A., McGarvey, A.C., MacDonald, H.R.*, et al.* (2016). Developing HSCs become Notch independent by the end of maturation in the AGM region. Blood *128*, 1567-1577.

Souroullas, G.P., and Goodell, M.A. (2011). A new allele of Lyl1 confirms its important role in hematopoietic stem cell function. Genesis *49*, 441-448.

Souroullas, G.P., Salmon, J.M., Sablitzky, F., Curtis, D.J., and Goodell, M.A. (2009). Adult hematopoietic stem and progenitor cells require either Lyl1 or Scl for survival. Cell stem cell *4*, 180-186.

Spangrude, G.J., Heimfeld, S., and Weissman, I.L. (1988). Purification and characterization of mouse hematopoietic stem cells. Science *241*, 58-62.

Stence, N., Waite, M., and Dailey, M.E. (2001). Dynamics of microglial activation: a confocal time-lapse analysis in hippocampal slices. Glia *33*, 256-266.

Sternberg, N., and Hamilton, D. (1981). Bacteriophage P1 site-specific recombination. I. Recombination between loxP sites. Journal of molecular biology *150*, 467-486.

Straub, A.C., Lohman, A.W., Billaud, M., Johnstone, S.R., Dwyer, S.T., Lee, M.Y., Bortz, P.S., Best, A.K., Columbus, L., Gaston, B., and Isakson, B.E. (2012). Endothelial cell expression of haemoglobin alpha regulates nitric oxide signalling. Nature *491*, 473-477.

Subramanian, A., Tamayo, P., Mootha, V.K., Mukherjee, S., Ebert, B.L., Gillette, M.A., Paulovich, A., Pomeroy, S.L., Golub, T.R., Lander, E.S., and Mesirov, J.P. (2005). Gene set enrichment analysis: a knowledge-based approach for interpreting genome-wide expression profiles. Proceedings of the National Academy of Sciences of the United States of America *102*, 15545-15550.

Sullivan, R.M., Wilson, D.A., Ravel, N., and Mouly, A.M. (2015). Olfactory memory networks: from emotional learning to social behaviors. Frontiers in behavioral neuroscience *9*, 36.

Sun, Y., Wang, Y., Li, J.H., Zhu, S.H., Tang, H.T., and Xia, Z.F. (2013). Macrophage migration inhibitory factor counter-regulates dexamethasone-induced annexin 1 expression and influences the release of eicosanoids in murine macrophages. Immunology *140*, 250-258.

Taoudi, S., and Medvinsky, A. (2007). Functional identification of the hematopoietic stem cell niche in the ventral domain of the embryonic dorsal aorta. Proc Natl Acad Sci U S A *104*, 9399-9403.

Thomas, D.M., Francescutti-Verbeem, D.M., and Kuhn, D.M. (2006). Gene expression profile of activated microglia under conditions associated with dopamine neuronal damage. Faseb J *20*, 515-517.

Tober, J., Koniski, A., McGrath, K.E., Vemishetti, R., Emerson, R., de Mesy-Bentley, K.K., Waugh, R., and Palis, J. (2007). The megakaryocyte lineage originates from hemangioblast precursors and is an integral component both of primitive and of definitive hematopoiesis. Blood *109*, 1433-1441.

Tober, J., McGrath, K.E., and Palis, J. (2008). Primitive erythropoiesis and megakaryopoiesis in the yolk sac are independent of c-myb. Blood *111*, 2636-2639.

Travnickova, J., Tran Chau, V., Julien, E., Mateos-Langerak, J., Gonzalez, C., Lelievre, E., Lutfalla, G., Tavian, M., and Kissa, K. (2015). Primitive macrophages control HSPC mobilization and definitive haematopoiesis. Nature communications *6*, 6227.

Tsai, F.Y., Keller, G., Kuo, F.C., Weiss, M., Chen, J., Rosenblatt, M., Alt, F.W., and Orkin, S.H. (1994). An early haematopoietic defect in mice lacking the transcription factor GATA-2. Nature *371*, 221-226.

Ueno, M., Fujita, Y., Tanaka, T., Nakamura, Y., Kikuta, J., Ishii, M., and Yamashita, T. (2013). Layer V cortical neurons require microglial support for survival during postnatal development. Nat Neurosci *16*, 543-551.

van de Laar, L., Saelens, W., De Prijck, S., Martens, L., Scott, C.L., Van Isterdael, G., Hoffmann, E., Beyaert, R., Saeys, Y., Lambrecht, B.N., and Guilliams, M. (2016). Yolk Sac Macrophages, Fetal Liver, and Adult Monocytes Can Colonize an Empty Niche and Develop into Functional Tissue-Resident Macrophages. Immunity *44*, 755-768.

van Furth, R., Cohn, Z.A., Hirsch, J.G., Humphrey, J.H., Spector, W.G., and Langevoort, H.L. (1972). The mononuclear phagocyte system: a new classification of macrophages, monocytes, and their precursor cells. Bulletin of the World Health Organization *46*, 845-852.

Vinck, M., Lima, B., Womelsdorf, T., Oostenveld, R., Singer, W., Neuenschwander, S., and Fries, P. (2010). Gamma-phase shifting in awake monkey visual cortex. J Neurosci *30*, 1250-1257.

Visvader, J., Begley, C.G., and Adams, J.M. (1991). Differential expression of the LYL, SCL and E2A helix-loop-helix genes within the hemopoietic system. Oncogene *6*, 187-194.

Vo, L.T., Kinney, M.A., Liu, X., Zhang, Y., Barragan, J., Sousa, P.M., Jha, D.K., Han, A., Cesana, M., Shao, Z.*, et al.* (2018). Regulation of embryonic haematopoietic multipotency by EZH1. Nature *553*, 506-510.

Vyas, P., Ault, K., Jackson, C.W., Orkin, S.H., and Shivdasani, R.A. (1999). Consequences of GATA-1 deficiency in megakaryocytes and platelets. Blood *93*, 2867-2875.

Wadman, I.A., Osada, H., Grütz, G.G., Agulnick, A.D., Westphal, H., Forster, A., and Rabbitts, T.H. (1997). The LIM-only protein Lmo2 is a bridging molecule assembling an erythroid, DNA-binding complex which includes the TAL1, E47, GATA-1 and Ldb1/NLI proteins. EMBO J *16*, 3145-3157.

Wang, Y., Szretter, K.J., Vermi, W., Gilfillan, S., Rossini, C., Cella, M., Barrow, A.D., Diamond, M.S., and Colonna, M. (2012). IL-34 is a tissue-restricted ligand of CSF1R required for the development of Langerhans cells and

microglia. Nature immunology *13*, 753-760.
Warren, A.J., Colledge, W.H., Carlton, M.B., Evans, M.J., Smith, A.J., and Rabbitts, T.H. (1994). The oncogenic cysteine-rich LIM domain protein rbtn2 is essential for erythroid development. Cell *78*, 45-57.
Wehrspaun, C.C., Haerty, W., and Ponting, C.P. (2015). Microglia recapitulate a hematopoietic master regulator network in¬†the aging human frontal cortex. Neurobiology of Aging *36*, 2443.e2449-2443.e2420.
Wilkinson, R.N., Pouget, C., Gering, M., Russell, A.J., Davies, S.G., Kimelman, D., and Patient, R. (2009). Hedgehog and Bmp polarize hematopoietic stem cell emergence in the zebrafish dorsal aorta. Developmental cell *16*, 909-916.
Wilson, N.K., Calero-Nieto, F.J., Ferreira, R., and Gottgens, B. (2011). Transcriptional regulation of haematopoietic transcription factors. Stem cell research & therapy *2*, 6.
Wilson, N.K., Foster, S.D., Wang, X., Knezevic, K., Schutte, J., Kaimakis, P., Chilarska, P.M., Kinston, S., Ouwehand, W.H., Dzierzak, E.*, et al.* (2010). Combinatorial transcriptional control in blood stem/progenitor cells: genome-wide analysis of ten major transcriptional regulators. Cell stem cell *7*, 532-544.
Wilson, N.K., Miranda-Saavedra, D., Kinston, S., Bonadies, N., Foster, S.D., Calero-Nieto, F., Dawson, M.A., Donaldson, I.J., Dumon, S., Frampton, J.*, et al.* (2009). The transcriptional program controlled by the stem cell leukemia gene Scl/Tal1 during early embryonic hematopoietic development. Blood *113*, 5456-5465.
Wynn, T.A., Chawla, A., and Pollard, J.W. (2013). Macrophage biology in development, homeostasis and disease. Nature *496*, 445-455.
Xu, J., Zhu, L., He, S., Wu, Y., Jin, W., Yu, T., Qu, J.Y., and Wen, Z. (2015). Temporal-Spatial Resolution Fate Mapping Reveals Distinct Origins for Embryonic and Adult Microglia in Zebrafish. Developmental cell *34*, 632-641.
Yamada, Y., Warren, A.J., Dobson, C., Forster, A., Pannell, R., and Rabbitts, T.H. (1988). The T cell leukemia LIM protein Lmo2 is necessary for adult mouse hematopoiesis. Proc Natl Acad Sci *95*, 3890-3895.
Yoder, M.C. (2014). Inducing definitive hematopoiesis in a dish. Nature biotechnology *32*, 539-541.
Yokomizo, T., and Dzierzak, E. (2010). Three-dimensional cartography of hematopoietic clusters in the vasculature of whole mouse embryos. Development *137*, 3651-3661.
Yokomizo, T., Watanabe, N., Umemoto, T., Matsuo, J., Harai, R., Kihara, Y., Nakamura, E., Tada, N., Sato, T., Takaku, T.*, et al.* (2019). Hlf marks the developmental pathway for hematopoietic stem cells but not for erythro-myeloid progenitors. The Journal of experimental medicine.
Yoshimoto, M., Montecino-Rodriguez, E., Ferkowicz, M.J., Porayette, P., Shelley, W.C., Conway, S.J., Dorshkind, K., and Yoder, M.C. (2011). Embryonic day 9 yolk sac and intra-embryonic hemogenic endothelium independently generate a B-1 and marginal zone progenitor lacking B-2 potential. Proceedings of the National Academy of Sciences of the United States of America *108*, 1468-1473.
Yu, X., Buttgereit, A., Lelios, I., Utz, S.G., Cansever, D., Becher, B., and Greter, M. (2017). The Cytokine TGF-beta Promotes the Development and Homeostasis of Alveolar Macrophages. Immunity *47*, 903-912 e904.
Zambrowicz, B.P., Imamoto, A., Fiering, S., Herzenberg, L.A., Kerr, W.G., and Soriano, P. (1997). Disruption of overlapping transcripts in the ROSA beta geo 26 gene trap strain leads to widespread expression of beta-galactosidase in mouse embryos and hematopoietic cells. Proceedings of the National Academy of Sciences of the United States of America *94*, 3789-3794.
Zaqout, S., and Kaindl, A.M. (2016). Golgi-Cox Staining Step by Step. Frontiers in Neuroanatomy *10*, 38.
Zhan, Y., Paolicelli, R.C., Sforazzini, F., Weinhard, L., Bolasco, G., Pagani, F., Vyssotski, A.L., Bifone, A., Gozzi, A., Ragozzino, D., and Gross, C.T. (2014). Deficient neuron-microglia signaling results in impaired functional brain connectivity and social behavior. Nat Neurosci *17*, 400-406.
Zhao, S., Guo, Y., Sheng, Q., and Shyr, Y. (2014). Advanced Heat Map and Clustering Analysis Using Heatmap3. BioMed Research International *2014*, 6.

Zhong, Y., Jiang, L., Hiai, H., Toyokuni, S., and Yamada, Y. (2007). Overexpression of a transcription factor LYL1 induces T- and B-cell lymphoma in mice. Oncogene *26*, 6937-6947.
Zhou, F., Li, X., Wang, W., Zhu, P., Zhou, J., He, W., Ding, M., Xiong, F., Zheng, X., Li, Z*., et al.* (2016a). Tracing haematopoietic stem cell formation at single-cell resolution. Nature *533*, 487-492.
Zhou, Y., Shi, L., Cui, X., Wang, S., and Luo, X. (2016b). Functional Connectivity of the Caudal Anterior Cingulate Cortex Is Decreased in Autism. PLoS One *11*, e0151879.
Zohren, F., Souroullas, G.P., Luo, M., Gerdemann, U., Imperato, M.R., Wilson, N.K., Gottgens, B., Lukov, G.L., and Goodell, M.A. (2012). The transcription factor Lyl-1 regulates lymphoid specification and the maintenance of early T lineage progenitors. Nature immunology *13*, 761-769.

université PARIS-SACLAY
ÉCOLE DOCTORALE
Structure et dynamique des systèmes vivants (SDSV)

Titre : Fonctions du facteur de transcription factor Lyl-1 au cours du développement hématopoïétique de l'embryon : Etude focalisée sur les macrophages du sac vitellin et sur les cellules souches hématopoïétiques.

Mots clés : Développement, Lyl-1, Sac Vitellin, Macrophage, Cellules Souches Hématopoïétiques.

Résumé : Pendant l'ontogenèse, les progéniteurs hématopoïétiques sont générés en 3 vagues indépendantes. Les 2 premières (primitive, puis transitoire définitive) ont lieu dans le sac vitellin (SV), avant la génération des Cellules Souches Hématopoïétiques (CSH), qui apparaissent plus tard au niveau de la région "Aorta-Gonad-Mesonephros" (AGM), lors de la 3ème vague, dite définitive. Tal1/SCL et son paralogue Lyl-1 appartiennent à un complexe transcriptionnel qui régule le développement hématopoïétique. Tal-1/SCL est indispensable à la spécification des progéniteurs hématopoïétiques des 3 vagues. Par contre, le rôle de Lyl-1 lors du développement hématopoïétique est mal connus.
Grâce au gène rapporteur lacZ des souris Lyl-1^{lacZ}, nous montrons que Lyl-1 marque et régule les progéniteurs macrophagiques primitifs (MΦ^{Prim}) du SV, ainsi que la microglie. Notre analyse en RNA-seq montre que l'ensemble des gènes exprimés par les progéniteurs MΦ^{Prim} est bien distinct de celui des progéniteurs MΦ transitoire définitifs, plus tardifs, reflétant le statut primitif des MΦ^{Prim}. De plus, l'invalidation de Lyl-1 influence les voies de signalisations de l'inflammation et conduit à une activation anormale des gènes de la microglie impliqués dans la régulation synaptique.
Lors de la 3ème vague du développement hématopoïétique, nous montrons que l'invalidation de Lyl-1 conduit à une diminution de l'activité des reconstitution à long terme des CSH de l'AGM à E10 et à une réduction de la population de CSH dans le foie fœtal à E12 et E14. La réduction de la population de CSH semble liée uniquement à un taux accru d'apoptose des CSH *Lyl-1*$^{LacZ/LacZ}$ uniquement au stade de l'AGM.
En conclusion, nos résultats montrent que Lyl-1 régule la production des progéniteurs MΦ primitifs, le développement de la microglie et celui des CSH, dont il contrôle la taille de la population, peu après leur génération.

Title : Functions of the transcription factor Lyl-1 in the hematopoietic development of the embryo: Focus on yolk sac macrophages and hematopoietic stem cells

Keywords: Development Lyl-1, yolk sac, Macrophage, Hematopoietic Stem Cells.

Abstract : During ontogeny, hematopoietic progenitors are generated in three independent waves, the first two (primitive and transient definitive) develop from the yolk sac (YS), before the appearance of Hematopoietic Stem Cells (HSC) that occurs later in the Aorta-Gonad-Mesonephros (AGM), in the third and definitive wave. Both Tal1/SCL and its paralog Lyl-1 belong to the transcriptional complex that regulates hematopoietic progenitor development. While Tal-1/SCL is mandatory for the specification of hematopoietic progenitors from the three embryonic waves, to date the functions of Lyl-1 during developmental hematopoiesis remains largely unknown.
By making use of the lacZ reporter from the Lyl-1^{lacZ} mice, we previously found that Lyl-1 marks and regulates YS macrophage progenitors from the primitive wave (MΦ^{Prim}), and embryonic microglia.
In a RNA-seq analysis, we show that MΦ^{Prim} gene expression landscape is clearly distinct from later transient definitive MΦ progenitors, reflecting their primitive status. Lyl-1 invalidation also influences some inflammatory signalling pathways and also leads to the abnormal activation of microglia genes involved in synaptic regulation. In the definitive wave, we found that Lyl-1 disruption leads to a reduced efficiency of long-term reconstitution by HSC from embryonic day (E)10 AGM and reduced HSC pool size in E12 and E14 fetal liver. The reduction of the HSC pool results from a higher apoptosis level in *Lyl-1*$^{LacZ/LacZ}$ HSCs restricted to the AGM stage.
Together, our data establish that Lyl-1 regulates the development of MΦ^{Prim} progenitors and HSC pool size soon after they are generated.

Université Paris-Saclay
Espace Technologique / Immeuble Discovery
Route de l'Orme aux Merisiers RD 128 / 91190 Saint-Aubin, France